GHENT UNIVERSITY

FACULTY OF SCIENCES

A&MS Atomic and Mass Spectrometry

DEPARTMENT OF CHEMISTRY

ATOMIC AND MASS SPECTROMETRY (A&MS) RESEARCH UNIT

# METHOD DEVELOPMENT FOR SPENT NUCLEAR FUEL CHARACTERISATION USING ISOTOPE DILUTION HPIC-SF-ICP-MS

Nancy Wanna

Student number: 01613721

Supervisor & promotor: Prof. Dr. Frank Vanhaecke

Mentor: Dr. Karen Van Hoecke

Co-promotor: Dr. Andrew Dobney

Co-mentor: Dr. Mirela Vasile

A dissertation submitted to Ghent University in partial fulfilment of the requirements for the degree of Doctor of Science: Chemistry

Academic year 2020–2021

sck cen Belgian Nuclear Research Centre

sck cen Academy

*For my family*

# Members of examination committee

**I. Voting members:**

**Chair:**

Prof. Dr. Mieke Adriaens
Ghent University
Department of Chemistry - WE06

**Secretary:**

Dr. Stepan Chernonozhkin
Ghent University
Department of Chemistry - WE06

**Other voting members:**

Dr. Laura Aldave De Las Heras
European Commission's Joint Research Center JRC Karlsruhe
Institute of Nuclear Safety and Security

Dr. Hélène Isnard
French Atomic Energy Commission CEA Saclay
Department of Physico-Chemistry

Prof. Dr. Anna Kaczmarek
Ghent University
Department of Chemistry - WE06

Prof. Dr. Frederic Lynen
Ghent University
Department of Organic and Macromolecular Chemistry - WE07

Prof. Dr. Laszlo Vincze
Ghent University
Department of Chemistry - WE06

**II. Non-voting members:**

Prof. Dr. Frank Vanhaecke
Ghent University
Department of Chemistry - WE06

Dr. Andrew Dobney
Belgian nuclear research center SCK CEN
Institute of Nuclear Materials Science

# Table of contents

# Acknowledgements

This PhD unraveled a world of opportunities for me to learn, grow and challenge myself in various ways that I can look back at with contentment. I am grateful to have been given the opportunity to perform research in the nuclear field and to share my work with the world. Therefore, I would like to thank the people who made all of this possible. First, I would like to thank my university supervisor and promotor Prof. Dr. Frank Vanhaecke for the opportunity to perform this PhD research and for his guidance and support. Since the day we met at Ghent University, I have been looking up to you as a guru of ICP-MS and at the same time as a friendly and down-to-earth person.

I would like to thank my mentor Dr. Karen Van Hoecke for her devotion, guidance, support and kindness. I will not forget the enormous amount of time and effort that you dedicated to make sure that everything is "going on the right track", starting from the 13$^{th}$ of January, 2017 when you met me at Brussel's airport with a train schedule and map, until the day this PhD is finalized. You are a role model of professionalism and leadership and the memories we shared together at work and in our respective personal lives will always be special to me.

I would like to thank my co-promotor Dr. Andrew Dobney for his support and for sharing his expertise with me throughout this PhD. It has been a pleasure learning from you not only about work, but about different aspects of life as well. Thank you for making time for me, my PhD and my life as an expat living in Belgium, for sharing the ups and downs with me throughout these four years and for motivating me whenever I was faced with difficulties along the way.

I am grateful for the support and guidance of my co-mentor Dr. Mirela Vasile. You have contributed to this PhD not only with time, effort and expertise about environmental samples but also with friendliness and kindness which made the work more enjoyable. Your time and people management skills are inspiring, and I look up to the way you give out everything in your power to reach your goal.

I would like to thank the Academy at the Belgian nuclear research center (SCK CEN) and especially Dr. Michèle Coeck and the scientific jury members for this opportunity of a life time. Also from SCK CEN, I would like to thank Prof. Dr. Thomas Cardinaels, Dr. Ingrid Geuens and Dr. Michel Bruggeman for including me in their respective groups: radiochemistry group (RCY), radiochemical analyses group (RCA) and low-level radioactivity measurements group (LRM). I am grateful to colleagues and supporting staff members of the RCA group, especially Dr. Lesley Adriaensen, Peter Van Bree, Els Verheyen, Luc Gelens, Prisca Verheyen, Karolien Van Rompaey, Loes Van Hout, Göran Verpoucke and Simon Sauvillers for the enjoyable work atmosphere, sharing their expertise, ensuring the safety of the work performed with radioactive samples and for their help and support throughout the four years of this PhD. I would also like to thank staff members of the RCY group especially Dr. Peter Zsabka, Dr. Karen Van Hecke and Dr. Mireille Gysemans for the enjoyable work atmosphere and friendly conversations, and staff members of the LRM group especially Karin Jacobs, Diana Verstrepen and Anke Hooyberghs for their time and help in preparing the environmental samples as well as for their

friendliness and kindness. I could not have written the R code without the help and support of Dr. Bart Rogiers, thank you for teaching me everything I know about R.

Since my first days at SCK CEN, I have met Yaana Bruneel and Dr. Yana Dekempeneer, who are both inspiring, supportive, kind and smart women that I am lucky to have as friends. I would like to thank fellow PhD students at the chemistry building of SCK CEN for the friendly conversations, the fruitful discussions and for sharing their expertise whenever needed.

I am grateful to helpful staff members of the atomic and mass spectrometry group at Ghent University, especially Dr. Stepan Chenonozhkin and Kris Latruwe for sharing their expertise on MC-ICP-MS and for the measurement of standards.

I would like to acknowledge the beautiful, supportive, life-loving and kind-hearted friends and family members (in Lebanon and all over the world) who were far away in distance but have never failed to support and encourage me no matter where they are. Thank you for keeping me in your prayers, for bringing me joy no matter the circumstances and for being my piece of home away from home.

A special gratitude goes to my dear husband Alexander. During these last four years, nothing would have been the same without you in my life. Thank you for your companionship and for enduring this PhD journey with me. I am looking forward to discovering together what the future holds for us. Life has been full of surprises and I have always been inspired by my two "little" brothers, Khalil and George, who can handle any situation without fear or panic. Thank you both, for your sense of humor, kindness and support. And last but undoubtedly not least, I would like to express my lifelong gratitude to my parents, Nazem and Antoinette, who have loved me unconditionally and supported all my decisions and journeys in life, even when it meant that I had to be thousands of kilometers away from them. The happiness and wellbeing of their children, is always their priority and it came at the expense of their health, energy and comfort. They have given me and my brothers everything we could ever need and more, and not a day goes by without me being grateful to God for giving me such amazing parents. I dedicate this dissertation to my parents and I hope I can always make them proud, to make their countless efforts worthwhile.

# Preface

This PhD project was performed at facilities on the site of the Belgian Nuclear Research Centre SCK CEN (Mol, Belgium) in collaboration with Ghent University (Ghent, Belgium), and was focused on developing an analytical method to characterize spent nuclear fuel (SNF) using high pressure ion chromatography (HPIC) coupled to a double focusing single collector sector field inductively coupled plasma-mass spectrometer (SF-ICP-MS).

Determining the isotopic and elemental composition of SNF, that is fuel which has undergone irradiation in a nuclear reactor, is essential for nuclear waste management and for evaluating the performance of the fuel. Post-irradiation examination of SNF includes destructive analysis for the determination of the mass fractions of long-lived actinides and lanthanides (fission products). The long-lived or stable nature of the nuclides of interest makes ICP-MS a more suitable method for their analysis and the method of choice for this work, rather than counting for example by using alpha-spectrometry. Isotope dilution mass spectrometry can be used as a primary method for determining mass fractions of uranium (U), plutonium (Pu) and neodymium (Nd), with the best precision and accuracy based on isotope ratio (IR) measurements using ICP-MS or, alternatively, by thermal ionization mass spectrometry (TIMS) in combination with alpha-spectrometry (e.g. for $^{238}$Pu). SF-ICP-MS is a single detector ICP-MS instrument well known for its flat top spectral peaks at low mass resolution, which increase the precision of IR measurements compared to quadrupole ICP-MS. Coupling HPIC on-line with ICP-MS (not possible with TIMS and alpha-spectrometry) offers a fast, and precise way to eliminate notorious isobaric interferences whilst reducing the analyst's exposure to radiation. The literature reports HPIC coupling to various types of ICP-MS instruments for the characterization of SNF. However, the overall precision obtained with isotope dilution when using HPIC coupled with a single detector SF-ICP-MS to determine the concentrations of U, Pu, Nd and Gd in SNF from one injection has not been reported previously. Therefore, the aim of this work was to separate U, Pu, Nd and Gd and to determine their mass fractions in SNF by means of isotope dilution HPIC-SF-ICP-MS. To accomplish this, the work was divided into four objectives as follows:

(1) Develop and validate a separation method for U, Pu and the lanthanides from one injection using HPIC-SF-ICP-MS. The first objective was tackled in different steps where, at each step, simulations with the Hydra/Medusa software package were performed to predict the complexes in solution. All Pu species in the sample had to be oxidised into Pu(VI) prior to the injection of the sample onto the column.

(2) Optimize the acquisition parameters with the SF-ICP-MS set-up and select a calculation method to obtain the most precise IR measurements. This optimization was accomplished by investigating different acquisition parameters with repeated injections of a Nd standard of natural isotopic abundance. Four mass windows (2, 25, 50 and 150 %), two dwell times (10 and 30 ms) and two different numbers of isotopes monitored per run (2 and 7) were investigated. At the same time, the three IR calculation methods most commonly reported in the literature were compared for their accuracy and precision, namely linear regression slope (LRS), point by point (PbP) rationing and peak area integration (PAI).

(3) Characterize two types of SNF (UOx and “Gd fuel”) using isotope dilution HPIC-SF-ICP-MS. Isotope dilution parameters (other than those investigated in the second objective) had to be optimized for on-line determination of Pu, Nd and Gd elemental mass fractions and a separate off-line determination of the U mass fraction in two types of SNF. This optimization included determining the lowest error magnification factor to obtain the most precise IR in the blend.

(4) Determine the overall uncertainty budget of isotope dilution HPIC-SF-ICP-MS, to compare this developed method to the ISO 17025 accredited isotope dilution TIMS & alpha-spectrometry method, which is currently used at SCK CEN. Uncertainty calculations were performed using the GUM Workbench software.

# Abbreviations

| | |
|---|---|
| PAR | 4-(2-pyridylazo) resorcinol |
| α-HIBA | Alpha-hydroxyisobutyric acid |
| ASTM | American Society for Testing and Materials |
| SCK CEN | Belgian Nuclear Research Centre |
| BP | Binary pump |
| CE | Capillary electrophoresis |
| CEA | Commissariat à l'Energie Atomique et aux énergies alternatives |
| CCQM | Consultative Committee for Amount of Substance |
| CITAC | Co-operation on International Traceability in Analytical Chemistry |
| DAD | Diode array detectors |
| DCP | Direct current plasma |
| EDF | Electricité de France |
| ESA | Electrostatic analyser |
| EGADSNF | Expert Group on Assay Data for Spent Nuclear Fuel |
| EGBUC | Expert Group on Burn-Up credit Criticality |
| FP | Fission product |
| GC | Gas chromatography |
| GDMS | Glow discharge mass spectrometry |
| HETP | Height equivalent to a theoretical plate |
| HPIC | High pressure ion chromatography |
| HPLC | High pressure liquid chromatography |
| HPGe | High purity germanium |
| HKED | Hybrid K-edge densitometry |
| ICP-MS | Inductively coupled plasma-mass spectrometry |
| ISO | International Organisation for Standardisation |
| IAEA | International Atomic Energy Agency |
| BIPM | International Bureau of Weights and Measures |
| OIML | International Organization of Legal Metrology |

| | |
|---|---|
| IC | Ion chromatography |
| IEC | Ion exchange chromatography |
| IUPAC | International Union of Pure and Applied Chemistry |
| IDMS | Isotope Dilution Mass Spectrometry |
| IR | Isotope ratio |
| JRC | Joint Research Centre |
| LOD | Limit of detection |
| LOQ | Limit of quantification |
| LRS | Linear regression slope |
| LSC | Liquid scintillation counting |
| K-bias | Mass bias correction factor |
| R | Mass resolution |
| MOx | Mixed oxide |
| MC | Multi-collector |
| NIST | National Institute of Standards and Technology |
| NIRAS | Nationale Instelling voor Radioactief Afval en Verrijkte Aplijtstoffen |
| NRD | Neutron resonance densitometry |
| NEA | Nuclear Energy Agency |
| ORNL | Oak Ridge National Laboratory |
| ONDRAF | Organisme National des Déchets Radioactifs et des Matières Fissiles Enrichies |
| PDET | Partial defect tester |
| PIPS | Passivated implanted planar silicon |
| PSI | Paul Scherrer Institute |
| PAI | Peak area integration |
| %FIMA | Percentage of fissions per initial metal atoms |
| PFA | Perfluoroalkoxy |
| PAD | Photodiode array detectors |
| PbP | Point-by-point |
| PEEK | Polyether ether ketone |
| PTFE | Polytetrafluoroethylene |

| | |
|---|---|
| PVF | Polyvinylfluoride |
| PWR | Pressurized water reactors |
| RF | Radiofrequency |
| REE | Rare earth elements |
| RSD | Relative standard deviation |
| RSC | Royal Society of Chemistry |
| STUK | Säteilyturvakeskus (radiation and nuclear safety authority in Finland) |
| SEM | Secondary electron multipliers |
| SIMS | Secondary ion mass spectrometry |
| SF | Sector field |
| SINRD | Self-indication neutron resonance densitometry |
| SP | Single pump |
| SNF | Spent nuclear fuel |
| SD | Standard deviation |
| SSB | Standard sample bracketing |
| TIMS | Thermal ionization mass spectrometry |
| UV-Vis | Ultraviolet-Visible |
| UOx | Uranium oxide |
| VWD | Variable wavelength detectors |

# Units used

| Name | Symbol | Description |
|---|---|---|
| Bar | bar | Unit of pressure equal to 100,000 Pa. |
| Barn | b | Unit used in particle physics to express the cross sectional area of nuclei. A barn is equal to $10^{-28}$ $m^2$. |
| Becquerel | Bq | SI unit of the activity referred to a radionuclide. Becquerel is the rate of radioactive decay of an unstable nuclide and is equal to one reciprocal second. |
| Electron volt | eV | Kinetic energy acquired by an electron in passing through a potential difference of one volt in vacuum. An eV is equal to $1.602176634 \cdot 10^{-19}$ J. |
| Equivalent | equiv | Unit for an amount of a substance in solution and is equal to the number of moles of an ion in solution multiplied by the valence of that ion. |
| Kelvin | K | SI unit of thermodynamic temperature and is equal to 1/273.16 of the triple point of water. |
| Megawatt electric | MWe | One million watts of electric capacity |
| Pascal | Pa | SI unit of pressure and is equal to newton per square meter. |
| Sievert | Sv | SI unit for dose equivalent and is equal to the joule per kilogram. |
| Unified atomic mass unit | u | Unit equal to 1/12 of the mass of a free carbon 12 atom, at rest and in its ground state. |

# Chapter 1 – Introduction and objectives

This first chapter provides a general overview of spent nuclear fuel (SNF), its management and characterization methods. The aim and objectives of this work will also be outlined in this chapter.

## 1.1 Spent nuclear fuel

SNF is part of the radioactive waste generated in nuclear power plants. According to the International Atomic Energy Agency (IAEA), SNF refers to fuel assemblies discharged from nuclear reactors after irradiation [1]. The nuclear fuel currently used in most reactors is based on uranium oxide with different enrichment values, depending on the reactor type. For example, the fuel used in light water reactors, such as pressurized water reactors (PWR) (Figure 1.1) and boiling water reactors, is enriched in $^{235}U$ up to 5 wt. %, while pressurized heavy water reactors use natural (~ 0.7 wt. % $^{235}U$) or slightly enriched (up to 1.2 wt. % $^{235}U$) uranium. After its mining, uranium is converted to uranium hexafluoride, which is in gaseous form, to be enriched [2]. After enrichment, uranium hexafluoride is converted to uranium dioxide (by "dry" or "wet" chemical processes [2]), which is subsequently compressed into fuel pellets (10 mm in diameter and 10-15 mm in height) which are then stacked into long tubes around 3-5 m in length, made of Zircaloy to make fuel rods for PWRs [3]. Zircaloy is an alloy of more than 95 wt. % zirconium, which has a very low absorption cross-section for thermal neutrons, high hardness and is durable and corrosion-resistant. Fuel rods (as many as 150 to 260) are grouped together into a specific geometry (square or hexagonal cross-section) using spacers to form a fuel assembly (Figure 1.1). Typically, a 1000 MWe PWR contains between 120 and 200 fuel assemblies. As shown in Figure 1.1, in a PWR, the reactor and steam generators are contained in a reinforced concrete structure (concrete and stainless steel) to protect these components from outside elements and to contain the radiation in case of any major accident.

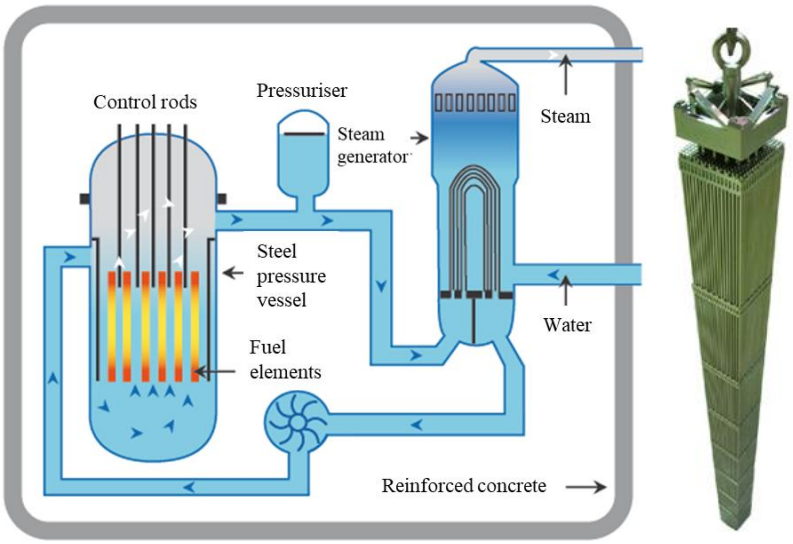


Figure 1.1 Schematic representation of a PWR (left) [4] and a PWR fuel assembly (right) [2]

When struck by a thermalized neutron, $^{235}U$ becomes unstable and undergoes fission. During fission, the $^{235}U$ atom splits into two smaller atoms, called fission products, having masses of around 95 and 140 atomic mass units (Figure 1.2), and releasing heat and 2 to 3 neutrons, which can support a fission chain reaction. To control a fission chain reaction, fissile material, neutrons, and material to slow down/retain neutrons are required. To sustain a fission chain reaction, neutrons are slowed in the reactor core by a moderator, which is usually water, but can be heavy water or graphite. To control or halt a fission chain reaction, neutron absorbers can be used in liquid form, such as boric acid dissolved in the primary water circuit, or in solid form, such as control rods (containing hafnium, boron or cadmium) or a burnable poison with high neutron absorption cross-section (such as gadolinium) can be included in the fuel to limit the excess reactivity. Liquid and solid neutron absorbers can also be used in combination to control the number of neutrons in a nuclear reactor. The neutron multiplication in a fission is characterized by the parameter *k*, defined in eq. 1.1 where $\eta$ is the number of neutrons produced in a fission to the number of neutrons absorbed, $\epsilon$ is the fast fission factor, which is the ratio of the total number of neutrons produced by all fissions to that of slow neutron fission, *p* is the resonance escape probability, which is the probability that neutrons avoid being captured and reach thermal energies where they may cause fission, *f* is the thermal utilization, which is the ratio of thermal neutrons absorbed in the fuel to the total number of thermal neutrons absorbed and $p_{fnl}$ and $p_{tnl}$ are the probabilities of fast and thermal neutron non-leakage, respectively [5]. A reactor is critical and has a constant power when $k = 1$, is supercritical and its power increases when $k > 1$, and is subcritical and its power decreases when $k < 1$.

$$k = \frac{Neutron\ production\ rate}{Neutron\ loss\ rate} = \eta.\epsilon.p.f.p_{fnl}.p_{tnl} \qquad \text{(eq. 1.1)}$$

Nuclear fuel is considered "spent" when it no longer contains enough $^{235}U$ atoms to sustain the fission chain reaction. This can happen 3 to 7 years after fuel loading, depending on the fuel and its location in the reactor core. Neutron capture by $^{238}U$ leads to the formation of plutonium and transuranic elements called minor actinides, such as neptunium, americium and curium, which can also undergo fission. SNF is highly radioactive as it emits alpha, beta, gamma and neutron radiation. The radiation level of SNF decreases over time as the radioactive elements decay. There are three main sources of radiation in SNF. These are (1) radioactive fission products (e.g. in increasing order of half-life from 5.2 days to $2.1 \cdot 10^5$ years: $^{133}Xe$, $^{131}I$, $^{85}Kr$, $^{152}Eu$, $^{90}Sr$, $^{137}Cs$ and $^{99}Tc$), (2) products of neutron capture by uranium such as plutonium (e.g. in increasing order of half-life from 14.3 to $3.7 \cdot 10^5$ years: $^{241}Pu$, $^{240}Pu$, $^{239}Pu$ and $^{242}Pu$) and minor actinides (e.g. in increasing order of half-life from 2.4 days to $2.1 \cdot 10^6$ years: $^{239}Np$, $^{242}Cm$, $^{244}Cm$, $^{241}Am$ and $^{237}Np$), and lastly (3) activation products formed by neutron capture in fuel cladding and structural materials in the fuel assembly (e.g. in increasing order of half-life from 2.7 to $3 \cdot 10^5$ years: $^{55}Fe$, $^{60}Co$, $^{14}C$, $^{94}Nb$, $^{59}Ni$ and $^{36}Cl$). Some components of SNF can be reusable, either for producing fresh fuel (uranium and plutonium) or for other uses, such as irradiation in a medical context (fission product: caesium).

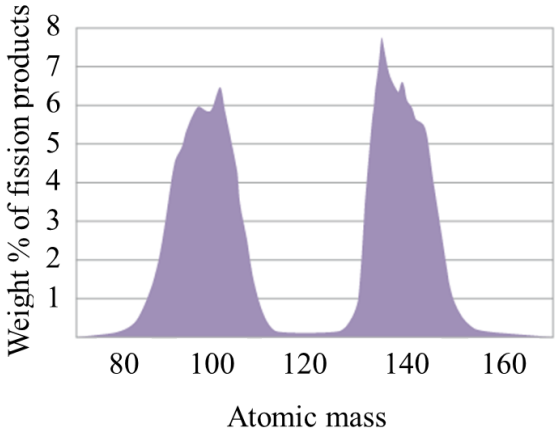


Figure 1.2 Distribution of fission products produced in a UOx fuel [6]

## 1.2 Radioactive waste management

Radioactive waste can be generated from a wide range of applications in addition to nuclear energy generation, such as the use of radioactive sources in medicine, research, agriculture and industry. The physical, chemical and radiological characteristics of waste vary widely depending on the application, but a common characteristic of all radioactive waste is its potential of being a hazard to people and to the environment. The analysis of radioactive waste is important for radioactive waste management prior to its disposal. National safety regulations are set for managing radioactive waste. However, the risk of radiation may transcend national borders. Therefore, the IAEA issued several international safety standards [7-9] and guides [10-13] providing recommendations for safe management and storage of radioactive waste to protect people and the environment. Radioactive waste management consists of the following steps: (1) collecting the radioactive waste, (2) processing it into a form suitable for safe storage and (3) storing it in surface or geological repositories depending on its classification. At various steps of the radioactive waste management process, the characterization of the different properties (e.g. physical, chemical and radiological) of radioactive waste is required and recorded to facilitate its management.

Radioactive waste is classified by the IAEA into six categories based on the radioactivity level and half-life (the time it takes for the radioactivity to decrease by half) of the waste [14] and ways for its safe management are indicated by the European Commission in the radioactive waste and spent fuel management directive 2011/70/Euratom [15]. Nevertheless, classification of radioactive waste can vary between countries. In Belgium, for example, NIRAS/ONDRAF (Nationale Instelling voor Radioactief Afval en verrijkte Splijtstoffen / Organisme National des Déchets Radioactifs et des matières Fissiles enrichies), the national organisation in charge of managing radioactive waste, classifies radioactive waste for final disposal into three categories: A (short-lived low and intermediate level waste), B (long-lived low and intermediate level waste) and C (short and long-lived high-level waste), which are based on the radioactivity content and the half-life of the waste similar to the IAEA classification. In contrast, the radiation and nuclear safety authority STUK (Säteilyturvakeskus) in Finland distinguishes between nuclear waste (spent nuclear fuel & low and intermediate nuclear waste) and radioactive waste

(conditioned solid waste, liquid waste, solid waste and airborne discharges), based on their disposal routes.

European countries have chosen to store their short-lived low and intermediate activity waste differently, by either opting for geological (e.g. Forsmark, Sweden) or near-surface storage (e.g. Aube, France). However, for long-lived high-level waste there is a general consensus that geological disposal is the safest option. Currently in Belgium, short-lived low and intermediate level waste undergoes intermediate near-surface storage, whilst the final disposal site in Dessel is still under construction according to NIRAS/ONDRAF [16].

### 1.3 Spent nuclear fuel management

Different strategies for managing SNF exist, since it can be regarded as a resource, and reprocessed to make new nuclear fuel (generating a closed fuel cycle), or it can be considered as radioactive waste after its removal from the reactor core and needing to be disposed of after decades of interim storage (open fuel cycle). The choice of spent nuclear fuel management strategy varies between countries, for example, France, the Russian Federation, China, India and Japan have chosen to reprocess their SNF, while the United States of America, Canada, Finland, Sweden and Germany opted for directly disposing their SNF. If classified as a resource, SNF assembly is dissolved in acid before separating uranium and plutonium from fission and activated products and transuranic elements (vitrified high level waste) and from the cladding and structural materials (intermediate level waste). Dissolving the SNF in acid does not achieve any separation of U and Pu; dissolution merely converts the solid SNF into solution form. The separation takes place after the dissolution, by a variety of processes, one of which is the PUREX process, a solvent extraction based process. SNF dissolves readily in a wide concentration range of nitric acid, with the consumption of protons and nitrate to form uranyl nitrate species. Many different chemical reactions with various stoichiometries can take place [17]. Uranium starts to precipitate from +/- pH 5 onwards under oxidizing conditions, hence only acidic conditions are used. Uranium and plutonium are then separated from each other and the uranium is isotopically enriched. Then, uranium and plutonium are converted into oxides that are used to make fresh mixed oxide fuel (MOx). Compared to the open fuel cycle, reprocessing involves additional steps, but reduces demand for uranium by 25 %. Both SNF and high-level waste require disposal in geological repositories, while intermediate level waste can be stored in near-surface or underground facilities. However, if classified as waste, SNF can be stored in water pools for up to 3 to 4 decades before being transported for interim storage or for disposal in a geological repository. Pools serve two functions: (1) protecting the workers from the radiation emitted by the SNF assemblies and (2) cooling the SNF assemblies by evacuating the heat through the circulating water. In geological disposal, SNF and high-level waste are encapsulated in a leak-tight container, isolated from the environment by multiple barriers and placed in tunnels at several hundred meters of depth. At different stages of SNF management, certain nuclides become more important (Figure 1.3). For example, during transportation and storage of SNF, short-lived radionuclides (such as volatile $^{131}I$) are significant in case of damage breaching the fuel rod cladding within one year of its discharge from the reactor core.

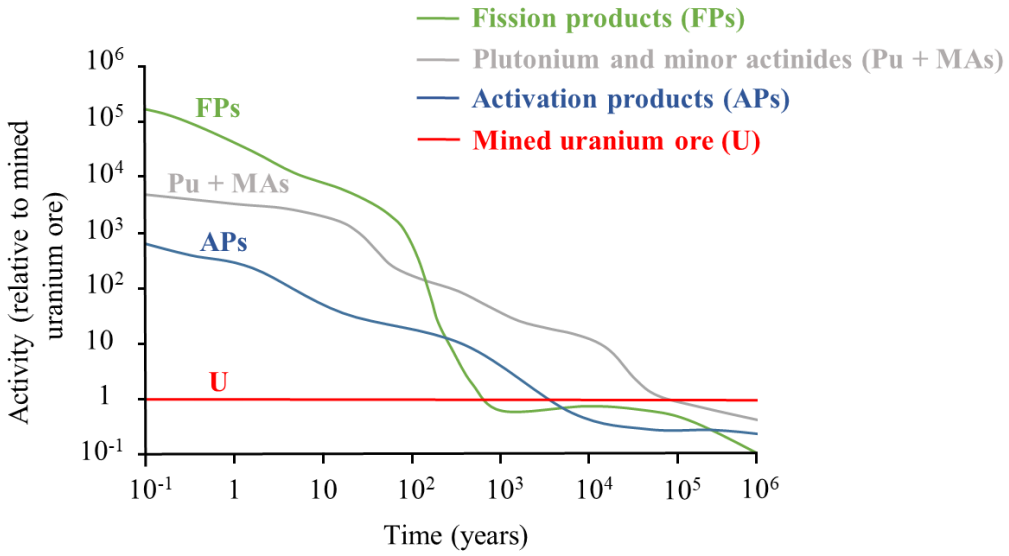


Figure 1.3 Trend of the activity of different SNF components relative to mined uranium ore with respect to time [3]

Shielding is a requirement throughout transportation and storage of SNF due to the hazard from $^{60}$Co and $^{137}$Cs, which are gamma emitters, and $^{240}$Pu and $^{242}$Cm, which are neutron emitters. Shielding is provided by 3 to 4 meters of water in pools where SNF is first stored (wet storage) after being discharged from the reactor core, before being transferred to dry storage where shielding is provided by the metal/concrete cask body and neutron absorbing materials. SNF is not moved to dry storage until after at least 5 to 10 years of storage in a reactor pool (depending on its capacity) connected directly to the reactor. Additional away-from-reactor storage might be needed, either wet or dry storage, if the capacity of the reactor pool is reached. Long-term dry storage for up to 100 years is now being considered due to the lack of final disposal facilities. The licence to construct the world's first geological repository (Onkalo) at the Olkiluoto site was granted in Finland in November 2015 [18] and the application for the operational license is scheduled to be submitted by the end of 2022 [19]. Additionally, cooling of SNF is required due to heat released by the beta emitting radionuclides $^{137}$Cs and $^{90}$Sr. Cooling ensures that no temperature limits will be exceeded in operational or accident conditions in order to protect the storage facility's structures, systems, components and the fuel from damage throughout the lifetime of the storage facility [1], thereby preventing release of radioactive material to the environment. In wet storage, cooling is provided by the pool water that is constantly circulated through heat exchangers, whereas in dry storage, cooling is provided by forced or natural air circulating around the containers of SNF [1]. Transport of SNF might be needed depending on the location of the nuclear power plant and SNF management facility. For transport of SNF, cylindrical containers are used, after first having passed a series of tests (drop, heat, immersion in water, etc.) to prove their robustness and thermoconductive and shielding properties, as recommended by the IAEA [1]. Design of the geological repositories must take into account the long-term heat release of $^{137}$Cs, $^{90}$Sr, $^{241}$Pu and $^{241}$Am and the mobility of long-lived radionuclides, such as $^{99}$Tc, $^{14}$C, $^{36}$Cl and $^{239}$Np, to ensure safe disposal of SNF. SNF still contains fissile uranium and plutonium radionuclides, which could become critical causing a chain reaction. Subcriticality must be ensured during

transport, storage, reprocessing and in geological repositories, for example, when stored in reactor pools, a subcritical geometry must be maintained and neutron absorbers can be added.

### 1.4 Spent nuclear fuel analysis

The composition of SNF depends on the amount of energy liberated by the fuel. An important characteristic of SNF is the "burn-up", which is the number of fissions undergone by the fuel [20] and the clearest way to express it, is as the percentage of fissile metal atoms that underwent fission (%FIMA). This is calculated as shown in eq. 1.2 [21], where *M* & *M'* are the numbers of heavy metal atoms before and after irradiation, *F* is the number of heavy metals that underwent fission, and is determined most frequently as $F = N/Y_{eff}$, *N* being the number of fission product atoms of a burn-up monitor nuclide (such as $^{148}$Nd) and $Y_{eff}$ being the effective fission product yield weighted by the yield for each fissile actinide.

$$\%FIMA = \frac{F}{M} = \frac{F}{F+M'} \qquad \text{(eq. 1.2)}$$

The %FIMA is most often calculated using $^{148}$Nd, although also other fission products can be used as burn-up monitors such as $^{137}$Cs, $^{139}$La and $^{144}$Ce. In order to use $^{137}$Cs for burn-up determination, it is essential to analyse a fuel sample that is large enough to be representative, because Cs is known to migrate from the centre of the fuel pellet towards its edge during irradiation due to the high radial temperature gradient between the pellet core (1200 °C) and rim (400-500 °C) [22]. In practice, the $^{144}$Ce half-life of 285 days can limit the use of this nuclide as burn-up monitor to only those SNFs with short cooling times [21]. The following properties of $^{148}$Nd make it the most used fission product monitor: (1) it is not volatile, does not migrate in the fuel pellet and has no volatile precursor, (2) it is stable and does not require decay corrections, (3) its fission yield is nearly the same for $^{235}$U (1.66 %) and $^{239}$Pu (1.65 %) [23], (4) it is not present in fresh nuclear fuel, (5) it can be corrected for natural neodymium contamination using $^{142}$Nd (which is stable and not a normal constituent of fresh fuel [24]), (6) it has a low neutron absorption cross-section (Table 1.4), which means that its probability of taking up another neutron is low.

The %FIMA (shown in eq.1.2) can be converted to gigawatt days per metric ton by consulting the ASTM E321 – 96 standard test method for burn-up determination [25]. SNF from UOx fuels with 3.5 % initial enrichment, 33 GWd·t(heavy metals)$^{-1}$ energy output and 3 years cooling time, contains (on a metals basis) almost 96 wt. % of uranium (including 1 % of fissile $^{235}$U), 1 wt. % of plutonium, 0.1 wt. % of minor actinides and 3 wt. % of fission products (Figure 1.4) [1]. For fuel with a higher burn-up, the amount of uranium remaining will be lower than 96 wt. % and the amounts of plutonium, minor actinides and fission products will be higher than 1, 0.1 and 3 wt. %, respectively (on a metals basis). In "Gd fuels", the fresh fuel is enriched to 5-10 wt. % in gadolinia ($Gd_2O_3$). As such, Gd is present as a major element within such fuels (before and after irradiation). Apart from the presence of the additional Gd, the composition of these "Gd fuels" is otherwise comparable to that of UOx fuels. The determination of the isotopic composition and content of Gd in "Gd fuels" after their irradiation enables the performance of Gd as burnable poison to be evaluated. Major fission products of $^{235}$U that have a fission yield higher than 5 % are presented in Table 1.1 [26]. Although the percentage of fissile material in

SNF is very low, the nature of this material makes it a target for nuclear safeguards. Burn-up credit is an accurate and realistic means to determine SNF reactivity, because it takes into account the reduction in the reactivity of nuclear fuel during irradiation due to the net reduction of fissile nuclides and to the production of neutron-absorbing nuclides (fission products and non-fissile actinides) [27]. Activities related to the assessment of nuclear criticality safety in member countries of the NEA (Nuclear Energy Agency) are coordinated by the Expert Group on Burn-Up credit Criticality (EGBUC). SNF characterization (assays and burn-up credit) is carried out for criticality safety and safeguards purposes using non-destructive and destructive analysis (explained in sections 1.4.5 and 1.4.6 of this chapter) to determine the concentrations and isotopic compositions of the main fuel elements (uranium, plutonium and gadolinium when it is added as a burnable poison in "Gd fuels" [28]) and those of a fission product monitor (neodymium).

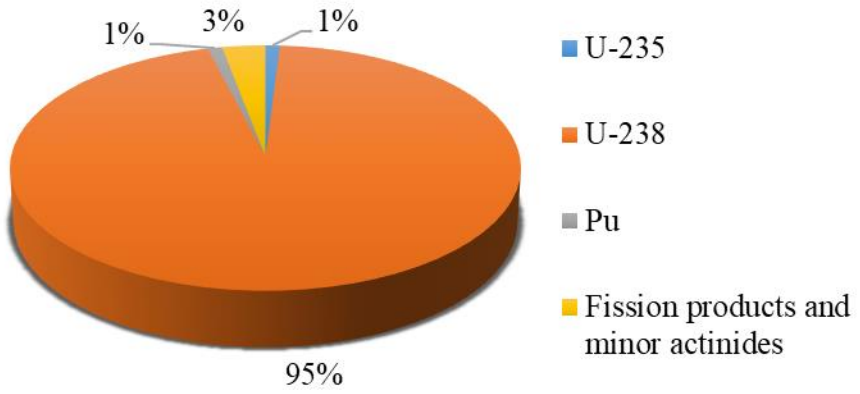


Figure 1.4 Composition of a UOx SNF with 3.5 % initial enrichment, 33 GWd.t(heavy metals)$^{-1}$ and 3 years cooling time [1]

Table 1.1 Fission products of $^{235}$U with fission yield higher than 5 % [26]

| Nuclide | Fission yield (% per fission of $^{235}$U) ± U (k=2) |
|---|---|
| $^{90}$Sr | 5.73 ± 0.13 |
| $^{95}$Zr | 6.502 ± 0.072 |
| $^{95}$Nb | 6.498 ± 0.072 |
| $^{99}$Mo | 6.132 ± 0.092 |
| $^{99}$Tc | 6.132 ± 0.092 |
| $^{133}$I | 6.59 ± 0.11 |
| $^{135}$I | 6.39 ± 0.22 |
| $^{133}$Xe | 6.6 ± 0.11 |
| $^{135}$Xe | 6.61 ± 0.22 |
| $^{137}$Cs | 6.221 ± 0.069 |
| $^{140}$Ba | 6.314 ± 0.095 |
| $^{140}$La | 6.315 ± 0.095 |
| $^{141}$Ce | 5.86 ± 0.15 |
| $^{144}$Ce | 5.474 ± 0.055 |
| $^{144}$Pr | 5.474 ± 0.055 |
| $^{144}$Nd | 5.475 ± 0.055 |

### 1.4.1 Uranium

Uranium has been formed within our Solar System by multiple supernovae from over 6 billion to about 200 million years ago [29]. As a result, uranium was present in the dust that eventually clogged together and cooled down to produce the Earth. Uranium is found naturally in trace amounts in different compartments of the Earth, such as soil (2 parts per million), water bodies (e.g. 0.3 parts per million in seawater [30]) and even air (2 $\mu Bq \cdot m^{-3}$). According to the United Nations Scientific Council, worldwide average dose rates due to ingestion (mainly from water) and inhalation of natural uranium nuclides are less than 1 µSv per year [31].

Uranium was discovered in 1789 by Klaproth and its radioactivity was demonstrated by Becquerel in 1896. Natural uranium has 92 protons in its nucleus, its electronic configuration is [Rn] $5f^3$ $6d^1$ $7s^2$ and it has three naturally occurring isotopes: $^{234}U$, $^{235}U$ and $^{238}U$, with characteristics as shown in Table 1.2. Nuclides with odd mass numbers (such as $^{235}U$ in Table 1.2) generally have a larger neutron capture cross-section compared to nuclides with an even mass number, which makes the probability of neutron absorption higher for nuclides with odd mass numbers than for those with even mass numbers (Oddo-Harkins rule) [32]. Atomic nuclei with even mass numbers are more stable when formed than those with odd mass numbers. This phenomenon can be explained by the nuclear shell model [32].

Table 1.2 Characteristics of naturally occurring uranium nuclides (the characteristics listed in this table were sourced from Nucleonica [33], except for the relative abundances which were calculated based on mole fractions obtained from IUPAC [34])

| Nuclide | Relative abundance (wt. %) | Half-life (years) | Specific activity ($Bq \cdot g^{-1}$) | Neutron absorption cross-section (b) | Decay mode |
|---|---|---|---|---|---|
| $^{234}U$ | 0.00531 (49) | $2.457 \cdot 10^5$ (3) | $2.300 \cdot 10^8$ (3) | 116 | α |
| $^{235}U$ | 0.71137 (59) | $7.038 \cdot 10^8$ (5) | $7.996 \cdot 10^4$ (6) | 697 | α |
| $^{238}U$ | 99.2833 (16) | $4.468 \cdot 10^9$ (3) | $1.2436 \cdot 10^4$ (8) | 12 | α |

Due to its electronic configuration, uranium is most stable in oxidation state VI, and is mainly found as $UO_2^{2+}$ (uranyl) in complexes [32]. The uranyl group can be detected in an infrared spectrum of a uranium compound by the presence of (1) a strong band in the region 920-980 $cm^{-1}$ due to the asymmetric O–U–O stretching vibration or (2) a band around 860 $cm^{-1}$ caused by the symmetric O–U–O stretching vibration in a Raman spectrum. Additionally, uranyl complexes have a yellow colour and a characteristic absorption peak around 25,000 $cm^{-1}$ (400 nm) which can be monitored using UV-Vis spectrometry.

### 1.4.2 Plutonium

Plutonium is a man-made element first produced in 1940 by Seaborg et al. by bombarding uranium with neutrons [35]. Plutonium found in the environment originates from anthropogenic sources (nuclear weapon testing, nuclear accidents, etc.). Characteristics of plutonium nuclides are shown in Table 1.3. Plutonium can be present in SNF either as a product of neutron capture by $^{238}U$ or it can be added to the fuel prior to its irradiation (MOx). Reactor-grade Pu is defined

as material composed of more than 18% of $^{240}$Pu [36]. The neutron cross-section of $^{240}$Pu (Table 1.3) limits its use in weapon grade Pu, which contains at least 93 % $^{239}$Pu [36].

Table 1.3 Characteristics of plutonium nuclides [33]

| Nuclide | Half-life (years) | Specific activity ($Bq \cdot g^{-1}$) | Neutron absorption cross-section (b) | Decay mode |
|---|---|---|---|---|
| $^{238}$Pu | 87.7 (3) | $6.34 \cdot 10^{11}$ (2) | 584 | α |
| $^{239}$Pu | $2.4114 \cdot 10^{4}$ (11) | $2.2947 \cdot 10^{9}$ (10) | 1,029 | α |
| $^{240}$Pu | $6.563 \cdot 10^{3}$ (5) | $8.396 \cdot 10^{9}$ (6) | 290 | α |
| $^{241}$Pu | 14.33 (4) | $3.829 \cdot 10^{12}$ (11) | 1,383 | β- |
| $^{242}$Pu | $3.735 \cdot 10^{5}$ (11) | $1.463 \cdot 10^{8}$ (4) | 30 | α |
| $^{244}$Pu | $8.00 \cdot 10^{7}$ (9) | $6.77 \cdot 10^{5}$ (8) | 12 | α |

Due to their similar redox potentials: E(Pu(III)/Pu(IV)) = 0.98V, E(Pu(IV)/Pu(V)) = 1.04 V and E(Pu(V)/Pu(VI)) = 0.94 V [32], multiple oxidation states III, IV, V and VI of plutonium can be present simultaneously in acidic solution. In alkaline solutions, plutonium can be found in oxidation states VII and even VIII (> 1 M sodium hydroxide) [37]. The oxidation states IV and VI of plutonium are the most stable ones in acidic solutions. Due to its large charge-to-radius ratio, plutonium (VI) readily strips oxygen atoms from water molecules and is present as $PuO_2^{2+}$ (plutonyl) which is stable in aqueous solutions [38].

### 1.4.3 Lanthanides

The lanthanide series consists of 15 elements in the periodic table from lanthanum to lutetium with atomic numbers from 57 to 71, and its elements are known to have very similar chemical properties, making their separation far from straightforward. Most lanthanides (including neodymium and gadolinium) are present in solution as $Ln^{3+}$ions having [Xe] $4f^n$ electronic configurations, nevertheless some lanthanides can also exist in solution as $Ln^{4+}$ (such as Ce) and $Ln^{2+}$ ions (such as Eu) [32]. The lanthanides differ in the number of electrons in the 4f orbital. As this orbital is positioned near the atomic nucleus, the electrons in the 4f orbital have only a limited effect on chemical bonding characteristics and speciation. Separation strategies therefore make use of the phenomenon called ‘lanthanide contraction’: Across the lanthanide series from La to Lu, the atomic and ionic radii are known to decrease as a result of the increasing effective nuclear charge (as is always the case within a period of the periodic table), however, the 4f electrons are less efficient in shielding the electrons inside the 5s and 5p orbitals from the positive nuclear charge, which leads to the “lanthanide contraction” [32]. Hence, the lanthanides share such similar chemistries [including oxidation state] that the possibilities of using the selectivity of an ion exchanger as the basis of a separation only can be rather limited for lanthanides.

#### 1.4.3.1 Neodymium

Neodymium was discovered in 1841 by Carl Gustav Mosander, who called it didymium (from “didymos”, which means twin in Greek) due to its similarity to lanthanum, which he had

discovered two years previously. In 1885, Carl Aeuer von Welsbach separated didymium into two elements and called these neodymium and praseodymium, both names deriving from the Greek meaning new and green twin, respectively [34]. Neodymium is the second most abundant lanthanide in the Earth's crust (40 parts per million) after cerium (66 parts per million) [32]. Each neodymium atom has 60 protons in its nucleus. Characteristics of naturally occurring Nd nuclides are listed in Table 1.4, which shows that neodymium nuclides are mostly stable ($^{142,\ 143,\ 145\ \&\ 146}$Nd) or have very long half-lives (more than $10^{15}$ years).

Table 1.4 Characteristics of naturally occurring neodymium nuclides (the characteristics listed in this table were sourced from Nucleonica [33], except for the relative abundances which were calculated based on mole fractions obtained from IUPAC [34])

| Nuclide | Relative abundance (wt. %) | Half-life (years) | Specific activity ($Bq \cdot g^{-1}$) | Neutron absorption cross-section (b) | Decay mode |
|---|---|---|---|---|---|
| $^{142}$Nd | 26.712 (44) | Stable | - | 27 | - |
| $^{143}$Nd | 12.062 (27) | Stable | - | 404 | - |
| $^{144}$Nd | 23.743 (25) | $2.29 \cdot 10^{15}$ (16) | $4.0 \cdot 10^{-2}$ (3) | 4 | α |
| $^{145}$Nd | 8.332 (13) | Stable | - | 60 | - |
| $^{146}$Nd | 17.388 (35) | Stable | - | 6 | - |
| $^{148}$Nd | 5.903 (22) | $2.7 \cdot 10^{18}$ | $3.3120 \cdot 10^{-5}$ (8) | 12 | 2β- |
| $^{150}$Nd | 5.860 (29) | $2.1 \cdot 10^{19}$ (5) | $4.2 \cdot 10^{-6}$ (10) | 6 | 2β- |

#### 1.4.3.2 Gadolinium

Gadolinium was discovered by Jean-Charles Galissard de Marignac in 1886 and was named by Paul-Emil Lecoq de Boisbaudran after gadolinite, the mineral in which it was found. Characteristics of gadolinium nuclides can be found in Table 1.5. Gadolinium nuclides are stable, except for $^{152}$Gd and $^{160}$Gd, which have long half-lives (more than $10^{14}$ years). When used as a burnable poison in nuclear fuels, the fuel is enriched to 5-10 wt. % in gadolinia ($Gd_2O_3$). As such, Gd is present as a major element within such fuels. During irradiation, gadolinium nuclides with large neutron absorption cross-sections, such as $^{155}$Gd and $^{157}$Gd (Table 1.5), capture neutrons thereby forming $^{156}$Gd and $^{158}$Gd, respectively. These resulting nuclides, however, have small neutron absorption cross-sections and thus constitute a dead-end for this decay chain reaction. Additionally, gadolinium nuclides can be produced in nuclear reactors by the fission of $^{235}$U and by the decay of fission products, but with low total yields ($< 10^{-4}$ %).

Table 1.5 Characteristics of naturally occurring gadolinium nuclides (the characteristics listed in this table were sourced from Nucleonica [33], except for the relative abundances which were calculated based on mole fractions obtained from IUPAC [34])

| Nuclide | Relative abundance (wt. %) | Half-life (years) | Specific activity ($Bq \cdot g^{-1}$) | Neutron absorption cross-section (b) | Decay mode |
|---|---|---|---|---|---|
| $^{152}Gd$ | 0.193 (29) | $1.08 \cdot 10^{14}$ (8) | $8.1 \cdot 10^{-1}$ (6) | 735 | α |
| $^{154}Gd$ | 2.134 (20) | Stable | - | 85 | - |
| $^{155}Gd$ | 14.581 (91) | Stable | - | 60,900 | - |
| $^{156}Gd$ | 20.297 (41) | Stable | - | 1,5 | - |
| $^{157}Gd$ | 15.617 (45) | Stable | - | 254,000 | - |
| $^{158}Gd$ | 24.946 (87) | Stable | - | 2.2 | - |
| $^{160}Gd$ | 22.232 (43) | $1.3 \cdot 10^{17}$ | $6.3622 \cdot 10^{-4}$ | 0.77 | 2β- |

### 1.4.4 Other spent fuel components

While burn-up determination requires the measurement of specific nuclides to assess the performance of the nuclear fuel, SNF characterization involves the measurement of many more nuclides formed during the irradiation of the fuel and is used to evaluate safety codes. Table 1.6 lists commonly measured nuclides for different safety-related SNF applications including burn-up determination.

Table 1.6 Commonly measured nuclides for different safety-related SNF applications (based on [21])

| Nuclide | Half-life (years) | Burn-up | Radiological safety | Waste management | SNF characterization |
|---|---|---|---|---|---|
| $^{79}Se$ | $2.95 \cdot 10^{5}$ | | | + | + |
| $^{95}Mo$ | Stable | + | | | + |
| $^{90}Sr$ | 28.9 | | + | + | + |
| $^{99}Tc$ | $2.111 \cdot 10^{5}$ | + | | + | + |
| $^{101}Ru$ | Stable | + | | | + |
| $^{106}Ru$ | 371.6 days | | + | | + |
| $^{103}Rh$ | Stable | + | | | + |
| $^{109}Ag$ | Stable | + | | | + |
| $^{125}Sb$ | 2.7586 | | + | | + |
| $^{129}I$ | $1.6 \cdot 10^{7}$ | | | + | + |
| $^{133}Cs$ | Stable | + | | | + |
| $^{134}Cs$ | 2.065 | | + | | + |
| $^{135}Cs$ | $2.3 \cdot 10^{6}$ | | | + | + |
| $^{137}Cs$ | 30 | + | + | + | + |
| $^{139}La$ | Stable | + | | | + |
| $^{142}Nd$ | Stable | | | | + |
| $^{143}Nd$ | Stable | + | | | + |
| $^{144}Nd$ | $2.29 \cdot 10^{15}$ | + | | | + |
| $^{145}Nd$ | Stable | + | | | + |
| $^{146}Nd$ | Stable | + | | | + |
| $^{148}Nd$ | $2.7 \cdot 10^{18}$ | + | | | + |
| $^{150}Nd$ | $2.1 \cdot 10^{19}$ | + | | | + |

Table 1.6 Commonly measured nuclides for different safety-related SNF applications (based on [21]) (continued)

| Nuclide | Half-life (years) | Burn-up | Radiological safety | Waste management | SNF characterization |
|---|---|---|---|---|---|
| $^{144}$Ce | 284.9 days | + | + | | + |
| $^{147}$Pm | 2.623 | + | | | + |
| $^{147}$Sm | $1.06 \cdot 10^{11}$ | + | | | + |
| $^{149}$Sm | Stable | + | | | + |
| $^{150}$Sm | Stable | + | | | + |
| $^{151}$Sm | 90 | + | | | + |
| $^{152}$Sm | Stable | + | | | + |
| $^{151}$Eu | Stable | + | | | + |
| $^{153}$Eu | Stable | + | | | + |
| $^{154}$Eu | 8.59 | + | + | | + |
| $^{155}$Eu | 4.753 | + | | | + |
| $^{152}$Gd | $1.08 \cdot 10^{14}$ | | | | + |
| $^{154}$Gd | Stable | | | | + |
| $^{155}$Gd | Stable | + | | | + |
| $^{156}$Gd | Stable | | | | + |
| $^{157}$Gd | Stable | | | | + |
| $^{158}$Gd | Stable | | | | + |
| $^{160}$Gd | $1.3 \cdot 10^{17}$ | | | | + |
| $^{234}$U | $2.457 \cdot 10^{5}$ | + | | + | + |
| $^{235}$U | $7.038 \cdot 10^{8}$ | + | | + | + |
| $^{236}$U | $2.342 \cdot 10^{7}$ | + | | + | + |
| $^{238}$U | $4.468 \cdot 10^{9}$ | + | | + | + |
| $^{237}$Np | $2.14 \cdot 10^{6}$ | + | | + | + |
| $^{238}$Pu | 87.7 | + | + | + | + |
| $^{239}$Pu | $2.4114 \cdot 10^{4}$ | + | + | + | + |
| $^{240}$Pu | $6.563 \cdot 10^{3}$ | + | + | + | + |
| $^{241}$Pu | 14.33 | + | | + | + |
| $^{242}$Pu | $3.735 \cdot 10^{5}$ | + | | + | + |
| $^{241}$Am | 433 | + | + | + | + |
| $^{243}$Am | 7370 | + | | + | + |
| $^{242}$Cm | 162.8 days | | + | | + |
| $^{243}$Cm | 29.1 | + | | | + |
| $^{244}$Cm | 18.1 | | + | | + |
| $^{245}$Cm | $8.5 \cdot 10^{3}$ | + | | + | + |

### 1.4.5 Non-Destructive analysis

Non-destructive passive or active analysis methods can be used to determine SNF characteristics in a fast and accurate way using computational codes. Passive methods are based on spontaneous radiation emission from the fuel itself, whereas active methods rely on external radiation sources. Several non-destructive analysis devices based on the monitoring of gamma rays, neutron emissions or Cherenkov light exist. Non-destructive analysis methods can be used to determine the burn-up and other characteristics of SNF based on computer codes, such as ALEPH [39] which links the Monte Carlo code MCNPX [40] to the burn-up code ORIGEN 2.2 [41]. ALEPH was developed by Wim Haeck and Bernard Verboomen at SCK CEN. An

example of a passive method is the PYTHON$^{TM}$ device [42], developed as a collaboration between EDF (Electricité de France) and CEA (Commissariat à l'Energie Atomique et aux énergies alternatives), which is a combination of a total gamma measurement, a passive neutron measurement and an online depletion code resulting in an accurate burnup determination within ± 2 % at a 95 % confidence level (k=2) [42]. Other non-destructive analysis methods exist, such as self-indication neutron resonance densitometry (SINRD), which is based on neutron measurements having uncertainties as high as 25 %, and the partial defect tester (PDET), which is based on neutron and gamma-ray measurements to detect partial defects in the fuel assembly and can be used to derive a semi-quantitative estimation of the burn-up. A device combining active and passive methods is the NAJA device [43], which includes passive and active neutron measurements combined with an on-line depletion code and gamma-spectrometry. The NAJA device is able to automatically determine the nature of the fuel (fresh or irradiated, UOx or MOx), the presence and kind of neutron absorber, the initial enrichment in $^{235}$U for a fresh UOx assembly and make accurate burn-up determinations with expanded uncertainties of ± 2 % at a 95 % confidence level (k=2) [43]. Neutron resonance densitometry (NRD) is an experimental active non-destructive method relying on neutron time-of-flight techniques, aiming to quantify uranium and plutonium nuclides in SNF in less than 20 minutes with less than 1 % resulting uncertainty [44].

The accuracy of the results obtained using computer codes is important in establishing the safety basis in SNF management [45]. Despite being a fast way to determine SNF characteristics, the results obtained by computational codes in non-destructive analysis must be validated by destructively analysing SNF samples using radiochemical analysis methods (explained in section 1.4.6 of this chapter). Thus, the accuracy of the results obtained using computer codes is tested by comparing experimental results obtained from destructive chemical analyses on real SNF samples with the corresponding results of the computer codes.

### 1.4.6 Destructive analysis

Interest in code validation using destructive analysis methods was acted upon by EGBUC in 2006, after a workshop on "The need for post-irradiation experiments to validate fuel depletion calculation methodologies" (held in Rez, Czech republic on May 11$^{th}$-12$^{th}$, 2006), with the establishment of a new expert group on assay data for spent nuclear fuel (EGADSNF). This expert group coordinates assay data activities and facilitates cooperation between NEA member countries in developing and implementing burn-up credit methods, taking into consideration the high cost of initiating new experimental assay programs (fuel transportation, hot-cell facilities, radiochemical analysis capabilities and requirements for waste management) [45]. The results obtained using destructive and non-destructive analysis methods are compared to validate computational codes. In Europe, SNF assay measurement and burn-up determination are conducted in several radiochemical analysis laboratories, including the Belgian Nuclear Research Centre (SCK CEN) in Belgium, the CEA in France, the European Commission's Joint Research Centre (JRC) in Germany and the Paul Scherrer Institute (PSI) in Switzerland.

Destructive analysis remains the most reliable analytical approach to determine nuclide-specific concentrations in SNF and can only be performed at specialised laboratories with hot-cells and radiometric or mass spectrometric analysis equipment [45].

SNF assay can be carried out using hybrid K-edge densitometry (HKED) to determine the elemental concentrations of uranium and plutonium from 0.5 $mg \cdot L^{-1}$ to several hundreds of $g \cdot L^{-1}$ with uncertainties ranging from 2 to 10 % (k = 2) respectively. Figure 1.5 shows the HKED device used at CEA [46]. The HKED device uses results from two measurements performed simultaneously on the sample: K-edge transmission and X-Ray fluorescence [46].

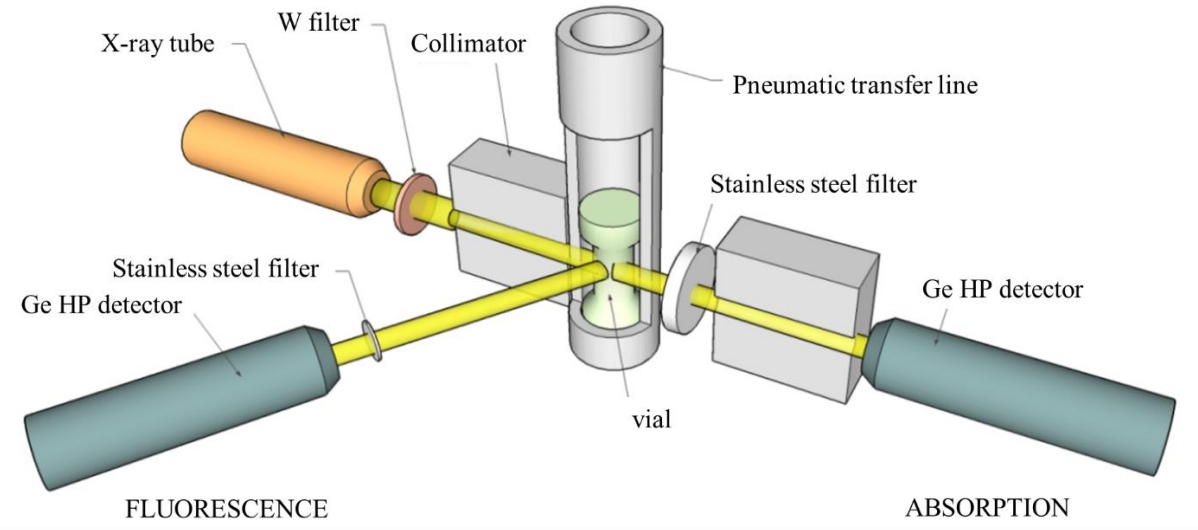


Figure 1.5 HKED device used at CEA [46]

The uranium elemental concentration in SNF can also be accurately determined using the titration method developed by Davies and Gray in 1964. No separation is required prior to the assay of uranium in SNF using the Davies and Gray titration unless interferences are present in milligram amounts or larger. First, uranyl in the sample is reduced to oxidation state IV by using excess Fe(II) in concentrated phosphoric-sulfamic acid, whilst the excess Fe(II) is oxidized selectively by nitric acid in the presence of Mo(VI) as a catalyst. Then, using potentiometric titration with vanadium as an electrochemical enhancer, U(IV) is titrated using a $K_2Cr_2O_7$ solution. The mass fraction of uranium ($C_U$) in the sample can then be determined by using eq. 1.3 [47], where $W$ is the atomic mass of uranium, $T$ is the titer of the titrating solution used (in $equivalent \cdot g^{-1}$), $m_c$ is the mass of the titrating solution used (in grams) to reach the endpoint and $m_a$ is the mass of the sample used (in grams).

$$C_U = WT\left(\frac{m_c}{2m_a}\right) \qquad \text{(eq. 1.3)}$$

The Davies and Gray titration is a fast, accurate and precise method to determine the uranium concentration with relatively little sample manipulation required. For SNF characterization, the titrator has to be installed inside a hot-cell.

The SNF burn-up is determined by using destructive analysis to measure the nuclide-specific concentration of a fission product monitor, usually $^{148}Nd$ [25], and those of the residual heavy

metal elements of the fuel: U and Pu [47-49]. Several destructive analysis methods are available, such as alpha spectrometry, liquid scintillation counting, gamma spectrometry, thermal ionization mass spectrometry (TIMS) and inductively coupled plasma-mass spectrometry (ICP-MS) [45]. SNF burn-up determination requires combining some of these radiometric and mass spectrometric methods.

For burn-up determination using destructive analysis, SNF sample preparation takes place inside a hot-cell where SNF pellets are dissolved, most commonly in 8 to 10 M nitric acid heated near its boiling point (86 °C) under reflux, to transfer uranium, the fission products, and most of the plutonium and the minor actinides into the solution. The nitric acid solution is then filtered and the residue is treated using a mixture of 8 M nitric acid and 0.1 M hydrofluoric acid to dissolve all the plutonium oxide. The filtered solution is then combined with the second solution before further gravimetric dilution in 1 M nitric acid to reduce the dose rate to a level permitted in laboratories, before removing it from the hot-cell. After dissolving the SNF sample and diluting the corresponding digest, chromatographic separation (off-line or on-line) is used to isolate the main fission products (neodymium, samarium, europium, gadolinium), uranium, plutonium and minor actinides into pure fractions prior to determining the nuclide-specific compositions and elemental concentrations of these elements by radiometric or mass spectrometric methods. Amongst the destructive analysis mass spectrometric methods, coupling on-line chromatography is only possible with ICP-MS. Such a hyphenated approach provides a rapid separation of the elements present in the SNF from one another, has a higher sample throughput, generates less radioactive waste and exposes the operator to less radiation compared to off-line chromatography.

#### 1.4.6.1. Radiometric methods

SNF contains various alpha-, beta- and gamma-emitting radionuclides that can be determined by using radiometric methods such as alpha spectrometry, gamma spectrometry and liquid scintillation counting. These radiometric methods require chromatographic separation of SNF elements into individual fractions to eliminate interfering radiation energies and to improve the limit of detection [45].

For measurement of short-lived alpha-emitting radionuclides in SNF, alpha spectrometry most commonly uses a passivated implanted planar silicon (PIPS) detector, which is placed inside a vacuum chamber, to absorb the high energy of an alpha particle (2-8 MeV) and convert it into an electronic signal (counts). PIPS detectors are usually calibrated for a range of 0 to 10 MeV by using standard alpha-emitting sources with known activities. Alpha spectrometry can be used to detect and quantify short-lived alpha-emitting radionuclides of uranium, plutonium, americium and curium in SNF with expanded relative uncertainties as low as 2 % in the best case at a 95 % confidence level (k = 2) [45]. However, alpha-spectrometry is incapable of separating the overlapping alpha-peaks of $^{239}$Pu (5105, 5144 and 5157 keV) and $^{240}$Pu (5124 and 5168 keV). Nevertheless, alpha spectrometry remains the method of choice to quantify shorter-lived radionuclides (e.g. $^{238}$Pu) when the plutonium is not completely separated from the highly concentrated uranium in SNF, which causes isobaric overlaps and hinders mass spectrometric analysis. Additionally, mass spectrometric methods, such as ICP-MS, can

encounter difficulties in the measurement of $^{238}$Pu if either the ICP-MS instrument has been used to measure high amounts of uranium causing a background signal and a higher detection limit at mass 238 [51] due to memory effects or if the reagents used during the sample preparation contain uranium [52].

Liquid scintillation counting (LSC) is a radiometric method that is used to measure beta-emitting radionuclides in SNF. In LSC, a fraction separated by chromatography is added to a scintillation cocktail that contains organic molecules which convert the kinetic energy of an alpha or a beta particle into light with a wavelength detectable with a photomultiplier tube. Most LSC systems are equipped with software to calculate the count rates measured. LSC can be used to determine the concentrations of the beta-emitting radionuclides $^{90}$Sr, $^{99}$Tc and $^{147}$Pm in SNF samples with a typical combined relative uncertainty of 2 % at a 95 % confidence level (k = 2) [45].

Finally, gamma spectrometry is used to measure gamma-emitting radionuclides either directly on a small aliquot (1-20 mL) of the SNF sample removed from the hot-cell (for fission products such as $^{137}$Cs, $^{144}$Ce, $^{154}$Eu and $^{155}$Eu, and minor actinides such as $^{241}$Am) or on separated fractions of the SNF sample (for $^{243}$Cm and $^{237}$Np) to eliminate gamma-emitters with overlapping gamma-rays. Detectors best suited for quantifying gamma-emitting radionuclides in SNF are high purity germanium detectors (HPGe), resulting in excellent peak resolution in SNF spectra. Detectors should be calibrated for energy, peak width and efficiency by using calibration sources with mixed radionuclide standards or a combination of standard sources [45]. The combined relative uncertainty of gamma-spectrometry measurements is usually higher than 3 % at a 95 % confidence level (k = 2) [45].

#### 1.4.6.2. Mass spectrometry methods

Mass spectrometric methods such as TIMS and ICP-MS can be used to determine the nuclide-specific composition and concentration of elements in SNF. To avoid isobaric overlaps, the elements present in SNF samples must be separated from one another by chromatography before they can be measured by TIMS or ICP-MS. Monoatomic isobaric interferences for plutonium, uranium, gadolinium and neodymium nuclides in SNF and the required mass resolutions (calculated according to the 10% valley definition [53]) needed to resolve them are presented in Table 1.7. According to the data in Table 1.7, a resolving power higher than that achievable by currently commercially available ICP-MS instruments (of both quadrupole and sector-field geometries) is needed to resolve the monoatomic isobaric interferences presented in Table 1.7. It is therefore required to chemically separate Pu, U, Nd and Gd using chromatography to eliminate the isobaric interferences which hinder their determination.

Table 1.7 Monoatomic isobaric interferences for Pu, U, Nd and Gd in SNF and the required mass resolutions (10% valley definition) to resolve them

| *m/z* | Element | Atomic weight ($g \cdot mol^{-1}$) | Required mass resolution (10% valley definition) |
|---|---|---|---|
| 142 | Nd | 141.9077289 | 93,300 |
| | Ce | 141.9092499 | |
| 144 | Nd | 143.9100929 | 40,424 |
| | Ce | 143.9136530 | |
| 144 | Nd | 143.9100929 | 75,209 |
| | Sm | 143.9120064 | |
| 148 | Sm | 147.9148290 | 71,454 |
| | Nd | 147.9168991 | |
| 150 | Sm | 149.9172822 | 41,423 |
| | Nd | 149.9209015 | |
| 152 | Sm | 151.9197390 | 2,540,465 |
| | Gd | 151.9197988 | |
| 154 | Gd | 153.9208734 | 114,628 |
| | Sm | 153.9222162 | |
| 154 | Gd | 153.9208734 | 72,860 |
| | Eu | 153.9229860 | |
| 155 | Gd | 154.9226298 | 573,152 |
| | Eu | 154.9229001 | |
| 238 | Pu | 238.0495583 | 193,742 |
| | U | 238.0507870 | |
| 241 | Am | 241.0568274 | 10,809,724 |
| | Pu | 241.0568497 | |
| 242 | Pu | 242.0587410 | 300,173 |
| | Am | 242.0595474 | |
| 244 | Cm | 244.0627507 | 167,892 |
| | Pu | 244.0642044 | |

When combined with isotope dilution, TIMS and ICP-MS can determine elemental concentrations in SNF with a combined relative uncertainty from 0.1 to 0.4 % at a 95 % confidence level (k = 2) [45]. ICP-MS is discussed in detail in chapter 3. Figure 1.6 shows a schematic representation of a nuclearized TIMS instrument.

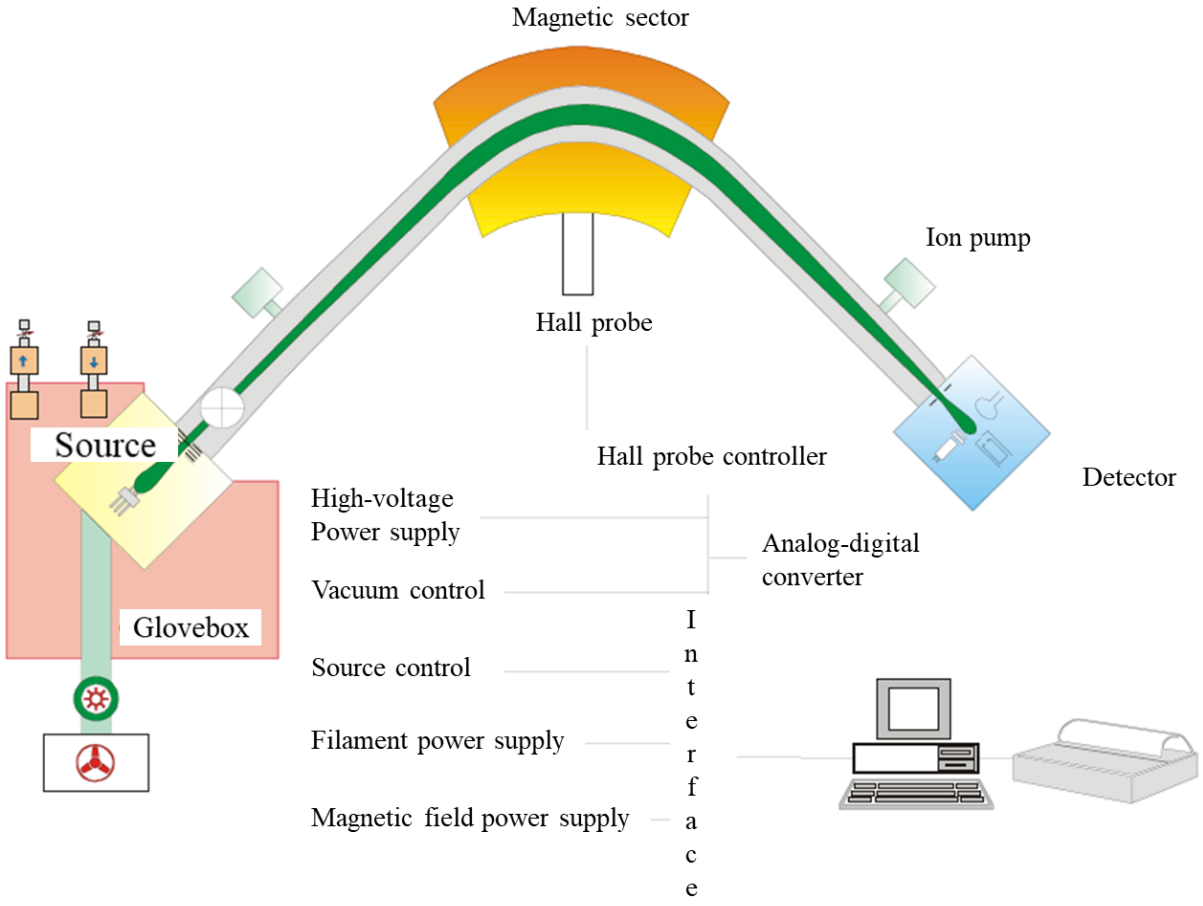


Figure 1.6 Schematic representation of a nuclearized TIMS instrument [54]

TIMS is a mono-elemental analysis technique in which a small amount (up to several micrograms) of the separated fractions of the SNF sample solution is deposited on a filament which is then placed inside the instrument's source housing. The source housing is then evacuated using a vacuum pump for several hours. Filaments are mostly made of rhenium because it has the highest work function of any metal (up to 5.8 eV) and a high enough melting point of about 2200 °C, which leads rhenium to provide the highest positive ion emission amongst metals [55]. The sample on the filament is heated by an electrical current passing through the filament, and positive ions are generated for elements with ionisation energies below 7.5 eV [55] (in comparison, ICP can ionize elements with much higher ionisation energies). The first ionisation energies of uranium, plutonium, neodymium and gadolinium are 6.05, 6.06, 5.48 and 6.15 eV, respectively, and therefore these elements can be ionized to singly-charged ions in either TIMS or ICP-MS. Ions are extracted (by a differential pump and/or extraction lens) and directed (by focusing lenses) towards the entrance of a magnetic sector field where they are separated based on their mass-to-charge ratio. The separated ions are then detected either sequentially (single collector) or simultaneously (multi-collector) setup. TIMS instruments were made commercially available at the end of the 1950s. Early TIMS instruments were single collector systems, which suffered from inaccuracy and imprecisions in isotope ratio (IR) measurements due to peak jumping (also referred to as dynamic scanning and involving altering the magnet settings to "jump" between the monitored masses in single-collector magnetic sector instruments.) that caused ion-beam fluctuations [56]. To overcome this issue,

multi-collector TIMS instruments were developed in the 1980s and 1990s by Finnigan MAT (Germany) and VG Isotopes (UK), and had as many as 9 Faraday cups. Nowadays, multi-collector TIMS instruments are equipped with both Faraday cups and ion counting detectors, such as Daly detectors or secondary electron multipliers (discussed in section 3.3.7 of chapter 3). TIMS analysis of SNF components is based on IR determination in conjunction with isotope dilution. Since the lighter nuclides evaporate more readily than the heavier nuclides, the initial ion beam composition becomes steadily more depleted of the lighter isotope, which results in a time-dependent mass bias (compared to a relatively stable mass bias over time in ICP-MS). Therefore, IRs determined by using TIMS must be corrected for mass fractionation using a reference IR of the same element (see section 3.2.3 in chapter 3), measured under the same conditions as the sample. The total evaporation method (also known as the flash evaporation method) is one way to overcome time-dependent mass fractionation in TIMS by measuring the ion signals of all isotopes of the element of interest until the entire deposited sample has been evaporated. When using the total evaporation method, calibration using isotopically certified reference materials to obtain absolute IRs is still necessary (see section 3.2.3 of chapter 3).

## 1.5 Aim and objectives

The aim of this PhD research project was to develop an accurate and precise methodology for the determination of the elemental mass fractions and nuclide-specific compositions of neodymium, gadolinium, plutonium and uranium in SNF using a sector field (SF) ICP-MS unit coupled with high pressure ion chromatography (HPIC). This project stems from SCK CEN's efforts to minimize the radiation risk to the operator and to increase sample throughput for SNF characterization, which is currently accomplished by separating SNF components using gravitational ion chromatography followed by their analyses using TIMS and alpha spectrometry (an ISO 17025 accredited method). The work was divided into four objectives: (1) developing and validating a separation method for the elements of interest using HPIC (discussed in chapter 4), (2) optimizing SF-ICP-MS parameters and finding a calculation method resulting in the best precision of IRs derived from transient signals (discussed in chapter 5), (3) characterizing SNF using isotope dilution HPIC-SF-ICP-MS (discussed in chapter 5) and (4) determining the overall uncertainty budget for isotope dilution HPIC-SF-ICP-MS and comparing it with those for isotope dilution TIMS and alpha-spectrometry (discussed in chapter 5).

## 1.6 References


[1] IAEA, “Storage of spent nuclear fuel SSG-15,” Vienna, 2012.

[2] World Nuclear Association, “Nuclear fuel and its fabrication,” 09 2020. [Online]. Available: https://www.world-nuclear.org/information-library/nuclear-fuel-cycle/conversion-enrichment-and-fabrication/fuel-fabrication.aspx. [Accessed 10 11 2020].

[3] IAEA, “Course on spent fuel storage,” IAEA, 2019.

[4] World Nuclear Association, “Nuclear power reactors,” World Nuclear Association, 10 2020. [Online]. Available: https://www.world-nuclear.org/information-library/nuclear-fuel-cycle/nuclear-power-reactors/nuclear-power-reactors.aspx. [Accessed 10 11 2020].

[5] R. Fullwood, Lecture notes for criticality safety, U. S. Department of Energy, 1992.

[6] World Nuclear Association, “Physics of uranium and nuclear energy,” 02 2018. [Online]. Available: https://www.world-nuclear.org/information-library/nuclear-fuel-cycle/introduction/physics-of-nuclear-energy.aspx. [Accessed 10 11 2020].

[7] IAEA, “Predisposal management of radioactive waste No. GSR Part 5,” Vienna, 2009.

[8] IAEA, “Disposal of radioactive waste No. SSR-5,” Vienna, 2011.

[9] IAEA, “Fundamental safety principles No. SF-1,” Vienna, 2016.

[10] IAEA, “Storage of radioactive waste No. WS-G-6.1,” Vienna, 2006.

[11] IAEA, “Borehole disposal facilities for radioactive waste No. SSG-1,” Vienna, 2009.

[12] IAEA, “Geological disposal facilities for radioactive waste No. SSG-14,” Vienna, 2011.

[13] IAEA, “Near surface disposal facilities for radioactive waste No. SSG-29,” Vienna, 2014.

[14] IAEA, “Classification of radioactive waste No. GSG-1,” Vienna, 2009.

[15] European Commission, “Radioactive waste and spent fuel,” European Commission, 09 2020. [Online]. Available: https://ec.europa.eu/energy/topics/nuclear-energy/radioactive-waste-and-spent-fuel_en. [Accessed 28 02 2021].

[16] NIRAS/ONDRAF, “Projet de stockage en surface à Dessel,” [Online]. Available: https://www.ondraf.be/projet-de-stockage-en-surface-dessel. [Accessed 04 11 2020].

[17] P. Marc, A. Magnaldo, A. Vaudano, T. Delahaye and E. Schaer, “Dissolution of uranium dioxide in nitric acid media: what do we know?,” EPJ N - Nuclear Sciences & Technologies, EDP Sciences, 3 (2017), pp.1-13, doi : 10.1051/epjn/2017005. cea-01516479

[18] Posiva press release, “Posiva is granted construction licence for final disposal facility of spent nuclear fuel,” 12 11 2015. [Online]. Available: http://www.posiva.fi/en/media/press_releases/posiva_is_granted_construction_licence_for_final_disposal_facility_of_spent_nuclear_fuel.3225.news. [Accessed 04 11 2020].

[19] IAEA, “Management of spent nuclear fuel from nuclear power reactors,” Vienna, 2020.

[20] J. Rein and B. Rider, “TID-17385, Burn-up determination of nuclear fuels,” Progress report, AEC research and development report, 1962.

[21] NEA, “Evaluation guide for the evaluated spent fuel assay database (SFCOMPO),” 2016.

[22] L. Van Brutzel, R. Dingreville and T. Bartel, “Nuclear fuel deformation phenomena,” NEA, 2015.

[23] B. Rider, C. Ruiz, J. Peterson and F. Smith, “Determination of Neodymium-148 in irradiated uranium and plutonium as a measure of burnup,” U. S. Atomic Energy Commission, 1967.

[24] CERCA, “Supply specification: Uranium high and low enriched category,” 278/1.

[25] ASTM, “Standard test method for atom percent fission in uranium and plutonium fuel (Neodymium-148 Method),” ASTM International, West Conshohocken, 2012.

[26] A. Koning, R. Forrest, M. Kellett, R. Mills, H. Henriksson and Y. Rugama, The JEFF-3.1 Nuclear Data Library, JEFF Report 21, OECD/NEA, Paris, France, 2006, ISBN 92-64-02314-3.

[27] G. You, C. Zhang and X. Pan, “Introduction of burn-up credit in nuclear criticality safety analysis,” *Procedia Engineering,* vol. 43, pp. 297-301, 2012.

[28] IAEA, “Characteristics and use of Urania-Gadolinia fuels,” IAEA, Vienna, 1995.

[29] World Nuclear Association, “The cosmic origins of uranium,” World Nuclear Association, 11 2016. [Online]. Available: https://www.world-nuclear.org/information-library/nuclear-fuel-cycle/uranium-resources/the-cosmic-origins-of-uranium.aspx. [Accessed 26 01 2021].

[30] T.-L. Ku, G. G. Mathieu and K. G. Knauss, “Uranium in open air ocean: concentration and isotopic composition,” *Deep Sea Research,* vol. 24, no. 11, pp. 1005-1017, 1977.

[31] United Nations, “Sources and effects of ionizing radiation Volume I : Sources,” in *United Nations Scientific Committee on the Effects of Atomic Radiation UNSCEAR 2000*, New York, 2000.

[32] S. Cotton, Lanthanide and actinide chemistry, Uppingham, Rutland: Wiley, 2006.

[33] Nucleonica, “Nuclide datasheets,” Nucleonica, 20 07 2020. [Online]. Available: https://www.nucleonica.com/Application/Datasheet.aspx. [Accessed 09 11 2020].

[34] J. R. De Laeter, J. K. Bohlke, P. De Bièvre, H. Hidaka, H. S. Peiser, K. J. R. Rosman and P. D. P. Taylor, "Atomic weights of the elements: Review 2000 (IUPAC technical report)," *Pure Applied Chemistry*, vol. 75, no. 6, pp. 683-800, 2003.

[35] J. J. Katz, G. T. Seaborg and L. R. Morss, The chemistry of the actinide elements, second edition, New York: Chapmann & Hall, 1986.

[36] K. L. Nash and J. C. Barley, Chemistry of radioactive materials in the nuclear fuel cycle, Woodhead publishing limited, 2011.

[37] I. Grenthe, X. Gaona, A. Plyasunov, L. Rao, W. H. Runde, B. Grambow, R. J. Konings, A. L. Smith and E. E. Moore, Second update on the chemical thermodynamics of uranium, neptunium, plutonium, americium and technetium NEA No. 7500, OECD, 2020.

[38] C. Ambard, "La spéciation du plutonium à l'état de traces par le couplage électrophorèse capillaire spectrométrie de masse à source plasma couplée par induction," Commissarisat de l'énergie atomique, 2007.

[39] W. Haeck and B. Verboomen, "ALEPH 1.1.2: A Monte Carlo burn-up code," SCK CEN-BLG-1003 Rev.0 open report, 2006.

[40] J. S. Hendricks, G. W. Mckinney, H. R. Trellue, J. W. Drukee, T. L. Roberts, H. W. Egdorf, J. P. Finch, M. L. Fensin, M. R. James, D. B. Pelowitz, L. S. Waters and F. X. Gallmeier, "MCNPX Version 2.6.A," Los Alamos National Laboratory Report: LA-UR-05-8225, 2005.

[41] A. G. Croff, "A user's manual for the ORIGEN2 computer code," Oak Ridge National Laboratory report ORNL/TM-7175, Oak Ridge, 1980.

[42] R. Berne, G. Bignan, G. Andrieu and D. Dethan, "A versatile passive and active non-destructive device for spent fuel assemblies monitoring," in *International conference on nuclear waste management and environmental remediation*, Prague, September 1993.

[43] G. Bignan and D. Janvier, "NAJA. A non-destructive automatic on line device for fuel assembly characterization and core load conformity control," in *ANS meeting "Advances in nuclear fuel management II"*, Myrtle Beach, March 1997.

[44] H. Harada, A. Kimura, F. Kitatani, M. Koizumi, H. Tsuchiya, B. Becker, S. Kopecky and P. Schillebeeckx, "Generalized analysis method for neutron resonance transmission analysis," *Journal of Nuclear Science and Technology,* vol. 52, no. 6, pp. 837-843, 2015.

[45] NEA, "Spent Nuclear Fuel Assay Data for Isotopic Validation," NEA, 2011.

[46] E. Esbelin, "Actinide L-line ED-XRF and Hybrid K-edge densitometer spectra processing," IAEA, 2014.

[47] L. M. Colletti, L. F. Walker and L. Tandon, "INFL guidelines on elemental assay," Los Alamos National Laboratory, 2013.

[48] F. Gueguen, H. Isnard, A. Nonell, L. Vio, T. Vercouter and F. Chartier, "Neodymium isotope ratio measurements by LC-MC-ICP-MS for nuclear applications: investigation of isotopic fractionation and mass bias correction," *J Anal At Spectrom*, vol. 30, no. 2, p. 443–452, 2015.

[49] K. Van Hoecke, J. Busse, M. Gysemans, L. Adriaensen, A. Dobney and T. Cardinaels, "Isolation of lanthanides from spent nuclear fuels by means of high performance ion chromatography (HPIC) prior to mass spectrometric analysis," *Journal of Radioanalytical and Nuclear Chemistry*, vol. 314, pp. 1727-1739, 2017.

[50] M. Moldovan, E. Krupp, A. Holliday and O. Donard, "High resolution sector field ICP-MS and multicollector ICP-MS as tools for trace metal speciation in environmental studies: a review," *Journal of Analytical Atomic Spectrometry*, vol. 19, pp. 815-822, 2004.

[51] H. Rameback, A. Tovedal, P. Lagerkvist, S. Jonsson and A. Vesterlund, "Alpha spectrometry and liquid scintillation counting for the measurement of Pu-238, Pu-239, Pu-240, Pu-241, Pu-242 and age," *Applied Radiation and Isotopes*, 2020.

[52] O. Donard, F. Bruneau, M. Moldovan, H. Garraud, V. Epov and D. Boust, "Multi-isotopic determination of plutonium (Pu-239, Pu-240, Pu-241 and Pu-242) in marine sediments using sector-field inductively coupled plasma mass spectrometry," *Analytica Chimica Acta*, vol. 587, pp. 170-179, 2007.

[53] K. K. Murray, R. K. Boyd, M. N. Eberlin, G. J. Langley, L. Li and Y. Naito, "Definitions of terms relating to mass spectrometry (IUPAC recommendations 2013)," *Pure Applied Chemistry*, vol. 85, no. 7, pp. 1515-1609, 2013.

[54] I. Gunther-Leopold, N. Kivel, J. Waldis and B. Wernli, "Characterization of nuclear fuels by ICP mass-spectrometric techniques," *Analytical and Bioanalytical Chemistry*, vol. 390, pp. 503-510, 2008.

[55] D. Smith, "Thermal ionization mass spectrometry," in *Inorganic mass spectrometry*, New York, Marcel Dekker, 2000, pp. 1-30.

[56] S. Burger, J. Vogl, U. Kloetzli, L. Nunes and M. Lavelle, "Thermal ionisation mass spectrometry," in *Sector field mass spectrometry for elemental and isotopic analysis*, The Royal Society of Chemistry, 2015, pp. 381-438.

# Chapter 2 – Ion chromatography

## 2.1 Introduction and overview

Since the separation method developed during this work is based on high-pressure ion chromatography (HPIC), this chapter is devoted to the principles of ion chromatography and to components of HPIC systems, and also contains an overview of the use of HPIC in nuclear applications.

Chromatography is defined by IUPAC as "a physical method of separation in which the components to be separated are distributed between two phases, one of which is stationary (stationary phase) while the other (mobile phase) moves in a definite direction" [1]. The stationary phase is usually packed inside a column. The components of the mixture are separated based on differences in their affinities towards the mobile and stationary phases as they move through the column. The Russian botanist Mikhail Semenovich Tswett is considered the father of chromatography with his work on using adsorption chromatography to separate plant pigments from one another [2-3]. In 1906, Tswett coined the term "chromatography", which originates from old Greek and means to write with colours, in his publications on chlorophyll in the German Botanical Journal [4-5]. The term "ion chromatography" (IC) refers to the chromatographic separation of anions and cations based on processes, such as ion exchange, ion pairing, ion exclusion, chelation, etc. [6-7]. Ion exchange chromatography (IEC) is the most widely used form of IC for the separation of metal ions and complexed transition metals [6]. In IEC, ions of the eluent and those from the sample compete for the oppositely charged sites on the stationary phase. When the stationary phase is negatively charged, it is used for cation exchange chromatography, and when it is positively charged, it is used for anion exchange chromatography. In 1975, Small, Stevens and Bauman laid the foundations of modern IEC with their work on the simultaneous separation of anionic and cationic species using IEC [9-11]. The term "ion chromatography" was introduced when the Dionex corporation (now part of Thermo Fisher Scientific) licensed their method for commercial development [7, 10].

Throughout the years, HPIC has proven to be a fast, robust, sensitive and selective method for the analysis of solutions. The identification of analytes in solution, as well as the determination of the different concentrations at which they are present, has been a major asset of HPIC thanks to the variety of detector types with which it can be coupled; these detector types include UV-Vis detectors, fluorescence detectors, conductivity detectors, potentiometric detectors and others. Furthermore, HPIC can be coupled on-line with techniques also providing information on the nuclide-specific composition of the analyte elements, such as inductively coupled-plasma mass spectrometry (ICP-MS).

## 2.2 Ion exchange chromatography theory

The basic principle of IEC, whether for anions or cations, is based on differences in the relative affinities of ions in the sample and the eluent for the stationary phase, thus leading to different ion-exchange equilibria. These differences in ion-exchange equilibria translate into the different ions spending different amounts of time bound to the stationary phase (also known as retention

time) or dissolved in the eluent prior to elution from the column. However, when the difference in ion-exchange equilibria is small, which is the case for the trivalent lanthanides for example, it is more effective to separate the sample ions from one another by using an eluent containing a ligand that complexes with the different ions to differing extents [11]. In this kind of separation, known as chelation IEC, there are two relevant equilibria (eq. 2.1 & 2.2) involving the ions in the sample ($M^{n+}$), stationary phase ($S^-$) and eluent ($E^-$):

$$M^{n+} + nS^-H^+ \rightleftharpoons S_nM + nH^+ \quad \text{(eq. 2.1)}$$

$$S_nM + nE^- \rightleftharpoons nS^- + ME_n \quad \text{(eq. 2.2)}$$

Here, the retention time is also affected by the type and concentration of eluent ions $E^-$, as well as the pH of the eluent.

### 2.2.1 Common terms in chromatography

A solution component eluting from the chromatographic column is characterized by the time it was retained on the column, commonly expressed as a retention time ($t_R$). The retention time of a component is measured at the maximum height of the component's chromatographic peak (see Figure 2.1). Additionally, the difference between the retention time of an unretained component ($t_M$) and that of the component of interest ($t_R$) is called the adjusted retention time ($t'_R$) (see Figure 2.1).

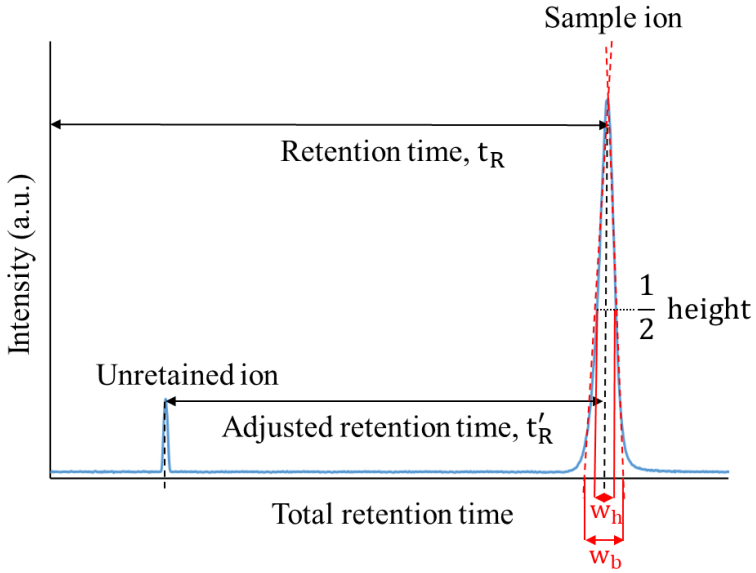


Figure 2.1 Schematic representation of a chromatographic peak and its attributes

The following terms are most commonly used for expressing the efficiency of the separation of components using chromatography. Based on IUPAC 2017 recommendations [12], two adjacent peaks are considered separated from one another at a peak resolution ($R_s$) of unity. The peak resolution can be calculated as shown in eq. 2.3 for two adjacent peaks eluting at retention

times $t_{R1}$ and $t_{R2}$, with $t_{R2}>t_{R1}$ and the second peak having a width at base ($w_b$) expressed in time units:

$$R_s = \frac{t_{R2}-t_{R1}}{w_b} \quad \text{(eq. 2.3)}$$

Alternatively, the peak resolution ($R_s$) can be calculated by Purnell's equation (eq. 2.4) using the number of plates ($N$), separation factor ($\alpha$) and the mean retention factor ($\bar{k}$).

$$R_s = \frac{\sqrt{N}}{4}\left(\frac{\alpha-1}{\alpha}\right)\left(\frac{\bar{k}}{\bar{k}+1}\right) \quad \text{(eq. 2.4)}$$

A second indicator for providing information on the separation of two adjacent peaks is the separation factor ($\alpha$), expressed as a number larger than one. The larger the separation factor, the more the maxima of two adjacent chromatographic peaks are separated. The separation factor can be calculated using eq. 2.4:

$$\alpha = \frac{t'_{R2}}{t'_{R1}} \quad \text{(eq. 2.5)}$$

where $t'_{R1}$ and $t'_{R2}$ are the adjusted retention times of two adjacent peaks appearing at retention times $t_{R2}$ and $t_{R1}$, with $t_{R2}>t_{R1}$.

Additionally, the retention factor ($k$) is used to determine the time a sample component resides in the stationary phase relative to the time it resides in the mobile phase and expresses "how much a sample component is retarded by the stationary phase" [12]. This retention factor ($k$) is the ratio of the adjusted retention time of the sample component ($t'_R$) and the retention time of an unretained component ($t_M$) (eq. 2.5).

$$k = \frac{t'_R}{t_M} \quad \text{(eq. 2.6)}$$

A common term used as an indication of the column efficiency, which influences the shape (width) of the peaks, is the number of theoretical plates ($N$). It is calculated based on the ratio of the retention time and the peak width (see Figure 2.1) at base ($w_b$) or at half height ($w_h$) (depending on how symmetric the peak shape is) as in eq. 2.6 which follows:

$$N = 16\left(\frac{t_R}{w_b}\right)^2 = 5.545\left(\frac{t_R}{w_h}\right)^2 \quad \text{(eq. 2.7)}$$

The higher the theoretical plate number, the higher the efficiency of the column. Therefore, an efficient column will result in narrow peaks. Under isocratic conditions, the effective number of plates (N*eff*) is used instead of $N$, and is calculated by replacing $t_R$ by $t'_R$ in eq. 2.7.

Finally, the resolution is affected by the height equivalent to a theoretical plate (*HETP*), which is the ratio of the column length and $N$ and is shown in eq. 2.7:

$$HETP = \frac{L}{N} \quad \text{(eq. 2.8)}$$

To obtain a better resolution under isocratic conditions, the HETP should be decreased [13].

## 2.3 Components of HPIC systems

Every HPIC system consists of the following key hardware components: (i) eluents, which make up the mobile phase, are placed in suitable reservoirs equipped with a degasser to eliminate air bubbles, (ii) a pump system with an optional gradient facility, (iii) a sample injection unit to introduce a known amount of sample onto the column for analysis, (iv) analytical column(s) for the separation of analyte ions from one another and a guard column to prevent contaminants damaging the analytical column and (v) a detector to quantify the separated sample ions, which is linked to a data processor that generates a digital record of the chromatograph on a computer screen. Each of these components are discussed into more detail in the following sub-sections. Polyether ether ketone (PEEK) is chosen for HPIC components (pumps, column heads, etc.) due to its ability to withstand high fluid pressures and its inert nature preventing any corrosion. Finally, all the components have to work together, therefore their characteristics must be compatible, for example the eluent should be suitable for the detector chosen, the elution conditions (flow rate, concentration, pH, etc.) should be appropriate for the column and detector, and rapid exchange of analytes between the phases must be prevalent.

### 2.3.1 Eluents

Eluents constitute the mobile phase in the chromatographic system and are prepared by dissolving acids or bases (buffers) in an aqueous solution. Eluents are stored in appropriately sized reservoirs, which for safety are placed in a leak tray. Prior to the introduction of eluents into the chromatographic system, the eluent should be filtered and degassed. It is advisable to use end-line nylon filters (0.2 or 0.45 µm) in each eluent take-up line to prevent the introduction of solid particles that could damage the pump(s) and column(s). To prevent the introduction of air bubbles into the HPIC system, the latter is equipped with a vacuum degassing module providing continuous online degassing of the eluent(s) prior to their introduction into the pump(s). Air bubbles cause random variations in the flow rate, damage the column stationary phase and lead to high noise in the signal if they reach the detector.

Several characteristics of the eluent affect the retention of the analytes of interest. Firstly, the ionic strength of the eluent is determined by the concentration of the buffer ions. The higher the ionic strength of the eluent, the faster the elution of the analyte ions from the stationary phase due to stronger ion pairing with the eluent ions [11]. Secondly, the pH of the eluent will determine the degree of dissociation [14], the net charge of the eluent ions in the mobile phase [11] and the form of the ion-exchange functional groups in the stationary phase. The charge of solute ions which are weak acids or bases (including carboxylate anions, fluoride, cyanide and most amines) will also depend on the pH of the eluent [15]. Thirdly, the eluent flow rate is inversely proportional to the retention time. However, increasing the flowrate is limited by the column's maximum operating pressure. Fourthly, the addition of organic solvent(s) to the eluent is suitable for the analysis of organic analyte ions, but does not affect the elution of inorganic analyte ions [14].

### 2.3.2 Pump system

The primary objective of the pump system is to force liquids through the chromatographic system in a stable, controllable and pressurized manner, whether that be introducing eluents onto the column (done by the analytical pump) or pumping liquids to be admixed with the column effluent prior to the detection stage (done by the post-column pump). The HPIC pump system can employ either a single pump (SP) or a binary pump (BP). The cost of pumps limit the maximum number of pumps supplied in commercially available HPIC systems to two. A SP system can deliver only one eluent at a time, whereas a BP system can mix two different eluents in any proportion and can also change that mixture over time. Changing the mixture of eluents over time is referred to as a gradient elution, as opposed to an isocratic elution. Alternatively, even more flexibility is obtained, at a lower cost, when a low-pressure quaternary gradient unit is installed prior to a pump, as indicated in Figure 2.2. Using a quaternary gradient unit permits mixing of up to four different solutions at pre-set proportions with respect to time by using a proportioning valve installed before the pump head. Each pump can consist of a single head or a dual head, and a pump system can be customized to have both types of pumps (single and dual headed). Pumps with a dual head, however, offer better accuracy in terms of flow rate delivery, and were therefore chosen for this work. The eluent passes successively through both pump heads, as shown in Figure 2.2. For eluent intake by the primary pump head, the piston is withdrawn from the pump head and the resulting suction closes the outlet check valve and opens the inlet check valve. Then, for eluent delivery from the primary pump head to the secondary pump head, the piston is inserted into the primary pump head, whereby the resulting pressure opens the outlet check valve and closes the inlet check valve. Meanwhile in the secondary pump head, the piston is retracted resulting in the eluent filling the secondary pump head. The secondary pump head releases eluent on the delivery stroke of its pump head. The two pump heads of the same pump operate anti-phase with each other, meaning that the delivery stroke of the secondary pump head is accompanied by a simultaneous refill stroke on the primary pump head. The secondary pump head is equipped with a pressure transducer to measure the pressure of the system. The pump motor speed is controlled by the instrument firmware installed on the computer connected to the HPIC system to ensure a constant flow rate versus the pressure.

The piston seal wash system consists of a peristaltic pump that rinses the main piston seals with deionized filtered water to prevent eluent crystallization on the piston surfaces.

In the gradient pump, a static mixer is placed after the secondary pump head to ensure that the eluents are mixed thoroughly. The static mixer is mandatory for the pump delivering the eluents to the column and optional for the post-column pump (if available).

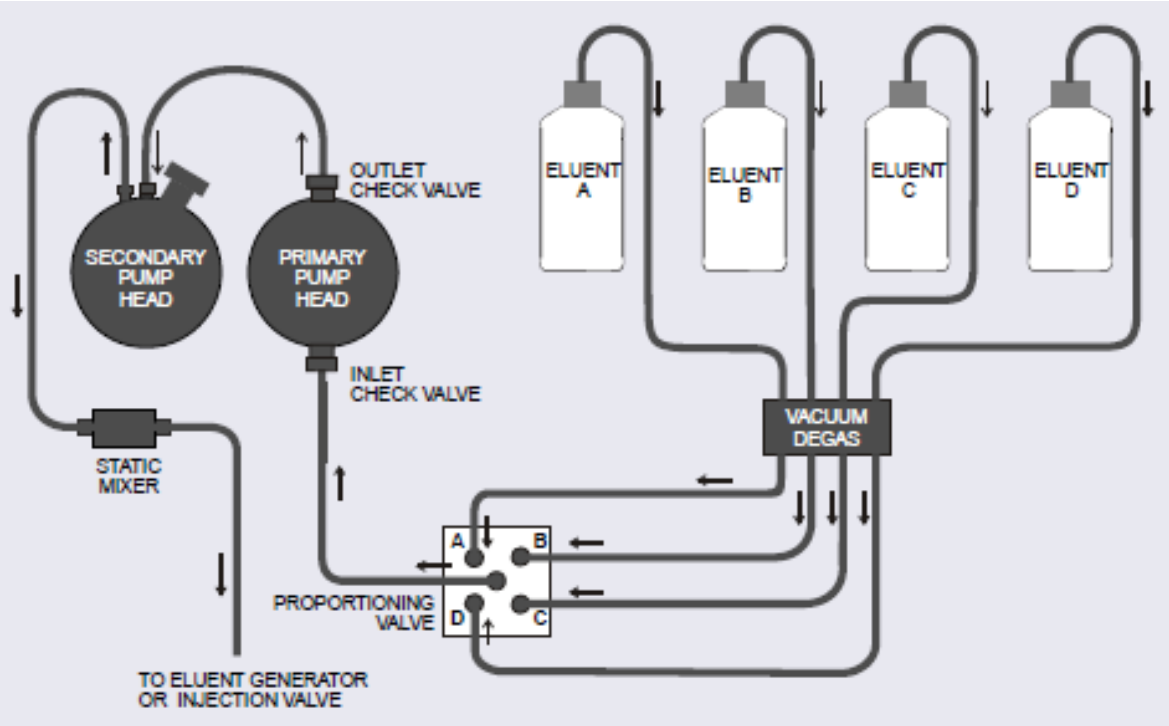


Figure 2.2 Schematic representation of a dual pump head with a quaternary low-pressure gradient unit [16]

### 2.3.3 Sample injection unit

The injection of the sample onto the column can be performed manually, using manual injection valves, or automatically, using automated valves, depending on the sample nature and the set-up requirements. Automated valves are more precise, safer and simpler to use than manual ones. The operating principle of any type of valve equipped with a sample loop (with a defined volume) is to fill the loop in the LOAD position and to flush the loop's content onto the column in the INJECT position. An example of a 6-port 2-way valve is presented in Figure 2.3.

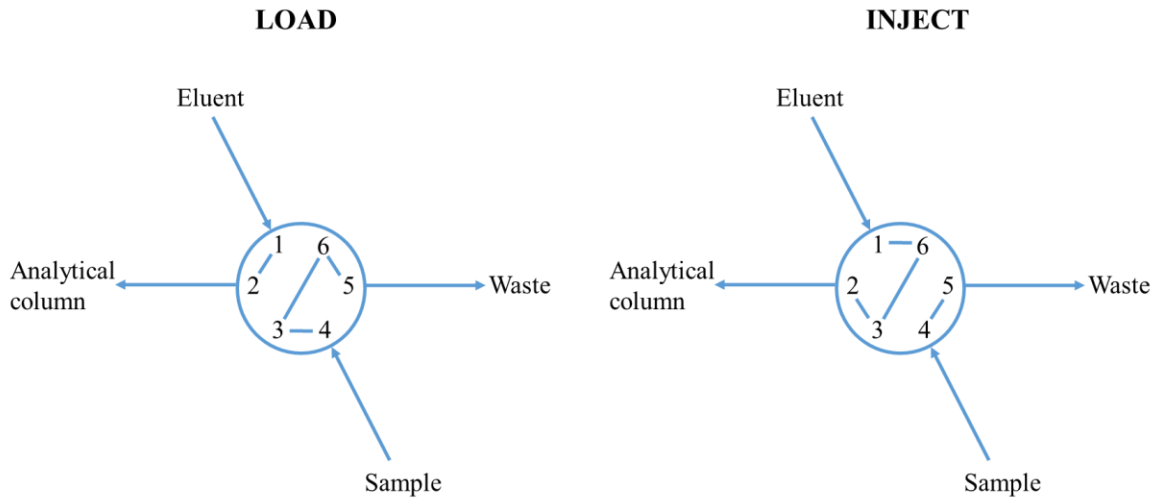


Figure 2.3 Positions of a 6-port 2-way valve equipped with a sample loop between ports 3 and 6

### 2.3.4 Stationary phases and columns

The stationary phase (or resin) in ion chromatography carries functional groups with a fixed charge. Respective counter-ions are located in the vicinity of the functional groups, resulting in electrical neutrality of the stationary phase [14]. The two main types of stationary phases are cationic exchangers for the separation of cations (or cationic complexes), and anionic exchangers for the separation of anions (or anionic complexes). Two types of cationic exchange resins exist, strong acid and weak acid cationic exchange resins. The main differences between these two types of cationic exchange resins are their cation exchange capabilities and the pH range over which they function. Strong acid cationic exchange resins function over the entire pH range [17]. Weak acid cation exchangers, however, are only effective above a pH of 4 and have a limited cation exchange capability. Strong acid cationic exchange resins are made by sulfonating latex particles and thus contain sulfonate functional groups ($–RSO_3^-$, pKa = -3) bound to the resin [11, 14]. The hydrogen counter-ion in these columns can be exchanged for another cation from the sample or the mobile phase. Examples of strong cationic exchange columns include IonPac CS10 or CS3 (Dionex), Luna SCX (Phenomenex) and Nucleosil SA (Macherey-Nagel). In contrast, weak acid cation exchangers consist of polymer-coated silica particles functionalized with carboxyl ($–RCO_2^-$, pKa < 3) groups (such as IonPac CS12, Dionex) or carboxyl and phosphonate ($–RPO_3H^–$, pKa = 1.1 – 2.3, or $–RPO_3^{2–}$, pKa = 5.3 – 7.2) groups (such as IonPac CS12A or CS15, Dionex) [11, 14]. One characteristic of weak acid cationic exchange resins is the dependence of the carboxyl group dissociation, and hence the ion-exchange capacity, on the pH of the sample [14].

Much like cationic exchange resins, strong base and weak base anionic exchange resins exist. Anionic exchange resins are formed in two steps, the first of which is the chloromethylation of a benzene ring in the styrene-divinylbenzene copolymer, followed by the reaction of the subsequent intermediate with an amine [11, 17]. Strong base anionic exchangers contain a quaternary ammonium functional group ($–NR_3^+$) bound to the resin's surface, and can function over the entire pH range. In contrast, weak base anionic exchangers are obtained by the reaction of a primary or secondary amine or ammonia with the chloromethylated copolymer and can only be used with solutions below a pH of 7 when the functional group is protonated [17]. Examples of anion exchange columns include PRP-X100 (Hamilton), LCA A01 (SYKAM), ExcelPak ICS-A23 (Yokogawa), in addition to more than 30 different anion exchange columns from IonPac AS1 to AS32 developed by Dionex.

Mixed-bed ion exchanger columns, containing both types of functional groups, are also available and can act as both anion and cation exchangers. Examples of mixed-bed columns include IONPAC CS5 and CS5A.

In addition to the functional groups present, columns can be defined according to their ion-exchange capacity, which is the number of ion-exchange sites per weight equivalent of the column resin and is commonly expressed as milliequivalent per gram resin ($mequiv.g^{-1}$) [11, 14]. Ion-exchange capacity is proportional to the size and amount of latex beads. The column capacity, usually specified by the manufacturer, indicates the maximum amount of analyte that can be injected onto the column. It is not unusual for the column capacity to deteriorate the more the column is used. This can be due to column aging or irreversible adsorption of ions

from the mobile phase onto the resin. Additionally, the column efficiency is an important indicator of its performance and is discussed in more detail in section 2.1 of this chapter.

Another important column feature is the resin's selectivity, defined as the strength at which sample ions pair with functional groups on the resin [18], and which can be used to estimate the elution order of ions from the column. The different factors affecting selectivity have been discussed widely in the literature and can be grouped into (1) sample ion properties and (2) resin properties [6, 11, 14, 19]. Moreover, the addition of non-ionic eluent modifiers (such as acetonitrile, methanol and others) to the mobile phase affects the selectivity by influencing the solvation of stationary phase functional groups and solute ions, by changing the ion-exchange affinity of hydrophobic ions, or by changing the $pK_a$ of those solutes which are weak acids or bases [15].

Finally, to prevent contaminants from reaching the column and thus, to prolong the life of the column, a guard column is usually placed before the separation column and is commonly a shorter column packed with the same stationary phase as the separation/analytical column [11, 19].

### 2.3.5 Detectors

The detector is responsible for turning a chemical attribute into a signal corresponding to the concentration or amount of sample ions eluting from the column. The choice of detector depends on the type of application. Several different types of detector can be used in ion chromatography, and these can be classified into two main categories: electrochemical and spectrometric detectors. Electrochemical detectors include conductivity [20-22], potentiometric [23-25] and amperometric detectors [26-28], while spectrometric detectors, are based on absorption of ultraviolet-visible electromagnetic radiation (UV-Vis) [29-30] or fluorescence detectors [11, 14]. Detailed information on electrochemical and fluorescence detectors can be found in the cited literature. Additionally, also other types of detectors can be coupled to HPIC, and these include atomic spectrometric techniques such as atomic emission spectrometry, atomic absorption spectrometry and inductively coupled plasma-mass spectrometry (ICP-MS). Since UV-Vis and ICP-MS were used in this work, they will be discussed separately below and in chapter 3, respectively.

#### 2.3.5.1 UV-Vis detectors

The operating principle of a UV-Vis spectrophotometer is rather simple. The solution entering the flow cell in the detector is irradiated with light of a specified wavelength and intensity ($I_0$). Then, the detector measures the intensity of the light exiting the solution ($I$). Based on the Beer-Lambert law, the absorbance ($A$), molar absorptivity ($\varepsilon$) and the optical path length of the flow cell ($L$) are used to determine the concentration of the solute ($c$) using the following equation (eq. 2.9):

$$A = log_{10}\left(\frac{I_0}{I}\right) = \varepsilon \cdot c \cdot L \qquad \text{(eq. 2.9)}$$

Different types of UV-Vis detectors for HPIC exist, of which two commonly used types are shown in Figure 2.4: variable wavelength detectors (VWD) and diode array detectors (DAD),

also known as photodiode array detectors (PAD). The main difference between these two types of detector is that with VWD, at any given time only one specific wavelength is monitored using a single photodiode detector, whereas with DAD, the full spectrum of light from the lamp passes through the sample in the flow cell and is detected simultaneously on a diode array detector.

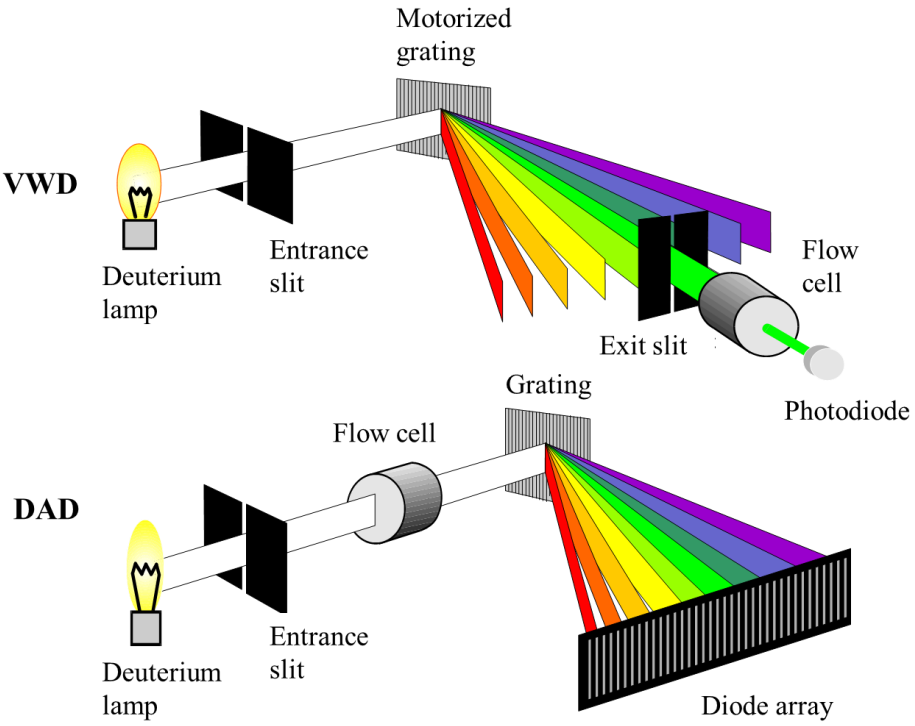


Figure 2.4 Simplified schematic representation of VWD and DAD components [31]

Additionally, there are two possible ways to detect species using a UV-Vis detector. If the species can absorb light in the UV-Vis region of the electromagnetic spectrum, then it can be detected by using direct detection, otherwise, it can be complexed with a colouring agent which absorbs light, using post-column derivatization. The UV range (from 100 to 400 nm) is most commonly used in direct detection, the UV radiation being generated by a Deuterium lamp, while the visible wavelength range (from 400 to 700 nm) is often used with post-column derivatization [11] where the light is provided by a Tungsten halogen lamp. Two of the most common colouring agents are 4-(2-pyridylazo)resorcinol (PAR), which has a red colour, and arsenazo III [Bis-(2-arsono-benzeneazo)-2,7-chromotropic acid], whose colour depends on the pH of the solution (with increasing pH, the colour of arsenazo III changes from reddish-purple to deep blue [32]). PAR forms chelate complexes with 34 metals [11] (including Cd, Co, Cu, Fe, Mn, Ni, Pb, Zn and the lanthanides) and absorbs between 520 and 535 nm. Arsenazo III is also mainly used for the detection of the lanthanides and actinides using UV-Vis spectroscopy and absorbs around 653 nm. Lower detection limits are obtained for the lanthanides when arsenazo III is used instead of PAR, which could be due to the different complexation behaviour of the two colouring agents with the lanthanides (as shown in Figure 2.5). Figure 2.5 shows the molecular structures of PAR and arsenazo III in their respective free and complexed forms.

| Colour agent | Free structure | Complexed structure |
|---|---|---|
| PAR | 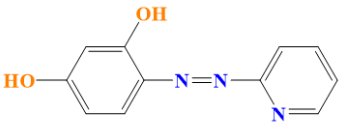 | 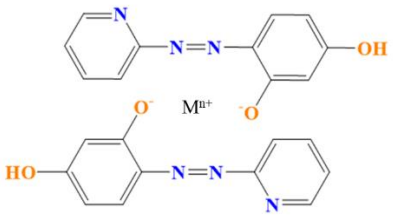 |
| Arsenazo III | 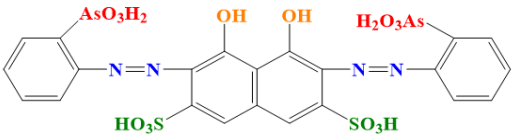 | 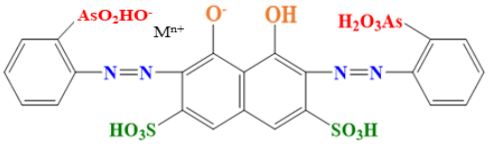 |

Figure 2.5 Structures of PAR and arsenazo III free and complexed with cation $M^{n+}$

The stoichiometry of metal-ligand complexes has been reported mainly as 1:2 for lanthanide-PAR [33] and 1:1 for complexes of arsenazo III with lanthanides and divalent cations (such as uranyl) [34]. Nonetheless, this complexation behaviour is pH and concentration dependent. PAR has three dissociation constants ($pKa_1$ ~ 3, $pKa_2$ ~ 5.5 and $pKa_3$ ~ 12) and therefore can exist in solution as either one of four differently protonated species: $H_3PAR^+$, $H_2PAR$, $HPAR^-$ or $PAR^{2-}$ (structures of PAR species can be found in Figure 2.6.), depending on the pH of the solution (Figure 2.6) [35-36]. Whereas arsenazo III is an octahydroxy weak acid ($RH_8$) with eight dissociation constants ($pKa_1$ < 1.3, $pKa_2$ < 1.3, $pKa_3$ = 2.6, $pKa_4$ = 4.3, $pKa_5$ = 6.7, $pKa_6$ = 8.8, $pKa_7$ = 10.6, $pKa_8$ = 11) [32] and can exist in solution as different protonated species shown in Figure 2.7 depending on the pH of the solution. The effect of the pH change in solution on the absorbance and stability of the 1:1 lanthanide-arsenazo III complexes has been previously reported by Rohwer et al. [37]. Moreover, when the lanthanides are in excess, they can form 1:1 complexes with PAR [35] with formation constants reported to increase from $10^{8.9}$ to $10^{10.7}$ going from La to Lu [38]. For 1:2 lanthanide-PAR complexes, formation constants have been reported to be in the range of $10^{9.2}$ to $10^{10.4}$ [39] and a molar absorptivity of 6.54 x $10^4$ $M^{-1}\cdot cm^{-1}$ has been reported for $Gd(PAR)_2$ complexes [33]. Whereas, under optimum pH conditions, formation constants of 1:1 lanthanide-arsenazo III complexes have been reported to be around $10^{1.3}$ to $10^{1.4}$ and molar absorptivity values vary between 8.16 x $10^4$ $M^{-1}\cdot cm^{-1}$ and 8.78 x $10^4$ $M^{-1}\cdot cm^{-1}$ have been reported when going across the lanthanide series from Ce to Dy [37].

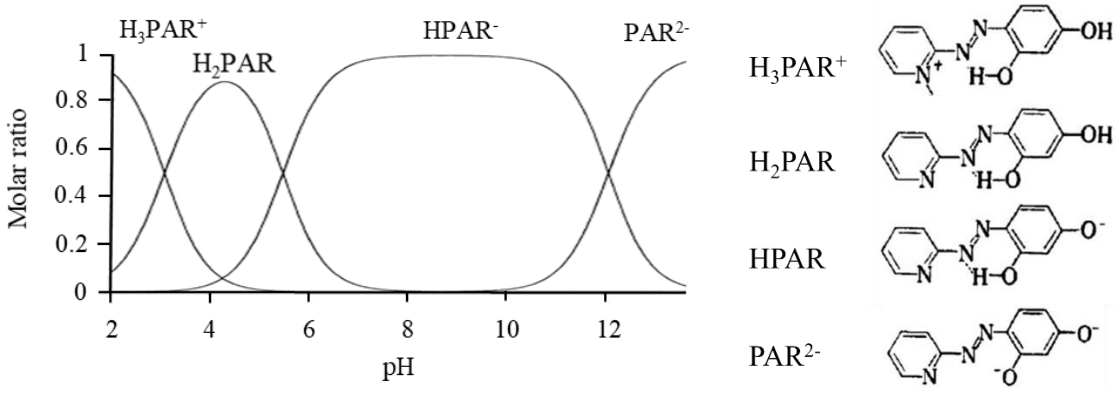


Figure 2.6 Distribution diagram of PAR species as a function of pH (left) [36] and structure of PAR species (right) [35]

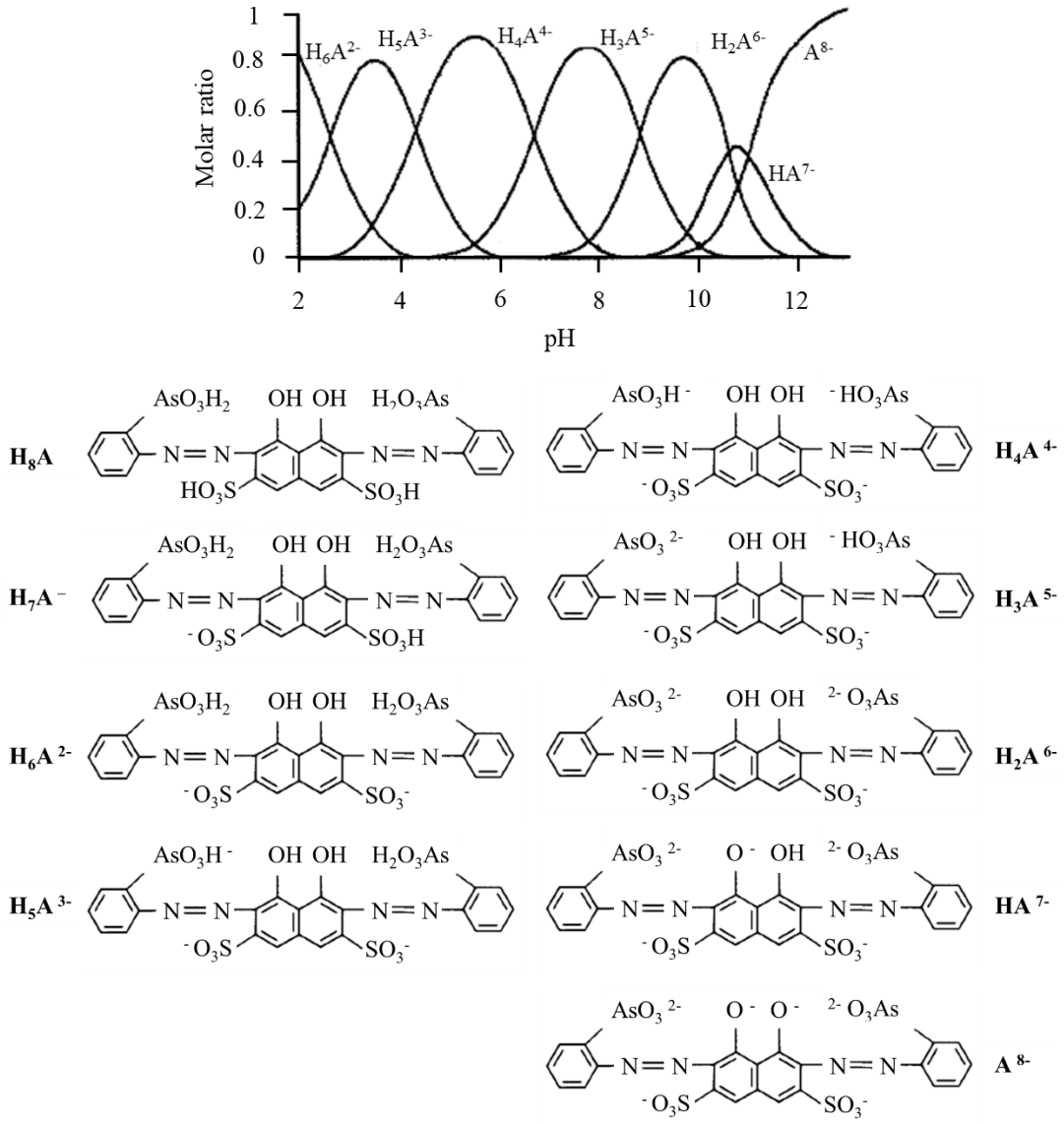


Figure 2.7 Distribution diagram of Arsenazo III species as a function of pH (2-13) [32] and structure of all Arsenazo III species (pH 0-13) [32]

## 2.4 Nuclear applications with HPIC

In the context of this PhD, HPIC was used in the characterization of nuclear samples. Table 2.1 gives an overview of literature employing HPIC for the separation of components in spent nuclear fuel (SNF). Overall, three categories of columns have been used for the separation of components in SNF, namely mixed-bed ion exchange columns, cation exchange columns, and reversed phase monolithic columns that were modified dynamically into cation exchange columns. Mixed-bed ion exchange columns can be used with oxalic acid to elute the lanthanides in the order of decreasing ionic radius (La to Lu) as negatively charged oxalate complexes, or with alpha-hydroxyisobutyric acid (α-HIBA) to elute the lanthanides in the opposite order as neutral species. The elution of Pu from mixed-bed ion exchange columns can be achieved by using either nitric acid or oxalic acid. Prior to its injection onto the column, an oxidizing agent is used to convert all Pu species in solution to one oxidation state. When nitric acid is used to elute Pu, the latter needs to be converted to Pu(VI) prior to its injection onto the column.

However, Pu(IV) is the preferred valency state when oxalic acid is used to elute Pu from a mixed-bed ion exchange column, since it is more stable than Pu(VI) at a pH of 4.8. Finally, U can be eluted either before or after the other SNF components, by using nitric acid or hydrochloric acid. However, since U is the major component of SNF, its elution prior to the other components is preferred to prevent its co-elution with other SNF components. Further information about spent nuclear fuel can be found in chapters 3-5.

### 2.4.1 Nuclearized HPIC-SF-ICP-MS setup

The HPIC system used in this work is flexible, in that it comprises various components including (i) a dual quaternary gradient pump system DP5000$^{+}$ (Thermo Fisher Scientific), (ii) mixed-bed ion exchange guard and separation columns (IonPac CG5A & CS5A, Dionex), (iii) an autosampler to perform the injections automatically, (iv) three automated stand-alone 6-port 2-way valves whose position and connections can be rearranged if desired, (v) a UV-Vis VWD detector making it possible to measure highly concentrated samples (mg·L$^{-1}$) and (vi) a nuclearized "*Element 2*" (Thermo Fisher Scientific) sector field (SF) ICP-MS instrument for the precise and accurate determination of the separated sample ions. Except the pump system and eluent bottles, all components of this setup were placed inside an alpha-glovebox since these come in contact with radioactive sample solutions. A schematic representation of the setup can be found in Chapter 4.

The chosen pump system permitted the use of up to four solutions with each pump which offers flexibility for separation method development. The analytical pump pumps the mobile phase into the columns and the post-column pump takes up the post-column reagent (used for UV-Vis detection) or internal standard solution (used for SF-ICP-MS analysis) to be admixed on-line with the column effluent in a T-piece before entering the chosen detector. The low pressure gradient of quaternary gradient pumps brings about inferior mixing and hence stability compared to binary pumps. Nevertheless, the price of a quaternary gradient pump is lower compared to a binary pump. Although a HPIC system consisting of two quaternary pumps was used in this work, one of the two quaternary pumps (the one pumping the internal standard or the post-column reagent) can be replaced by a binary pump since only 2 solutions were used with this particular pump (the internal standard or post-column reagent solution and water for rinsing the tubes). The flow rate used in both pumps was 0.125 mL·min$^{-1}$.

The mixed-bed ion exchange CS5A column has a hydrophobic microporous 55 % cross-linked divinylbenzene resin core (with a particle diameter of 9 µm) that has been agglomerated with two layers of permeable latex particles (the manufacturing process of CS5A is shown in Figure 2.8), which carry the actual cation and anion exchange functional groups. One layer is a fully sulfonated latex layer for cation-exchange. The other layer is a fully aminated latex layer for anion-exchange. This characteristic of mixed bed ion exchange columns offers the flexibility needed during separation method development in terms of the eluent to be chosen for complexing with the analytes of interest. Therefore, the CG5A guard column and CS5A analytical column were chosen for this work as mixed bed ion exchange columns for their ability to separate transition and lanthanide metals. These columns are supplied in one length (250 mm for CS5A and 50 mm for CG5A) and two different internal diameters (2 and 4 mm for each of CS5A and CG5A). An increase in the internal diameter of a column is also

associated with an increase in the flow rate used. This correlation is shown in eq. 2.10 which is used to calculate the new volumetric flowrate ($F_2$) needed to keep the linear flow rate constant when changing the internal diameter of a column from $D_1$ to $D_2$. $F_1$ *is* the old volumetric flowrate. Therefore, the smaller internal diameter of 2 mm was chosen for this setup to better match the uptake rate of the nebulizer of the SF-ICP-MS.

$$F_2 = \frac{(D_1)^2}{(D_2)^2} \cdot F_1 \qquad \text{(eq. 2.10)}$$

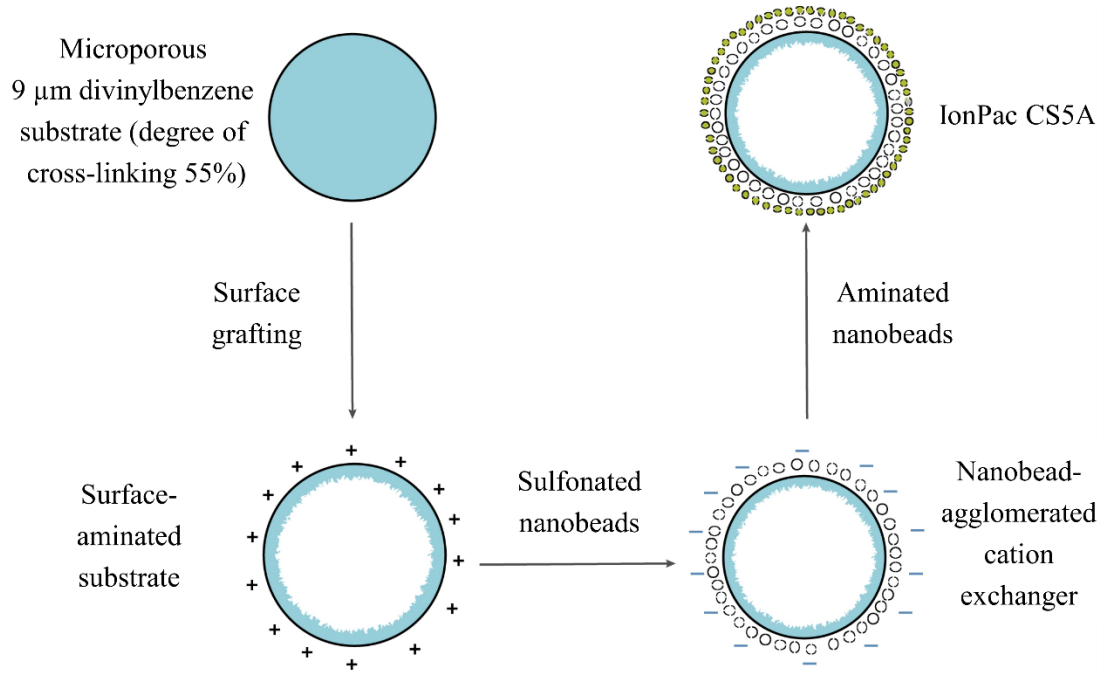


Figure 2.8 Schematic representation of the steps in the manufacturing process of CS5A column [14]

The use of columns with smaller particle sizes, as is the case in ultra-high pressure liquid chromatography (UHPLC), was not considered for this work. This would shorten the separation method and result in narrower chromatographic peaks, but would create an additional challenge to collect sufficient spectrometric data within the short elution time of the chromatographic peak. Poorer peak definition is expected to lead to poorer accuracy and precision of isotope ratios. In addition, further speeding up of the chromatographic method would not offer any substantial practical benefit due to the very low number of SNF samples that actually need to be measured on any given day and in view of the time consuming sampling, licensing and actual transport of samples and sample preparation in a nuclear hot cell, which all together can take weeks or months to achieve.

The positions of the three valves could either be changed manually or programmed into the method setup, using the Chromeleon 7.2 software (Thermo Fisher Scientific). The first valve was equipped with a sample loop and was used to inject automatically and accurately 25 µL of

the sample solution onto the columns. This automation was also useful in reducing the radiation exposure of the analyst.

A UV-Vis detector had also been installed in the glovebox as an alternative detection technique to SF-ICP-MS. The choice of two detection techniques offers flexibility when developing a chromatographic separation. For example, using the UV-Vis detector during the chromatographic method development can avoid unnecessary introduction of high concentrations of organic acids into the SF-ICP-MS unit and thus prevents clogging the orifices of the nebuliser and/or sampler and skimmer cones with salt deposits.

After being admixed on-line with the corresponding post-column reagent, the column effluent entered the second valve which directed the flow to either the UV-Vis detector or to the third valve. During the analysis of SNF samples, the second valve was connected to a fraction collecting system instead of to the UV-Vis detector, to collect the eluting U fractions for off-line analysis. The command for the second valve to change positions and direct the flow of column effluent to the fraction collection system for a specified time interval was included in the method setup in Chromeleon 7.2 software. The collected U fractions were admixed with the internal standard, thus causing a dilution by a factor of two, which was useful in preventing high concentrations of U from being introduced into the SF-ICP-MS instrument.

Finally, if the column effluent reaches the third valve, it can either be introduced into the nebulizer of the SF-ICP-MS unit or directed to waste (in the case of highly concentrated rinsing solutions, or time regions of the chromatogram that are not needed for the analysis). In this way, the risk of irreversible contamination of the SF-ICP-MS unit with highly concentrated matrices is reduced.

## 2.5 Conclusion

Overall, the basic components of a HPIC set-up consist of eluent(s), a pump(s) system, an injector, column(s) and a detector. The characteristics of different components of an HPIC set-up depend on the type of analysis of interest. Additionally, it is essential to configure the HPIC set-up in a coherent and fit-for-purpose manner. The set-up used in this work offered the possibility to determine analytes by using either UV-Vis or SF-ICP-MS detection. Since the concept of UV-Vis detection in HPIC was discussed in this chapter, the next chapter will be dedicated to ICP-MS and specifically SF-ICP-MS.

Table 2.1 Overview of HPIC methods applied for characterization of SNF

| Column name | Column type | Column dimensions (id x length in mm) | Column capacity ($\mu eq.col^{-1}$) | Injection volume (µL) | Analytes (in elution order) | Eluent(s) | Flow rate ($mL.min^{-1}$) | Total elution time (min) | Oxidizing agent | Detector | Reference(s) |
|---|---|---|---|---|---|---|---|---|---|---|---|
| IonPac CG5 + CS5 | Mixed bed IEC | 4 x 250 | $-SO_3^-$: 30+150<br>$-NR_3^+$: 14+70 | 200 | Lanthanides (La, Ce, Pr, Nd, Pm, Sm, Eu & Gd) | 0.1 M oxalic acid-0.19 M lithium hydroxide | - | 25 | - | ELAN 5000 quadrupole ICP-MS | [40-41] |
| IonPac CG10 + CS10 | Cation exchange | 4 x 250 | $-SO_3^-$: 80 | 200 | Actinides: Np, Pu, U, Am & Cm<br>Fission products: Rb, Cs, Sr & Y | 1 M nitric acid | - | - | Silver(II) to oxidize Pu to Pu(VI) in 5 min | ELAN 5000 quadrupole ICP-MS | [40-42] |
| IonPac CG5 + CS5 | Mixed bed IEC | 4 x 250 | $-SO_3^-$: 30+150<br>$-NR_3^+$: 14+70 | 1000 | Lanthanides (Lu to La)<br>Pu<br>U | 0.04-0.26 M α-HIBA 0.4 M nitric acid - 1 M HCl | 1 | 35 & 7 | 250 µL of 6 M perchloric acid to oxidize Pu to Pu(VI) | $PQ2^+$ quadrupole ICP-MS | [43] |
| IonPac CG5A + CS5A | Mixed bed IEC | 2 x 250 | $-SO_3^-$: 1+5<br>$-NR_3^+$: 2+10 | 25 | Pu<br>U | 0.4 M nitric acid - 1 M HCl | 0.25 | 10 | Perchloric acid to oxidize Pu to Pu(VI) | Neptune MC-ICP-MS | [44] |
| IonPac CG5A + CS5A | Mixed bed IEC | - | - | 250 | Actinides (Np, Pu, Am & Cm) and lanthanides (La, Ce, Pr, Nd, Pm, Sm, Eu & Gd) + U | 0.1 M oxalic acid-0.19 M lithium hydroxide + 2 M HCl | 1 | 32 | 0.2 M sodium nitrite to oxidize Pu to Pu(IV) in 10 min | ELAN 5000 quadrupole ICP-MS | [45] |
| Reversed phase monolith + camphor-10-sulfonic acid (CSA) | Cation exchange | 4.6 x 100 | - | - | Pu+U, lanthanides (Sm, Nd, Pr, Ce, La)<br>Pu, U | 0.02 M CSA - 0.1 M α-HIBA (pH 3.1 with $NH_3$)<br>0.1 M α-HIBA (pH 3.75) | 2 | 35 & 8 | Sodium nitrite to oxidize Pu to Pu(IV) | UV-Vis at 655 nm with $10^{-4}$ M Arsenazo III | [46] |

| | | | | | | | | | | | |
|---|---|---|---|---|---|---|---|---|---|---|---|
| LUNA SCX | Cation exchange | 4.6 x 250 | - | | Lanthanides (Gd, Eu, Sm, Nd, Pr, Ce, La) | 0.1 M α-HIBA pH 3.6 – 0.2 M α-HIBA pH 4.5 | 1 | 32 | - | Neptune Plus MC-ICP-MS | [47] |
| Shodex IC R-621 | Cation exchange | 6 x 50 | | 50 | Lanthanides (Dy, Gd, Eu, Sm, Nd, Pr, Ce, Lu) | 0.1 M α-HIBA (pH 4.6 with $NH_4OH$), 0.5 & 1.0 M α-HIBA (pH 4.5 with $NH_4OH$) | 0.5 | 90 | - | UV-Vis at 655 nm with $2.10^{-4}$ M Arsenazo III in 1 M acetic acid | [48] |
| IonPac CG10 + CS10 | Cation exchange | 4 x 250 | $-SO_3^-$: 80 | 50 | U – Lanthanides, Pu, U & Am | 1 M HCl - 0.04 – 0.26 M α-HIBA (pH 4.5 with $NH_4OH$), 0.4 M $HNO_3$ – 1 M HCl – 0.26 M α-HIBA (pH 4.5 with $NH_4OH$), | 1 | 30 | $10^{-3}$ M potassium permanganate in 1 M nitric acid to oxidize Pu to Pu(VI) overnight | UV-Vis at 650 nm with $3.10^{-4}$ M Arsenazo III, $PQ2^+$ quadrupole ICP-MS | [49] |
| Reversed phase monolith + n-octane sulfonic acid | Cation exchange | 4.6 x 250 | - | 100 | Lanthanides, Pu & U | 0.05 – 0.15 M α-HIBA pH6.5 + 0.15 – 0.3 M α-HIBA pH 3.5, 0.1 M hydroxylamine hydrochloride in 5 M HCl & 0.5 M $HNO_3$ | 1 | 50 | 30 % $H_2O_2$ + 3 M $HNO_3$ to oxidize Pu to Pu(IV) | UV-Vis at 653 nm with $1.5.10^{-4}$ M Arsenazo III + 0.01 M urea in 0.1 M $HNO_3$ | [50] |
| IonPac CG5A + CS5A | Mixed bed IEC | 2 x 250 | $-SO_3^-$: 1+5 $-NR_3^+$: 2+10 | 250 | Lanthanides | 0.04 – 0.26 M α-HIBA (pH 4.5 with $NH_4OH$) | 0.3 | 47 | - | Quadrupole ICP-MS | [51] |
| IonPac CG5A + CS5A | Mixed bed IEC | 4 x 250 | $-SO_3^-$: 4+20 $-NR_3^+$: 8+40 | 50 | Fission products (Cs, Sr, Y, La, Ce, Pr, Nd, Pm, Sm) | 6mM PDCA (with 90 mM acetic acid, buffered to pH 4.8 with $NH_4OH$); 150 mM oxalic acid (buffered to pH 4.8 with $NH_4OH$); and 100 mM DGA (buffered to pH 4.8 with $NH_4OH$) | 1 | 52 | - | Quadrupole ICP-MS | [52] |

## 2.6 References


[1] L. Ettre, "Nomenclature for chromatography (IUPAC recommendations 1993)," *Pure & applied chemistry,* vol. 65, no. 4, pp. 819-872, 1993.

[2] L. S. Ettre, Chapters in the evolution of chromatography, Imperial College Press, 2008.

[3] A. Rodrigues, C. Pereira, L. Pais, A. Ribeiro, A. Ribeiro, M. Silva, N. Graca and J. Santos, "Chapter 1 - Principles of simulated moving bed," in *Simulated moving bed technology: Principles, design and process applications*, Elsevier, 2015.

[4] M. Tswett, "Adsorption analysis and chromatographic method. Application to the chemistry of chlorophyll," *Ber. Dtsch. Bot. Ges.,* vol. 24, pp. 384-392, 1906a.

[5] M. Tswett, "Physical-chemical studies of chlorophyll Adsorption," *Ber. Dtsch. Bot. Ges.*, vol. 24, pp. 316-326, 1906b.

[6] J. Lemmon, "Ion chromatography," *Encylopaedia of Materials: Science and Technology*, pp. 4280-4284, 2001.

[7] P. R. Haddad and P. E. Jackson, Ion chromatography - principles and applications, Elsevier Science, 2003.

[8] W. Rieman and H. Walton, Ion Exchange in Analytical Chemistry, Pergamon Press, 1970.

[9] H. Small, T. Stevens and W. Bauman, *Analytical Chemistry,* vol. 47, p. 1801, 1975.

[10] R. E. Smith, Ion chromatography applications, CRC Press, 1990.

[11] J. S. Fritz and D. T. Gjerde, Ion chromatography, Wiley VCH, 2009.

[12] T. A. Maryutina, E. Y. Savonina, P. S. Fedotov, R. M. Smith, H. Siren and D. B. Hibbert, "Terminology of separation methods (IUPAC Recommendations 2017)," *Pure Applied Chemistry,* vol. 90, no. 1, pp. 181-231, 2018.

[13] E. Stauffer, J. A. Dolan and R. Newman, "Chapter 8 - Gas chromatography and gas chromatography - Mass spectrometry," in *Fire Debris Analysis*, ACADEMIC PRESS, 2008, pp. 235-293.

[14] J. Weiss, Handbook of ion chromatography, Wiley VCH.

[15] C. A. Pohl, J. R. Stillian and P. E. Jackson, "Factors controlling ion-exchange selectivity in suppressed ion chromatography," *Journal of Chromatography A,* vol. 789, pp. 29-41, 1997.

[16] *Dionex ICS-5000+ chromatography system operator's manual,* Thermo Fisher Scientific, 2012.

[17] F. J. Dechow, "Chapter 16: Chromatography," in *Fermentation and Biochemical Engineering Handbook,* Elsevier, 2014, pp. 319-359.

[18] J. S. Fritz, "Factors affecting selectivity in ion chromatography," *Journal of Chromatography A,* vol. 1085, pp. 8-17, 2005.

[19] SeQuant, A practical guide to ion chromatography, ISBN 978-91-631-8056-9 ed., Umea: SeQuant, 2007.

[20] J. Ouyang, J. L. Duan, W. R. Baeyens and J. R. Delanghe, "A simple method for the study of salbutamol pharmacokinetics by ion chromatography with direct conductivity detection," *Talanta,* vol. 65, pp. 1-6, 2005.

[21] C. Guan, J. Ouyang, Q. Li, B. Liu and W. R. Baeyens, "Simultaneous determination of catecholamines by ion chromatography with direct conductivity detection," *Talanta,* vol. 50, pp. 1197-1203, 2000.

[22] S. D. Kumar, V. Tripathi, N. Shenoy and B. Maiti, "Chloride analysis in magnesium metal using ion chromatography with conductometric detection," *Journal of Chromatography A,* vol. 1046, pp. 155-158, 2004.

[23] P. R. Haddad and P. W. Alexander, "Ion chromatography of Mg, Ca, Sr and Ba ions using a metallic copper electrode as a potentiometric detector," *Journal of Chromatography,* vol. 294, pp. 397-402, 1984.

[24] S. Egashira, "Potentiometric detector with a glass electrode for the ion-exchange chromatography of carboxylic acids," *Journal of Chromatography,* vol. 202, pp. 37-43, 1980.

[25] S. H. Han, K. S. Lee, G. S. Cha, D. Liu and M. Trojanowicz, "Potentiometric detection in ion chromatography using multi-ionophore membrane electrodes," *Journal of Chromatography,* vol. 648, pp. 283-288, 1993.

[26] Q. Xu, C. Xu, Q. Wang, K. Tanaka, H. Toada, W. Zhang and L. Jin, "Application of a single electrode, modified with polydiphenylamine and dodecyl sulfate, for the simultaneous amperometric determination of electro-inactive anions and cations in ion chromatography," *Journal of Chromatography A,* vol. 997, pp. 65-71, 2003.

[27] T. T. Christison and J. S. Rohrer, "Direct determination of free cyanide in drinking water by ion chromatography with pulsed amperometric detection," *Journal of Chromatography A,* vol. 1155, pp. 31-39, 2007.

[28] B. M. De Borba and J. S. Rohrer, "Determination of biogenic amines in alcoholic beverages by ion chromatography with suppressed conductivity detection and integrated pulsed amperometric detection," *Journal of Chromatography A,* vol. 1155, pp. 22-30, 2007.

[29] M. Frankowski and A. Ziola-Frankowska, "Speciation analysis of aluminium and aluminium fluoride complexes by HPIC-UVVIS," *Talanta,* vol. 82, pp. 1763-1769, 2010.

[30] R. J. Williams, "Determination of inorganic anions by ion chromatography with ultraviolet absorbance detection," *Analytical Chemistry,* vol. 55, pp. 851-854, 1983.

[31] M. Dong and J. Wysocki, “Ultraviolet detectors: perspectives, principles and practices,” *LCGC North America,* vol. 37, no. 10, pp. 750-759, 2019.

[32] I. Nemcova and B. Metal, “Dissociation constants of Arsenazo III,” *Talanta,* vol. 33, no. 10, pp. 841-842, 1986.

[33] S. Steinberg, V. Hodge and L. Becerra-Hernandez, “Investigation of the interaction of Gadolinium with several organic ligands and humic acid by ligand competition using 4-(2-pyridylazo)-resorcinol (PAR),” *Environments,* vol. 7, no. 69, 2020.

[34] S. B. Savvin, Arsenazo III: Methods of photometric determination of actinide elements, Moscow: Atomizdat, 1966.

[35] T. Iwamoto, “Acid-Base Property and Metal Chelate Formation of 4-(2-Pyridylazo)-resorcinol,” *Bulletin of the Chemical Society of Japan,* vol. 34, no. 5, 1961.

[36] J. Ghasemi, A. Niazi, M. Kubista and A. Elbergali, “Spectrophotometric determination of acidity constants of 4-(2-pyridylazo)resorcinol in binary methanol–water mixtures,” *Analytica Chimica Acta,* vol. 455, pp. 335-342, 2002.

[37] H. Rohwer and E. Hosten, “pH dependence of the reactions of arsenazo III with the lanthanides,” *Analytica Chimica Acta,* vol. 339, pp. 271-277, 1997.

[38] E. Ohyoshi, “Spectrophotometric determination of formation constants of 1:1 complexes of lanthanides with 4-(2-pyridylazo)resorcinol (PAR),” *Talanta,* vol. 31, no. 12, pp. 1129-1132, 1984.

[39] K. N. Munshi and A. K. Dey, “Determination of lanthanides using 4-(2-pyridylazo)-resorcinol,” *Michrochimica Acta,* vol. 59, pp. 751-756, 1971.

[40] J. Barrero-Moreno, J. Garcia Alonso, P. Arbore, G. Nicolaou and L. Koch, “Characterization of spent nuclear fuels by ion chromatography-inductively coupled plasma mass spectrometry,” *J Anal Atom Spectrom,* vol. 11, pp. 929-936, 1996.

[41] M. Betti, “Use of ion chromatography for the determination of fission products and actinides in nuclear applications,” *Journal of chromatography A,* vol. 789, pp. 369-379, 1997.

[42] J. Barrero Moreno, M. Betti and J. Garcia Alonso, “Determination of neptunium and plutonium in the presence of high concentrations of uranium by ion chromatography-inductively coupled plasma mass spectrometry,” *Journal of Analytical Atomic spectrometry,* vol. 12, pp. 355-361, 1997.

[43] I. Gunther-Leopold, F. Gabler, B. Wernli and Z. Kopajtic, “Characterization of spent nuclear fuels by an on-line coupled HPLC-ICP-MS system,” Paul Scherrer Institute Scientific Report, Switzerland, 2000.

[44] I. Gunther-Leopold, J. Waldis, B. Wernli and Z. Kopajtic, “Measurement of Plutonium isotope ratios in nuclear fuel samples by HPLC-MC-ICP-MS,” *International Journal of Mass Spectrometry,* vol. 242, pp. 197-202, 2005.

[45] L. Perna, F. Bocci, L. Aldave de las Heras, J. De Pablo and M. Betti, “Studies on simultaneous separation and determination of lanthanides and actinides by ion chromatography inductively coupled plasma mass spectrometry combined with isotope dilution mass spectrometry,” *Journal of Analytical Atomic Spectrometry,* vol. 17, pp. 1166-1171, 2002.

[46] S. Bera, R. Balasubramanian, Arpita Datta, R. Sajimol, S. Nalini, T. S. Lakshmi Narasimhan, M. P. Antony, N. Sivaraman, K. Nagarajan and P. R. Vasudeva Rao, “Burn-Up Measurements on Dissolver Solution of Mixed Oxide Fuel Using HPLC-Mass Spectrometric Method,” *International Journal of Analytical Mass Spectrometry and Chromatography,* vol. 1, pp. 55-60, 2013.

[47] F. Gueguen, H. Isnard, A. Nonell, L. Vio, T. Vercouter and F. Chartier, “Neodymium isotope ratio measurements by LC-MC-ICPMS for nuclear applications: investigation of isotopic fractionation and mass bias correction,” *Journal of Analytical Atomic Spectrometry,* vol. 30, pp. 443-452, 2015.

[48] K. Van Hoecke, J. Busse, M. Gysemans, L. Adriaensen, A. Dobney and T. Cardinaels, “Isolation of lanthanides from spent nuclear fuels by means of high pressure ion chromatography (HPIC) prior to mass spectrometric analysis,” *Journal of Radioanalytical and Nuclear Chemistry,* vol. 314, pp. 1727-1739, 2017.

[49] S. Röllin, Z. Kopatjtic, B. Wernli and B. Magyar, “Determination of Lanthanides and Actinides in Uranium Materials by High Performance Liquid Chromatography with Inductively Coupled Plasma Mass Spectrometric Detection,” *Journal of Chromatography,* vol. 739, pp. 139-149, 1996.

[50] P. Kumar, P. Jaison, V. Telmore, P. Sumana and S. Aggarwal, “Determination of lanthanides, Thorium, Uranium and Plutonium in irradiated (Th, PU)O2 by liquid chromatography using α-Hydroxyiso Butyric Acid (α-HIBA),” *International Journal of Analytical Mass Spectrometry and Chromatography,* vol. 01, pp. 72-80, 2013.

[51] S. F. Wolf, D. L. Bowers and J. C. Cunnane, “Analysis of high burnup spent nuclear fuel by ICP-MS,” *Journal of Radioanalytical and Nuclear Chemistry,* vol. 263, pp. 581-586, 2005.

[52] B. D. Roach, E. K. Fenske, D. C. Glasgow, J. D. Partridge, T. J. Keever and J. M. Glaquinto, “Rapid concentration and isotopic measurements of ultra-trace $^{235}$U fission products with comparison to an ORIGEN isotope depletion model,” *Talanta,* vol. 205, 120079, 2019.

# Chapter 3 – Inductively coupled plasma-mass spectrometry

## 3.1 Introduction and overview

In this PhD, high-pressure ion chromatography (HPIC) was coupled to a single-collector double-focusing sector field (SF) inductively coupled plasma-mass spectrometry (ICP-MS) instrument to perform nuclide-specific analyses. Since chapter 2 was devoted to HPIC, this chapter focuses on the basic principles and major components of ICP-MS and its application in the nuclear field. ICP-MS is an important analysis technique permitting the determination of nearly all elements of the periodic table along with their nuclide-specific composition. In comparison with other mass spectrometric techniques, such as thermal ionization mass spectrometry (TIMS), glow discharge mass spectrometry (GDMS) or secondary ion mass spectrometry (SIMS), ICP-MS can be used to analyse aqueous solutions easily and rapidly [1].

Common types of mass separators used in ICP-MS include the magnetic field, quadrupole filter and time-of-flight analyser. SF-ICP-MS instruments, as the name implies, are based on a magnetic sector field as the mass separator, and can be of the either single (magnetic field only) or double (with an electrostatic field in addition) focusing type. Two types of SF-ICP-MS instruments exist, based on the number of detectors: (1) single-collector instruments and (2) multi-collector instruments. Single-collector instruments, are equipped with one detector that detects ions with different mass-to-charge (*m/z*) ratios sequentially, and are operated under dynamic (scanning or peak hopping/jumping) conditions. In contrast, multi-collector instruments are equipped with several parallel detectors that can detect ions at different *m/z* ratios simultaneously, and are usually operated under static conditions (fixed magnetic field and acceleration voltage). Single-collector ICP-MS instruments are used for the accurate determination of elements at trace to ultra-trace concentrations, and their characteristic flat-top peaks (at low mass resolution) are valuable for precise IR measurements (RSD ≥ 0.05 %) and thus isotope dilution mass spectrometry (IDMS), which is the reason it was selected for this work. The first SF-ICP-MS instrument, "*Plasmatrace*", was produced in 1988 by VG Elemental. However, the complexity of operation and the high purchase price of the first SF-ICP-MS instruments limited the adoption of this type of instrument, especially with the existence of the much less expensive quadrupole-based ICP-MS instruments.

It was not long after the first commercial availability of ICP-MS instruments that their coupling to speciation techniques became of interest. For example, the coupling of HPIC to a quadrupole ICP-MS was published as long ago as 1986 for multi-elemental separation and detection of separated metals [2] and 1989 for the determination of arsenic species [3]. A general increase in the number of publications related to coupling HPIC to ICP-MS can be seen over the years (Figure 3.1).

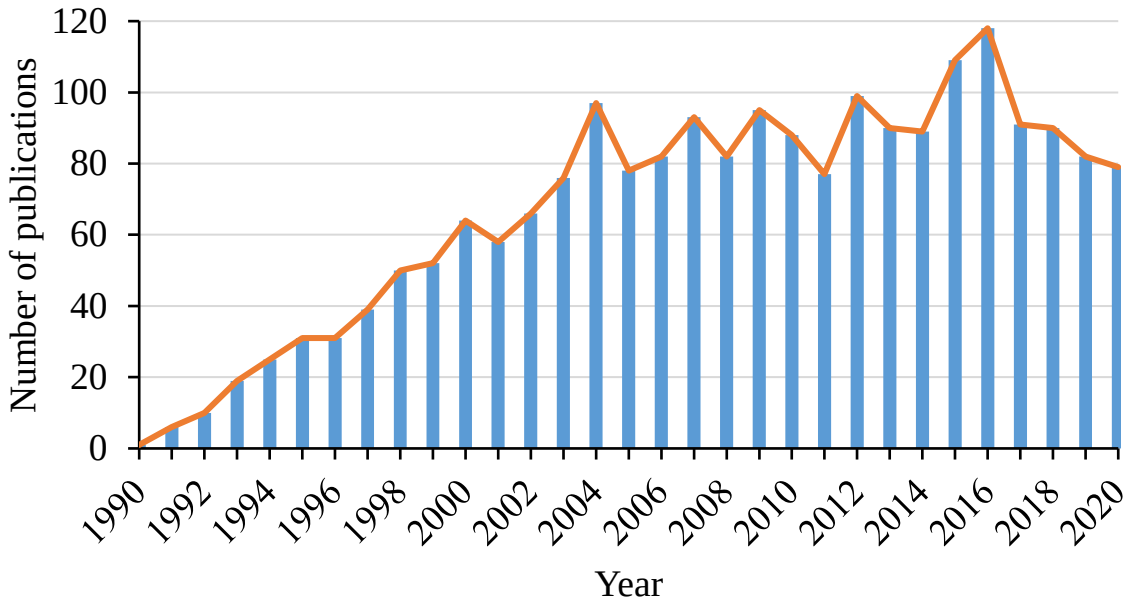


Figure 3.1 Evolution of the number of publications related to the hyphenation of HPIC with ICP-MS over the years based on data extracted from Web of Science on October 05, 2020 with "HPIC" and "ICP-MS" as search terms

## 3.2 Background on SF-ICP-MS

### 3.2.1 Operating principle

The basic principle of operation of a SF-ICP-MS is no exception to the common mass spectrometers' operating principle, which consists of ionization of the sample components in an ion source, separating the ions based on their *m/z* ratio using a mass separator and finally detecting the ions and converting them to a quantifiable signal using a detector. In ICP-MS, the mass separator is operated under vacuum ($10^{-6}$ – $10^{-10}$ Pa), whereas the ion source can be placed at ambient pressure (101,325 Pa). The magnetic sector is the core of a sector field mass spectrometer, and its operating principle is discussed in section 3.3.6 of this chapter.

### 3.2.2 Isotope ratio measurement

Isotope ratio (IR), defined in IUPAC as "the ratio of the number of atoms (*N*) of one isotope to the number of atoms of another isotope of the same chemical element in the same system" [4]. Thus, the isotope-number ratio of an element *E* with isotopes *i* and *j* in phase *P*, is calculated using the following equation.

$$R = \frac{N(^{i}E)_P}{N(^{j}E)_P} \qquad \text{(eq. 3.1)}$$

IR measurement is essential for the determination of the mass fractions of elements with the highest precision and accuracy using isotope dilution (further information in section 3.2.6.3 of this chapter). The precision of an IR is commonly expressed as the repeatability (RSD %) of IRs acquired in the different runs carried out in off-line mode (no transient signals). Different IR precisions can be obtained with different mass spectrometric instruments. For example,

single-collector SF-ICP-MS instruments provide more precise IRs than quadrupole-based instruments (explained in section 3.3.6 of this chapter). However, single-collector ICP-MS generally yield poorer precisions (RSD ≥ 0.05 %) than multi-collector ICP-MS instruments (RSD ≥ 0.002 %), owing to the simultaneous measurement of the different isotopes of interest.

It is worth mentioning that TIMS was widely considered the benchmark technique for accurate and precise (RSD < 0.01 %) IR measurement. However, with the introduction of the first multi-collector ICP-MS unit, the "*Plasma 54*" from VG Elemental (Winsford, UK) in 1992, TIMS is gradually being replaced by multi-collector ICP-MS, due mainly to the higher sample throughput possible with ICP-MS and the higher ionization energy of the ICP ion source [5]. This is illustrated by the fact that 60 percent of laboratories which acquired multi-collector ICP-MS also have one or more TIMS instruments [6]. Nevertheless, ICP-MS has several notorious factors limiting its performance in comparison with TIMS including: abundance sensitivity, instrumental mass discrimination leading to biased IR data (see 3.2.3), dead time when using an electron multiplier as detector (see 3.2.4) and spectral interferences (see 3.2.5). Abundance sensitivity is defined by IUPAC as "a measure of the contribution of the peak tail of a major isotope (with a certain *m/z* value) to an adjacent *m/z* value" [4], and is determined by the resolution power of the ICP-MS instrument used.

### 3.2.3 Instrumental mass bias

Mass spectrometric measurement of an IR is hindered by instrumental isotopic fractionation, which is sometimes referred to as "instrumental mass fractionation", "instrumental mass discrimination" or "instrumental mass bias". All these variations on a theme describe the sum of effects occurring within all regions of the instrument that contribute to the difference (denoted by a K-factor as shown in eq. 3.2) between the measured isotope ratio ($R_{meas}$) and the true isotope ratio ($R_{true}$). This difference will be referred to as *mass bias* throughout this dissertation. If mass bias is not taken into account, erroneous IRs are obtained. The understanding of the effects causing mass bias is still limited; however, there is a general consensus among mass spectrometrists on classifying these effects into either mass-dependent or mass-independent effects. Only mass-dependent fractionation will be considered in this dissertation, as causes of mass-independent effects are under debate. A couple of effects causing mass-independent bias are the nuclear field shift and the magnetic isotope effect and are discussed into further detail in the following literature: [7-9]. Mass-dependent effects include the space-charge effect and the nozzle separation effect [10], and lead to erroneous raw IR result. The space-charge effect takes place mainly after the skimmer cone and is considered the main contributor to mass bias, being caused by mutual repulsion (coulombic interaction) between ions of similar charges which leads to lighter ions being removed to a greater extent from the ion beam than heavier ions. The nozzle separation effect affects the extraction of ions from the ICP by the interface, causing heavier ions to be sampled more efficiently than the lighter ones. The space-charge effect and the nozzle separation effect do not counteract each other, but increase the mass bias in the same direction.

Different correction models have been presented to correct for mass-dependent effects of mass bias, of which the most popular are presented in eqs. 3.3 – 3.6, where $\varepsilon$ is the mass bias per atomic mass unit and $\beta$ is the fractionation factor.

$$K_{bias} = \frac{R_{true}}{R_{meas}} \quad \text{(eq. 3.2)}$$

$$\text{Linear law:} \quad K_{lin} = \frac{R_{true}}{R_{meas}} = (1 + \varepsilon_{lin} \cdot \Delta m) \quad \text{(eq. 3.3)}$$

$$\text{Power law:} \quad K_{pow} = \frac{R_{true}}{R_{meas}} = (1 + \varepsilon_{pow})^{\Delta m} \quad \text{(eq. 3.4)}$$

$$\text{Exponential law:} \quad K_{exp} = \frac{R_{true}}{R_{meas}} = e^{\varepsilon_{exp} \cdot \Delta m} \quad \text{(eq. 3.5)}$$

$$\text{Russell's law:} \quad K_{bias} = \frac{R_{true}}{R_{meas}} = \left(\frac{m_2}{m_1}\right)^{\beta} \quad \text{(eq. 3.6)}$$

The choice of one model over the other depends on the type of instrument being used. Based on a study by Quétel et al., when using single-collector ICP-MS, the different models yield similar results and uncertainties, and hence, the use of the simple linear model is sufficient to correct for mass bias [11]. The power and exponential laws are sometimes used to correct the instrumental mass bias with multi-collector instruments. On the other hand, Russell's law, published in 1978 [12], is different from the other models and takes into account the actual isotopic masses instead of the difference in mass between them.

It is possible to calibrate IRs for the effect of mass bias by establishing a relationship between the measured and true IRs, which are obtained by measuring certified reference materials or a constant IR in the sample itself. The calibration can be done using internal calibration, where the calibrant (reference) and the measurand are analysed simultaneously, i.e. in the same solution, or alternatively using external calibration, where the calibrant and measurand are measured sequentially in different solutions [13]. Both internal and external calibration methods can be performed with IRs of the same element (intra-elemental) or of a different element (inter-elemental) [14]. A requirement for implementing internal calibration methods is the existence of a (sufficiently) constant IR, either of the same element as the measurand (e.g. using $^{146}Nd/^{144}Nd$ for calculating the fractionation factor and correcting for $^{142}Nd/^{144}Nd$ in the same sample), or of a different element than the measurand (e.g. adding Zr to the sample and using $^{90}Zr/^{91}Zr$ to correct $^{87}Sr/^{86}Sr$ for mass bias). However, finding a constant IR is not applicable to spent nuclear fuel samples due to their varying nuclide-specific compositions. It is usually possible to add to the sample an isotopically certified reference material of an element close in mass to that in the sample, however the complex composition of spent nuclear fuels makes it hard to find a suitable reference material with an element which is not present in the sample. When an external reference material is added to the sample, it is advisable to have the calibrant and measurand at the same concentration, which could be a limiting factor with high concentrations especially when using separation columns with limited capacity. In such cases, external calibration, also known as standard-sample bracketing, is the simplest approach when using a sequential ICP-MS instrument coupled with HPIC to characterize spent nuclear fuel. In this approach, an isotopically certified reference material having a similar isotopic composition and concentration as the measurand is measured sequentially with the sample, with the

standards (the isotopically certified reference material) bracketing the sample(s). The K-factor determined from two sequential standards, through averaging or interpolation, is applied to the sample between them. It is preferable to isolate the analytes from the matrix prior to their analysis when using external calibration. If this is not possible, matrix- and concentration-matching between the samples and the standards is required for this external calibration method to work successfully [13]. In this work, the sample analytes were always separated from the matrix using HPIC prior to the analysis with SF-ICP-MS.

### 3.2.4 Dead time

The dead time (τ) is the time period during which a pulse-counting electron multiplier is unresponsive to incoming ions due to handling the pulse generated by a previous ion by the associated electronics. While handling a pulse, the electron multiplier is incapable of determining a subsequent pulse [15], resulting in count rate losses and a shift from the linear response of the detector, which needs to be accounted for when aiming at accurate IR measurements. Different methods exist to correct the measured count rate for dead time, such as the one developed by Russ [16], by Held and Taylor [17], or the one by Baxter et al. [18] that was used in this work. In this last approach, the automatic dead time correction is first disabled in the instrument's software. Then, different concentrations of elements having at least one pair of isotopes with a ratio significantly different from unity are measured in counting mode. The IRs measured in this work were $^{238}U/^{235}U$ ($R_{true}$ = 137.8), $^{138}Ba/^{137}Ba$ ($R_{true}$ = 6.4) and $^{175}Lu/^{176}Lu$ ($R_{true}$ = 37.5) in Spex standards (Boom Laboratoriumleverancier, Meppel, The Netherlands) with natural isotopic compositions (except for U that was depleted in $^{235}U$). The measured signal intensities for the major isotope should be higher than $10^6$ counts per second (cps) but within the pulse-counting range limit of the detector, that is less than ~ 5 x $10^6$ cps for the "*Element 2*" used in this work. Additionally, it is advisable to avoid excessively high count rates to avoid the onset of sag, resulting in additional count rate loss [18-19]. The dead time is then correlated to the measured signal intensities of the major ($I_{meas,M}$) and minor ($I_{meas,m}$) isotopes and can be calculated using the slope ($a$) and intercept ($b$) of the fitted data points (eqs. 3.7, 3.8 & 3.9):

$$\frac{I_{meas,M}}{I_{meas,m}} = \tau.\left(1 - \frac{R_{true}}{K_{bias}}\right).I_{meas,M} + \frac{R_{true}}{K_{bias}} \quad \text{(eq. 3.7)}$$

$$= a.I_{meas,M} + b \quad \text{(eq. 3.8)}$$

$$\tau = \frac{a}{1-b} \quad \text{(eq. 3.9)}$$

An example of the dead time calculation performed in this work using Ba isotopes is shown in Figure 3.2.

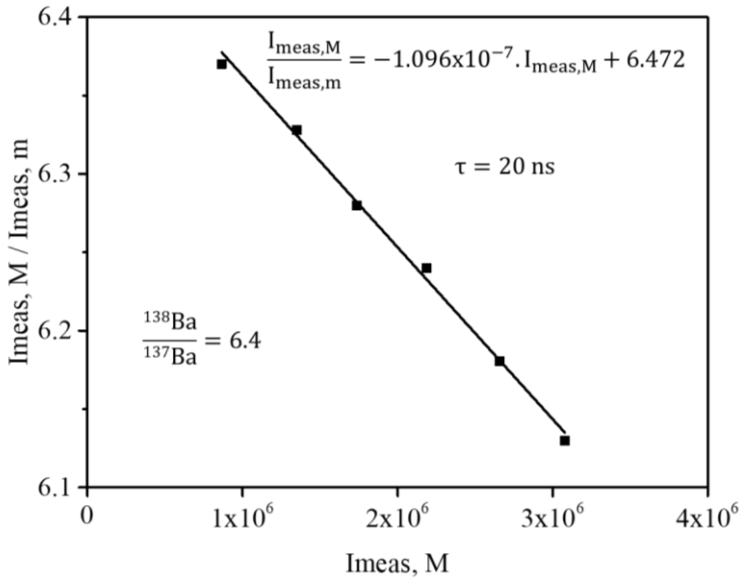


Figure 3.2 Dead time calculated using Ba isotopes following the dead time correction approach developed by Appelblad and Baxter

The dead time obtained with the three isotope pairs was found to be similar (20 ns) and was set in the instrument software for automatic correction of the measured intensities.

### 3.2.5 Spectral interferences

Different types of spectral interferences can occur for two or more ions having the same nominal *m/z* ratio such as monoatomic ions of isobaric nuclides (e.g. $^{144}Ce^+$ and $^{144}Nd^+$), polyatomic oxide ions (e.g. $^{142}CeO^+$ and $^{158}Gd^+$), hydroxide ions (e.g. $^{238}UH^+$ and $^{239}Pu$) and others. Even though spectral interferences can be avoided by appropriate sample preparation for matrix elimination or the separation of the elements of interest (e.g. using chromatography) prior to the introduction of the sample into the ICP-MS, argon (Ar)-based ions (e.g. $^{40}ArO^+$, $^{40}ArN^+$ and $^{40}Ar_2^+$) generated in Ar based ICP can still interfere with sample analytes (e.g. at *m/z* 56, 54 and 80), leading to erroneous IR measurements. An unambiguous way to eliminate most spectral interferences in modern SF-ICP-MS instruments is to use high mass resolution setting [5]. If possible, interference corrections can be done based on isotopic reference values.

### 3.2.6 Quantification methods

In addition to IR measurements, ICP-MS is an accurate tool for elemental quantification. Various quantification strategies exist for ICP-MS and the choice of one method over the others depends on the desired precision and accuracy, the type of certified reference materials available and the amount of sample available. In this chapter, external calibration (one or multiple point calibration) and internal calibration methods such as standard addition and isotope dilution will be discussed, as well as noise correction using internal normalisation. For any calibration method, the traceability of the result should be evident, commencing with the gravimetric preparation of standards and samples until the amount of substance in the sample has been determined.

### 3.2.6.1 External calibration

In external calibration, a correlation is established between the concentration of a substance in the standard and the response registered by the instrument. Several standards containing different concentrations distributed equally over the range of expected sample concentrations, are measured. The measured intensities, or peak areas in the case of transient signals, are then plotted against the corresponding concentrations and a linear regression line is fitted though the data points. That a calibration fit is satisfactory can be evaluated by the closeness of the regression coefficient ($R^2$) to unity and by the mean squared weighted deviation. The concentration in the sample is then obtained by interpolation using the equation of the linear regression (slope and intercept). It is possible to use one-point calibration if the concentration of an analyte in the standard is as close as possible to the concentration of that analyte in the sample. This calibration method does not take into account potential spectral interference and/or non-spectral interference (matrix effect) and could lead to an erroneous estimation of the amounts of sample analytes if the latter are not separated from the matrix prior to the analysis.

### 3.2.6.2 Standard addition

Internal calibration using the method of standard additions is a suitable way to matrix-match the sample and the standard. The sample is split into different aliquots into which increasing known amounts of the standard are spiked, leaving one sample aliquot without standard. The spiked and unspiked samples are then measured and their corresponding signals are recorded. The recorded signals are then plotted against their corresponding spiked standard amount as shown in Figure 3.3. The signal of the unspiked sample will be at x = 0. The amount of analyte in the sample is then determined by extrapolating the linear regression to the x-axis. According to the RSC's Analytical Methods Committee, it is possible to spike only one sample aliquot if the spiked amount is at least five times the amount of substance in the sample [20]. It is crucial for the sample and spiked standard to reach chemical equilibrium prior to measurement to avoid erroneous results.

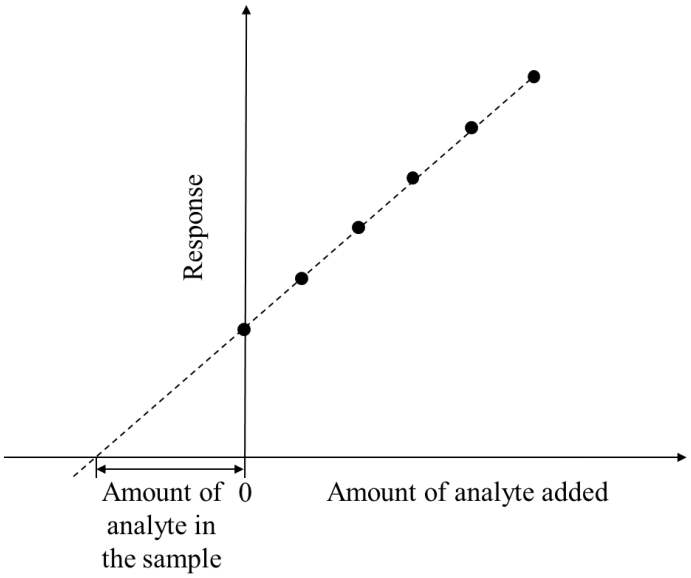


Figure 3.3 Principle of the method of standard additions

#### 3.2.6.3 Isotope dilution

A primary method is defined by CCQM as "a method having the highest metrological qualities, whose operation can be completely described and understood and for which a complete uncertainty statement can be written down in terms of SI units" [21]. For accurate and precise trace element analysis, IDMS is considered to have the potential of being a primary method of the highest metrological quality by CCQM of BIPM [21-22] (Consultative Committee for Amount of Substance of the International Bureau of Weights and Measures), generally providing better accuracy and precision compared to other calibration techniques. In IDMS analysis, a sample with an unknown concentration of an element (having at least two isotopes) is mixed and chemically equilibrated with a known amount of a spike isotopically enriched in a minor isotope of that element [23]. The ratio of that enriched isotope to a reference isotope in the blend or mixture is then measured using mass spectrometry [24]. For the best results when using a highly enriched spike, the absolute amount of spike should be approximately equal to that of the analyte in the blend [23], however a factor of 10 higher or lower is usually acceptable [24]; alternatively, as a rule of thumb, the ratio in the blend should approach the square root of the multiplication of the sample and spike ratios [25]. To determine the blend ratio which can be measured with the best precision, the error magnification factor can be used (refer to section 5.3.2.1). Isotope dilution can be performed in batch or online. In batch isotope dilution, optimum blending is achieved by mixing the spike and the sample on a weight basis at the beginning of the analytical process [24]. Whereas in online isotope dilution, the isotopically enriched spike is mixed online at a constant flow rate with the flow containing the sample. To apply online isotope dilution, compound-independent sensitivity has to be demonstrated [26]. A major disadvantage of online isotope dilution in comparison to batch isotope dilution is that any loss of compound prior to isotopic equilibration cannot be corrected for [26]. Although this work included coupling of HPIC to SF-ICP-MS and IDMS was performed using transient signals, batch isotope dilution was preferred over online isotope dilution as the sample and the spike added to the sample then experience the same conditions (oxidation, separation, etc.) in the mixture and no additional bias is intentionally introduced. Additionally, the measurement of spikes separately from the samples was not performed in this work to avoid potentially contaminating the instrument with high amounts of the enriched isotopes. The spikes used in isotope dilution HPIC-SF-ICP-MS experiments in this work and their isotopic compositions are presented in Table 3.1. Therefore, the isotopic amounts (and their uncertainties) reported on the certificate of the reference materials used were corrected for radioactive decay if necessary (such as for all monitored Pu isotopes) and used in isotope dilution calculations. An example of measured transient signals in the sample and the blend of spent nuclear fuel using HPIC-SF-ICP-MS can be found in Figure 3.4.

Table 3.1 Isotopic compositions of Pu- and U-enriched certified reference materials and Nd and Gd in-house produced and characterised enriched standards used for spiking in isotope dilution HPIC-SF-ICP-MS

| (Certified) reference material | Nuclide | Amount fraction (·100) (U, k=2) |
|---|---|---|
| IRMM-049d* | $n(^{238}Pu)/n(Pu)$ | 0.46898 (72) |
| | $n(^{239}Pu)/n(Pu)$ | 0.21046 (12) |
| | $n(^{240}Pu)/n(Pu)$ | 4.3611 (47) |
| | $n(^{241}Pu)/n(Pu)$ | 0.17760 (60) |
| | $n(^{242}Pu)/n(Pu)$ | 94.7575 (50) |
| | $n(^{244}Pu)/n(Pu)$ | 0.024365 (50) |
| | | |
| IRMM-040a | $n(^{233}U)/n(U)$ | 98.0430 (57) |
| | $n(^{234}U)/n(U)$ | 0.91454 (20) |
| | $n(^{235}U)/n(U)$ | 0.2142 (55) |
| | $n(^{236}U)/n(U)$ | 0.02412 (29) |
| | $n(^{238}U)/n(U)$ | 0.8041 (19) |
| | | |
| Nd-146 spike produced in-house | $n(^{142}Nd)/n(Nd)$ | 0.43650 (97) |
| | $n(^{143}Nd)/n(Nd)$ | 0.29826 (80) |
| | $n(^{144}Nd)/n(Nd)$ | 0.7719 (21) |
| | $n(^{145}Nd)/n(Nd)$ | 0.6416 (13) |
| | $n(^{146}Nd)/n(Nd)$ | 97.5234 (33) |
| | $n(^{148}Nd)/n(Nd)$ | 0.2255 (11) |
| | $n(^{150}Nd)/n(Nd)$ | 0.1028 (15) |
| | | |
| Gd-157 spike characterised in-house | $n(^{153}Gd)/n(Gd)$ | 0.0040 (29) |
| | $n(^{154}Gd)/n(Gd)$ | 0.0396 (14) |
| | $n(^{155}Gd)/n(Gd)$ | 0.2928 (55) |
| | $n(^{156}Gd)/n(Gd)$ | 1.675 (21) |
| | $n(^{157}Gd)/n(Gd)$ | 88.37 (20) |
| | $n(^{158}Gd)/n(Gd)$ | 9.07 (18) |
| | $n(^{160}Gd)/n(Gd)$ | 0.547 (30) |

*Values decay-corrected for UOx HPIC-SF-ICP-MS date of analysis (2020-02-27)

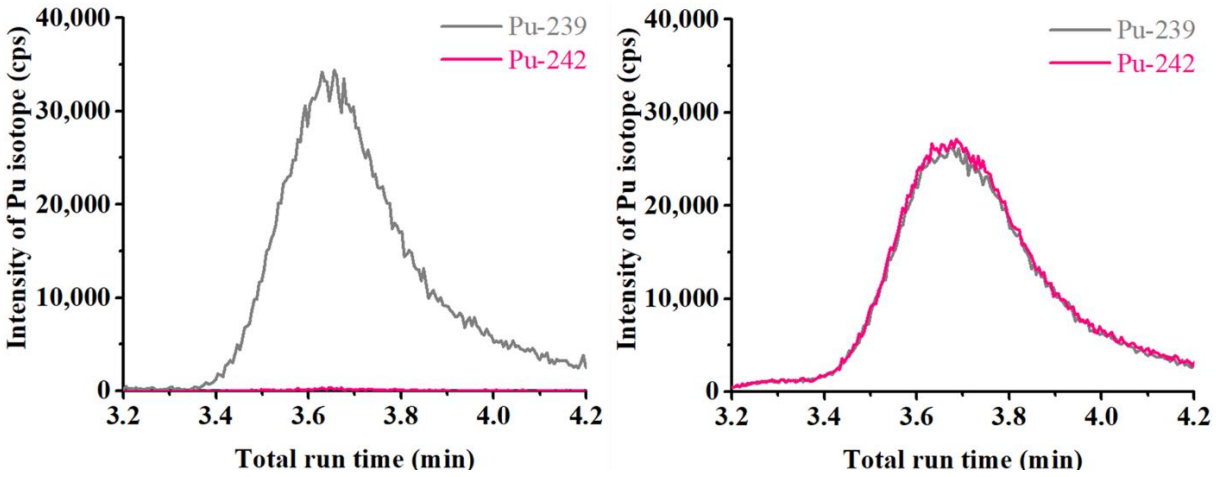


Figure 3.4 HPIC-SF-ICP-MS chromatograms of $^{239}$Pu and $^{240}$Pu in the sample (left) and the blend (right)

The principle of IDMS is as follows: let $n_x$ and $n_y$ be the number of moles of the poly-isotopic element in the sample and the spike, respectively. Then, the number of moles of the same element in the blend can be expressed as $n_b$, which corresponds to the following mass balance:

$$n_b = n_x + n_y \qquad \text{(eq. 3.10)}$$

Using eq 3.11, $n_x$ can be obtained from $n_y$, $R_y$ (known ratio in the spike), $\Sigma R_{i,y}$ (the sum of all isotope amount ratios in the spike), the measurement of the isotope amount ratio in sample ($R_x$) and blend ($R_b$) and the sum of all the isotope amount ratios in the sample ($\Sigma R_{i,x}$).

$$n_x = n_y \cdot \frac{R_y - R_b}{R_b - R_x} \cdot \frac{\Sigma R_{i,x}}{\Sigma R_{i,y}} \qquad \text{(eq. 3.11)}$$

The number of moles ($n$) can be substituted by the mass fraction ($w$) using the correlation:

$$n = \frac{w.m}{M} \qquad \text{(eq. 3.12)}$$

where, $m$ is the weighed mass (in g) and $M$ is the molar mass (in g.mol$^{-1}$). Therefore, eq. 3.11 becomes:

$$w_x = w_y \cdot \frac{m_y}{m_x} \cdot \frac{M_x}{M_y} \cdot \frac{R_y - R_b}{R_b - R_x} \cdot \frac{\Sigma R_{i,x}}{\Sigma R_{i,y}} \text{ [27]} \qquad \text{(eq. 3.13)}$$

The determination of the mass fraction in nuclear samples is used to make SI-traceable measurements. The correlation shown in eq. 3.13 is the primary IDMS equation, which is simpler than other isotope dilution forms (secondary, tertiary and quaternary IDMS) and is suitable for routine analysis. The main advantage of IDMS is that to quantify the element's mass fraction, IRs are used, which are neither affected by incomplete recovery during sample pre-treatment [1, 23] nor by instabilities of instrumental parameters [28]. This is more accurate than other calibration techniques that use signal intensities [22, 28] normalised to those of an internal reference for quantification instead. Additionally, measuring IRs cancels out any matrix

effects [23-24] because the spike and reference isotopes are affected by the matrix to the same extent (within the isotope precision offered by single-collector ICP-MS).

Despite being classified as a primary method, IDMS does not entail accurate results unless various prerequisites are met, such as isotopic equilibration within the blend. Any loss in sample or spike prior to isotopic equilibration can be an important source of error [24]. Nevertheless, total isotopic equilibration can be accomplished relatively quickly in single-phase systems (such as water) [22]. Additional features of IDMS that can be considered as limitations include its limitation in applicability to elements with at least two isotopes, the signal of which can be monitored interference-free. Furthermore, IDMS can be time-consuming since it requires the pre-determination of analyte mass fraction in the sample using a more traditional approach to make adequate decisions about the amounts of sample and spike to be mixed. In the case of nuclear samples, mass fractions of Pu, U and Nd in the fuel can be estimated from nuclear material accountancy data and the irradiation history of the fuel. Additionally, contamination during the sample preparation process cannot be corrected for. Finally, IDMS is a costly analysis specifically in terms of purchase of certified enriched spikes (if available), but also because of the need to know the isotopic composition of the sample [which if not of natural isotopic composition will require either information from the customer or an actual additional analysis using another calibration method (external calibration for example)] prior to isotope dilution, in order to determine the amount of sample and spike to be combined to produce the blend. However, enriched spikes can be used for many analyses, so whilst the upfront purchase costs of enriched spikes can be daunting, once purchased, their costs become divided over many analyses.

#### 3.2.6.4 Internal normalization

In mass spectrometry, internal normalization is used to correct for drift in sensitivity of the instrument during a measurement performed for elemental quantification. Internal normalization is performed by adding a non-analyte single-element standard into solutions of the calibration standards, samples and blanks. Chemical properties of the internal standard should be similar to those of the analyte of interest. An internal standard can be used with external calibration and standard additions to normalize the signal intensity of the analyte, however, this is not done with isotope dilution which uses IRs instead of signal intensities, with these IRs being much more resistant to sensitivity changes than signal intensities are.

### 3.3 Components of single-collector SF-ICP-MS

The main use of single-collector SF-ICP-MS is the determination of elements at trace to ultra-trace levels. Moreover, it shows a capability of fit-for-purpose precision in IR measurements owing to the capability of fast scanning / peak jumping and the flat-top peaks in low resolution mode making it fit-for-purpose in IDMS. Nevertheless, multi-collector mass spectrometers are the best equipped to obtain the best achievable IR precision. Figure 3.5 shows a schematic representation of SF-ICP-MS components. The following components of single-collector SF-ICP-MS, specifically the "*Element 2*", will be discussed in this section: (1) the sample introduction system, introducing the sample (or a representative part thereof) into the plasma, (2) the ICP, ionizing the sample analytes, (3) the interface, transporting the ions from

atmospheric pressure into the reduced pressure zone, (4) the ion transfer optics, accelerating the ions towards the mass analyser and focusing the ion beam, (5) the sector field mass separator, separating the ions according to their *m/z* ratio, (6) the slit system, permitting to switch between resolutions, (7) the lens filter, eliminating the impact of abundance sensitivity, (8) the detector and (9) the vacuum system, removing gas particles which could possibly interfere by colliding with the ion beam.

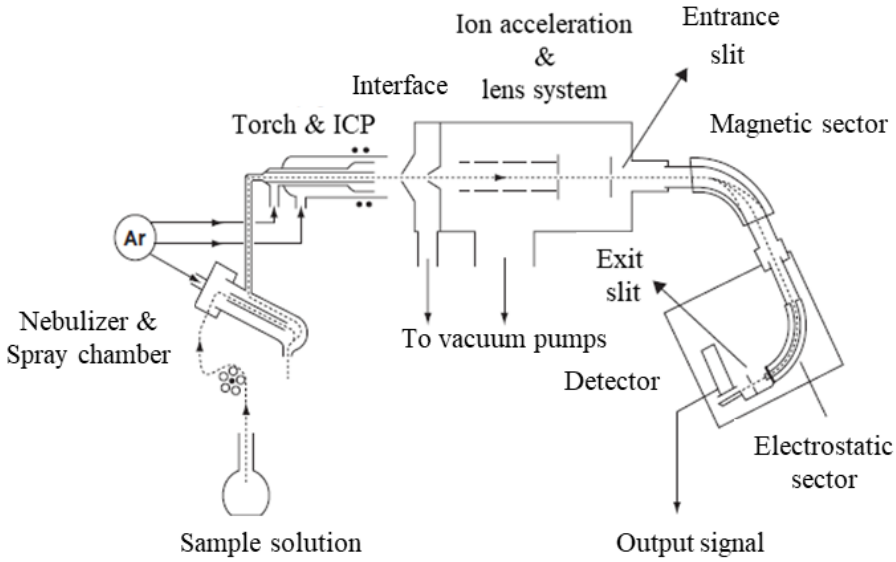


Figure 3.5 Schematic representation of a double-focusing SF-ICP-MS unit with its various components [5]

### 3.3.1 Sample introduction system

The sample introduction system converts the sample into a form compatible with the plasma (wet/dry aerosol or gas) and introduces it into the plasma. The sample introduction system was called the "Achilles' heel" of ICP-MS [29].This 1984 title still holds, especially since most of the problems that can occur with ICP-MS take place in the sample introduction system. The sample introduction system is under ambient pressure, which permits the continuous introduction of sample into the plasma, rendering sample introduction simpler than with other types of mass spectrometers where the ion source is operated at $10^{-6}$-$10^{-10}$ Pa (TIMS) or at 100 Pa (GDMS) [30]. Liquid samples are first pumped using a peristaltic pump, or a chromatographic pump in case of HPIC coupled to ICP-MS, into a nebulizer where the liquid is converted into an aerosol (mist of droplets), which then enters the spray chamber where a limited amount of droplets make their way into the plasma. Different types of nebulizers exist, some of which do not necessitate the use of a pump to introduce the sample, since they rely on the sample being sucked by the positive pressure of the nebulizer gas, a phenomenon referred to as the "venturi effect". The nebulizer gas is the gas flowing in the nebulizer and breaking up the sample solution into an aerosol. The most commonly used types of nebulizers are the concentric nebulizer, which delivers < 20 % of the sample into the plasma when operated at flowrates between 0.1 to 1 mL·min$^{-1}$ [31], and the crossflow nebulizer designs. When ICP-MS is coupled to nano-HPLC or capillary electrophoresis (CE), low-flow nebulizers (such as micro-concentric and micromist nebulizers), which are reduced in size and made of inert polymer

materials, are required to operate at low flowrates in the $\mu L \cdot min^{-1}$ range and are efficient (up to 100 %) in introducing the sample aerosols generated into the plasma [32]. Nebulizers are generally made of glass or quartz, however various types of polymers, such as perfluoroalkoxy (PFA), polytetrafluoroethylene (PTFE) or polyvinylfluoride (PVF) can be used for their corrosion-resistant and inert properties, which make them suitable for trace element analysis.

After being converted into an aerosol, the sample enters the spray chamber where the larger droplets (> 8 µm in diameter [33]) strike the walls of the spray chamber or settle out by gravity to be drained away, leaving only the smaller ones to reach the plasma and therefore reducing the sample introduction efficiency by 10 to 100 times [5]. Another function of the spray chamber is to smooth out fluctuations in the flowrate induced by the pump, thereby improving the signal stability. Scott-type (also known as double-pass) spray chambers and cyclonic spray chambers are the most commonly used types of spray chamber and are illustrated in Figure 3.6. Both types can be made of glass or from polymers. However, longer washout time can be observed for polymeric spray chambers due to their beading and thus lower wettability than glass [33]. The finest aerosol can be obtained with the Scott-type spray chamber design [34] whereas a broader particle size distribution and higher introduction efficiency are obtained with cyclonic spray chamber [5, 35]. The signal stability can be increased by combining both types of spray chambers [36].

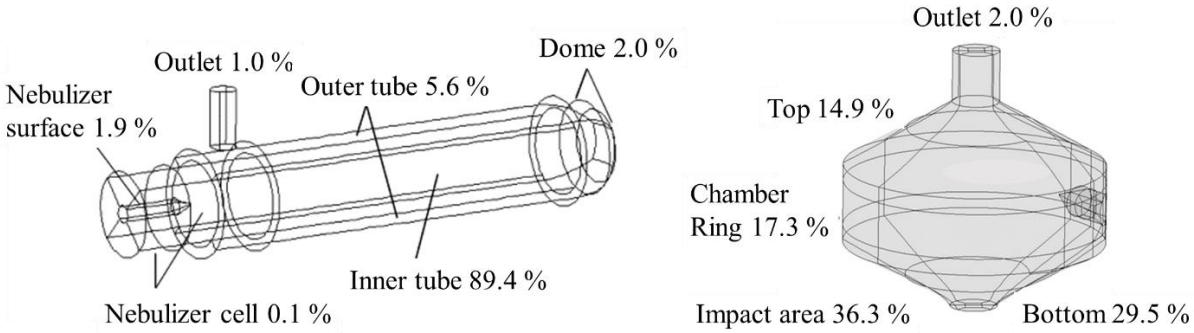


Figure 3.6 Aerosol droplet distribution in a Scott type spray chamber (left) [34] and in a cyclonic spray chamber (right) [35]

Coupling the sample introduction system of an ICP-MS to HPIC is rather simple compared to the considerations that need to be taken with other chromatographic techniques, such as gas chromatography (GC) and CE. In GC, it is necessary to avoid condensation of the gaseous analytes eluting from the column prior to their introduction into the ICP. Therefore, the interface of the ICP-MS has to be heated to maintain the efficiency of the GC separation (resolution and peak shapes). To this end, several manufacturers, such as Agilent and Perkin Elmer, provide interfaces with a heated transfer line. However, the interest in GC-ICP-MS has been decreasing due to a lack of real sample applications and stable and reliable standards required for quantitative analysis [37]. Similarly, special considerations must be taken into account when coupling ICP-MS to CE, where the electrical circuit needs to be closed at the end of the CE capillary for a continuous electrical circuit to be applied [38]. In contrast, the only consideration in the coupling of HPIC to ICP-MS is the type of nebulizer to be used, which depends on the operating flow rate of the separation column and the chemical inertness/material of the

nebulizer. Additionally, a leak tight ferrule connection must be used at the nebulizer inlet when HPIC is coupled to ICP-MS to prevent any sample loss and introduction of air.

### 3.3.2 Inductively coupled plasma

The ICP is essentially a quasi-neutral ionized gas with charged and neutral particles and is currently the most widely adopted ionization source in mass spectrometry. Ar is the most commonly used gas for ICP, and was the one used in this work. Nevertheless, mixed-gas ICP and He ICP also exist and can be used when Ar ICP is not suitable [39]. Sample aerosol droplets make their way through the torch into the Ar ICP while being carried by a flow of Ar (sample gas ~ 1 $L \cdot min^{-1}$), and are desolvated, the salt particles thus formed are vaporized and atomized and these atoms subsequently ionized in the different zones of the 7,000 – 10,000 K ICP (as noted in Figure 3.7). The torch consists of three concentric quartz tubes (Figure 3.8) through which Ar flows at different rates. In the "*Element 2*", the end of the torch is surrounded by a copper water-cooled load coil through which a radiofrequency (RF) current of ~ 27 MHz passes and generates a magnetic field of the same frequency around and inside the load coil. A high-voltage spark seeds the plasma gas with free electrons capable of ionizing Ar atoms to "ignite" the ICP. The ICP is maintained by the collision-induced ionization of Ar as long as the cool gas (~ 15-20 $L \cdot min^{-1}$) keeps feeding Ar into the plasma and as long as the RF energy is supplied. In addition, the cool gas forms a physical barrier between the plasma and the torch, preventing the torch from melting. The auxiliary gas (~ 1 $L \cdot min^{-1}$) can be used to optimize the position of the ICP, whereas the sample gas transports the sample through the plasma, puncturing a hole in the centre, giving the plasma a toroidal shape. As the sample passes through the centre of the ICP, it is surrounded by high temperatures for a relatively long time (approximately 2 ms), compared with other ionization sources such as direct current plasma (DCP) where the sample travels along the outside of the discharge and does not experience high temperatures for as long as in an ICP [40]. Another advantage of ICP is its high ionization energy, which allows the simultaneous ionization of different elements including those with high ionization energies (such as W, Re, Os, Hf), a characteristic which is not possible with thermal ionization sources for example where only one element can be ionized at a time [41]. Characteristics of the ICP can be optimized according to the analyte species. For example, the higher the RF power applied to the ICP, the hotter the plasma becomes, which makes it suitable for analysing species with high ionization energies [40]. Additionally, the sensitivity of the instrument can be adjusted by changing the position of the torch or by changing the nebulizer gas flow rate, and thus the position of the plasma with respect to the interface, from the instrument software.

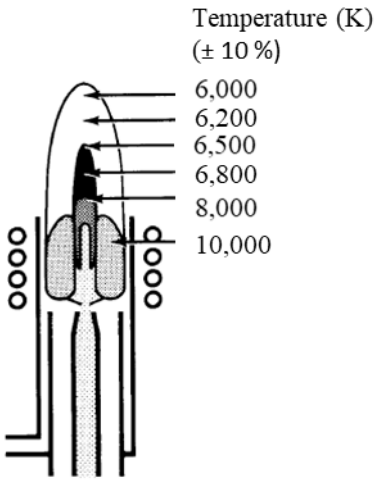


Figure 3.7 Ionisation temperatures for different regions of the ICP [40]

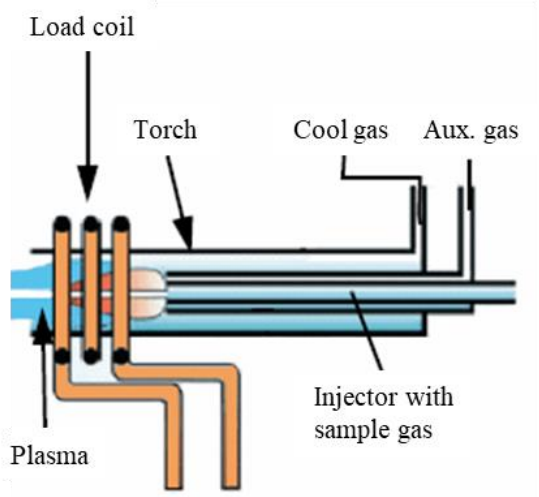


Figure 3.8 Torch and load coil arrangement from "*Element 2*" manual (source: Thermo Fisher Scientific ©)

The ICP consists mainly of Ar, but also contains traces of H, O, N and C as impurities in commercial Ar gas. Since the ionization energy of Ar is around 15.8 eV, the plasma contains enough energy to generate singly charged ions for most elements of the periodic table having a first ionization energy between 4 and 12 eV [42]. For elements having a second ionization energy lower than 15.8 eV, doubly charged ions can also be formed. The degree of ionization (in percentage) of an element in the ICP can be obtained from the Saha-Eggert equation [15]. Ions can be formed in the ICP by various non-selective processes, the most likely being electron impact, as described in eq. 3.14.

$$M + e^- \rightarrow M^+ + 2e^- \qquad \text{(eq. 3.14)}$$

Ions can also be formed in the ICP to a lesser extent by charge transfer (as shown in eq. 3.15) and by Penning ionization (as shown in eq. 3.16).

$$M + Ar^+ \rightarrow M^+ + Ar \qquad \text{(eq. 3.15)}$$

$$M + Ar^* \rightarrow M^+ + Ar + e^- \qquad \text{(eq. 3.16)}$$

Several polyatomic ions and doubly charged ions are thought to be formed due to a secondary electrical discharge caused by capacitive coupling between the ICP and the grounded interface [43]. This secondary discharge can be eliminated by the use of a centrally grounded load coil, two interlaced and oppositely charged load coils or a grounded guard electrode between the load coil and the torch [44]. The latter approach is used in the "*Element 2*".

### 3.3.3 Interface

After their formation in the ICP, ions pass through the interface which is at reduced pressure (10 – 100 Pa). The interface is generally made of two coaxial metal cones (sampler and skimmer cones) both of which have a small central orifice (around 1 mm for the sampler cone and around 0.4 mm for the skimmer cone) for the passage of ions generated in the plasma (illustrated in Figure 3.9). The cones can be made of heat-conducting materials such as Ni or Al, however, for analysing corrosive solutions, Pt-covered cones are ideal. Upon entry into the interface region between the cones, the dramatic reduction in pressure causes a supersonic expansion of the extracted plasma, of which the central part passes through the skimmer cone aperture. This supersonic expansion is a major contributor to the mass bias observed in ICP-MS, since the lighter mass ions are more easily diffusing away from the centre of the ion beam than the heavier mass ions. The positive ions of this beam are then selected and directed towards the ion transfer optics, commonly using a negatively charged extraction lens.

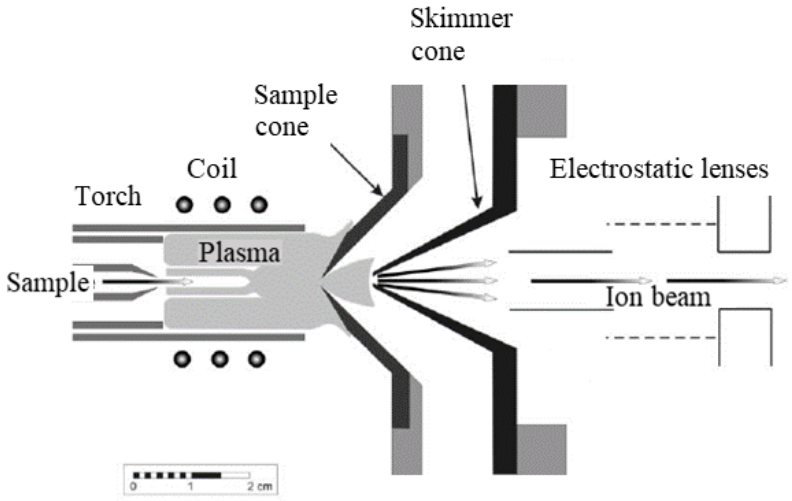


Figure 3.9 Schematic cross-section of ICP and interface [41]

### 3.3.4 Ion transfer optics

The ion transfer optics consist of one or more electrostatically controlled lenses (cylindrical or quadrupole) designed to extract, focus and accelerate the ion beam before it enters the mass separation component through its entrance slit. Additionally, the lens system shapes the original circular profile of the ion beam into a rectangular profile in accordance with the geometry of the entrance slit in the "*Element 2*". The ions exiting through the orifice of the skimmer cone are accelerated over a potential difference of between 4,000 to 10,000 V, depending on the type of SF-ICP-MS instrument. In SF-ICP-MS, ions are accelerated up to three times than in quadrupole instruments, which is why SF instruments are more sensitive and have a more

uniform response throughout the mass range (2 to 260 u) [44]. The angular divergence of the ion beam is inversely proportional to the acceleration voltage, which is why high acceleration voltages are preferred [15]. The curved shape of SF-ICP-MS instruments (shown in Figure 3.5) hinders neutral species and photons from reaching the detector, causing an increased background or signal instability. Additionally, electrons and neutral particles are removed by the vacuum pumps after the interface region. An illustration of the ion transfer optics of the "*Element 2*" is shown in Figure 3.10.

Figure 3.10 Ion transfer optics (source: Thermo Fisher Scientific ©)

### 3.3.5 Slit system

A pneumatic slit system defines the geometry of the ion beam and the mass resolution. The mass resolution can be selected by changing the width of the entrance and exit slits located at the entrance and exit of the mass separator components, respectively. Mass resolution (R) is defined by IUPAC as "the observed *m/z* value divided by the smallest difference Δ(*m/z)* for two ions that can be separated" [4]. Higher mass resolution is obtained by using narrower slits, lower mass resolution is obtained by using wider slits. However, as the resolution is increased, fewer ions pass through the slits and thus the intensity decreases [42]. In a single-collector double-focusing "*Element 2"* or "*Element XR"* unit (Thermo Fisher Scientific, Bremen, Germany), the resolution is determined by one of three slit openings on the slit holder (Figure 3.11), permitting to change between low (R = 400), medium (R = 4,000) and high resolution (R = 10,000) in less than one second. In low resolution, the ion beam width is narrower than the exit slit, resulting in flat-top peaks. The spectral peaks become more triangular when increasing the resolution. The resolution is set by the user in the instrument's software and the Ar pressure in the Bourdon tube (see Figure 3.11) changes accordingly (1 bar for medium R, ~ 2.8 bar for low R and ~ 6 bar for high R), causing a proportional change in the dimensions of the Bourdon tube, and thus in the position of the slit support, located at the free end of the Bourdon tube, to one of the three resolution settings.

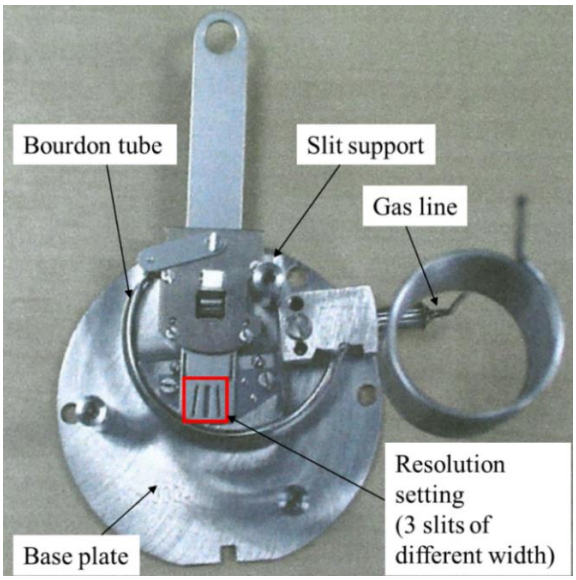


Figure 3.11 Variable entrance/exit slit unit for "*Element 2*" (source: Thermo Fisher Scientific ©)

### 3.3.6 Sector field mass separator

The mass separator in double-focusing SF-ICP-MS instruments consists of a magnetic sector and an electrostatic analyser (ESA), separating ions based on their *m/z* ratio. The double-focusing property originates from the energy dispersion of the magnetic and electric sectors being equal in magnitude but opposite in direction, which leads to focusing both the ion angles (first focusing) and energies (second focusing). When an ICP is used as the ionization source, it is beneficial to have a double-focusing setup since the energy spread of ions is large (up to 20 eV), compared to other instruments equipped with "gentler" ionization sources, such as TIMS [5]. Additionally, thanks to their double-focusing capabilities, SF mass analysers show a higher resolution than traditional quadrupole mass analysers. The forward and reverse Nier-Johnson geometries (Figure 3.12) are most widely used in commercial SF-ICP-MS instruments. The Nier-Johnson geometry was developed at the University of Minnesota in the 1950s [45] and is currently mainly applied in multi-collector SF-ICP-MS instruments. In this geometry, the ion beam is first deflected by 90° in the ESA and then by 60° in the magnetic field. In the reverse Nier-Johnson geometry, the same angles of deflection are used, but the magnetic sector is placed before the ESA. The reverse Nier-Johnson geometry is used mainly in single-collector SF-ICP-MS instruments. Since a reverse Nier-Johnson double-focusing SF-ICP-MS instrument was used in this work, the magnetic sector will be described before the electrostatic analyser in the following sections.

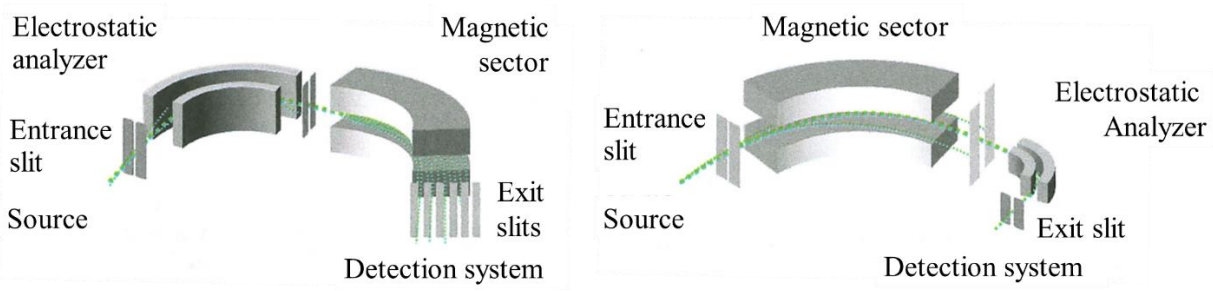


Figure 3.12 Schematic representation of forward (left) and reverse (right) Nier-Johnson geometries [15]

After the ion transfer optics, ions enter the magnet where they are subjected to a magnetic field perpendicular to the plane of the ion beam, thus the ions move in a circular path and are dispersed (Figure 3.13) with respect to their masses and kinetic energies. The radius ($r_m$) of the ion's circular path can be calculated from eq. 3.17, using the accelerating voltage ($V$), the magnetic flux density ($B$) and the ionic mass ($m$) and charge ($z$). This equation is derived from the equilibrium between the Lorentz force acting as the centripetal force exerted on the ions.

$$r_m = \frac{1}{B}\sqrt{\frac{2mV}{z}} \qquad \text{(eq. 3.17)}$$

After exiting the magnetic field, ions having the same *m/z* ratio are focused on a single point, although only one *m/z* ratio is focused perfectly on that single point depending on the magnet setting. In Figure 3.13 lines with the same colour illustrate paths of ions with the same *m/z* ratio.

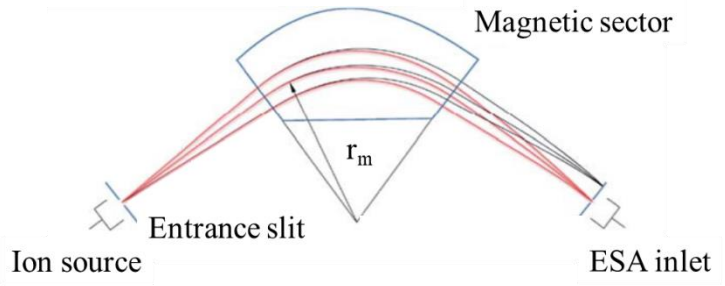


Figure 3.13 Sketch of a magnetic sector [46]

Upon exiting the magnetic sector, the ions enter the radial ESA (Figure 3.14) where they are dispersed according only to their energies. The radius ($r_e$) of the ion's circular path in the electric field can be determined from eq. 3.18. The ESA also provides angular focusing, as does the magnetic sector.

$$r_e = \frac{2V}{zE} \qquad \text{(eq. 3.18)}$$

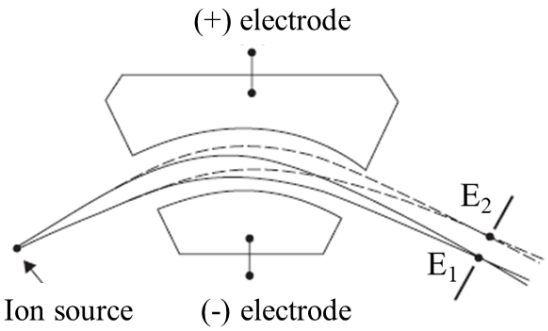


Figure 3.14 Circular path of ions with different kinetic energies ($E_1$ and $E_2$) in ESA [5]

Based on eq. 3.16, there are different ways to acquire a mass spectrum with a single-collector double-focusing SF-ICP-MS instrument: by changing either the magnetic field B (magnetic scanning or B-scanning) or the acceleration voltage (electric scanning or E-scanning). B-scanning is considered relatively slow, taking into account that it takes about 20 milliseconds for the magnet to settle (due to magnet hysteresis) after changing the magnetic field and measure at a specific mass compared to only 1-2 ms for a quadrupole; a full mass scan (0-250 u) would take approximately 200 ms with a magnet compared to about 100 milliseconds with a quadrupole [42]. E-scanning is faster than B-scanning, but is restricted to a partial mass range due to the loss of sensitivity. Nonetheless, a better IR precision is obtained with E-scanning and low mass resolution (better than 0.05% RSD) compared to B-scanning and to a quadrupole-based instrument [5]. However, under optimum conditions, IR precisions less than 0.1 % RSD can be obtained using quadrupole-based instruments equipped with a collision cell and applying collisional damping [47].

The detection of transient signals with single-collector SF-ICP-MS instruments was not considered for a long time due to the relatively slow scanning speed of such mass separators [48]. However, this changed with the introduction of laminated water-cooled magnets for SF-ICP-MS instruments, resulting in minimal magnet hysteresis (instability after magnet jump) thus improving mass stability [46] and permitting scanning the entire mass range at speeds close to that of quadrupole-based instruments [49].

### 3.3.7 Detection system

After the separation of ions based on their *m/z* ratios, ions pass through the exit slit and impinge on the detector located at the end of the mass spectrometer. The aim of the detector is to detect the ions of interest, to amplify and convert the signal into a current form, suitable for data processing. In modern SF-ICP-MS instruments, secondary electron multipliers (SEM) and Faraday cups are the most commonly used detectors. Faraday cups are used mainly for the detection and quantification of high ion currents [50] in multi-collector SF-ICP-MS instruments for simultaneous detection of multiple ions, resulting in highly precise IR measurements. Nevertheless, single-collector SF-ICP-MS instruments also benefit from using Faraday cups in addition to the SEM, as is the case in the "*Element XR"* and "*AttoM"* (Nu Instruments Limited),

to increase the linear dynamic range of the instrument from 9 to 12 orders of magnitude. In contrast, a SEM is several orders of magnitude more sensitive than a Faraday cup [51] and is currently the most commonly used ion detector in single-collector SF-ICP-MS instrumentation. The principle of SEM operation (illustrated in Figure 3.15) is as follows: when reaching the SEM, each ion impinges on a conversion dynode releasing one or more secondary electrons. The secondary electrons are then accelerated due to a potential difference between the front end and the back end of the detector. These accelerated secondary electrons hit a second dynode releasing multiple electrons. This process is repeated at 12-24 dynodes resulting in a cascade or avalanche of $10^4$-$10^8$ secondary electrons, depending on the type and energy of the incident primary particle [5, 15, 51]. The dynodes are made of copper - beryllium (2 %) and silver - magnesium (2-4 %) alloys [51] with curved shapes (Figure 3.15) and their successive potential difference depends on the voltage applied to the multiplier [15]. A SEM can be operated in ion-counting (also called pulse-counting) mode for counting individual incoming pulses when signal intensities are low, but when the signal is high the analogue mode can be used where the intensity of a continuously variable current proportional to the number of incoming ions is measured. SEM detectors offer increased sensitivities by a factor of $10^5$-$10^8$ in comparison to Faraday cup detectors, plus a faster response time. Additionally, SEM detectors suffer from mass discrimination due to the increased speed of the lighter ions compared to heavier ions, and are subject to dead time (discussed in 3.2.4).

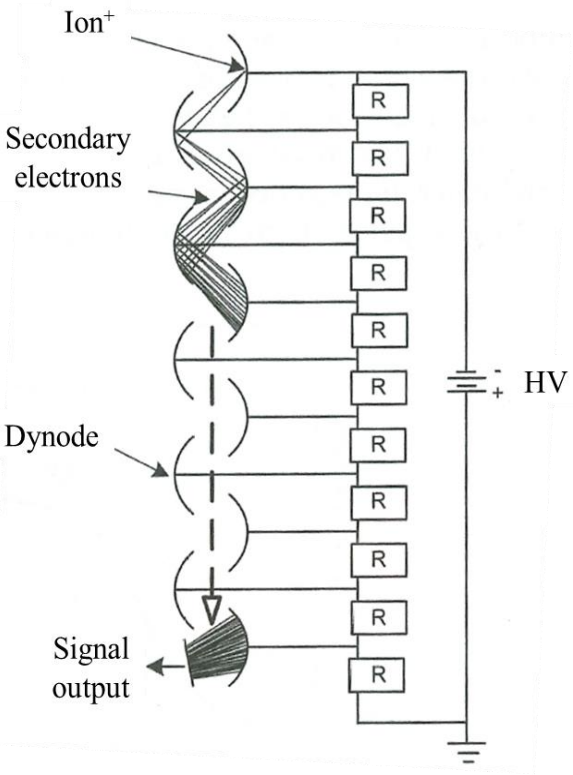


Figure 3.15 Schematic representation of SEM operation [15]

### 3.3.8 Vacuum system

The ion path in SF-ICP-MS is long, compared to that in quadrupole ICP-MS [15]. To prevent any collisions or interferences of the ion beam with air particles, the ion transfer optics system, mass separator, detector and all parts in between, are placed under high vacuum ($10^{-6}$ – $10^{-10}$ Pa) by using a differential pumping system. In the "*Element 2*", a rotary pump is connected to the interface region and is called the interface pump. The interface pump operates separately from the high-vacuum system and is switched off when the plasma is shut down. Directly behind the interface region, a slide valve is automatically closed when the plasma is shut down to maintain the high vacuum behind the slide valve. After the interface, four turbo pumps ensure high vacuum in the transfer lens and focusing system (two turbo pumps), the flight tube in the magnet (one turbo pump) and in the ESA and detector (one turbo pump).

### 3.4 Nuclear application of ICP-MS

Determining the nuclide-specific composition of a nuclear fuel is essential before, as well as after its irradiation in the nuclear reactor, for purposes of licensing, non-proliferation of nuclear material (safeguards), understanding reactor operation and nuclear waste management [52]. The nuclide-specific characterization of nuclear fuel that has been irradiated, spent nuclear fuel (SNF), requires accurate and precise IR measurements of uranium (U), plutonium (Pu) and neodymium (Nd), the last of which is used as a fission product (FP) monitor [52-53]. The determination of nuclide-specific concentrations of gadolinium (Gd) nuclides can also be of interest in the case of alternative/experimental fuels, such as gadolinium nuclear fuel in which Gd is included in the fuel assembly as a burnable neutron absorber to improve reactor performance [54]. As fuels used in nuclear power reactors contain high amounts of fissile material, this implies a high reactivity, especially at the beginning-of-life. This high reactivity can often not be compensated for solely by control rod insertion or the presence of boron in the primary coolant. The use of burnable poisons (e.g., Gd in the form of gadolinium oxide) located inside the fuel rods was proposed as a solution to this issue [54]. Such fuel rods are inserted in the fuel assembly at specific positions, and can have a Gd content up to 10 wt% and a U enrichment similar to that of the surrounding $UO_2$ fuel rods. The composition of the fuel depends mainly on the reactor type (light water, heavy water, etc). For example, for its use in a light water reactor, natural U (0.72% $^{235}U$) [52] is enriched in $^{235}U$ (3–5%) [52, 55]. During irradiation, U is partially consumed, thereby creating transuranium elements (mainly Pu) and FP, 40% of which consists of rare earth elements (REE) [55], including two-thirds of the lanthanide series - lanthanum (La) to erbium (Er) - with maximum yields for Nd and cerium (Ce) [55]. After irradiation, U accounts for 95.5% of the non-oxide mass [55]. Plutonium can be present in SNF either as a product of neutron capture by $^{238}U$ or it can have been added to the fuel prior to its irradiation [mixed oxide fuel (MOx)]. Reactor grade Pu is defined as material composed of more than 18% $^{240}Pu$ [55]. The relatively high neutron cross-section of $^{240}Pu$ limits its use in weapon-grade Pu, which contains at least 93 % $^{239}Pu$ [55]. To determine the Pu isotopic composition in SNF, measuring $^{238}Pu$, $^{239}Pu$, $^{240}Pu$, $^{241}Pu$, $^{242}Pu$, and $^{244}Pu$ is of interest due to their high abundance. There are different techniques in the nuclear analysis laboratory's "toolbox" which can be used independently or interchangeably for the analysis of spent nuclear fuel [52]. Alpha spectrometry has been used traditionally for determination of the Pu isotopes in SNF [52]. However it is incapable of resolving the energies of alpha-particles from $^{239}Pu$ and $^{240}Pu$, and it cannot measure $^{241}Pu$, which undergoes beta decay, thereby providing incomplete information only. Furthermore, long measurement times are often necessary because of the long half-life of the Pu isotopes, except for $^{238}Pu$. Alternatively, thermal ionization mass spectrometry (TIMS) is a well-known technique applied routinely to determine the Pu isotopic composition and content in SNF [56]. However, the sample preparation required for TIMS and the measurement itself are much more time-consuming than for inductively coupled plasma-mass spectrometry (ICP-MS). This led to an increasing application of ICP-MS for the determination of the nuclide-specific composition of SNF, instead of TIMS [52, 57]. The main advantages of ICP-MS lie in its broad elemental coverage, capability to measure ions of multiple elements per run, high sample throughput and relatively low purchase cost [57-58]. However, isobaric overlap must be eliminated for the accurate measurement of the isotopic

compositions of U, Pu and REE in SNF. The occurrence of notorious isobaric interferences, such as the overlap of the signals of $^{238}U^{+}$ and $^{238}Pu^{+}$ and of $^{142}Ce^{+}$ and $^{142}Nd^{+}$, and the formation of interfering polyatomic ions, such as $^{238}U_1H^{+}$ jeopardizing the accurate determination of $^{239}Pu^{+}$, hinder ICP-MS analysis, but can be eliminated by using HPIC prior to introduction of the sample into the mass spectrometer for the most time-efficient and safest characterization of SNF [59-61]. Other complicating factors in ICP-MS are the effects of inadequate abundance sensitivity (section 3.2.2 of this chapter) [58], the mass bias effect (section 3.2.3 of this chapter) [52], and detector dead time (section 3.2.4 of this chapter), all of which the user must take into account.

### 3.4.1 Nuclearization of a single-detector double-focusing SF-ICP-MS

This section provides technical information about the HPIC-SF-ICP-MS setup used in this work. Personnel of SCK CEN, including the mentor and co-promotor of this PhD project were involved in selecting the instruments, as well as in customizing, setting up and optimizing the technical parameters of the glovebox setup. On the other hand, the PhD student was in charge of operating, maintaining and troubleshooting the HPIC and SF-ICP-MS parts when needed. This included tasks such as changing Rheodyne valves placed inside the glovebox and re-installing the Chromeleon software on the computer controlling the HPIC parts. Pictures of the instrumental setup outside and inside the glovebox are shown in Figures 3.16 – 3.18. To accomplish this nuclearization of an "*Element 2*" coupled to an alpha-glovebox, many considerations had to be taken into account. Those considerations related to the instrument's characteristics will be discussed first, followed by the characteristics of the alpha-glovebox. For the nuclearized "*Element 2*", the interface region was elongated by the manufacturer (Thermo Fisher Scientific, Bremen, Germany) such that it can be physically fitted in the wall of the glovebox. A glovebox frame was provided to the manufacturer for the exact measurements and dimensions of the glovebox. The sample introduction system and the torch box had to be placed inside the glovebox due to the radioactive nature of the samples (due mainly to the presence of Pu in the samples). Since the interface of a nuclearized "*Element 2*" is longer than that in a regular "*Element 2*", the manufacturer suggested to use the longer extraction lens of a Neptune for the nuclearized "*Element 2*" in our laboratory. In order to make manipulation of the torch as convenient as possible inside the glovebox, the torch box was placed on a stainless steel rail mechanism which can be opened electronically by a switch on the outside of the glovebox (Figure 3.19). The switch regulates the Ar gas pressure (by means of electronic valves installed) on both sides of a piston to move the torch box either away from or closer to the interface. Additionally, the building's ventilation system did not provide a sufficient extraction flow rate (minimum 45 $m^3 \cdot h^{-1}$) from the torchbox, resulting in the inability to ignite the plasma in a closed glovebox. To make up for the 15-25 $m^3 \cdot h^{-1}$ extraction flowrate deficit, a Jacomex fan (model MKV 006-R, Figure 3.20) was purchased from TCPS (Rotselaar, Belgium) and connected in series with the extraction line of the glovebox at one end and to the building ventilation circuit at the other end. The fan is equipped with a regulator and can automatically and dynamically compensate for the extraction flowrate deficit, due to its coupling with an electronic box equipped with an alarm in case the exhaust airflow is below a preset value. The glovebox in which the torchbox is placed is equipped with a range of detectors capable of launching an

alarm signal, including a water sensor of which the alarm is activated if liquid deeper than 2 mm is detected inside the glovebox, and a temperature alarm if the temperature inside the glovebox exceeds 45°C. There is also a Dwyer photohelic® differential pressure meter that gives an alarm in case the underpressure inside the glovebox is outside of the preset limits (*i.e.* 30 and 40 mm water column). In response to an alarm or an electricity shutdown, magnetic valves in the $O_2$ and Ar supply lines, close automatically for safety reasons. Having made all the above mentioned adjustments, the nuclearized "*Element 2*" SF-ICP-MS can be safely operated alone or in hyphenation with HPIC, which was done in this work. More details on the hyphenated setup will be given in the next chapter.

Figure 3.16 "*Element 2*" glovebox setup

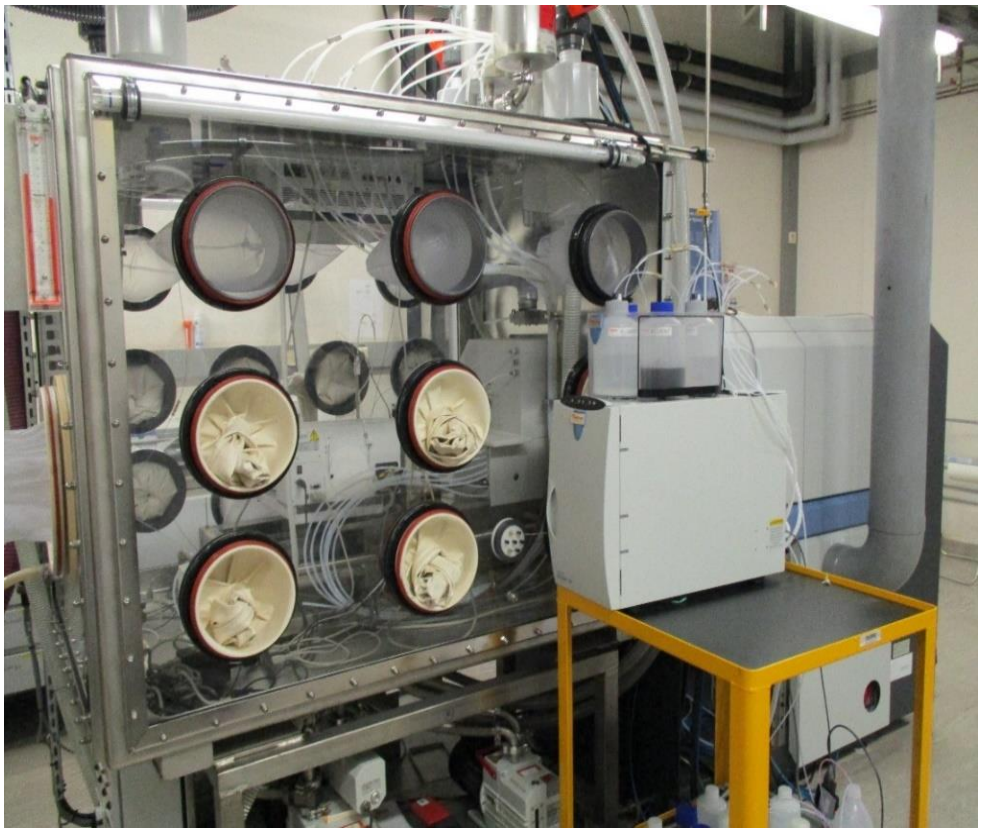

Figure 3.17 HPIC setup at the side of glovebox

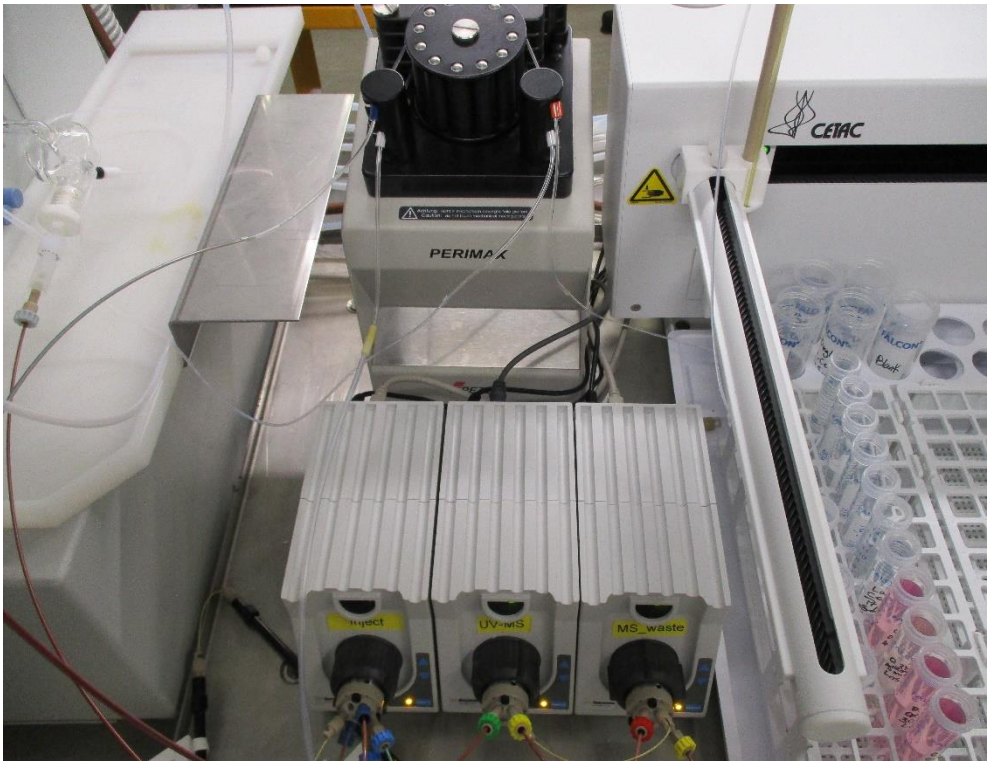


Figure 3.18 Instrumental setup inside the glovebox

Figure 3.19 Electronic box under the glovebox

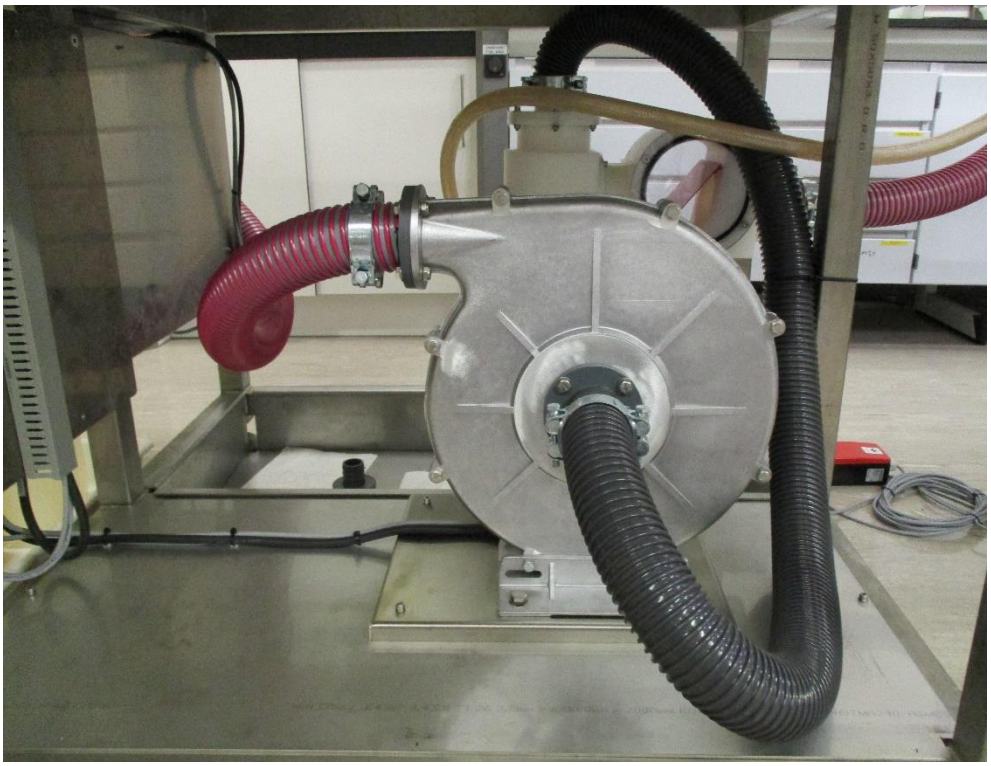

Figure 3.20 External fan

## 3.5 References


[1] J. S. Becker, "Inorganic mass spectrometry of radionuclides," in *Handbook of radioactivity analysis*, 3rd edition 2012 ed., Elsevier, 2012, pp. 833-870.

[2] J. J. Thompson and R. S. Houk, "Inductively coupled plasma mass spectrometric detection for multielement flow injection analysis and elemental speciation by reversed phase liquid chromatography," *Analytical Chemistry,* vol. 58, pp. 2541-2548, 1986.

[3] D. Beauchemin, K. Siu, J. W. McLaren and S. S. Berman, "Determination of arsenic species by high-performance liquid chromatography-inductively coupled plasma mass spectrometry," *Journal of Analytical and Atomic Spectrometry,* vol. 4, pp. 285-289, 1989.

[4] K. K. Murray, R. K. Boyd, M. N. Eberlin, G. J. Langley, L. Li and Y. Naito, "Definitions of terms relating to mass spectrometry (IUPAC recommendations 2013)," *Pure Applied Chemistry,* vol. 85, no. 7, pp. 1515-1609, 2013.

[5] F. Vanhaecke, "Single-collector inductively coupled plasma mass spectrometry," in *Isotopic analysis: Fundamentals and applications using ICP-MS*, Wiley-VCH Verlag & Co. KGaA, 2012, pp. 31-76.

[6] C. B. Douthitt, "The evolution and applications of multicollector ICPMS (MC-ICPMS)," *Analytical and Bioanalytical Chemistry,* vol. 390, pp. 437-440, 2008.

[7] K. Newman, P. A. Freedman, J. Williams, N. S. Belshaw and A. N. Halliday, "High sensitivity skimmers and non-linear mass dependent fractionation in ICP-MS," *Journal of Analytical and Atomic Spectrometry,* vol. 24, pp. 742-751, 2009.

[8] L. Yang, S. Tong, L. Zhou, Z. Hu, Z. Mester and J. Meija, "A critical review on isotopic fractionation correction methods for accurate isotope amount ratio measurements by MC-ICP-MS," *Journal of Analytical and Atomic Spectrometry,* vol. 33, pp. 1849-1861, 2018.

[9] F. Vanhaecke and K. Kyser, "The isotopic composition of the elements," in *Isotopic analysis: fundamentals and applications using ICP-MS*, Wiley-VCH Verlag GmbH & Co. KGaA, 2012, pp. 1-30.

[10] K. G. Heumann, J. Vogl, G. Rädlinger and J. Vogl, "Precision and accuracy in isotope ratio measurements by plasma source mass spectrometry," *Journal of Analytical Atomic Spectrometry,* vol. 13, pp. 1001-1008, 1998.

[11] C. R. Quétel, J. Volg, T. Prohaska and S. Nelms, "Comparative performance study of ICP-MS mass spectrometers by means of U "isotopic measurements"," *Journal of Analytical Chemistry,* vol. 368, pp. 148-155, 2000.

[12] W. A. Russell, D. A. Papanastassiou and T. A. Tombrello, "Ca isotope fractionation on the Earth and other Solar System materials," *Geochimica et Cosmochimica Acta,* vol. 42, pp. 1075-1090, 1978.

[13] J. Irregeher, J. Vogl, J. Santner and T. Prohaska, “Measurement strategies,” in *Sector field mass spectrometry for elemental and isotopic analysis*, The Royal Society of Chemistry, 2015, pp. 126-151.

[14] J. Meija, L. Yang, Z. Mester and R. E. Sturgeon, “Correction of instrumental mass discrimination for isotope ratio determination with multi-collector inductively coupled plasma mass spectrometry,” in *Isotopic analysis*, Wiley-VCH Verlag GmbH & Co. KGaA, 2012, pp. 113-137.

[15] L. Rottmann, N. Jakubowski, S. Konegger-Kappel, O. Hanousek and T. Prohaska, “Technical Background,” in *Sector field mass spectrometry for elemental and isotopic analysis*, The Royal Society of Chemistry, 2015, pp. 44-96.

[16] G. I. Russ, “Isotope ratio measurements using ICP-MS,” in *Applications of Inductively Coupled Plasma Mass Spectrometry (eds. A.R. Date and A.L. Gray)*, London, Chapman and Hall, pp. 90-114.

[17] A. Held and P. D. Taylor, “A calculation method based on isotope ratios for the determination of dead time and its uncertainty in ICP-MS and application of the method to investigating some features of a continuous dynode multiplier,” *Journal of Atomic and Analytical Chemistry*, vol. 14, pp. 1075-1079, 1999.

[18] P. K. Appelblad and D. C. Baxter, “A model for calculating dead time and mass discrimination correction factors from inductively coupled plasma mass spectrometry calibration curves,” *Journal of Analytical and Atomic Spectrometry,* vol. 15, pp. 557-560, 2000.

[19] F. Vanhaecke, G. de Wannemacker, L. Moens, R. Dams, C. Latkoczy, T. Prohaska and G. Stingeder, “Dependence of detector dead time on analyte mass number in inductively coupled plasma mass spectrometry,” *Journal of Analytical Atomic Spectrometry,* vol. 13, pp. 567-571, 1998.

[20] amc, “Standard additions: myth and reality AMCTB No 37,” March 2009.

[21] T. J. Quinn, “Primary methods of measurement and primary standards,” *Metrologia*, vol. 34, pp. 61 - 65, 1997.

[22] L. Yang and R. E. Sturgeon, “High accuracy and precision isotope dilution mass spectrometry: An application to the determination of Mo in seawater,” *Journal of Analytical Atomic Spectrometry,* vol. 24, pp. 1327 - 1335, 2009.

[23] K. Heumann, “Determination of trace elements and elemental species using isotope dilution inductively coupled plasma mass spectrometry,” in *Isotopic analysis: fundamentals and applications using ICP-MS*, Wiley, 2012, pp. 189-233.

[24] P. Rodriguez-Gonzalez and J. Ignacio Garcia Alonso, “Mass Spectrometry: Isotope dilution mass spectrometry,” in *Encyclopaedia of analytical science*, vol. 6, Elsevier, 2019.

[25] F. Vanhaecke, L. Balcaen and P. Taylor, “Use of ICP-MS for isotope ratio measurements,” in *Inductively coupled plasma spectrometry and its applications*, Blackwell Publishing Ltd, 2007, pp. 160-225.

[26] J. Ignacio Garcia Alonso and P. Rodriguez-Gonzalez, Isotope Dilution Mass Spectrometry, The Royal Society of Chemistry, 2013.

[27] E. Pagliano, Z. Mester and J. Meija, “Reduction of measurement uncertainty by experimental design in high-order (double, triple, and quadruple) isotope dilution mass spectrometry: application to GC-MS measurement of bromide,” *Analytical and Biochemistry,* vol. 405, pp. 2879 - 2887, 2013.

[28] P. Rodriguez-Gonzalez, J. Manuel Merchante-Gayon, J. Ignacio Garcia Alonso and A. Sanz-Medel, “Isotope dilution analysis for elemental speciation: A tutorial review,” *Spectrochimica Acta Part B,* vol. 60, pp. 151 - 207, 2005.

[29] R. F. Browner and A. W. Boorn, “Sample introduction: the Achilles' heel of atomic spectroscopy?,” *Analytical Chemistry,* vol. 56, no. 7, pp. 786A-798A, 1984.

[30] T. Prohaska, “General overview,” in *Sector field mass spectrometry for elemental and isotopic analysis*, The Royal Society of Chemistry, 2015, pp. 29-43.

[31] C. B'Hymer and J. A. Caruso, “Nebulizer sample introduction for elemental speciation,” in *Comprehensive analytical chemistry*, Elsevier, 2000, pp. 213-226.

[32] K. Inagaki, S.-i. Fujii, A. Takatsu and K. Chiba, “High performance concentric nebulizer for low-flow rate liquid sample introduction to ICP-MS,” *Journal of Analytical Atomic Spectrometry,* vol. 26, pp. 623-630, 2011.

[33] P. Gaines, “Sample introduction for ICP-MS and ICP-OES,” *Spectroscopy solutions for materials analysis,* January 2005.

[34] G. Schaldach, L. Berger, I. Razilov and H. Berndt, “Characterization of a double-pass spray chamber for ICP spectrometry by computer simulation (CFD),” *Spectrochimica Acta B,* vol. 57, pp. 1505-1520, 2002.

[35] G. Schaldach, L. Berger, I. Razilov and H. Berndt, “Characterization of a cyclone spray chamber for ICP spectrometry by computer simulation,” *Journal of Analytical and Atomic Spectrometry,* vol. 17, pp. 334-344, 2002.

[36] R. S. Olofsson, I. Rodushkin and M. D. Axelsson, “Performance characteristics of a tandem spray chamber arrangement in double focusing sector field ICP-MS,” *Journal of Analytical and Atomic Spectrometry,* vol. 15, pp. 727-729, 2000.

[37] J. Garcia-Bellido, L. Freije-Carrelo, M. Moldovan and J. R. Encinar, “Recent advances in GC-ICP-MS: Focus on the current and future impact of MS/MS technology,” *Trends in Analytical Chemistry,* 2020.

[38] G. Alvarez-Llamas, M. del Rosario Fernandez de laCampa and A. Sanz-Medel, “ICP-MS for specific detection in capillary electrophoresis,” *Trends in Analytical Chemistry,* vol. 24, pp. 28-36, 2005.

[39] A. Montaser and H. Zhang, “Mass spectrometry with mixed-gas and Helium ICPs,” in *Inductively coupled plasma mass spectrometry*, Wiley-VCH Inc., 1998, pp. 809-890.

[40] C. B. Boss and K. J. Fredeen, Concepts, instrumentation and techniques in inductively coupled plasma optical emission spectrometry, USA: PerkinElmer, Inc., 2004.

[41] J. Košler and P. Sylvester, “Present trends and the future of Zircon in geochronology: Laser ablation ICPMS,” *Rev Mineral Geochem,* vol. 53, pp. 243-275, 2003.

[42] R. Thomas, Practical guide to ICP-MS, Marcel Dekker, Inc., 2004.

[43] G. O'Connor and E. H. Evans, “Fundamental aspects of inductively coupled plasma - mass spectrometry (ICP-MS),” in *Inductively coupled plasma spectrometry and its applications*, Blackwell Publishing Ltd, 2007, pp. 134-159.

[44] N. Jakubowski, M. Horsky, P. H. Roos, F. Vanhaecke and T. Prohaska, “Inductively coupled plasma mass spectrometry,” in *Sector field mass spectrometry for elemental and isotopic analysis*, The Royal Society of Chemistry, 2015, pp. 208-318.

[45] E. G. N. Johnson and O. Alfred, *Physics Reviews,* vol. 91, pp. 10-17, 1953.

[46] N. Jakubowski, T. Prohaska, L. Rottmann and F. Vanhaecke, “Inductively coupled plasma- and glow discharge plasma-sector field mass spectrometry,” *Journal of Analytical and Atomic Spectrometry,* vol. 26, pp. 693-726, 2011.

[47] P. R. R. Mason, K. Kaspers and M. J. Van Bergen, “Determination of sulfur isotope ratios and concentrations in water samples using ICP-MS incorporating hexapole ion optics,” *Journal of Analytical Atomic Spectrometry,* vol. 14, pp. 1067-1074, 1999.

[48] N. Jakubowski, L. Moens and F. Vanhaecke, “Sector field mass spectrometers in ICP-MS,” *Spectrochimica Acta Part B,* vol. 53, pp. 1739-1763, 1998.

[49] D. L. Miles and J. M. Cook, “Geological applications of plasma spectrometry,” in *Inductively coupled plasma spectrometry and its applications*, Blackwell Publishing Ltd., 2007, pp. 277-337.

[50] M. Rehkämper, M. Schönbächler and C. H. Stirling, “Multiple collector ICP-MS: Introduction to instrumentation, measurement techniques and analytical capabilities,” *Geostandards Newsletter,* vol. 25, pp. 23-40, 2001.

[51] J. S. Becker, Inorganic mass spectrometry: Principles and applications, John Wiley & Sons, Ltd., 2007.

[52] S. C. Szechenyi and M. Ketterer, “Nuclear Applications,” in *Isotopic analysis: Fundamentals and applications using ICP-MS*, Wiley, 2012, pp. 419-432.

[53] ASTM, “Standard test method for atom percent fission in uranium and plutonium fuel (Neodymium-148 Method),” ASTM International, West Conshohocken, 2012.

[54] IAEA, “Characteristics and use of Urania-Gadolinia fuels,” IAEA, Vienna, 1995.

[55] K. L. Nash and J. C. Barley, Chemistry of radioactive materials in the nuclear fuel cycle, Woodhead publishing limited, 2011.

[56] S. K. Aggarwal, S. Kumar, M. K. Saxena, P. M. Shah and H. Chand Jain, “Investigations for isobaric interference of 238Pu at 238U during thermal ionization mass spectrometry of uranium and plutonium from the same filament loading,” *International Journal of Mass Spectrometry and Ion Processes,* vol. 151, pp. 127 - 135, 1995.

[57] J. S. Becker, “Mass spectrometry of long-lived radionuclides,” *Spectrochimica Acta Part B,* vol. 58, pp. 1757 - 1784, 2003.

[58] M. E. Ketterer and S. C. Szechenyi, “Determination of plutonium and other transuranic elements by inductively coupled plasma mass spectrometry: A historical perspective and new frontiers in the environmental sciences,” *Spectrochimica Acta Part B,* vol. 63, pp. 719 - 737, 2008.

[59] I. Gunther-Leopold, J. Waldis, B. Wernli and Z. Kopajtic, “Measurement of Plutonium isotope ratios in nuclear fuel samples by HPLC-MC-ICP-MS,” *International Journal of Mass Spectrometry,* vol. 242, pp. 197-202, 2005.

[60] J. Barrero Moreno, M. Betti and J. Garcia Alonso, “Determination of neptunium and plutonium in the presence of high concentrations of uranium by ion chromatography-inductively coupled plasma mass spectrometry,” *Journal of Analytical Atomic spectrometry,* vol. 12, pp. 355-361, 1997.

[61] S. Bera, R. Balasubramanian, Arpita Datta, R. Sajimol, S. Nalini, T. S. Lakshmi Narasimhan, M. P. Antony, N. Sivaraman, K. Nagarajan and P. R. Vasudeva Rao, “Burn-Up Measurements on Dissolver Solution of Mixed Oxide Fuel Using HPLC-Mass Spectrometric Method,” *International Journal of Analytical Mass Spectrometry and Chromatography,* vol. 1, pp. 55-60, 2013.

# Chapter 4 – HPIC-SF-ICP-MS separation method development and validation

This chapter describes the work related to the first objective of this PhD: the development and validation of a separation method for the lanthanides, uranium and plutonium using HPIC-SF-ICP-MS for the characterization of SNF and environmental soil samples. The separation method was developed using samples made from mixing mono-elemental standards, whereas the method validation was performed on real SNF and environmental soil samples. Isotope ratios (IRs) were not evaluated during the separation method development and validation. Portions of this chapter have been taken from a previous publication in volume 1617 of the peer-reviewed Journal of chromatography A (impact factor 4.049 in 2019) [1].

## 4.1 Introduction

The aim of this step of the work is to separate the target elements (plutonium, uranium, neodymium and gadolinium) from each other in order to quantify them and their corresponding nuclides in the following step. To perform the separation safely and precisely, HPIC was chosen over gravitational ion chromatography. The gravitational ion chromatographic separation of the lanthanides is notorious for the time it takes (up to 2 weeks) and hence its labour intensiveness, the dose rate the operator is exposed to (up to 2 $mSv \cdot h^{-1}$) and the increased risk of radioactive contamination of the separation. Additionally, the samples used for HPIC-SF-ICP-MS are diluted 100-fold more (less than 20 µg of SNF and a uranium mass fraction of 1.6 $\mu g \cdot g^{-1}$ were needed for the HPIC-SF-ICP-MS analysis) than the ones used for gravitational ion chromatography followed by thermal ionization mass spectrometry & alpha-spectrometry (2 mg of SNF and a uranium mass fraction of 160 $\mu g \cdot g^{-1}$ were needed). Therefore, the dose rate measured for the samples to be handled by the operator using HPIC-SF-ICP-MS for SNF analysis, is as low as the dosimeters can measure (< 1.15 $\mu Sv \cdot h^{-1}$). Moreover, a higher dilution can be made in the hot cell for HPIC separation to keep the radiation risk to a minimum. For HPIC-SF-ICP-MS, the minimum volume needed for one injection of a sample was 0.5 mL of which 25 µL were injected onto the column.

In previous studies, HPIC has been coupled to quadrupole-based and to multi-collector sector field ICP-MS instruments (as was shown in Table 2.1 of chapter 2) to determine IRs based on transient signals of analytes eluting from the different types of ion exchange columns. However, no previous study has investigated the coupling of HPIC to a single-collector SF-ICP-MS instrument to study lanthanides and actinides in various sample matrices. Nevertheless, the use of a single-collector sector field instrument can be advantageous for applications that require high sensitivity, but are less demanding in terms of IR precision (more details in chapter 3). A SF-ICP-MS unit offers a substantially higher sensitivity than does a MC- ICP-MS instrument, because it uses an electron multiplier for ion detection, while MC-ICP-MS uses Faraday collectors for this purpose. As a result, the concentrations of radionuclides in the samples to be

measured by SF-ICP-MS can be much lower than those required for measurement by MC-ICP-MS. The purchase cost of a SF-ICP-MS instrument is also considerably lower (2 to 3-fold) than that for MC-ICP-MS instrumentation [2]. Another advantage of SF-ICP-MS over MC-ICP-MS is the higher number of nuclides that can be monitored in one injection or measurement method. Although the analyte nuclides are not monitored simultaneously, the single detector of a SF-ICP-MS instrument is not as limited by a certain mass range and maximum number of isotopes that can be monitored, as is the case for a MC-ICP-MS instrument, in which the (custom) detector configuration determines the maximum number and mass range of isotopes that can be monitored simultaneously. Modern quadrupole ICP-MS instruments also offer high sensitivity in different matrices, but their compact design and small size render handling and maintenance inconvenient after their nuclearization in a glovebox. The size, thickness and flexibility of the gloves worn when working with the glovebox combined with the very restricted access to the small instrumental components (of a quadrupole instrument) make any maintenance work (especially manipulating tools and screws) to be performed on a nuclearized quadrupole ICP-MS challenging. In addition, the flat-top peaks obtainable with SF-ICP-MS (at low mass resolution and even at medium mass resolution with an exit slit wider than the entrance slit [3]) result in better IR precisions than those attainable with quadrupole-based ICP-MS [2, 4] (see section 3.2.2 of chapter 3). These flat-top peaks are a characteristic of the mass spectrometer design, and, when measuring in low resolution mode, this holds true whether measuring off-line or on-line. Therefore, the coupling of HPIC to SF-ICP-MS to measure radionuclides offers a fit-for-purpose precision and sensitivity.

With this in mind, the objective of the current chapter does not involve measurement IRs, but is strictly focused on the separation of lanthanides, uranium and plutonium in different sample matrices and the quantification of concentrations of neodymium, gadolinium, uranium and plutonium nuclides from transient signals using external calibration.

## 4.2 Methods

### 4.2.1 Setup timings

A schematic representation of the HPIC-SF-ICP-MS setup, which was described in section 2.4.1 of chapter 2, is shown in Figure 4.1, where the blue rectangle represents the glovebox outline. Due to the unusually long distance between pump and injector in the setup, it takes a long time for the eluent to reach the column, and thus it was important to determine experimentally the time needed for the eluent to reach the different components (columns and detector) before developing the separation method. The time needed for the eluent to reach the inlet of the guard column was determined using a coloured Arsenazo III solution and a chronometer, with the tubing disconnected from the column. In contrast, the time needed for the eluent to reach the ICP-MS detector could be determined visually by a shift in the baseline of the chromatograms.

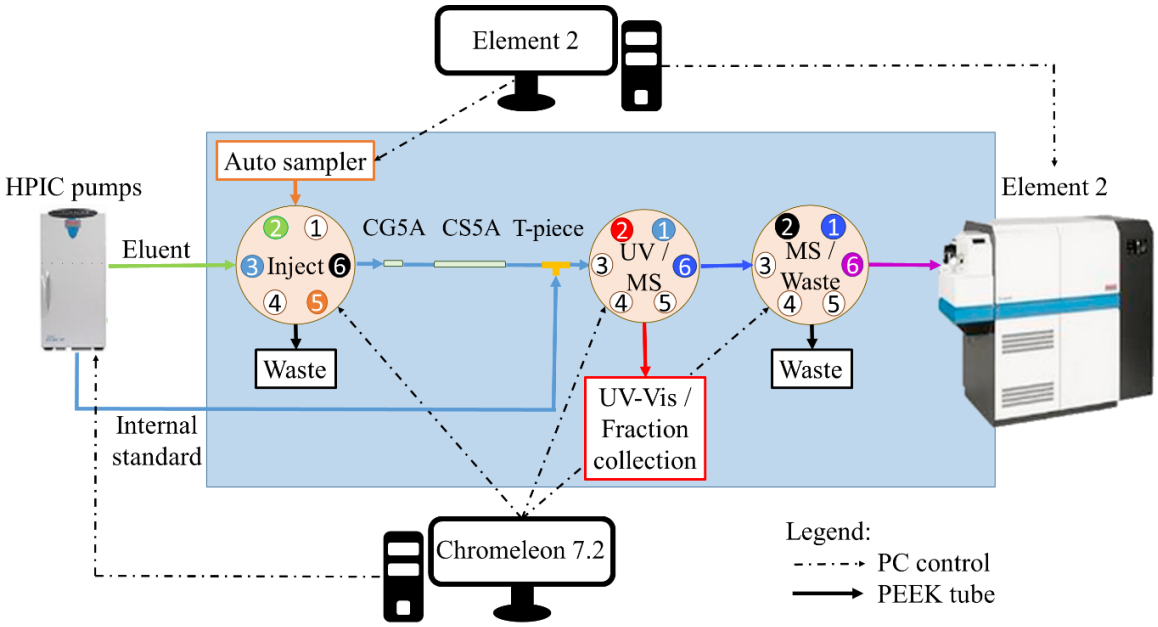


Figure 4.1 Schematic representation of the HPIC-SF-ICP-MS setup (the blue opaque rectangle represents the glovebox outline)

### 4.2.2 SF-ICP-MS acquisition parameters

The SF-ICP-MS parameters used during the development and validation of the separation method are presented in Table 4.1.

Table 4.1 SF-ICP-MS parameters during the separation method development and validation

| Parameter | Value / Description |
|---|---|
| Mass resolution | 400 |
| Scan optimization | Speed |
| Scan type | E-Scan |
| RF power | 1250 W |
| Detector dead time | 17 ns |
| Runs | 450 |
| Passes | 1 |
| Dwell time per nuclide | 10 ms |
| Mass window | 150 % |
| Integration window | 40 % |
| Cool gas flowrate | 16 $L \cdot min^{-1}$ |
| Auxiliary gas flowrate | 0.8 $L \cdot min^{-1}$ |
| Nebulizer gas flowrate | 1.06 $L \cdot min^{-1}$ |
| Internal standard | $^{205}Tl$ in 0.75 M $HNO_3$ |
| Nuclides monitored | $^{139}La$, $^{140}Ce$, $^{141}Pr$, $^{142}Nd$, $^{143}Nd$, $^{144}Nd$, $^{145}Nd$, $^{146}Nd$, $^{148}Nd$, $^{150}Nd$, $^{147}Sm$, $^{152}Sm$, $^{153}Eu$, $^{155}Gd$, $^{156}Gd$, $^{157}Gd$, $^{158}Gd$, $^{160}Gd$, $^{175}Lu$, $^{205}Tl$, $^{235}U$, $^{238}U$, $^{239}Pu$, $^{240}Pu$, $^{241}Pu$, $^{242}Pu$, $^{244}Pu$ |
| Used magnet masses (u) | 139.905, 151.919, 234.040 & 238.049 |

### 4.2.3 HPIC-SF-ICP-MS separation method development

#### 4.2.3.1 Separation of lanthanides

First, standard solutions (mixtures of Spex single-element standards diluted to 2.5 $\mu g \cdot L^{-1}$ for each element) covering the full mass range of the lanthanides (La, Ce, Pr, Nd, Sm, Eu, Gd and Lu) were injected onto the column. A gradient elution using a mobile phase with an oxalic acid concentration ranging from 0.1 to 0.15 M oxalic acid buffered to pH 4.5 with $NH_4OH$ was used to separate these lanthanides within the shortest possible run time. This gradient elution program is the same as the oxalic acid gradient presented in the overall elution method presented in Table 4.2. Peak resolutions ($R_s$) and the separation factors ($\alpha$), both of which were calculated following IUPAC recommendations [5], were used to assess the separation of the peaks.

#### 4.2.3.2 Separation of uranium and lanthanides

Subsequently, U was also included in the synthetic solutions (2.5 $\mu g \cdot L^{-1}$) and different eluents were tested for their ability to elute U before or after the lanthanides without disturbing the lanthanide separation. Different molarities of HCl (0.5 and 1 M), as well as 0.1 M oxalic acid buffered to a pH of 0.6 by addition of concentrated HCl, were tested for eluting U from the column, either before or after lanthanide elution. Speciation of the lanthanides and U under the different circumstances was predicted using Hydra/Medusa simulations.

#### 4.2.3.3 Separation of plutonium, uranium and lanthanides

Finally, $^{242}Pu$ was also included in the synthetic mixtures of U and lanthanides in order to optimize the HPIC-SF-ICP-MS method for separation and quantification of Pu, U, Nd and Gd within a single injection. This step was addressed as follows: Oxidation of plutonium. Pu (2.5 $\mu g \cdot L^{-1}$) was oxidized to Pu(VI) in 40 nM $KMnO_4$ 12 hours prior to injection onto the column. The influence of temperature and concentration of nitric acid on the Pu(VI) peak position and width was investigated.

The elution of Pu from the column, after oxidation with $KMnO_4$ at room temperature, was investigated for different concentrations of nitric acid (0.4, 0.6, 0.8 and 1 M) and for 0.1 M oxalic acid at pH 4.5. In the final method including the determination of Pu, U and lanthanides, elution commenced with 1 M nitric acid, followed by a gradient of nitric acid - water and 0.1–0.15 M oxalic acid at pH 4.5, as is shown in Table 4.2. The columns were washed and conditioned with 1 M nitric acid at the end of each run to re-equilibrate the column before the next injection and to prevent any U & Pu cross-contamination.

Table 4.2 HPIC elution program for the separation of plutonium, uranium and the lanthanides

| Total run time range (min) | 1 M $HNO_3$ (%) | Water (%) | 0.1 M oxalic acid pH 4.5 (%) | 0.3 M oxalic acid pH 4.5 (%) | Rate of variation (%·min$^{-1}$) |
|---|---|---|---|---|---|
| 0-5 | 100-75 | 0 | 0 | 0 | 5 |
| 5-15 | 0 | 100 | 0 | 0 | 0 |
| 15-25 | 0 | 0 | 100 | 0 | 0 |
| 25-29 | 0 | 0 | 100-85 | 0-15 | 1.5 |
| 29-39 | 0 | 0 | 85-75 | 15-25 | 1 |
| 39-49 | 100 | 0 | 0 | 0 | 0 |

### 4.2.4 HPIC-SF-ICP-MS separation method validation

Once the HPIC-SF-ICP-MS separation method had been optimized, its analytical figures of merit were determined.

#### 4.2.4.1 Linearity

Six different concentrations in the working range of each element of interest (Nd, Gd, U and Pu) were injected onto the column consecutively and were eluted using their respective mobile phase within the overall gradient elution program. Each data point of the monitored nuclides was then normalized versus the concomitant data point for the $^{205}$Tl internal standard (see section 3.2.6.4) using an Excel macro. The normalized data points were then fitted to a Gaussian model, using OriginLab, and the peak area under each curve was integrated and plotted versus the respective injected nuclide-specific concentration. The linear regression curves based on the calibration points of each nuclide of Nd, Gd, U and Pu monitored were inspected in terms of their regression coefficient ($R^2 > 0.9995$) and residuals.

#### 4.2.4.2 Repeatability and intermediate precision

Repeatability of the injections was investigated on the same day (6 injections) and over a one-month period for each element using its corresponding eluent. The average retention times of the major isotopes of each element and their 2SD standard deviations were used to assess method repeatability.

#### 4.2.4.3 Limit of detection (LOD) & Limit of quantification (LOQ)

The limit of detection for each isotope of Nd, Gd, U and Pu monitored (Table 4.1) was determined based on eq. 4.1 [6]. The blank equivalent concentration BEC (µg·L$^{-1}$) was obtained by dividing the intercept by the slope using the LINEST function in Excel.

$$LOD = BEC + 3SD_{blank} \quad \text{(eq. 4.1)}$$

In this equation, SD blank indicates the standard deviation of the blank concentration over 6 injections due to the limited number of blank injections performed. Moreover, the LOQ was derived from the LOD as shown in eq. 4.2 [6].

$$LOQ = 3.3LOD \quad \text{(eq. 4.2)}$$

The nuclide-specific LOD and LOQ obtained as mass concentrations in the samples injected were then converted to masses by multiplying with the volume of the sample injected.

### 4.2.5 Other matrices

#### 4.2.5.1 Spent nuclear fuel matrix

A sample of an irradiated gadolinium nuclear fuel diluted in 1 M $HNO_3$ was available in-house. This sample was diluted further to a uranium concentration of 500 $\mu g \cdot L^{-1}$, and spiked with 2.5 $\mu g \cdot L^{-1}$ of La, Ce, Pr, Sm, Eu, Lu (to cover the full range of lanthanides and be certain that all lanthanides elute from the column) and 10 $\mu g \cdot L^{-1}$ of Nd. This solution generated peaks (i.e. transient ICP-MS signals) with sufficiently high intensities to demonstrate the chromatographic separation of these elements. $KMnO_4$ was added to the sample as explained in section 4.2.3.3 of chapter 4. The concentrations of Nd and Gd nuclides were determined by first integrating their respective peak areas from their transient signals, which were normalized against the transient signal of the $^{205}Tl$ internal standard (see section 3.2.6.4), and then by interpolating their respective concentrations from external calibration curves established for each nuclide (*i*) (eq. 4.3). For Nd nuclides, the spiked concentration was subtracted from the concentration determined based on the peak area from eq. 4.3. The concentrations of Nd and Gd nuclides were then compared to those obtained previously by means of thermal ionization mass spectrometry (TIMS).

$$concentration_i = peak\ area_i \cdot calibration\ curve\ slope_i \quad \text{(eq. 4.3)}$$

#### 4.2.5.2 Environmental soil matrix

The applicability of the final separation method to environmental samples was verified by analysing a reference material (IAEA-375 certified soil standard). Sample preparation consisted of microwave-assisted acid digestion (Synergy SP-D, CEM) of 0.5 g of IAEA-375 at 175 °C for 10 min in 3 mL of concentrated hydrofluoric acid, 7 mL of concentrated nitric acid and 3 mL of concentrated hydrogen peroxide. The sample was then evaporated to dryness on a hotplate, after which the residue was dissolved in 10 mL of 0.3 M nitric acid and additionally spiked with 2.5 $\mu g \cdot L^{-1}$ of $^{242}Pu$. The concentrations of $^{242}Pu$ and of $^{238}U$ in the sample were then determined using external calibration, and compared with the calculated concentration of spiked $^{242}Pu$ and the recommended value for $^{238}U$ on the IAEA-375 certificate.

## 4.3 Results and discussion

### 4.3.1 Setup timings

It was found that, at a flowrate of 0.125 $mL \cdot min^{-1}$, it takes the eluent 3.1 minutes to reach the inlet of the guard column and 9.2 minutes in total to reach the ICP-MS detector after passing through the column. The latter time is deduced from the higher background in the HPIC-SF-

ICP-MS chromatograms when the eluent is changed from water to oxalic acid. Therefore, any change in the eluent composition will only be detected after 9.2 minutes.

### 4.3.2 HPIC-SF-ICP-MS separation method development

#### 4.3.2.1 Separation of lanthanides

Using a gradient of oxalic acid concentrations from 0.1 to 0.15 M at a pH of 4.5 resulted in the lanthanides eluting from the column in the order La to Lu (Figure 4.2), with a resolution ($R_s$) > 0.7 and a separation factor ($\alpha$) > 1.1, as shown in Table 4.3. This separation permits quality assurance of burn-up determination by investigating results obtained using lanthanides used as burn-up monitors other than $^{148}$Nd, including $^{139}$La, $^{144}$Ce, $^{143+144}$Nd, $^{145+146}$Nd and $^{150}$Nd.

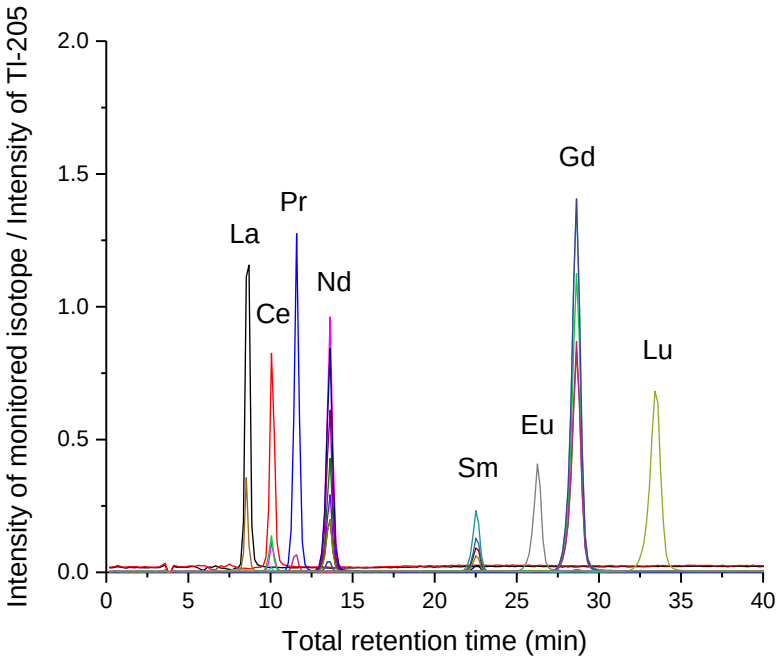


Figure 4.2 HPIC-SF-ICP-MS chromatogram of the separation of lanthanides (different colours refer to different monitored masses)

Table 4.3 Peak resolutions and separation factors of the lanthanides determined according to IUPAC recommendations [5] from three injections of a synthetic mixture of mono-elemental standards

| Element | Retention time range (min) | Average retention time (min) (RSD %) | Peak resolution ($R_s$) | Separation factor ($\alpha$) |
|---|---|---|---|---|
| La | 8.6 – 8.9 | 8.7 (1.4) | 1.0 | 1.2 |
| Ce | 10.1 | 10.1 (0.2) | 0.7 | 1.1 |
| Pr | 11.4 – 11.6 | 11.6 (1.1) | 1.0 | 1.2 |
| Nd | 13.2 – 13.8 | 13.5 (2.3) | 4.4 | 1.6 |
| Sm | 21.3 - 22.9 | 22.2 (3.8) | 1.4 | 1.2 |
| Eu | 24.6 - 26.4 | 25.8 (4.0) | 1.0 | 1.1 |
| Gd | 27.6 - 28.6 | 28.3 (2.0) | 1.5 | 1.1 |
| Lu | 31.0 - 33.4 | 32.1 (3.8) | - | - |

Lanthanides exist in solution as trivalent ions, with almost identical chemical properties, which makes their separation based solely on the selectivity of the ion exchanger challenging [4, 7]. However, the use of a complexing agent, such as oxalate [4, 8-11], permits the separation of lanthanide oxalate complexes based on their different stability constants by means of anion exchange chromatography [7].

Oxalic acid is the simplest dicarboxylic acid, has the chemical formula $C_2O_4H_2$ and the structural formula as shown in Figure 4.3 below. The dissociation of the diprotonated oxalic acid into its conjugate base form (the oxalate anion $C_2O_4^{2-}$) occurs following eq. 4.4 and 4.5 below.

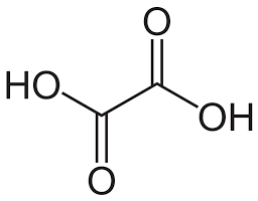


Figure 4.3 Structural formula of oxalic acid ($C_2O_4H_2$)

$$C_2O_4H_2 \rightleftarrows C_2O_4H^- + H^+ \ (\mathrm{pKa_1} = 1.23) \qquad \text{(eq. 4.4)}$$

$$C_2O_4H^- \rightleftarrows {C_2O_4}^{2-} + H^+ \ (\mathrm{pKa_2} = 4.19) \qquad \text{(eq. 4.5)}$$

At a pH of 4.5, oxalic acid (acid dissociation constant $pKa_2 = 4.19$) is highly dissociated (eq. 4.5) into its conjugate base form, which causes extensive complex formation ($Ln(C_2O_4)_3^{3-}$ [12]) with the trivalent lanthanides (eq. 4.6). The lanthanides were found to elute in the increasing order of their stability constants ($\log\beta_3$) with oxalate (10.3 to 13.4), *i.e.* from La to Lu,. The stability constants of the smaller (thus heavier) lanthanides are larger due to their higher charge density, which is caused by the decrease in ionic radius along the lanthanide series as shown in Table 4.4 [7]. The stronger the negatively charged complexes, the more strongly they bind to the ion exchange resin. The latter effect is dominant and gives an explanation for the higher

concentration of oxalic acid needed to elute the smaller lanthanides from the CS5A column [13]. This elution order is in agreement with that reported previously by Perna et al. [9], namely that the elution of lanthanides complexed with oxalate proceeds in the order of increasing atomic numbers such that La is eluted first due to its weakest stability constant with oxalate ($\log\beta_3 = 10.3$).

$$Ln^{3+} + 3{C_2O_4}^{2-} \rightleftarrows Ln(C_2O_4)_3{}^{3-} \qquad \text{(eq. 4.6)}$$

Table 4.4 Ionic radii of lanthanide cations $Ln^{3+}$ [7]

| $Ln^{3+}$ | $La^{3+}$ | $Ce^{3+}$ | $Pr^{3+}$ | $Nd^{3+}$ | $Sm^{3+}$ | $Eu^{3+}$ | $Gd^{3+}$ | $Lu^{3+}$ |
|---|---|---|---|---|---|---|---|---|
| Ionic radius (pm) | 103.2 | 101.0 | 99.0 | 98.3 | 95.8 | 94.7 | 93.8 | 86.1 |

The lanthanides do not have a characteristic coordination number, however based on research performed in the past 20 years, analysis of coordination numbers of lanthanides indicates that lanthanides are most commonly found (60 % of known structures) in coordination numbers 8 and 9 in complexes [7]. Therefore, lanthanides would be likely to have coordination number 8 or 9 in complexes with the bidentate oxalate ligand and would be found as $[Ln(C_2O_4)_3(H_2O)_2]$ or $[Ln(C_2O_4)_3(H_2O)_3]$ in solution. Given that in complexes with a specific ligand, such as oxalate, the coordination number of the lanthanides commonly depends on their size [7], the coordination numbers of the lanthanides would be expected to increase from 8 (for La up to Sm/Eu) to 9 moving across the lanthanide series (based on lanthanides contraction). This means that complexes of the lighter lanthanides (from La to Sm/Eu) would have a square antiprismatic or dodecahedral structure (Figure 4.4), whereas the heavier lanthanides (from Eu/Gd up to Lu) would have a tricapped trigonal prismatic structure [7] shown in Figure 4.4.

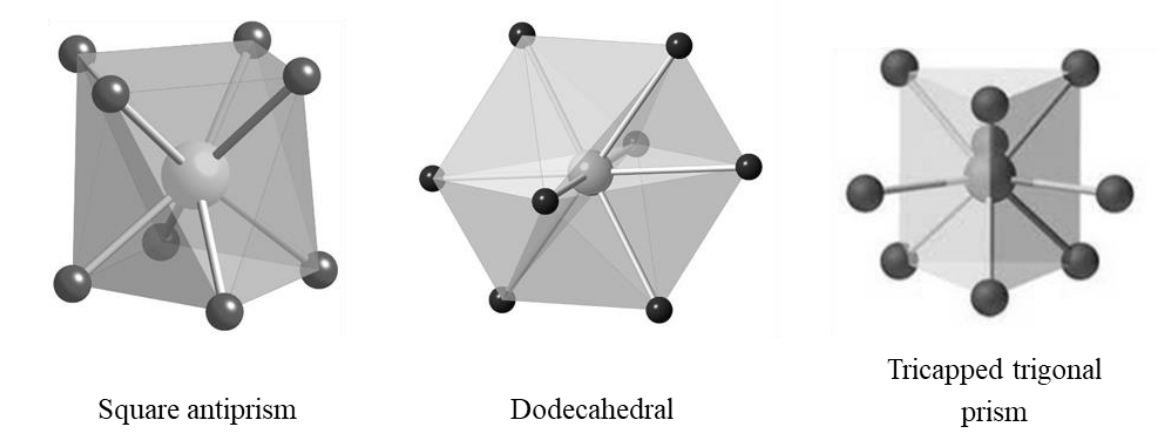


Figure 4.4 Expected geometries of lanthanides with oxalate in solution (taken from https://www.chemtube3d.com)

The lanthanides, which were injected onto the column as cations binding to the cation exchange sites, elute upon complexing with oxalic acid as negatively charged complexes. However, these negatively charged complexes do not co-elute, but instead are separated from one another due to their interactions with the anion exchange sites present in the column, thereby making use of the essential characteristic of a mixed bed ion exchange column to load and separate species

with opposite charge. The heavier lanthanide ions are smaller in ionic radius than the lighter ones (Table 4.4) and thus have a higher charge density, thereby increasing their affinity towards the anion exchange sites of the resin. In this case, the ion interactions between resin and negatively charged complexes are dominant and more pronounced for the heavier/smaller lanthanides [12]. Thus, elution of the heavier lanthanides requires a higher oxalic acid concentration than that used for the lighter lanthanides (0.1 M). Hence, a gradient of 0.1–0.15 M oxalic acid at a pH of 4.5 was used in order to elute the lanthanides in 35 min. This total run time is close to the 25 min achieved in other studies that used the same type of column (CS5A) to elute the lanthanides (La, Ce, Pr, Nd, Sm, Eu and Gd) with 0.1 M oxalic acid [8] and similar to the time needed (33 min) to elute the lanthanides with a gradient of 0.04–0.26 M α-HIBA in the reverse order (from Lu to La) [4]. However, using oxalic acid (up to 0.15 M) instead of α-HIBA (up to 0.26 M) would be beneficial since lower concentrations of organic acid would be introduced into the SF-ICP-MS unit.

Eluting the lanthanides in less than 40 min demonstrates that the HPIC-SF-ICP-MS method brings significant time-savings compared to other analytical methods for the separation of lanthanides, such as gravitational ion exchange chromatography that can take up to 2 weeks for irradiated nuclear fuels. Unlike other studies, we chose to adjust the pH of oxalic acid to 4.5 using ammonium hydroxide instead of lithium hydroxide [8-10] to avoid contamination of the HPIC column and SF-ICP-MS unit with lithium. Moreover, eluting the lanthanides in the order La to Lu as oxalate complexes, instead of using other complexing agents (e.g. α-HIBA) to elute the lanthanides in the reverse order, saves time since Nd elutes within the first 15 minutes after injection compared to approximately 25 minutes otherwise. This is useful when analysing UOx SNF for burn-up determination since the run can be shortened and stopped after Nd has eluted from the column.

Finally, oxalic acid salt deposition in both the spray chamber and the torch injector tube, as well as carbon depositions on the cones of the SF-ICP-MS instrument, were avoided by limiting the concentration of oxalic acid to 0.15 M.

#### 4.3.2.2 Separation of uranium and lanthanides

The ASTM standard practice C1845 describes the elution of uranium using 1 M HCl followed by that of the lanthanides with a gradient of concentrations from 0.04 to 0.26 M α-HIBA at a pH of 4.5 from a cation exchange column [14]. For the purpose of this paper, a mixed bed ion exchange column is preferable since it elutes Nd faster and thus reduces the total run time. In addition, no decrease in sensitivity was observed when introducing 0.15 M oxalic acid for longer time periods into the mass spectrometer, unlike the decrease in signal sensitivity observed for the higher α-HIBA concentrations needed to separate the lanthanides (personal communication). U exists in solution as the uranyl cation $UO_2^{2+}$, which can be eluted from the CS5A column as a complex with chloride ions [4, 9] with a stability constant $\log K_1 = -0.1$ [7]. Therefore, in the first elution method, 0.5 M HCl was introduced onto the column after the oxalic acid gradient. However, this resulted in two distinct peaks for U [Figure 4.5 (a)]. It was hypothesized that the two peaks correspond to different uranyl species, which, according to the Hydra/Medusa speciation diagram (see Appendix Figure S4.1), would be $UO_2Cl^+$ and $UO_2$(ox).

To obtain just one uranyl species in solution, the elution order was reversed by using HCl as the initial mobile phase, followed by the oxalic acid gradient. Under these conditions, one broad peak was observed for U, but the lanthanides were no longer separated from one another (see Appendix Figure S4.2). A Hydra/Medusa speciation diagram shows two species, $UO_2Cl^+$ and $UO_2^{2+}$, which could overlap to generate the observed broad peak. It was hypothesized that residual HCl in the pre-column tubing was mixing with the incoming oxalic acid eluent, thereby causing a decrease in the pH (< 4.5) such that the lanthanides were no longer separated. This hypothesis was supported by experiments in which the column was flushed with water (to remove HCl) before starting the oxalic acid gradient elution. Under the latter conditions, the separation of the lanthanides was partially restored, but peak overlapping still occurred. Finally, when 0.1 M oxalic acid at pH 0.6 was used to elute U after the lanthanides, a narrow U peak was obtained [Figure 4.5 (b)]. This peak corresponds to the neutral species $UO_2$(ox), as revealed in the Hydra/Medusa speciation diagram in the Appendix (Figure S4.3), which does not bind to the column and hence elutes as a sharp peak. The complex formation equilibrium constants of uranyl with oxalic acid have been reported in the literature to be $LogK_1 = 4.63$, $LogK_2 = 4.05$ and $LogK_3 = 3.31$, respectively [9]. For determination of both lanthanides and uranium (without plutonium) in a sample, this gradient elution method of 0.1–0.15 M oxalic acid at pH of 4.5 followed by an isocratic elution with 0.1 M oxalic acid at pH of 0.6 is fit-for-purpose.

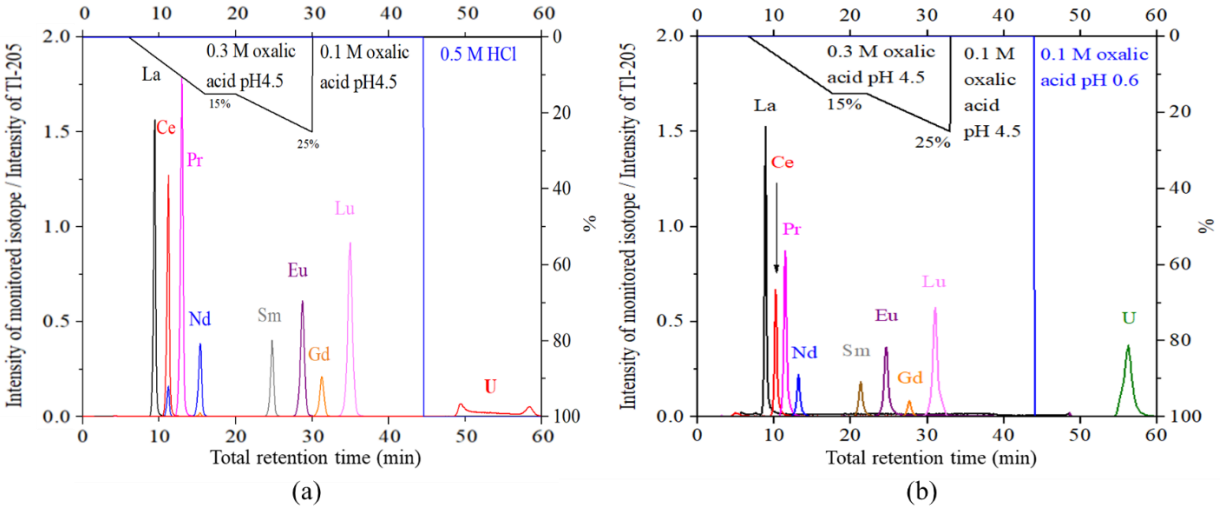


Figure 4.5 HPIC-SF-ICP-MS chromatogram of lanthanides and U using a gradient of 0.1–0.15 M oxalic acid at pH 4.5, followed by isocratic elution with (a) 0.5 M HCl and (b) 0.1 M oxalic acid at pH of 0.6

#### 4.3.2.3 Separation of plutonium, uranium and lanthanides

##### 4.3.2.3.i Oxidation of plutonium

Due to the electrochemical properties of Pu, different Pu oxidation states ranging from +III to +VI can co-exist in solution [15-19] and each of the four states can form various complexes [16], resulting in several Pu species eluting separately from an ion exchange column [15-16]. For quantitative isotopic analysis, such as IR measurements, it is preferable to have only one peak for Pu. To achieve this, all Pu species were converted to Pu(VI) (which is stable in solution

and elutes as a sharp peak) by oxidation with $KMnO_4$ [4, 20-21]. As a result of its high ionic charge, Pu(VI) readily strips oxygen atoms from water molecules and is present in aqueous solutions as $PuO_2^{2+}$, known as the plutonyl ion [17].

#### 4.3.2.3.ii Elution of plutonium, uranium and lanthanides

Previous studies have reported that plutonyl can be eluted from the column used by complexing it with nitrate ions [4, 19]. Therefore, different concentrations of nitric acid were used to elute plutonyl from the column, and the resulting peaks were found to increase in intensity and become narrower with increasing nitric acid concentration over the range 0.4 to 1 M. However, for nitric acid concentrations < 1 M, a small peak preceding the one of plutonyl (Figure 4.6) was observed and attributed to hydrolysis of plutonyl. This behaviour was also predicted by the corresponding Hydra/Medusa speciation diagram (Appendix Figure S4.4), which indicated an increase in the concentration of the hydrolyzed $(PuO_2)_2(OH)_2$ species with increasing pH, or in other words, at lower nitric acid concentrations. Therefore, 1 M nitric acid was used to elute Pu as a single peak from the column.

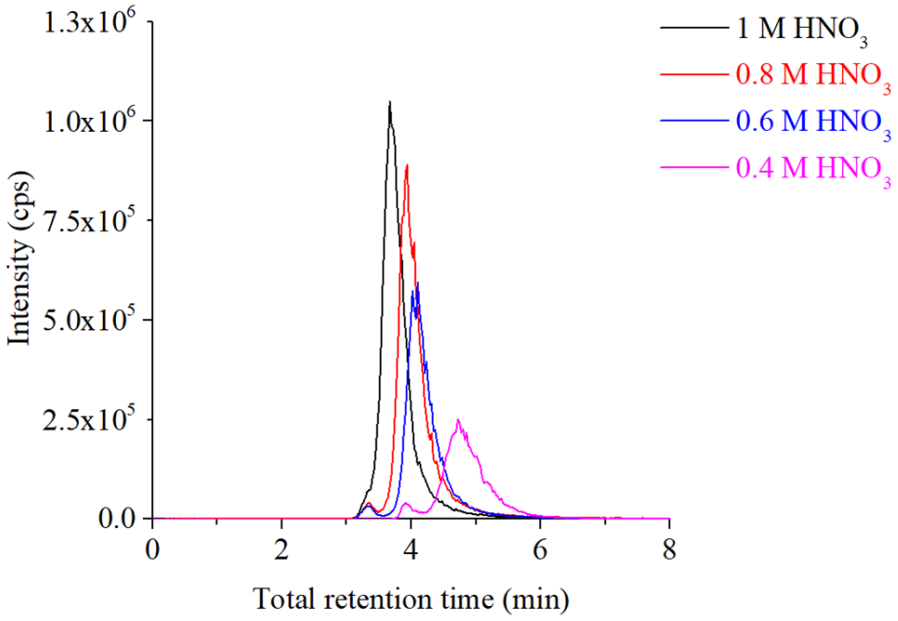


Figure 4.6 Elution of Pu with different concentrations of $HNO_3$

The influence of temperature and concentration of nitric acid during the oxidation of Pu with $KMnO_4$, on the plutonyl peak shape is shown in Figure 4.7. It can be seen in Figure 4.7 that the plutonyl peak is symmetrical when 2 % $HNO_3$ is used during the oxidation with $KMnO_4$. The effect of temperature on the plutonyl peak shape was found to be negligible. Therefore, once $KMnO_4$ was added to the samples, which were prepared in 2 % $HNO_3$, they were left at room temperature for 12 hours to convert all Pu species to Pu(VI).

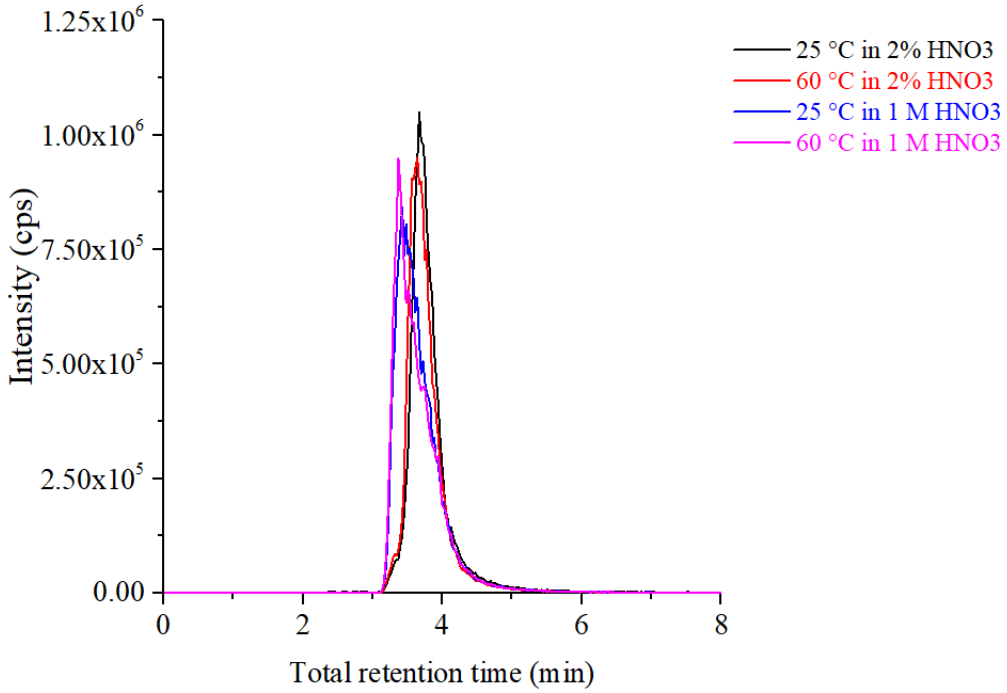


Figure 4.7 HPIC-SF-ICP-MS chromatogram comparing the elution of Pu after its oxidation to Pu(VI) with $KMnO_4$ under different conditions

It was also found that uranyl eluted from the column as a complex with nitrate, yielding a peak that did not interfere with the Pu peak. The complexation of uranyl with nitrate has been reported previously in the literature, with a stability constant $\log K_1 = -0.3$ [7]. Despite uranyl being isostructural to plutonyl, the metal-O bond is shorter in the plutonyl ion due to the smaller ionic radius (and thus a higher charge density) for Pu compared to U (due to the actinides contraction similar to lanthanides contraction). This results in plutonyl having a higher charge density than uranyl such that plutonyl forms stronger complexes with nitrate causing Pu to elute first from the column with nitrate ligands in the eluent. Plutonyl nitrate complexes $[PuO_2(NO_3)_2(H_2O)_2]$ and uranyl nitrate complexes $[UO_2(NO_3)_2(H_2O)_2]$ both have a distorted hexagonal bipyramidal structure [22] (plutonyl nitrate structure is shown in Figure 4.8). However, the unit cell volume (equal to the cell-edge length cubed) is smaller for plutonyl nitrate than for uranyl nitrate, which could be due to the actinides contraction.

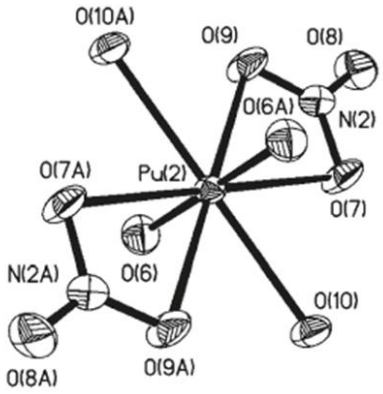


Figure 4.8 Structure of plutonyl nitrate $[PuO_2(NO_3)_2(H_2O)_2]$ [22]

Subsequently, the elution behaviour of Pu(VI) with 0.1 M oxalic acid at pH 4.5 was investigated, in order to decide the final elution order of Pu, U and the lanthanides. In this case, multiple Pu peaks were observed (Figure 4.9). This could be due to the reduction of plutonyl to $Pu^{4+}$, $Pu^{3+}$ and $PuO_2^{+}$ in the oxalic acid medium [23] (section 2.4 of chapter 2) and/or to formation of different complexes of plutonyl with oxalate (Hydra/Medusa speciation diagram in Appendix Figure S4.5). Hence, in order to avoid multiple plutonium peaks, Pu must be eluted before the introduction of oxalic acid into the column (therefore, prior to elution of the lanthanides).

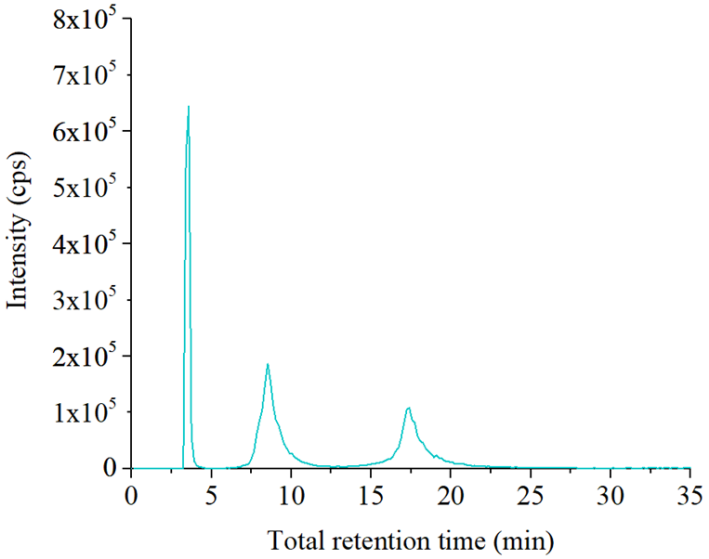


Figure 4.9 Elution of Pu with 0.1 M oxalic acid pH 4.5

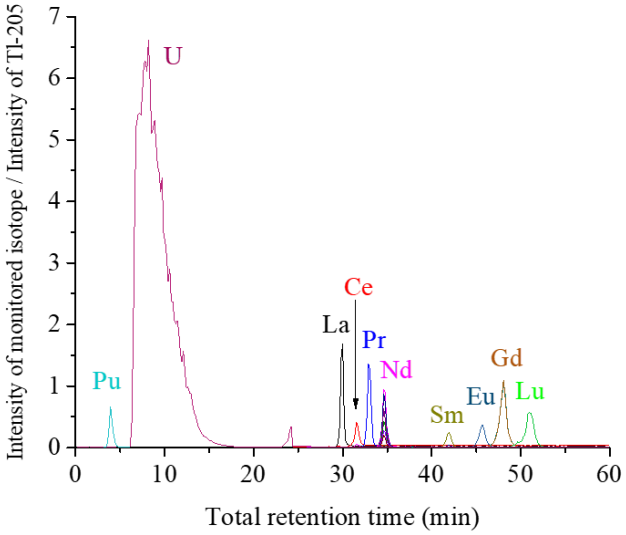


Figure 4.10 HPIC-SF-ICP-MS chromatogram of the separation of Pu, U and the lanthanides in a synthetics mixture

Finally, Pu was included in a synthetic mixture of U and lanthanides to elute all components in a single chromatographic run. This resulted in plutonyl and uranyl both eluting as neutral nitrate complexes (albeit with different stability constants and thus, retention times), followed by the lanthanides as oxalate complexes (Figure 4.10).

Given that Am interferes with Pu at more than one mass (241 and 242), it is important to chromatographically separate it from Pu to avoid erroneous determination of the elemental and nuclide-specific mass fractions of Pu in SNF samples. However, Am is present as $Am^{3+}$ in solution, and is expected to elute as $Am(C_2O_4)_3^{3-}$ with oxalic acid eluent based on results obtained by Perna et al. [9]. Using our separation method for the SNF samples measured, the peak observed at mass 241 during the elution of Ce (Figure 4.11) corresponds to $^{241}Am$ eluting as $Am(C_2O_4)_3^{3-}$ from the column. This result confirms that Am elutes separately from Pu using our separation method, therefore eliminating isobaric interferences between Am and Pu and avoiding erroneous determination of elemental and nuclide specific Pu mass fractions in SNF samples.

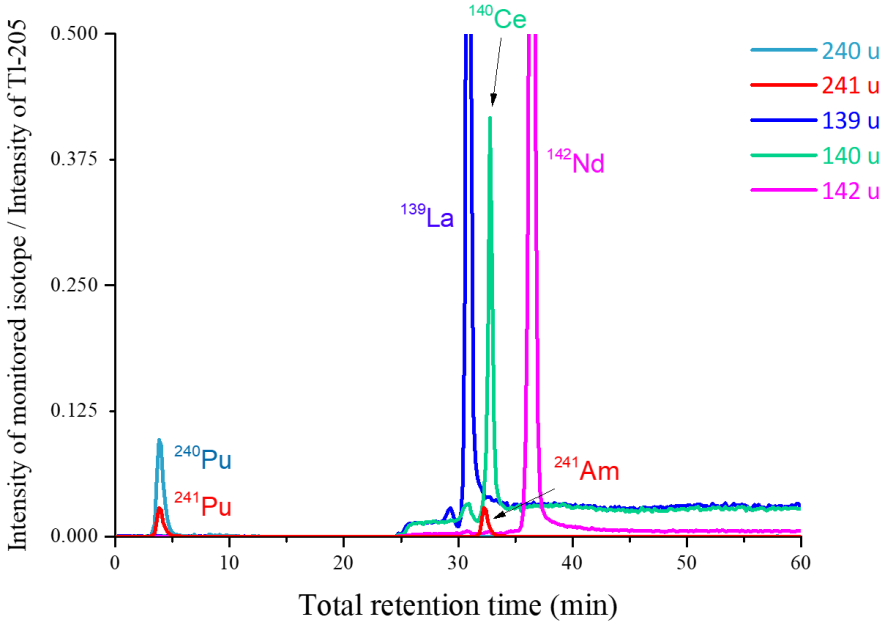


Figure 4.11 HPIC-SF-ICP-MS chromatograph of $^{241}Am$ elution using 0.1 M oxalic acid buffered to pH 4.5 using $NH_4OH$

Rinsing with water between the nitric acid and oxalic acid eluents was necessary to avoid a decrease in the pH of the oxalic acid that would otherwise lead to a poorer resolution in the separation of the lanthanides. When the oxalic acid reaches the ICP-MS introduction system (t = 23 min) a peak arising from the disequilibration in the ICP appears in the $^{238}U$ signal. This peak is quantifiable and does not interfere with any other signal. If needed, by automatically switching the second 6-port-2-way valve, the eluted U can be collected in a Falcon tube, which can contain an appropriate diluent and internal standard. The fraction collected in this way can serve later for determination of IRs by means of continuous aspiration into the SF-ICP-MS instrument. Moreover, the use of OPTIMA™ grade nitric acid was found to be essential to avoid accumulation of lanthanides on the column during the first 5 min of the final elution program, during which nitric acid is used as the eluent. The use of this grade of nitric acid was preferred due to its ultra-low concentrations of lanthanides (< 10 ppt). Accumulation of lanthanides using OPTIMA™ grade nitric acid was ≤0.079 pg, compared to ≤8.1 pg with trace metal grade nitric acid. The lanthanide impurities present in nitric acid would accumulate on

the column during the first part of the final elution program. Introducing oxalic acid onto the column in the next step of the final elution program would then elute both the accumulated lanthanides due to impurities, as well as those lanthanides originating from the actual injected sample, giving rise to an increase in blank concentrations and hence LODs. Therefore, the use of OPTIMA$^{TM}$ grade (or equivalent purity) nitric acid is recommended. Finally, the introduction of the $^{205}$Tl internal standard through the post-column reagent pump and its mixing with the column effluent allows short-term changes in sensitivity to be corrected (see section 3.2.6.4). In addition, the pH of the column effluent is lowered by the matrix (0.75 M nitric acid) of the post-column medium. As a result, the nitric acid concentration of the nebulized sample is adjusted to the default concentration of 0.3 M, which improves the stability of the ICP-MS signal.

### 4.3.3 HPIC-SF-ICP-MS separation method validation

#### 4.3.3.1. Linearity

The lowest calibration point was set at a concentration higher than the method LOQ whilst the upper calibration point was set at 4 times the concentration of Nd, Gd, Pu and U standards in the synthetic mixture used during method optimization to avoid exceeding the column capacity. These concentrations were chosen such that signal count rates in the effluent lay within the pulse counting range of the electron multiplier in the SF-ICP-MS instrument. The linearity of the calibration line was assessed in terms of regression statistics. The correlation coefficients of the linear regression plots were found to be > 0.9995 for all evaluated nuclides of Nd, Gd, Pu and U (Figures S4.7 – S4.10 in this chapter's appendix). Furthermore, the residuals indicated a good fit between the data and the regression model. The plot of the residuals versus the nuclide concentration showed a random distribution of the residuals around zero (Figures S4.11 – S4.14 in this chapter's appendix). This demonstrates that the method is at least linear in the working range of 1–10 $\mu g \cdot L^{-1}$ for Nd, 10–100 $\mu g \cdot L^{-1}$ for Gd, 1–10 $\mu g \cdot L^{-1}$ for Pu and 0.5–24 $\mu g \cdot L^{-1}$ for U.

#### 4.3.3.2. Repeatability and intermediate precision

The variation in the retention time of the monitored analytes was negligible within one day, as is shown in Table 4.5. Furthermore, over a period of 1 month, the retention time of Gd was found to increase by up to 4 min and that of Nd by less than 1 min, while no significant difference was observed for Pu and U. Any observed shift in retention times did not deteriorate the separation between the elements, but nonetheless indicated the impact of the eluent's pH [24] and thus the concentration of ammonium hydroxide in solution, on the repeatability of the lanthanide separations.

Table 4.5 Average retention time with the standard deviation (SD) and the relative standard deviation (RSD) of six replicates of a Pu, U, Nd and Gd standard

| Nuclide | Retention time (min) | SD (min) | RSD (%) |
|---|---|---|---|
| $^{242}$Pu | 3.91 | 0.02 | 0.6 |
| $^{238}$U | 18.50 | 0.19 | 1.0 |
| $^{142}$Nd | 15.57 | 0.07 | 0.5 |
| $^{158}$Gd | 31.59 | 0.10 | 0.3 |

#### 4.3.3.3. LOD and LOQ

The calculated nuclide-specific LOD and LOQ values are reported in Table 4.6 (not enough data to determine LODs and LOQs for all nuclides of U and Pu). These values give an overview of the capabilities of this HPIC-SF-ICP-MS method. The LOD values obtained with HPIC-SF-ICP-MS fall short of those achieved with SF-ICP-MS alone, which are in the range of fg amounts. This is due to the dilution of the injected sample volume (25 µL) by the eluent and post-column added internal standard (about 0.5 mL) and to the fact that an ICP's pneumatic nebulizer with relatively large internal volumes cannot equilibrate quickly enough to the fast changing concentration of the analyte eluting from the HPIC column in a small volume (e.g. 25 µL) [15]. Nevertheless, the limits of detection achieved by this HPIC-SF-ICP-MS method are lower than those reported by another study (2.91 $\mu g \cdot L^{-1}$ for U and 0.026 $\mu g \cdot L^{-1}$ for Pu [15]) that used HPIC coupled to a quadrupole-based ICP-MS unit.

Table 4.6 LOD and LOQ for the monitored nuclides

| Nuclide | Nuclide-specific LOD ($\mu g \cdot L^{-1}$) | Nuclide-specific LOQ ($\mu g \cdot L^{-1}$) |
|---|---|---|
| $^{142}$Nd | 0.067 | 0.22 |
| $^{143}$Nd | 0.031 | 0.10 |
| $^{144}$Nd | 0.070 | 0.23 |
| $^{145}$Nd | 0.022 | 0.073 |
| $^{146}$Nd | 0.055 | 0.18 |
| $^{148}$Nd | 0.019 | 0.063 |
| $^{150}$Nd | 0.016 | 0.054 |
| $^{155}$Gd | 0.047 | 0.16 |
| $^{156}$Gd | 0.074 | 0.25 |
| $^{157}$Gd | 0.050 | 0.17 |
| $^{158}$Gd | 0.066 | 0.22 |
| $^{160}$Gd | 0.082 | 0.27 |
| $^{238}$U | 0.065 | 0.21 |
| $^{240}$Pu | 0.0029 | 0.0096 |
| $^{242}$Pu | 0.015 | 0.048 |
| $^{244}$Pu | 0.00042 | 0.0014 |

### 4.3.4 Other matrices

#### 4.3.4.1 Spent nuclear fuel matrix

In the HPIC-SF-ICP-MS chromatogram (see Figure 4.12) of the Gd-containing nuclear fuel, Pu, U and the lanthanides were eluted using the final optimized method and the same peak order and resolution as observed with synthetic solutions was obtained, which demonstrates the applicability of the method to a SNF matrix. The on-line separation method permits IRs to be measured in SNF samples since all spectral interference from isobaric nuclides were resolved. Since U is the main component of SNF with a concentration at least a hundred times higher than that of the lanthanides [4], eluting U prior to the lanthanides avoids matrix interferences hampering quantification of the lanthanides. Using HPIC-SF-ICP-MS for the analysis of SNF instead of gravitational ion chromatography followed by TIMS not only saves time, it also reduces the amount of radiation to which the operator is exposed.

Furthermore, a comparison of Nd and Gd nuclide-specific concentrations, in a spent "Gd fuel", obtained by external calibration with HPIC-SF-ICP-MS (see 4.2.5.1) and those obtained by means of isotope dilution TIMS is summarized in Table 4.7. However, no external precision value is reported since the results are based on a single measurement and the ultimate goal of this work is to quantify the nuclide specific mass fractions of Pu, U, Nd and Gd using isotope dilution and not using external calibration. Nevertheless, the uncertainties obtained using external calibration are expected to be of the order of 5 to 10 % (k=2) (see section 3.2.6.1 of chapter 3).

Nd is a fission product formed by irradiation of the fuel. While Gd is also formed by fission, but in lower amounts than Nd, Gd can also be mixed in as a burnable poison in the fuel assembly for improving the reactor performance (see section 1.4.3.2 of chapter 1) [25]. The nuclide-specific concentrations of the Nd isotopes obtained by HPIC-SF-ICP-MS lie within a range of ± 6 % of those obtained by TIMS, whereas the nuclide-specific concentrations of the Gd isotopes lie within a range of ± 11 % of those obtained by TIMS. For this particular nuclear fuel, the concentration of $^{157}$Gd in the diluted sample was below the nuclide-specific LOQ for $^{157}$Gd (0.17 $\mu g \cdot L^{-1}$). The low concentration of $^{157}$Gd is due to the high neutron absorption cross-sections of $^{157}$Gd compared to those of the other Gd isotopes (see section 1.4.3.2 of chapter 1) [25]. As a result of its high neutron absorption cross-section, during irradiation of the fuel, $^{157}$Gd is transformed into $^{158}$Gd, thereby drastically decreasing the concentration of $^{157}$Gd compared to those present in the original fuel. The low abundance of $^{157}$Gd, after irradiation, contributes to the discrepancy between HPIC-SF-ICP-MS data and TIMS data for this Gd isotope. Theoretically, the intensity of $^{157}$Gd chromatographic peak should be higher than that of $^{152}$Gd, however, the measured intensity of the $^{157}$Gd chromatographic peak was less than the one measured for $^{152}$Gd (Figure S4.6 in the Appendix of this chapter), which implies an erroneous result for $^{157}$Gd since the concentration of $^{152}$Gd was 102 % of that determined by TIMS. Since this sample was only measured once, verification of the $^{157}$Gd data could not be done. Given that data shown in Table 4.7 was obtained at an early stage of the verification of the quantitative aspect of the HPIC-SF-ICP-MS method and that the ultimate goal of this work is to quantify nuclide-specific concentrations using isotope dilution (and not by external calibration), not all

relevant nuclides were measured (including $^{150}$Nd and $^{154}$Gd) which is why concentrations for these nuclides are missing in Table 4.6.

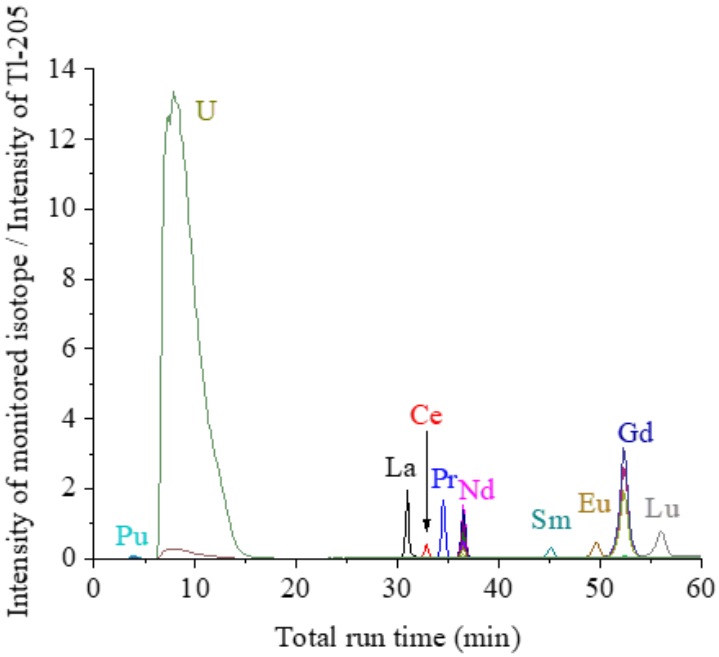


Figure 4.12 HPIC-SF-ICP-MS chromatogram of the separation of Pu, U and the lanthanides in a spent "Gd fuel" sample

Table 4.7 Comparison of nuclide-specific concentrations obtained using HPIC-SF-ICP-MS with external calibration and TIMS for Nd and Gd nuclides in a Gd SNF

| Nuclide | Nuclide-specific concentration (ng·g$^{-1}$) by HPIC-SF-ICP-MS | Nuclide-specific concentration (ng·g$^{-1}$) by TIMS | HPIC-SF-ICP-MS / TIMS (·100) |
|---|---|---|---|
| $^{142}$Nd | 0.00089 | 0.00090 | 98.1 |
| $^{143}$Nd | 0.153 | 0.158 | 96.9 |
| $^{144}$Nd | 0.164 | 0.167 | 98.3 |
| $^{145}$Nd | 0.107 | 0.113 | 94.7 |
| $^{146}$Nd | 0.099 | 0.101 | 98.4 |
| $^{148}$Nd | 0.059 | 0.059 | 99.3 |
| $^{152}$Gd | 0.109 | 0.107 | 101.4 |
| $^{155}$Gd | 0.54 | 0.53 | 100.6 |
| $^{156}$Gd | 25.85 | 25.78 | 100.3 |
| $^{157}$Gd | 0.03 | 0.22 | 15.5 |
| $^{158}$Gd | 30.11 | 30.79 | 97.8 |
| $^{160}$Gd | 18.34 | 16.54 | 110.8 |

#### 4.3.4.2 Environmental soil matrix

The soil standard material contains 0.03 pg of Pu per gram soil material (concentration expected in solution = 0.14 ng·L$^{-1}$). The chromatographic peak corresponding to such a low concentration

of any Pu isotope would not be detectable with this hyphenated method. Therefore, $^{242}$Pu was spiked into the standard material to raise the intensity of the $^{242}$Pu chromatographic peak above the quantification limit. The HPIC-SF-ICP-MS chromatogram resulting from the $^{242}$Pu spiked soil sample is shown in Figure 4.13. Pu, U and the lanthanides were eluted in separate peaks and in the same order as with the synthetic mixtures and the SNF matrix. This extends the applicability of this separation method to soil samples. The recovery of spiked $^{242}$Pu was found to be 105 % and that of U was 97 % of the recommended value on the IAEA-375 certificate, which is within the 95 % confidence interval mentioned on the reference standard certificate. No external precision is reported since the results are based on a single measurement.

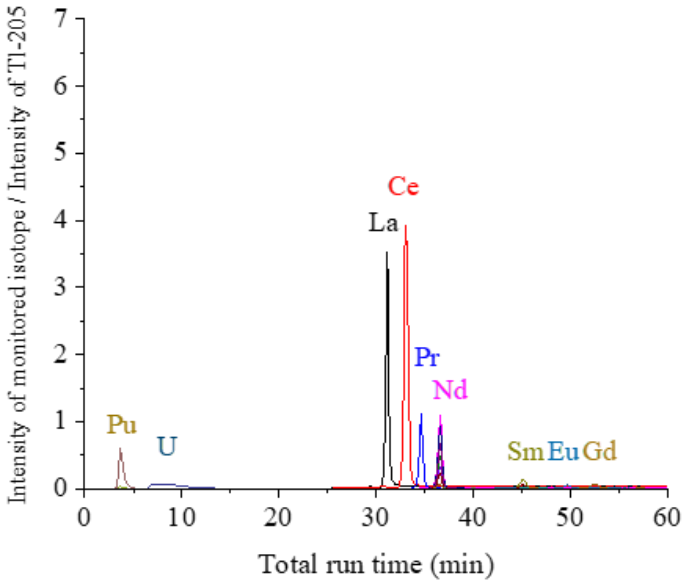


Figure 4.13 HPIC-SF-ICP-MS chromatogram for the separation of Pu, U and the lanthanides in the environmental soil standard IAEA-375

## 4.4 Conclusions and outlook

In conclusion, a HPIC method for the separation of Pu, U and the lanthanides was developed successfully with the aid of simulated speciation diagrams from Hydra/Medusa. This HPIC separation method eliminates isobaric overlaps which hinder the determination of Pu, U, Nd and Gd mass fractions in SNF, does not use high concentrations of organic acid which can clog the orifices of the sampler and skimmer cones, and employs $NH_4OH$ (for pH adjustment) instead of LiOH to avoid unnecessary contamination of the HPIC column and SF-ICP-MS unit with lithium. Additionally, this separation method is applicable to widely different matrices (SNF and soil matrices) in terms of uranium content.

In a single run, Pu and U were eluted separately with 1 M nitric acid as neutral plutonyl and uranyl nitrate complexes, respectively, before the lanthanides, which were eluted as anionic oxalate complexes by using a gradient of 0.1–0.15 M oxalic acid at pH 4.5. All analytes eluted as single peaks, suitable for quantitative analysis (such as IR determination). The method was found to result in linearly increasing pulse count signals over the range 1–10 $\mu g \cdot L^{-1}$ for Nd, 10–100 $\mu g \cdot L^{-1}$ for Gd, 1–10 $\mu g \cdot L^{-1}$ for Pu and 0.5–24 $\mu g \cdot L^{-1}$ for U nuclides. The chromatographic method was repeatable, however, it is important to control accurately the pH

(4.5 ± 0.05) of the oxalic acid eluent. The overall method saves time (requires ≤60 min) and reduces the radiation dose of the analyst compared to gravitational ion exchange chromatography which can take a couple of weeks for the elution of the lanthanides.

Finally, the developed method was applied to two significantly different matrices: (i) spent nuclear fuel matrix and (ii) environmental soil matrix. Nuclide-specific concentrations, derived from HPIC-SF-ICP-MS analysis using external calibration, for Nd and Gd nuclides in a Gd spent nuclear fuel were 92–106 % and 89–111 %, respectively, of those obtained using TIMS.

The determined concentrations of Pu and U were 105 % and 97 %, respectively, compared to their theoretical concentration in a $^{242}$Pu spiked soil sample.

The method validation of the external calibration indicates that it is possible to quantify four elements, Pu, U, Nd and Gd. Nevertheless, also other lanthanides, such as La, Ce, Pr, Sm, Eu and Lu can be quantified if necessary.

Isotope dilution mass spectrometry (IDMS) is more suitable to analysis of SNF, with smaller measurement uncertainties than those achievable with external calibration, but determining IRs on transient signals brings its own challenges, which were tackled in the next step of the PhD.

## 4.5 References


[1] N. N. Wanna, K. Van Hoecke, A. Dobney, M. Vasile, T. Cardinaels and F. Vanhaecke, "Determination of the lanthanides, uranium and plutonium by means of on-line high-pressure ion chromatography coupled with sector field inductively coupled plasma-mass spectrometry to characterize nuclear samples," *Journal of Chromatography A,* vol. 1617, 2020.

[2] M. Moldovan, E. Krupp, A. Holliday and O. Donard, "High resolution sector field ICP-MS and multicollector ICP-MS as tools for trace metal speciation in environmental studies: a review," *Journal of Analytical Atomic Spectrometry,* vol. 19, pp. 815-822, 2004.

[3] M. Florez, M. Aramendia, M. Resano, A. Lapena, L. Balcaen and F. Vanhaecke, "Isotope ratio mapping by means of laser ablation-single collector-ICP-mass spectrometry: Zn tracer studies in thin sections of Daphnia magna," *Journal of Analytical and Atomic Spectrometry,* vol. 28, pp. 1005-1015, 2013.

[4] I. Gunther-Leopold, F. Gabler, B. Wernli and Z. Kopajtic, "Characterization of spent nuclear fuels by an on-line coupled HPLC-ICP-MS system," Paul Scherrer Institute Scientific Report, Switzerland, 2000.

[5] T. A. Maryutina, E. Y. Savonina, P. S. Fedotov, R. M. Smith, H. Siren and D. B. Hibbert, "Terminology of separation methods (IUPAC Recommendations 2017)," *Pure Applied Chemistry,* vol. 90, no. 1, pp. 181-231, 2018.

[6] V. Thomsen, D. Schatzlein and D. Mercuro, "Limits of detection in spectroscopy," Spectroscopy vol 11, no. 12, pp. 112-114, 2003.

[7] S. Cotton, Lanthanide and actinide chemistry, Uppingham, Rutland: Wiley, 2006.

[8] J. Barrero Moreno, J. Garcia Alonso, P. Arbore, G. Nicolaou and L. Koch, "Characterization of spent nuclear fuels by ion chromatography-inductively coupled plasma mass spectrometry," *Journal of Analytical Atomic Spectrometry,* vol. 11, pp. 929-935, 1996.

[9] L. Perna, Chromatographic separations for fission products and actinides determination by different analytical techniques: mass spectrometry and radiometry, Barcelona: Universidad Politécnica de Catalunya, 2003.

[10] M. Betti, "Use of ion chromatography for the determination of fission products and actinides in nuclear applications," *Journal of chromatography A,* vol. 789, pp. 369-379, 1997.

[11] J. Ignacio Garcia Alonso, F. Sena, P. Arbore, M. Betti and L. Koch, "Determination of fission products and actinides in spent nuclear fuels by isotope dilution ion chromatography inductively coupled plasma mass spectrometry," *Journal of analytical and atomic spectrometry,* vol. 10, pp. 381-393, 1995.

[12] E. Borai, R. Hassan, M. El-Dessouky and A. Ghonem, "Efficient separation of lanthanides using poly(styrene-divinyl benzene) aminated anion exchanger," in *ESENSA-08 9th International conference of nuclear sciences and applications*, Sharm El-Sheikh, 2008.

[13] Dionex, "Ion chromatography of lanthanide metals," Technical note TN 23 (1991).

[14] ASTM C1845-16, "Standard practice for the separation of lanthanide elements from uranium matrices using high pressure ion chromatography (HPIC) for isotopic analyses by inductively coupled plasma mass spectrometry (ICP-MS)," ASTM International, West Conshohocken, PA, 2016.

[15] J. Barrero Moreno, M. Betti and J. Garcia Alonso, "Determination of neptunium and plutonium in the presence of high concentrations of uranium by ion chromatography-inductively coupled plasma mass spectrometry," *Journal of Analytical Atomic spectrometry,* vol. 12, pp. 355-361, 1997.

[16] D. Clark, "The chemical complexities of Plutonium," *Los Alamos Science,* vol. 26, pp. 364-381, 2000.

[17] C. Ambard, "La spéciation du plutonium à l'état de traces par le couplage électrophorèse capillaire spectrométrie de masse à source plasma couplée par induction," Commissarisat de l'énergie atomique, 2007.

[18] B. Harvey, H. Heal, A. Maddock and E. Rowley, "The chemistry of plutonium," *Journal of the chemical society,* no. 0, pp. 1010-1021, 1947.

[19] I. Gunther-Leopold, J. Waldis, B. Wernli and Z. Kopajtic, "Measurement of Plutonium isotope ratios in nuclear fuel samples by HPLC-MC-ICP-MS," *International Journal of Mass Spectrometry,* vol. 242, pp. 197-202, 2005.

[20] S. Rollin, Z. Kopatjtic, B. Wernli and B. Magyar, "Determination of lanthanides and actionides in Uranium materials by high-performance liquid chromatography with inductively coupled plasma mass spectrometric detection," *Journal of Chromatography A,* vol. 739, pp. 139-149, 1996.

[21] E. Vassileva, E. Han and I. Levy, "Determination of low-level plutonium in seawater by sector field inductively coupled plasma mass spectrometry: method validation," Springer, 2016.

[22] A. Gaunt, I. May, M. Neu, S. Reilly and B. Scott, "Structural and spectroscopic characterization of plutonyl(VI) nitrate under acidic conditions," *Inorganic Chemistry,* vol. 50, pp. 4244-4246, 2011.

[23] D. Reed, D. Wygmans, S. Aase and J. Banaszak, "Reduction of Np(VI) and Pu(VI) by organic chelating agents," Argonne, 1939.

[24] K. Van Hoecke, J. Busse, M. Gysemans, L. Adriaensen, A. Dobney and T. Cardinaels, "Isolation of lanthanides from spent nuclear fuels by means of high performance ion

chromatography (HPIC) prior to mass spectrometric analysis," *Journal of Radioanalytical and Nuclear Chemistry*, vol. 314, pp. 1727-1739, 2017.

[25] IAEA, "Characteristics and use of Urania-Gadolinia fuels," IAEA, Vienna, 1995.

# Appendix chapter 4

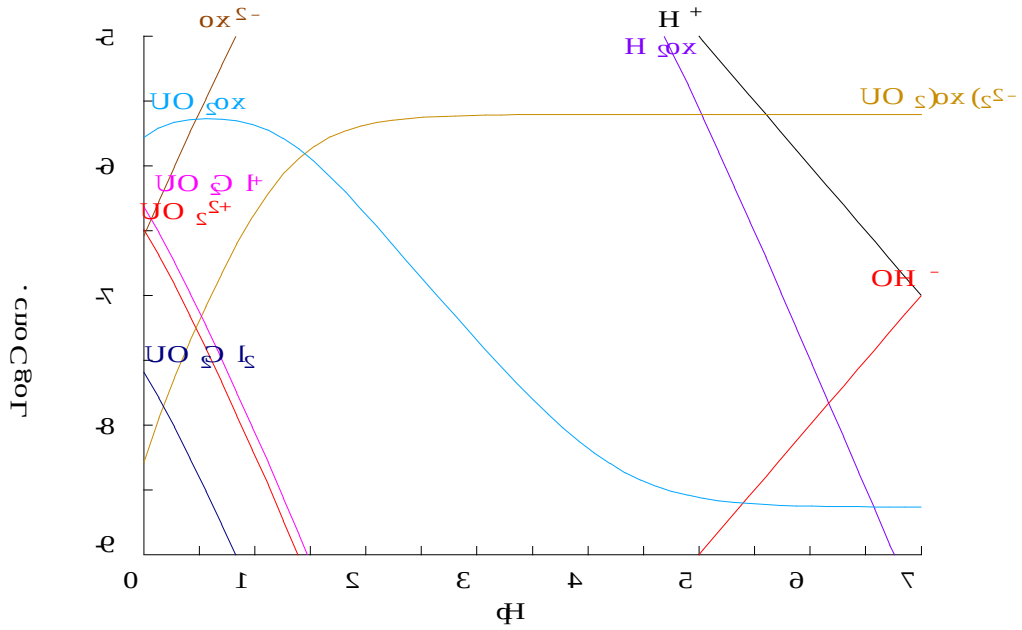

Figure S4.1 Hydra/Medusa graph of uranyl, oxalate and chloride

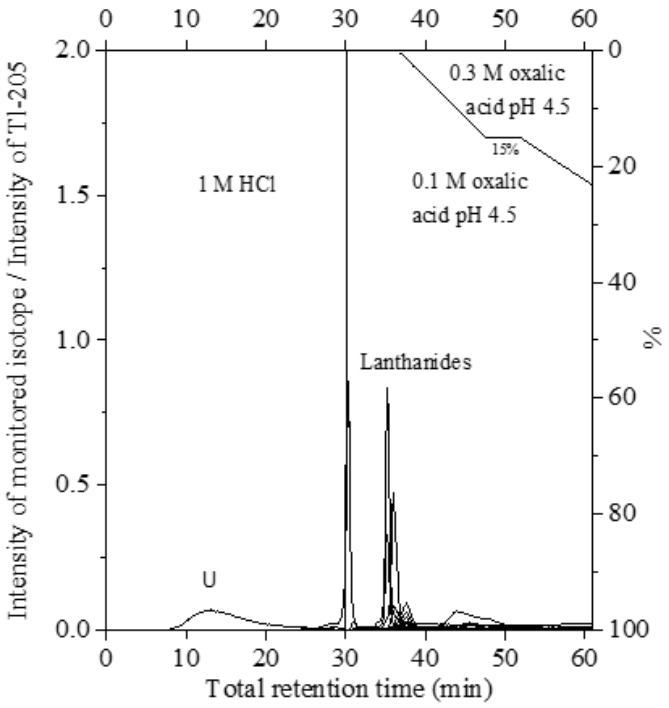


Figure S4.2 HPIC-SF-ICP-MS chromatogram showing isocratic elution of U using 1 M HCl, followed by a gradient elution of the lanthanides with 0.1 - 0.15 M oxalic acid at pH of 4.5

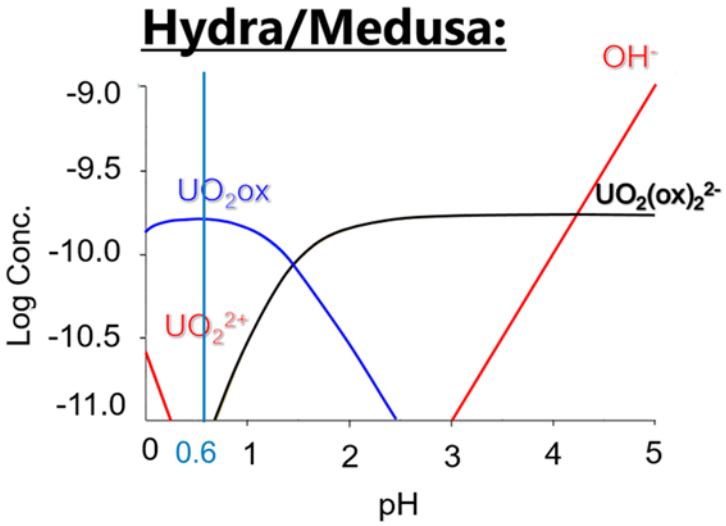


Figure S4.3 Hydra/Medusa speciation graph of uranyl and oxalate

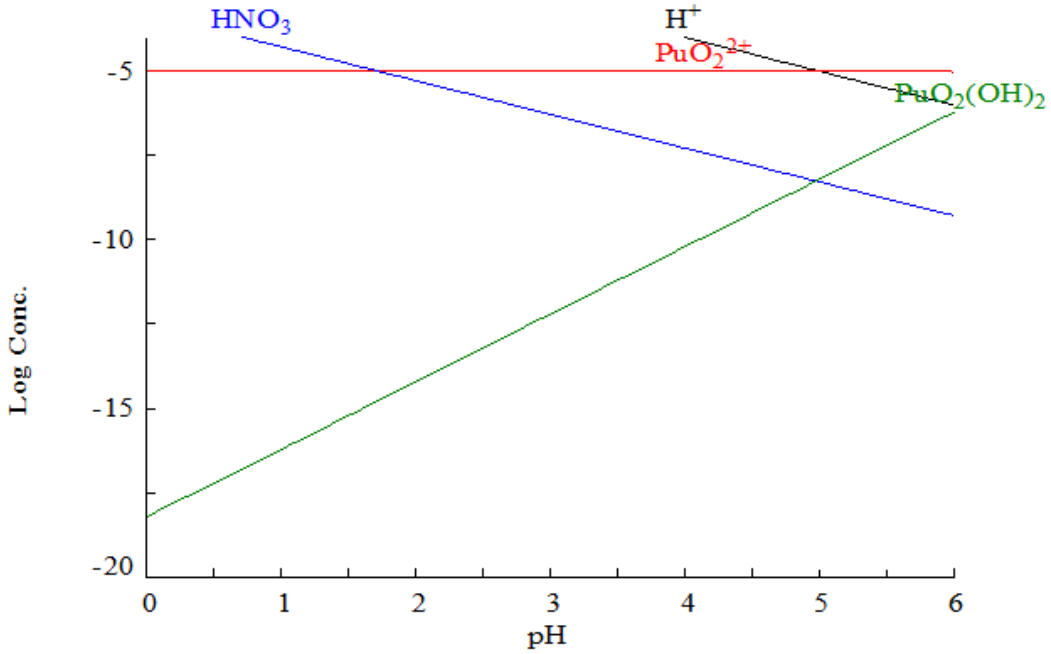


Figure S4.4 Hydra/Medusa speciation graph of Pu(VI) and nitric acid in solution

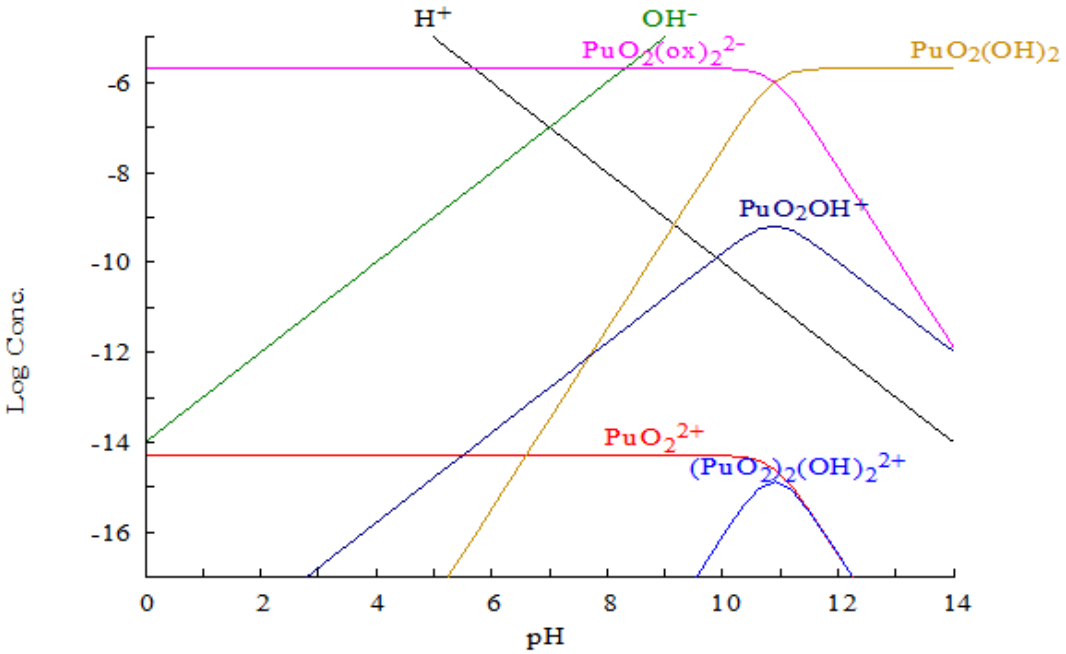


Figure S4.5 Hydra/Medusa speciation graph of Pu(VI) and oxalic acid

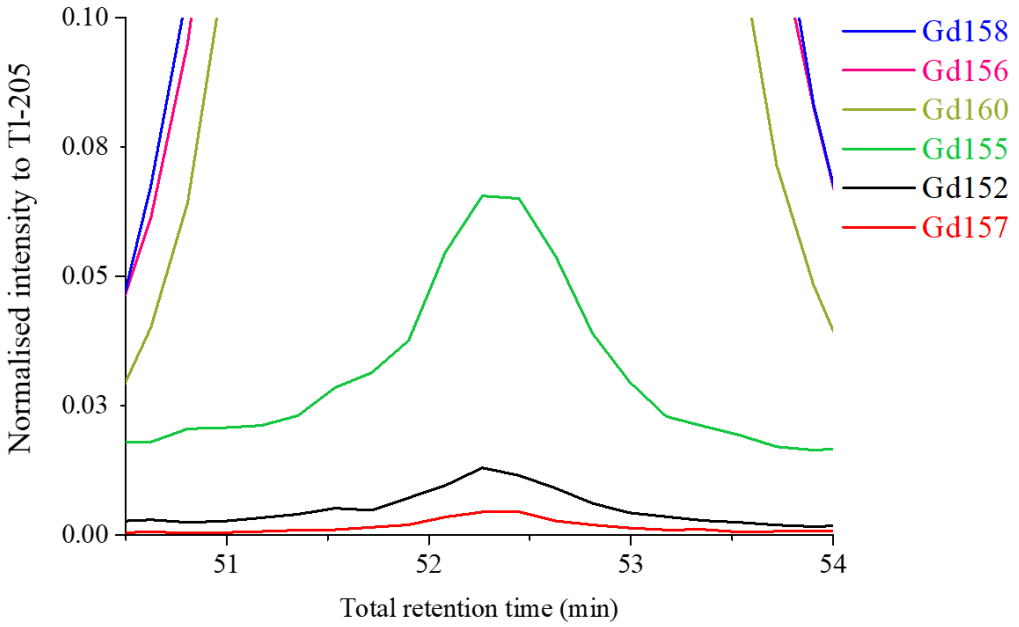


Figure S4.6 Chromatograph of Gd nuclides obtained from the injection of a “Gd fuel” onto the HPIC-SF-ICP-MS set-up

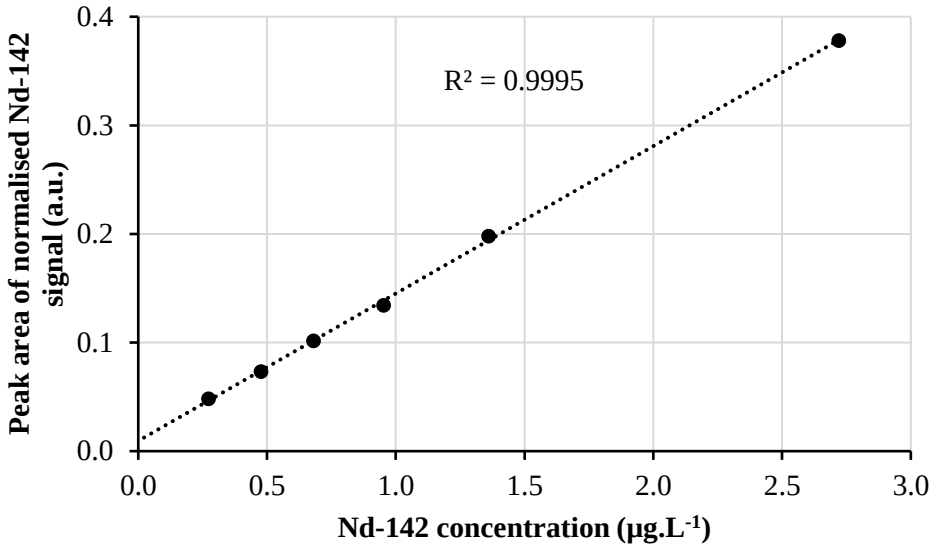
R² = 0.9995
Peak area of normalised Nd-142 signal (a.u.)
Nd-142 concentration (µg.L-1)
0.0
0.1
0.2
0.3
0.4
0.5
1.0
1.5
2.0
2.5
3.0

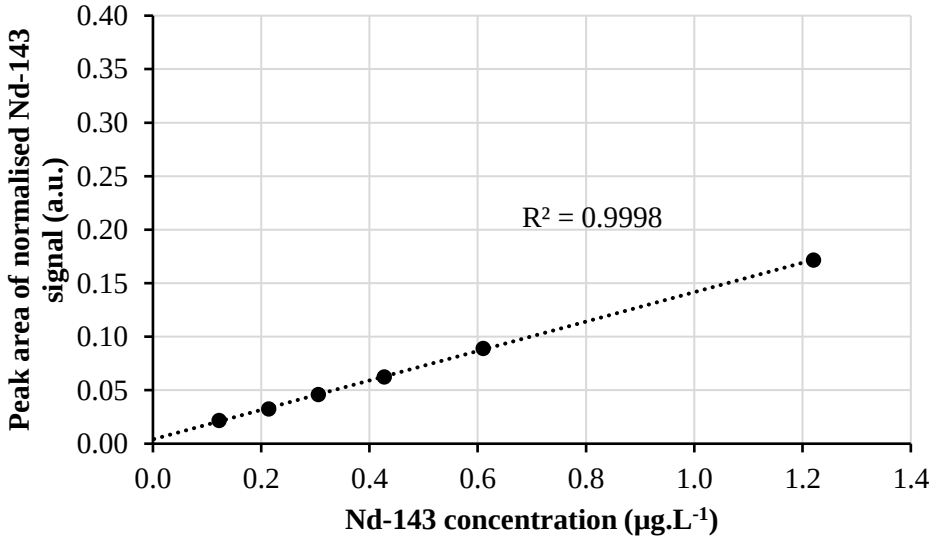
R² = 0.9998
Peak area of normalised Nd-143 signal (a.u.)
Nd-143 concentration (µg.L-1)
0.00
0.05
0.10
0.15
0.20
0.25
0.30
0.35
0.40
0.2
0.4
0.6
0.8
1.0
1.2
1.4

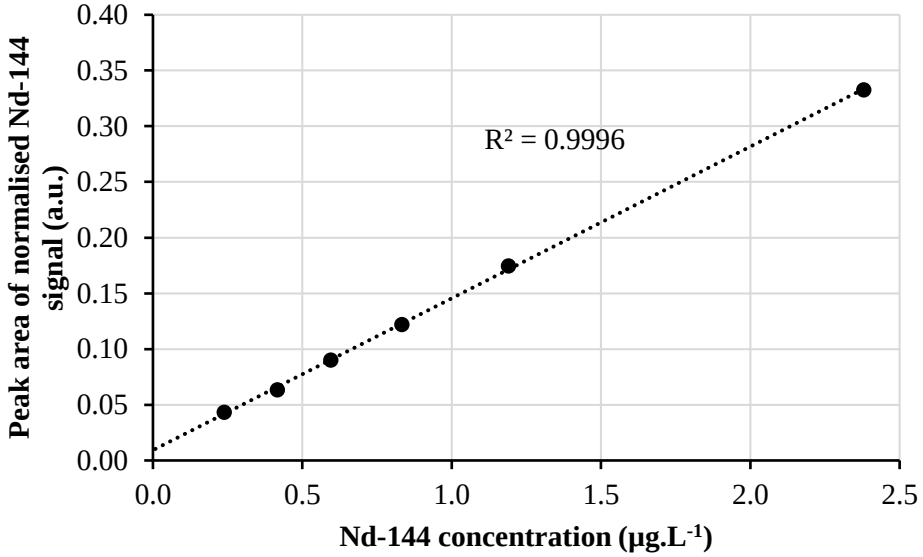
R² = 0.9996
Peak area of normalised Nd-144 signal (a.u.)
Nd-144 concentration (µg.L-1)
0.00
0.05
0.10
0.15
0.20
0.25
0.30
0.35
0.40
0.5
1.0
1.5
2.0
2.5

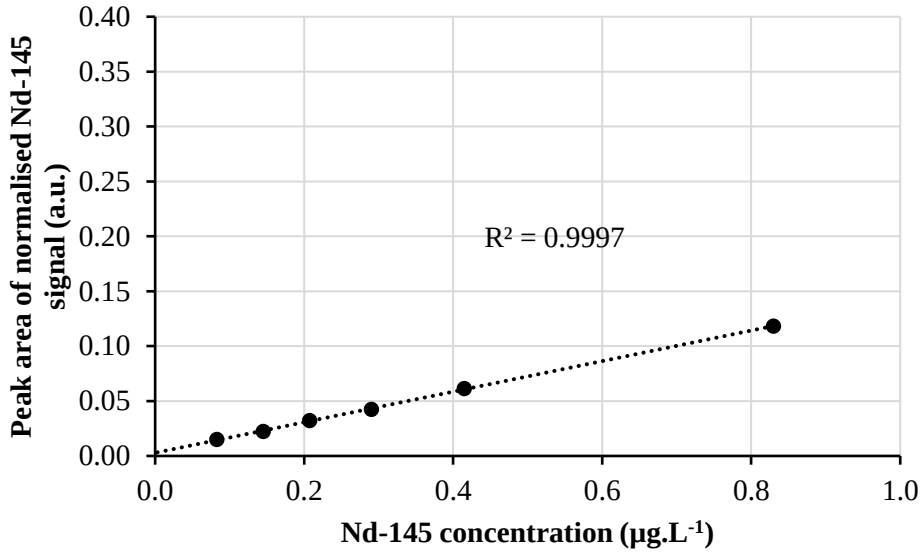
Peak area of normalised Nd-145 signal (a.u.)
0.40
0.35
0.30
0.25
0.20
0.15
0.10
0.05
0.00
R² = 0.9997
0.0
0.2
0.4
0.6
0.8
1.0
Nd-145 concentration (µg.L-1)

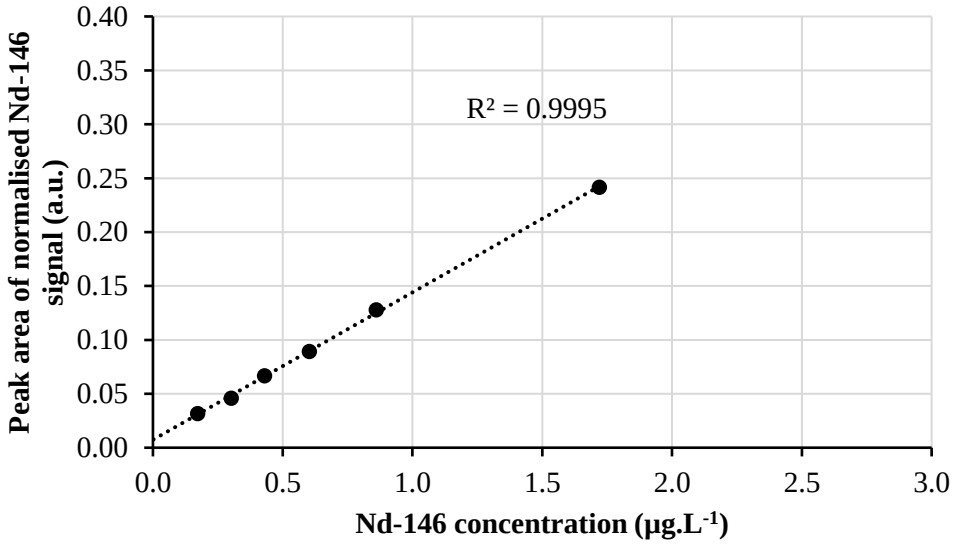
Peak area of normalised Nd-146 signal (a.u.)
0.40
0.35
0.30
0.25
0.20
0.15
0.10
0.05
0.00
R² = 0.9995
0.0
0.5
1.0
1.5
2.0
2.5
3.0
Nd-146 concentration (µg.L-1)

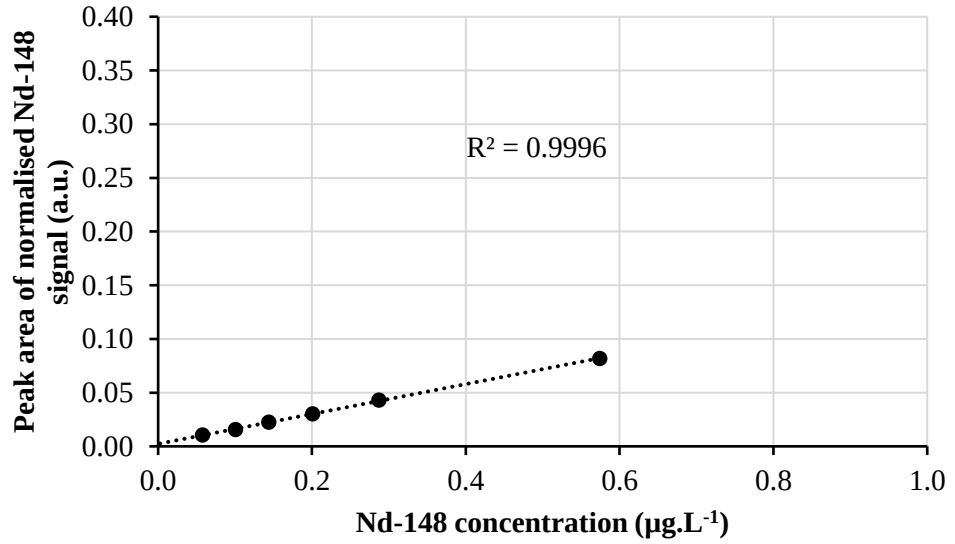


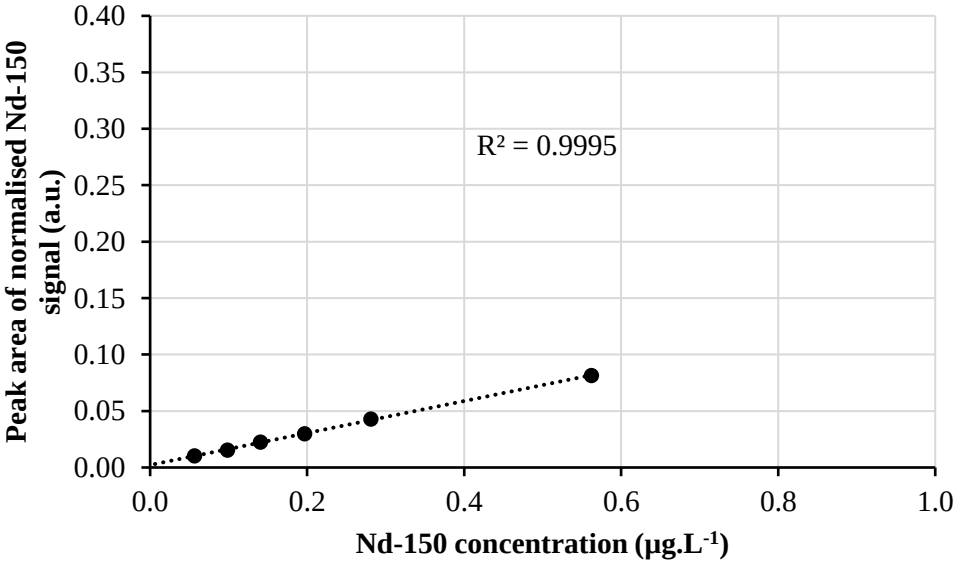


Figure S4.7 Nd nuclide-specific calibration curves obtained with HPIC-SF-ICP-MS

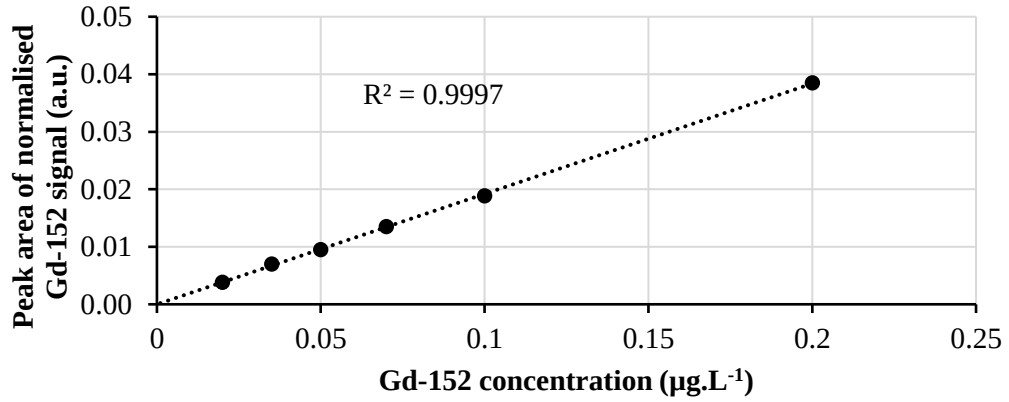
Peak area of normalised Gd-152 signal (a.u.)
0.05
0.04
0.03
0.02
0.01
0.00
R² = 0.9997
0
0.05
0.1
0.15
0.2
0.25
Gd-152 concentration (µg.L-1)

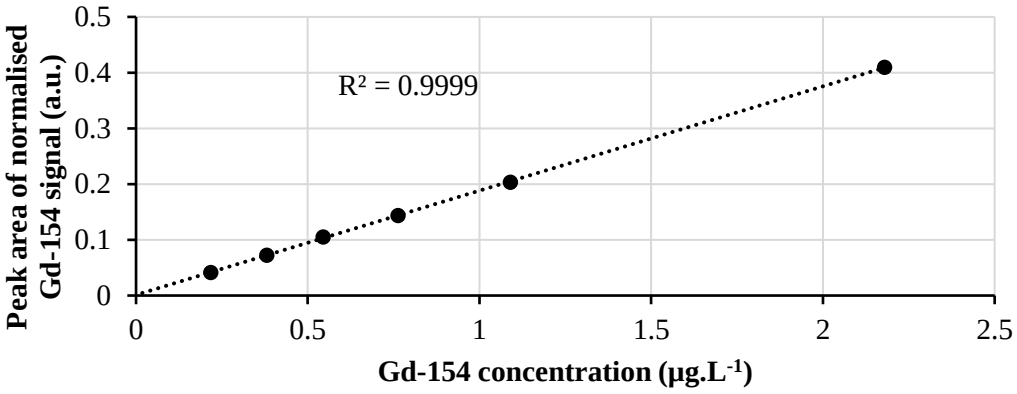
Peak area of normalised Gd-154 signal (a.u.)
0.5
0.4
0.3
0.2
0.1
0
R² = 0.9999
0
0.5
1
1.5
2
2.5
Gd-154 concentration (µg.L-1)

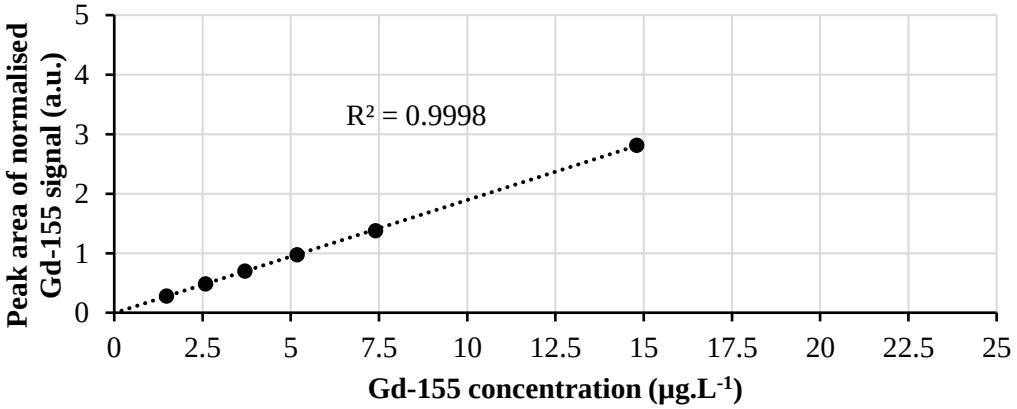
Peak area of normalised Gd-155 signal (a.u.)
5
4
3
2
1
0
R² = 0.9998
0
2.5
5
7.5
10
12.5
15
17.5
20
22.5
25
Gd-155 concentration (µg.L-1)

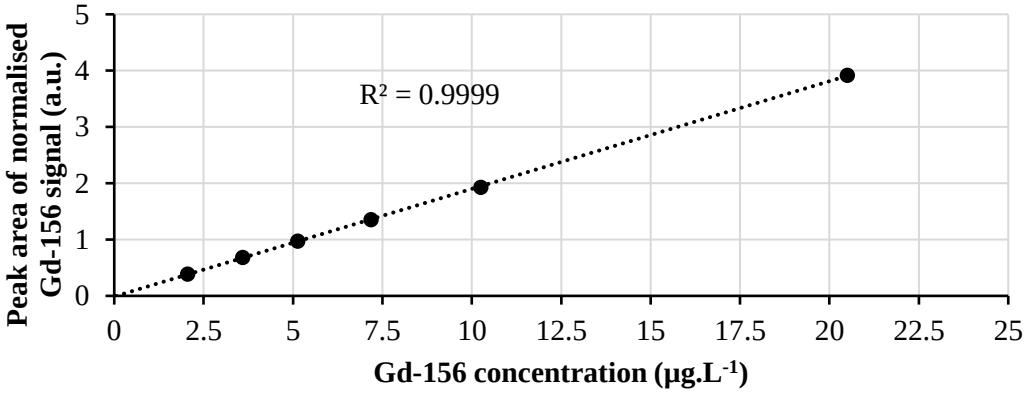
Peak area of normalised Gd-156 signal (a.u.)
5
4
3
2
1
0
R² = 0.9999
0
2.5
5
7.5
10
12.5
15
17.5
20
22.5
25
Gd-156 concentration (µg.L-1)

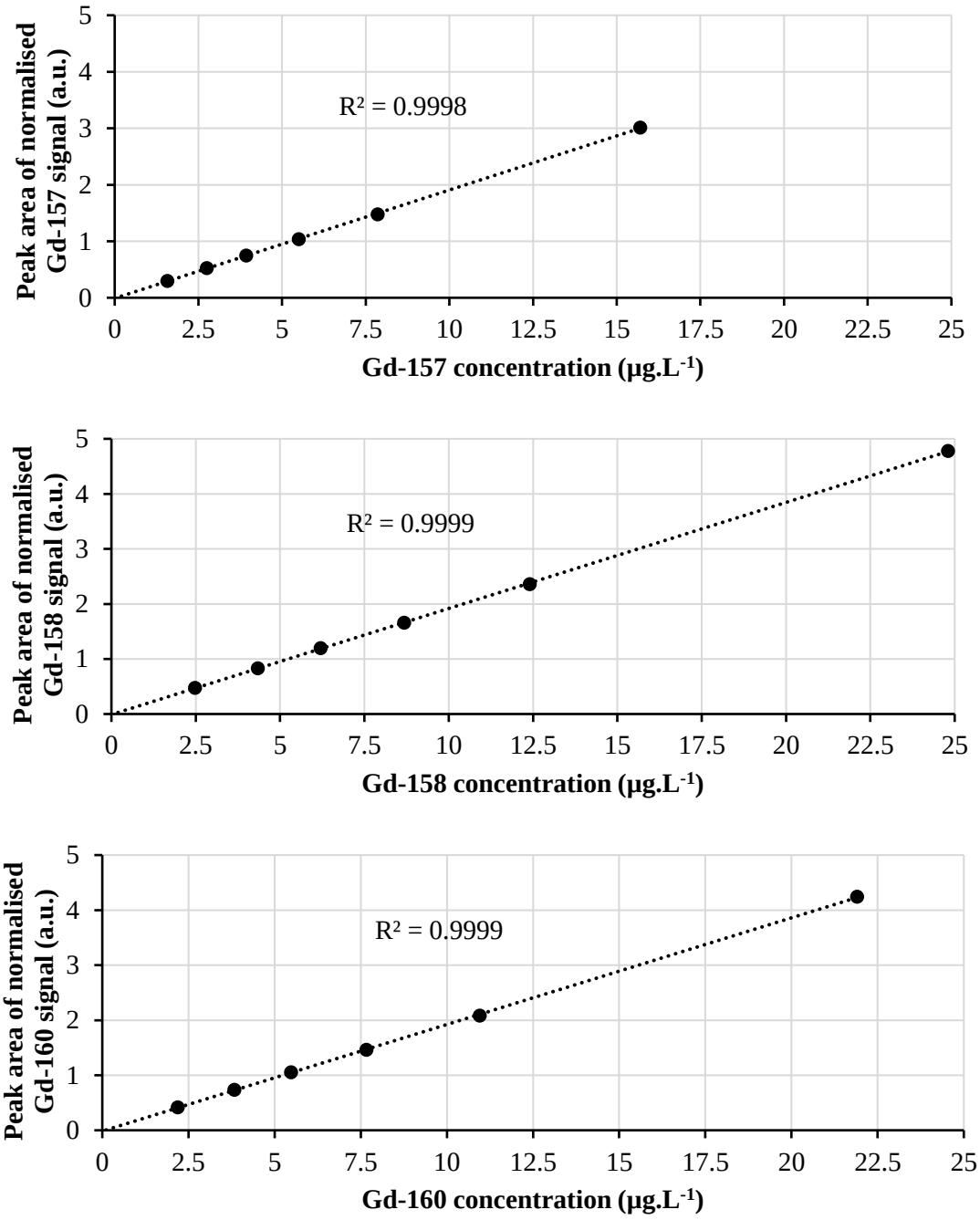


Figure S4.8 Gd nuclide-specific calibration curves obtained with HPIC-SF-ICP-MS

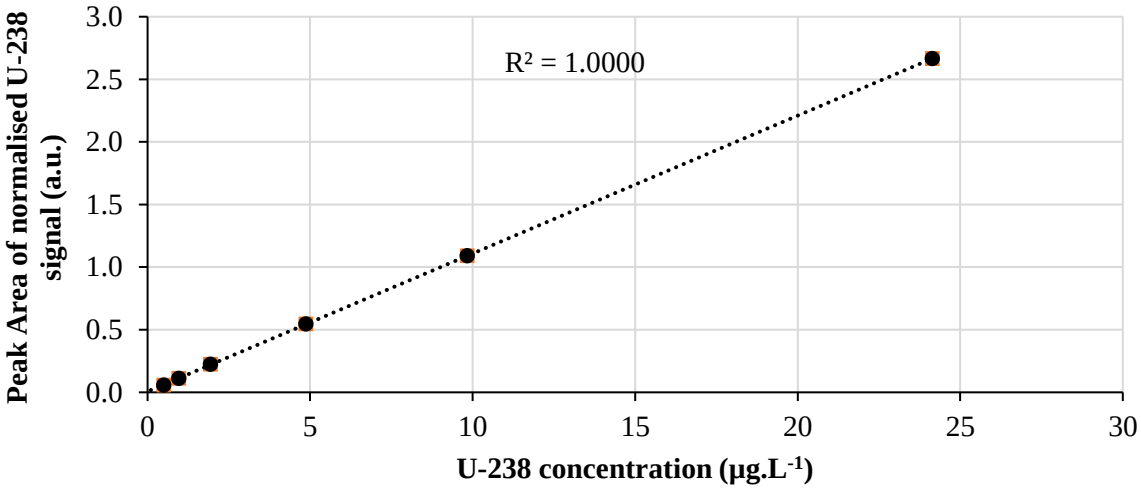


Figure S4.9 Calibration curve for $^{238}U$ obtained with HPIC-SF-ICP-MS

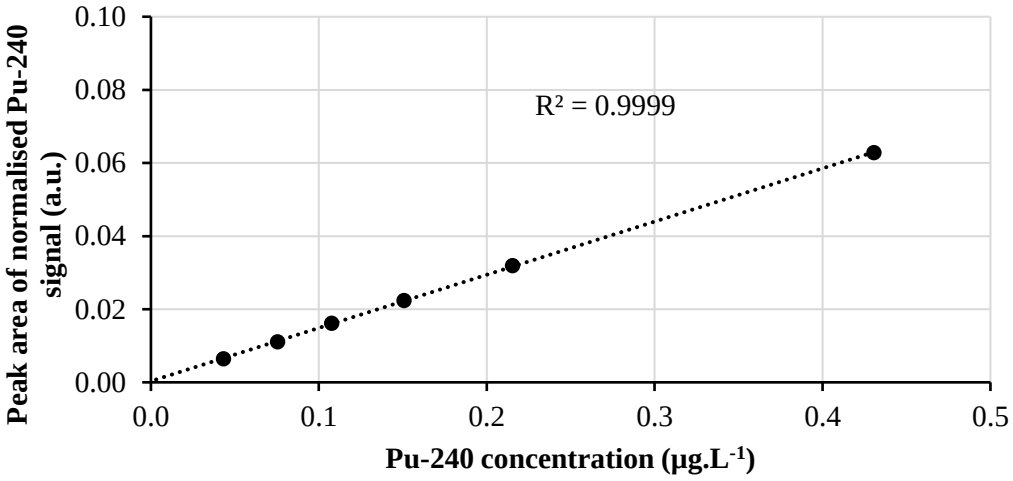


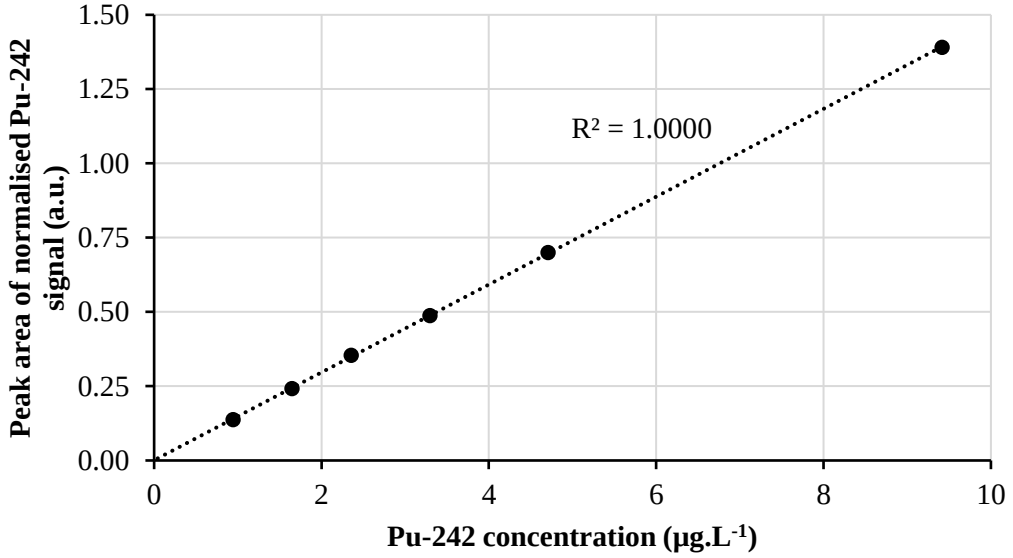


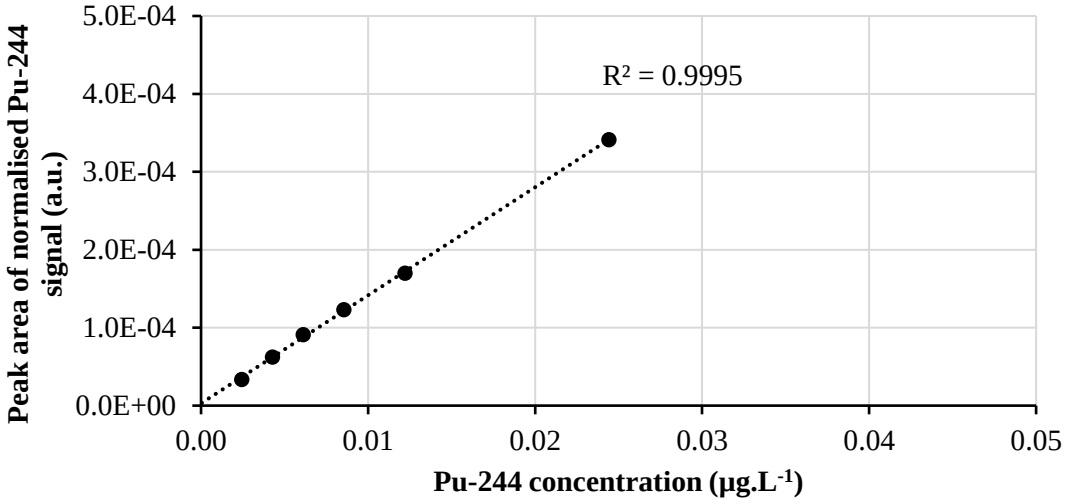


Figure S4.10 Calibration curves for monitored Pu isotopes obtained with HPIC-SF-ICP-MS

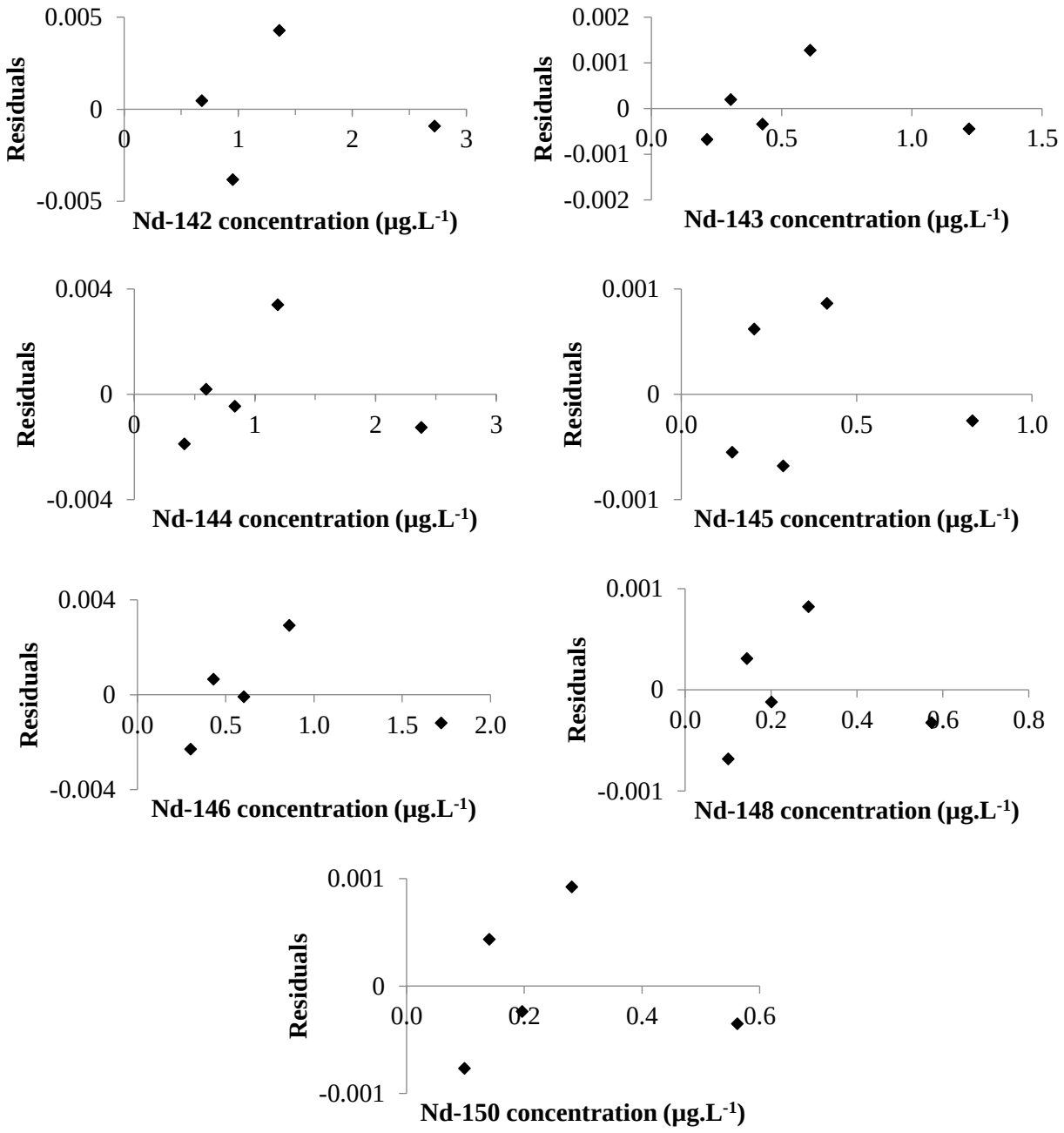


Figure S4.11 Residuals of linear regression for all nuclide-specific Nd calibration curves obtained with HPIC-SF-ICP-MS

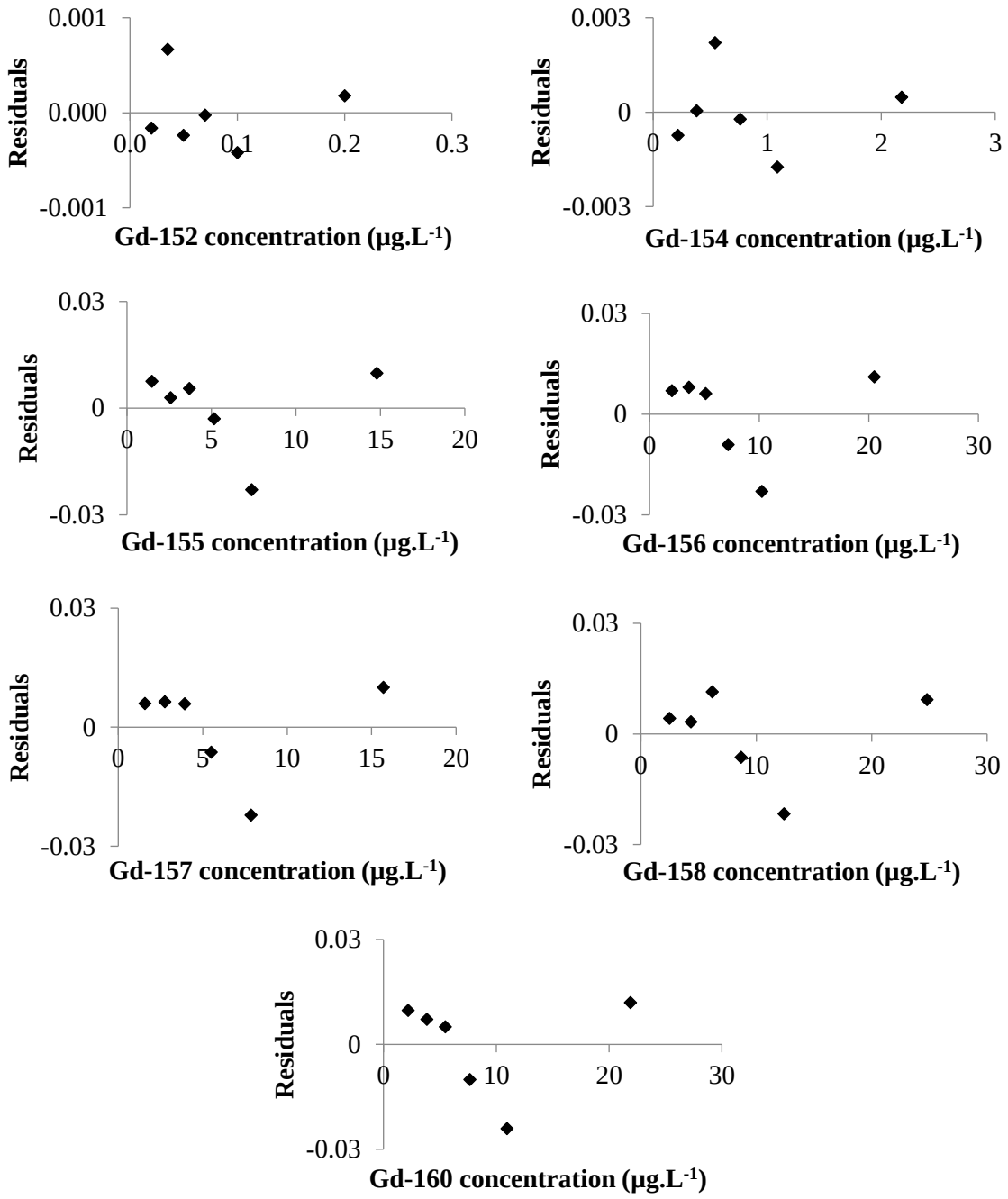


Figure S4.12 Plots of residuals for all nuclide-specific Gd calibration curves obtained with HPIC-SF-ICP-MS

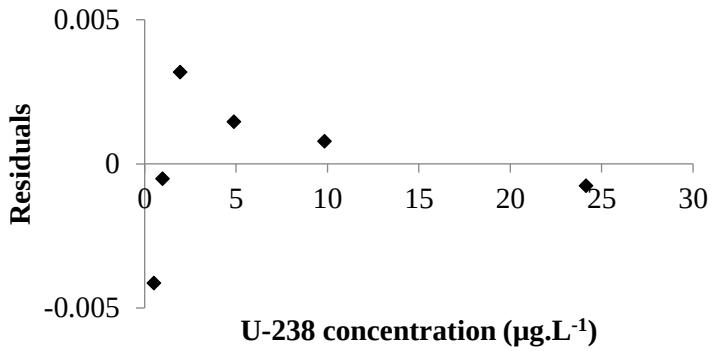


Figure S4.13 Plot of residuals for $^{238}U$ calibration curve

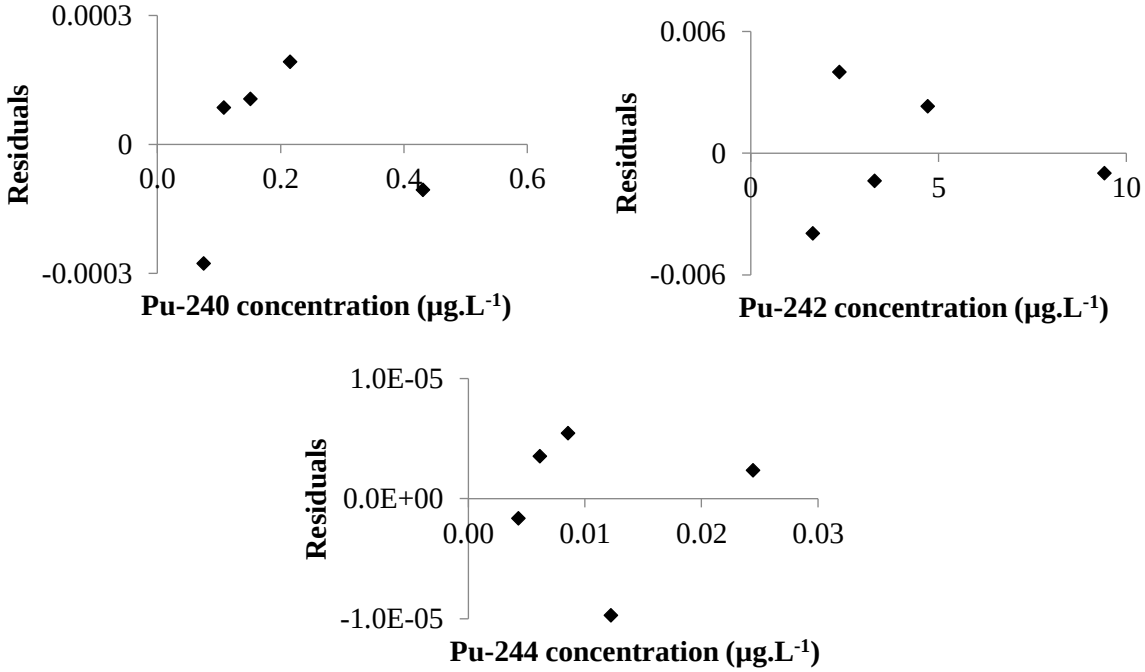


Figure S4.14 Plots of residuals for the Pu nuclide-specific calibration curves obtained with HPIC-SF-ICP-MS

# Chapter 5 – Optimization of isotope dilution HPIC-SF-ICP-MS

This chapter describes the work related to the second objective of this PhD: namely the optimization of an isotope dilution HPIC-SF-ICP-MS method to quantify neodymium, gadolinium, uranium and plutonium in SNF. The work towards this objective was divided into three steps. The first step was to optimize the acquisition parameters for SF-ICP-MS and to select a calculation method to obtain the most precise isotope ratios (IRs). The second step was to characterize two types of SNF by using isotope dilution HPIC-SF-ICP-MS. Finally, the overall uncertainty budget of isotope dilution HPIC-SF-ICP-MS was determined in order to compare the precision of the mass fractions obtained by using the optimized method with those obtained by using the ISO 17025 accredited isotope dilution TIMS & alpha spectrometry method. Portions of this chapter have been taken from a previous publication in volume 221 of the peer-reviewed journal Talanta (impact factor 5.339 in 2019) [1].

## 5.1 Introduction

After the HPIC separation method development, different calculation methods, SF-ICP-MS parameters and sample preparation steps were investigated to obtain the lowest uncertainties on elemental mass fractions determined by isotope dilution mass spectrometry (IDMS) using the single detector SF-ICP-MS hyphenated to HPIC. The precision of IRs is known to be a major contributor to the uncertainty of IDMS and therefore IRs were the first target of the investigation. Different acquisition parameters (mentioned in section 5.2.3.2 of chapter 5) as well as different calculation methods (see section 5.2.3.3 of chapter 5) were considered in order to determine IRs from transient signals with the best precision compared to the theoretical precision calculated from Poisson statistics (eq. 5.1). Other contributors to the uncertainty of IDMS, such as the IR in the blend and weighing uncertainties, were also taken into account and optimized. The expanded uncertainty of IDMS using the optimized HPIC-SF-ICP-MS method for the characterization of SNF was determined using a bottom-up approach with the aid of GUM Workbench software and compared to the time consuming but accurate isotope dilution TIMS & alpha spectrometry method.

## 5.2 Materials and methods

### 5.2.1 Standards and spikes

Materials with Nd of natural isotopic composition were obtained from VWR International (Leuven, Belgium) and Johnson Matthey (JMC-311). For the determination of the instrumental mass bias, the following certified isotopic reference materials were used: NBS-947 for Pu and NBS-005 for U, both sourced from the National Institute of Standards and Technology (NIST, Gaithersburg, MD, USA), Gd Spex Certiprep mono-elemental standard solution was purchased from Boom Laboratoriumleverancier (Meppel, The Netherlands). For isotope dilution mass

spectrometry, the following spikes were used: $^{146}$Nd spike obtained from Oak Ridge National Laboratory (ORNL, Oak Ridge, TN, USA), [the elemental Nd concentration of the enriched $^{146}$Nd spike was quantified by reverse IDMS using TIMS against $Nd_2O_3$ of natural isotopic composition (Specpure, Johnson Matthey Chemicals Limited, London, UK) and the uncertainty on the concentration obtained was 1.5% (2s))], $^{157}$Gd spike supplied by Isoflex (San Francisco, CA, USA), and the elemental Gd concentration was quantified by reverse IDMS using TIMS against $Gd_2O_3$ of natural isotopic composition (see section 3.2.6.3 for the isotopic compositions of the $^{146}$Nd and $^{157}$Gd spikes), and $^{233}$U (IRMM-040a) and $^{242}$Pu (IRMM-049d) certified isotopic reference materials obtained from the European Commission's Joint Research Centre (JRC, Geel, Belgium - formerly known as IRMM - Institute for Reference Materials and Measurements).

### 5.2.2 Fuel samples

Two types of SNF samples were analysed by isotope dilution HPIC-SF-ICP-MS: a uranium oxide (UOx) SNF and an experimental Gd-enriched SNF, for which the abbreviation "Gd fuel" is used [2].

### 5.2.3 Optimization of IR precision in transient signals

The precision of an IR derived from transient signals was studied by using the IRs of a natural neodymium standard material (JMC-311) diluted to a 10 $ng \cdot g^{-1}$ elemental mass fraction. Neodymium was favoured due to its non-radioactive and multi-isotopic nature (7 isotopes), as well as its presence as a fission product in both types of SNF analysed. The precisions of the IRs of interest, from SF-ICP-MS measurements performed on-line coupled with HPIC were compared with off-line measurements of the same IRs on five days over a one-month period. The precision (single injection) and repeatability (repeatability of 10 injections performed on the same day) obtained for these IRs were used as metrics to compare three methods (see 5.2.3.3) of calculating the IR. The intensity of each nuclide in the procedural blank was always subtracted from that of the corresponding nuclide in the sample/standard.

#### 5.2.3.1 HPIC method for Nd

To elute the injected neodymium (0.25 ng) from the columns, an isocratic flow rate of 0.125 $mL \cdot min^{-1}$ of 0.1 M oxalic acid buffered to pH 4.5 using ammonium hydroxide was employed. The column effluent was admixed with 0.75 M $HNO_3$ at an equal flow rate to acidify the column effluent before introducing it into the SF-ICP-MS. Further details about the instrumental setup can be found in chapters 2 and 4.

#### 5.2.3.2 SF-ICP-MS method for Nd

The influence of several data acquisition parameters on the precisions of the neodymium IRs calculated from transient signals was investigated. The effects of different mass windows (illustrated in Figure S5.1 in the appendix of this chapter), dwell times and numbers of monitored nuclides on the IR precision were investigated. Table 5.1 provides an overview of

the SF-ICP-MS parameters used during the optimization of acquisition parameters for IR measurements. The linearity of the mass bias correction factor (K-bias) over the monitored mass range was also investigated.

Table 5.1 SF-ICP-MS data acquisition parameters used during the assessment of IR precisions attainable from transient signals

| Parameter | Value/ Description |
|---|---|
| Mass resolution | 400 |
| Scan optimization | Speed |
| Scan type | E-Scan |
| Detection mode | Counting |
| Dwell time per nuclide | 10 or 30 ms |
| Mass window | 2, 25, 50 or 150 % |
| Integration window | Equal to mass window |
| Samples per peak | 20 |
| Nuclides monitored | $^{142}$Nd & $^{146}$Nd, or, $^{142}$Nd, $^{143}$Nd, $^{144}$Nd, $^{145}$Nd, $^{146}$Nd, $^{148}$Nd & $^{150}$Nd |

Standard sample bracketing (SSB) was used to correct for the instrumental mass bias. This implies that a standard (of known isotopic composition and concentration) was injected onto the column before and after the sample to determine a mass bias correction factor from each standard injection. The average mass bias correction factor of the two standard injections was then used to correct the sample result for mass bias. During optimization of the acquisition parameters using neodymium IR measurements, correction for the instrumental mass bias was accomplished using the linear model, as shown in eq. 3.3 in chapter 3 (section 3.2.3 of chapter 3).

The experimentally obtained precisions of the mass bias corrected IRs, when using different mass windows, were compared with the theoretical (best obtainable) precision, which was calculated according to eq. 5.1 [3], where $I_a$ and $I_b$ are the number of counts measured for isotopes a and b respectively.

$$RSD\ (\%) = 100 \cdot \sqrt{\frac{1}{I_a} + \frac{1}{I_b}} \qquad \text{(eq. 5.1)}$$

#### 5.2.3.3 Calculation methods of IRs from transient signals

IRs were determined from the co-eluting chromatographic peaks of the nuclides monitored (of that element). Once the optimum mass window was determined, the contribution of the chromatographic peak shoulders was investigated by considering data from 50% and 100 % of the chromatographic peak width for IR calculations, since, according to counting statistics, the

precision of the IRs obtained from the chromatographic peak shoulders is worse than that obtained in the peak centre [4].

#### 5.2.3.3.i Point by point method

In this calculation method, the point-by-point or PbP method, the raw IRs within the selected area of the chromatographic peak are averaged [5], as shown in Figure 5.1. The uncertainty on the calculated IR is considered to be the standard deviation of the averaged ratios obtained through error propagation.

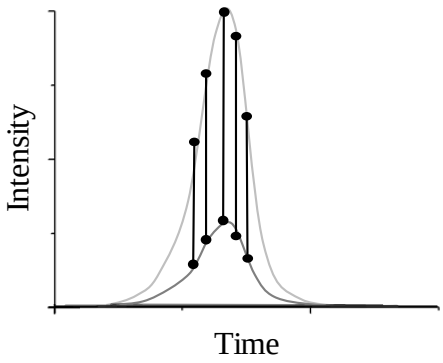


Figure 5.1 Point by Point (PbP) calculation method of the raw IR from transient signals

#### 5.2.3.3.ii Linear regression slope method

To calculate the raw IR using the linear regression slope (LRS), the intensities of the two nuclides are plotted as a function of one another and the IR is taken to be the slope of the linear regression line fitted to the data points [3, 5] (Figure 5.2 below). The equation of the linear regression line [3] is determined by using the least squares regression method (the LINEST function in Excel) as shown in eq. 5.2, where $a$ is the IR and $u_a$ represents the internal precision of a single measurement of an IR.

$$y = (a \pm u_a)x + (b \pm u_b) \qquad \text{(eq. 5.2)}$$

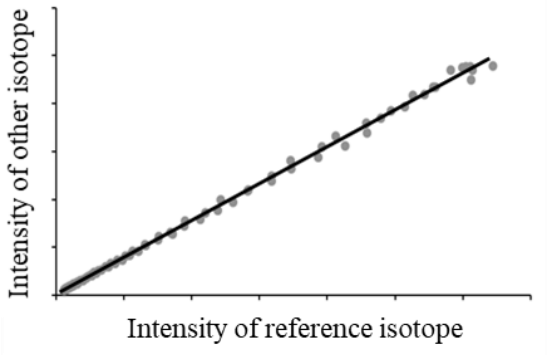


Figure 5.2 Linear regression slope (LRS) calculation method of the raw IR from transient signals

#### 5.2.3.3.iii Peak area integration method

To obtain raw IRs using the peak area integration (PAI) method, the area under the chromatographic peak of each nuclide measured (Figure 5.3) is divided by that of the measured reference nuclide [5]. For each nuclide monitored, the area under the chromatographic peak was calculated by summing areas of the integrated trapezoidal sections between two consecutively measured data points. The shape of the chromatographic peaks obtained using HPIC-SF-ICP-MS is skewed due to the sequential scanning of the different masses by the single collector SF-ICP-MS unit used. Therefore, fitting of the chromatographic peaks could not be done automatically. Different fittings (e.g. Gaussian fit and Boltzmann fit) were tried in OriginLab, but finally the fitting was done manually in Excel.

The standard deviation of the raw intensity is obtained using Poisson counting statistics (eq. 5.3) and propagated using the laws of error propagation [6] to calculate the uncertainty on the IR.

$$s = \sqrt{number\ of\ counts} \qquad \text{(eq. 5.3)}$$

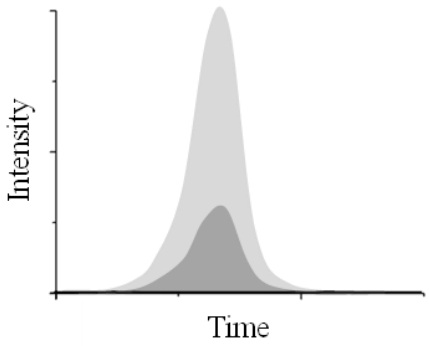


Figure 5.3 Peak area integration (PAI) calculation method of the raw IR from transient signals

#### 5.2.3.4 Calculation methods of IRs from continuous nebulization

The data acquisition parameters used for continuous nebulization measurements are listed in Table 5.2. During nebulization of a sample, the recorded intensity of each nuclide is divided by that of the reference nuclide. The ratios obtained thus are averaged and their standard deviation is considered to be the uncertainty on the IR. Ratios lying outside the 2SD margin from the average were omitted when calculating the IR.

Table 5.2 SF-ICP-MS parameters used during continuous nebulization for optimizing IR precision

| Parameter | Value/ Description |
|---|---|
| Mass resolution | 400 |
| Scan optimization | Mass accuracy |
| Scan type | E-Scan |
| Detection mode | Counting |
| Dwell time per nuclide | 10 ms |
| Mass window | 25 % |
| Integration window | 25 % |
| Samples per peak | 20 |
| Nuclides monitored | $^{142}$Nd, $^{143}$Nd, $^{144}$Nd, $^{145}$Nd, $^{146}$Nd, $^{148}$Nd & $^{150}$Nd |

### 5.2.4 Isotope dilution

Figure 5.4 illustrates the workflow of isotope dilution HPIC-SF-ICP-MS used in this work to characterize the UOx and "Gd fuel". The spikes and $KMnO_4$ were added to the samples at least 12 hours before the analysis, to ensure sufficient time for isotopic equilibration and to convert all Pu to the desired oxidation state (+VI) (see section 4.2.3.3 of chapter 4), respectively. Tuning resulted in an oxide level ($MO^+/M^+$ ratio) lower than 8% of the corresponding element signal before starting the measurement sequence. The results obtained with isotope dilution HPIC-SF-ICP-MS were compared to those previously obtained using off-line gravitational chromatography followed by isotope dilution TIMS & alpha-spectrometry. Since isotope dilution HPIC-SF-ICP-MS analyses were performed later than the isotope dilution TIMS & alpha-spectrometry analyses (see Table 5.3 for dates), the date of the TIMS & alpha-spectrometry analyses were used as a reference date. The isotope dilution HPIC-SF-ICP-MS data was corrected to this reference date for the decay of $^{241}$Pu, with a half-life of 14.33 years, to $^{241}$Am. At SCK CEN, the TIMS measurement of Pu is usually carried out within 10 days from the date of the off-line chromatographic separation of Pu from U and Am. This is a pragmatic approach that seeks to avoid the need to correct for ingrowth of $^{241}$Am, since over this short timeframe any change would be negligible. The date for Pu-Am separation by off-line gravitational chromatography, the date of Am analysis by alpha-spectrometry (and Am mass fractions in the analysed fuel samples) and the date of Pu analysis by isotope dilution TIMS & alpha-spectrometry are listed in Table 5.3.

Since both the UOx and the Gd-fuel samples were cooled for more than 4 years (time elapsed between EOL and DOA at SCK CEN laboratories), $^{144}$Ce (half-life around 9 months) will have decayed substantially to $^{144}$Nd during this cooling period. The activity of $^{144}$Ce in the samples was also found to be below the detection limit ($5.7 \cdot 10^{-05}$ mg·g$^{-1}$ fuel). Therefore, it is not possible to distinguish between $^{144}$Nd formed as a fission product and $^{144}$Nd formed by the decay of $^{144}$Ce at the time of analysis.

Nuclide-specific mass fractions of $^{154}$Eu, $^{155}$Eu, $^{154}$Gd, $^{155}$Gd in the "Gd fuel" are presented in Table 5.4, from which it can be inferred that the decay of $^{154}$Eu and $^{155}$Eu into $^{154}$Gd and $^{155}$Gd,

respectively, would have only a minor effect on the mass fractions of these Gd nuclides since their mass fractions in the "Gd fuel" were already 1000 times higher than those of these Eu nuclides (unlike in UOx spent nuclear fuels where the mass fractions of Eu and Gd are similar).

Table 5.3 Pu-Am gravitational chromatographic separation date and Pu analysis dates using TIMS & alpha-spectrometry and HPIC-SF-ICP-MS

| Sample | Date of Pu-Am separation | Date of Pu TIMS & alpha-spectrometry analysis | Date of Pu HPIC-SF-ICP-MS analysis | Date of Am analysis | Mass fraction of $^{241}$Am in fuel ($mg \cdot g^{-1}$) ± U (k=2) |
|---|---|---|---|---|---|
| UOx | 2019-10-01 | 2019-10-08 | 2020-02-26 (n = 2) 2020-02-27 | 2020-02-18 (by gamma-spectrometry) | 0.477 ± 0.17 |
| Gd fuel | 2018-02-14 | 2018-02-22 | 2020-01-06 2020-02-24 2020-02-25 | 2017-02-13 (by alpha-spectrometry) | 0.1468 ± 0.0089 |

Table 5.4 Nuclide-specific mass fractions of Eu and Gd nuclides in the "Gd fuel" measured using isotope dilution TIMS & alpha-spectrometry

| Sample | Date of analysis | Nuclide | Mass fraction in fuel at date of analysis ($mg \cdot g^{-1}$) |
|---|---|---|---|
| Gd fuel | 2017-05 | $^{154}$Eu | $9.83 \cdot 10^{-4}$ |
| | | $^{155}$Eu | $2 \cdot 10^{-4}$ |
| | 2018-05 | $^{154}$Gd | 1.74 |
| | | $^{155}$Gd | 1.7 |

#### 5.2.4.1 Instrumental methods

##### 5.2.4.1.i HPIC method

The elution method for the separation of Pu, U and the lanthanides in one run, as described in section 4.2.3.3 of chapter 4, was used. The uranium fraction was collected between 4.25 and 21.67 minutes by automatically diverting the flow of the column effluent away from the SF-ICP-MS nebulizer and towards the fraction collection system by using a 6-port 2-way valve. After collection of this uranium fraction, the flow was automatically redirected back towards the inlet system of the SF-ICP-MS unit for on-line measurement. The uranium fraction was analysed later off-line by using continuous nebulization for sample introduction.

##### 5.2.4.1.ii SF-ICP-MS method

The SF-ICP-MS parameters used during the on-line and off-line isotope dilution analyses are listed in Table 5.5. Figure S5.2 in the appendix of this chapter shows a sequence as used by the software of the "*Element 2"* used in this work for the analysis of a spent "Gd fuel" using isotope dilution HPIC-SF-ICP-MS. Based on the elution times of the elements of interest, the list of

nuclides to be monitored was changed in the SF-ICP-MS measurement method during the same injection. During the elution of Nd, $^{140}$Ce was monitored in order to be able to correct for any potential contribution to the $^{142}$Nd signal (*counts*) from $^{142}$Ce using eq.5.4 (*A* is the isotopic abundance reported by IUPAC, $(n(^{142}Nd)/n(^{146}Nd))_{meas}$ and $(n(^{140}Ce)/n(^{146}Nd))_{meas}$ are the measured IRs for $^{142}$Nd and $^{140}$Ce relative to $^{146}$Nd and $(n(^{142}Nd)/n(^{146}Nd))_{interference\ corr}$ is the interference corrected IR for $^{142}$Nd relative to $^{146}$Nd).

$$(n(^{142}Nd)/n(^{146}Nd))_{interference\ corr}=(n(^{142}Nd)/n(^{146}Nd))_{meas}-\left(\frac{A(^{142}Ce)\cdot(n(^{140}Ce)/n(^{146}Nd))_{meas}}{A(^{140}Ce)}\right) \quad \text{(eq. 5.4)}$$

Table 5.5 SF-ICP-MS parameters during on-line and off-line isotope dilution

| Parameter | On-line (transient signal) | | | Off-line (continuous nebulization) |
|---|---|---|---|---|
| Cool gas flow rate | 16 L·min$^{-1}$ | | | |
| Auxiliary gas flow rate | 0.8 L·min$^{-1}$ | | | |
| Nebulizer gas flow rate | 1.06 L·min$^{-1}$ | | | |
| Mass resolution | 400 | | | |
| Scan type | E-Scan | | | |
| RF power | 1250 W | | | |
| Detector dead time | 17 ns | | | |
| Detection mode | Counting | | | |
| Dwell time per nuclide | 10 ms | | | |
| Settling time | 1 ms | | | |
| Scan optimization | Speed | | | Mass accuracy |
| | Pu | Nd | Gd | U |
| Runs | 830 | 740 | 645 | 350 |
| Passes | 1 | | | 1 |
| Mass window | 25 % | | | 2 % |
| Integration window | 25 % | | | 2 % |
| Samples per peaks | 20 | | | 250 |
| Nuclides monitored during elution of Pu peak (total run time 0-4.25 mins) | $^{238}$Pu, $^{239}$Pu, $^{240}$Pu, $^{241}$Pu, $^{242}$Pu & $^{244}$Pu | | | - |
| Nuclides monitored during analysis of U in collected fraction (total run time 4.25-21.67 mins) | - | | | $^{233}$U, $^{234}$U, $^{235}$U, $^{236}$U & $^{238}$U |
| Nuclides monitored during elution of Nd peak (total run time 35-40 mins) | $^{140}$Ce, $^{142}$Nd, $^{143}$Nd, $^{144}$Nd, $^{145}$Nd, $^{146}$Nd, $^{148}$Nd & $^{150}$Nd | | | - |
| Nuclides monitored during elution of Gd peak (total run time 50-60 mins) | $^{152}$Gd, $^{154}$Gd, $^{155}$Gd, $^{156}$Gd, $^{157}$Gd, $^{158}$Gd & $^{160}$Gd | | | - |

#### 5.2.4.1.iii TIMS and alpha-spectrometry method

Nuclear fuel samples were dissolved in a 10 M $HNO_3$/0.1 M HF mixture, inside a shielded hot-cell. After dilution of an aliquot of that mother solution in 1 M $HNO_3$, an aliquot of the diluted sample was subjected to a redox cycle in order to convert all Pu to Pu(IV), after which all target

elements were converted into their chloride forms by evaporation and re-dissolution in HCl. Pu and U were separated from the fission products + REE + Am + Cm by their elution with 0.35 M $HNO_3$ and 8.0 M $HNO_3$, respectively, on a Dowex 1X4 column. Ce (as Ce IV) was separated from the unretained fission products + REE + Am + Cm fraction using a mixed $PbO_2$ – Dowex 1X4 column that retains tetravalent ions. The unretained actinides, fission products and trivalent REE were converted to chloride forms and eluted from a column loaded with a Ln resin, Gd eluting last under a nitric acid gradient elution. These purified U, Pu, Nd and Gd fractions were subsequently analysed by TIMS using classical evaporation from non zone-refined triple filaments and ion signal monitoring by Faraday collectors. All IRs were corrected for mass bias fractionation.

For alpha spectrometric analyses, measurements were made on the unseparated dilution of the mother solution. Standard and sample sources were prepared by weighing and evaporating a small aliquot on a tantalum disc (three separate discs for each sample or standard). Total alpha measurements were performed using efficiency-calibrated solid scintillation ZnS-detectors. Measurements of the alpha energy groups, i.e. $^{239}Pu$ + $^{240}Pu$, $^{238}Pu$ + $^{241}Am$, were performed using energy-calibrated PIPS (Passivated ion Implanted Planar Silicon) detectors that permit the identification of the alpha-emitters and the determination of their relative contributions to the total alpha activity.

#### 5.2.4.2 Calculation methods

The peak area integration (PAI) method was used to determine IRs from transient signals of Pu, Nd and Gd. Standard sample bracketing (SSB) was used for external correction of the instrumental mass bias. The two nuclides selected for each element for IDMS purposes are shown in Table 5.6.

Table 5.6 Pairs of nuclides selected for IDMS

| Element | Spike nuclide | Reference nuclide |
|---|---|---|
| Pu | $^{242}Pu$ | $^{239}Pu$ |
| U | $^{233}U$ | $^{238}U$ |
| Nd | $^{148}Nd$ | $^{146}Nd$ |
| Gd | $^{157}Gd$ | $^{156}Gd$ |

The single isotope dilution equation (eq. 3.13 in section 3.2.6.3 of chapter 3) was used to determine the mass fractions of the selected elements in the different spent nuclear fuel types. This version of IDMS was used due to its simplicity for routine analysis, requiring the fewest variables to be measured [7]. Based on the measured IRs in the sample ($R_{i,x}$), the amount fractions of the different Pu, U, Nd and Gd nuclides present in the sample were determined.

An uncertainty budget for IDMS was derived based on the bottom-up approach, following the rules given in the Eurachem/CITAC guide CG 4 [6]. The uncertainty calculation was performed by using GUM Workbench software (Metrodata GmbH, Germany) [8]. A cause and effect diagram, known as an Ishikawa or fishbone diagram, was used to illustrate the uncertainty

sources. The following sources of uncertainty and their corresponding standard uncertainties were considered:

- Raw IR calculation using PAI for transient signals after blank subtraction.
- Mass bias correction using IR reference values derived from IUPAC abundances [9] for Gd nuclides. For Nd, however, the IRs measured (on JMC-311) by MC-ICP-MS were chosen as reference values (to correct for instrumental mass bias Russell's law (see eq. 3.6) was used with a value of 0.7219 for the $^{146}Nd/^{144}Nd$ ratio). For U and Pu, the reference IRs were obtained from the certificates of the corresponding standards.
- Uncertainties introduced through weighing during the dilution of the spikes, samples and preparation of the blend. The minimum mass used throughout all different serial dilutions was 250 mg. The repeatability, readability and linearity specifications of the balance (Mettler Toledo MS205DU) were taken into account in calculating the expanded weighing uncertainty. Uncertainty for the correction of air buoyancy was calculated based on international recommendation R 111 – 1 issued by OIML (International organization of legal metrology) [10].
- IRs for Pu and U nuclides in the spike ($R_{i,y}$) were taken from the corresponding certificates.
- IRs for Nd and Gd nuclides in the spike solutions were based on values measured with TIMS since no certificates were available.
- Uncertainties in the sum of the ratios in the sample ($\Sigma R_{i,x}$) and in the spike ($\Sigma R_{i,y}$).

The expanded uncertainties (k =2) associated with the elemental mass fractions of Pu, U, Nd and Gd determined from both on-line and off-line isotope dilution HPIC-SF-ICP-MS measurements were compared with equivalent data available from previous analyses of the same SNF samples by means of off-line gravitational chromatography followed by TIMS (Sector 54 from VG) or alpha spectrometry [Alpha Analyst from Mirion Technologies (Canberra BNLS) NV] in the case of $^{238}Pu$.

Figure 5.4 Simplified diagram of isotope dilution HPIC-SF-ICP-MS workflow (*i* refers to a monitored nuclide, *w* is the mass fraction, *m* is the weight measured with a balance, *M* is the molecular weight, *E* is the element of interest corresponding to *i*, *n* is the number of moles, *K* is the mass bias correction factor, *A* is the abundance of the lighter isotope (*l*) and heavier isotope (*h*), *R* is the IR and $R(i)_y$ is obtained from the certificate)

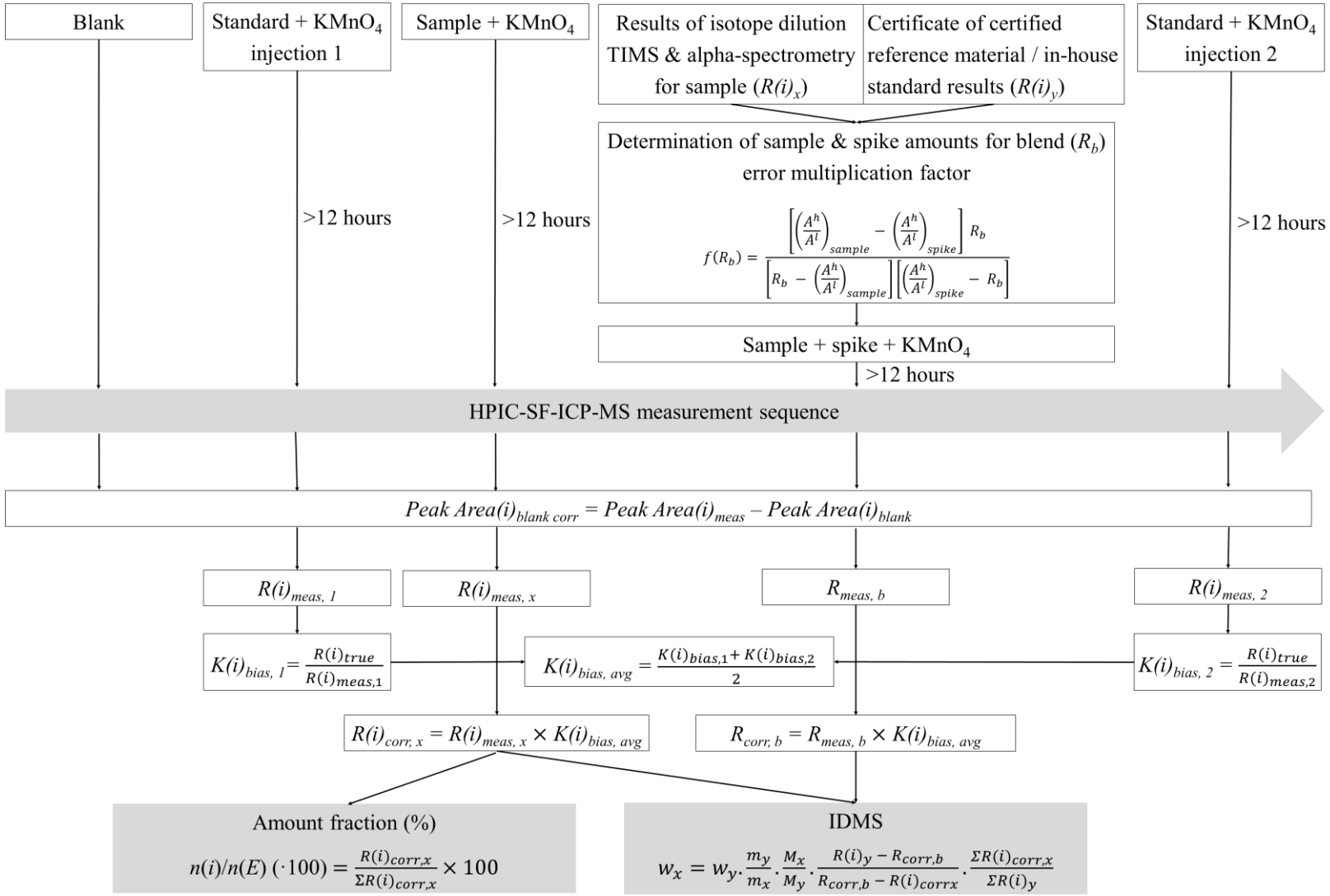

## 5.3 Results and discussion

### 5.3.1 Optimization of IR precision in transient signals

With a mass window of 150 %, to acquire all of the 20 samples per flat top peak, the effect of two dwell times (10 and 30 ms) on the precision of Nd IRs from transient signals was investigated. The shorter dwell time resulted in a faster sequential acquisition of the nuclides and increased the number of data points per chromatographic peak, as illustrated in Figure S5.1 in the appendix of this chapter. The precision on the IRs, calculated by using PbP and LRS, was improved when using the shorter dwell time (10 ms) (illustrated using the example of $^{142}Nd/^{146}Nd$ in Figure 5.5), which is in agreement with the literature [11, 12] that for instruments with sequential acquisition (such as SF-ICP-MS) the uncertainty in the IR improves with faster switching between the nuclides monitored. With PAI, however, the time dependency is irrelevant and the effect of spectral skew is eliminated, thereby significantly improving the precision of IRs compared to those calculated by PbP or LRS, as shown in Figure 5.5. Spectral skew arises from the sequential acquisition of the signal at different masses, and is translated into a biased IR, because the second measured mass is monitored at a later stage during peak elution. Therefore, the second measured mass is biased in a positive sense in comparison to the first measured mass when the elution peak is increasing, while the opposite is observed when the elution peak is decreasing [13]. As a consequence of spectral skew, PbP provides the least precise IRs in transient signals from HPIC-SF-ICP-MS.

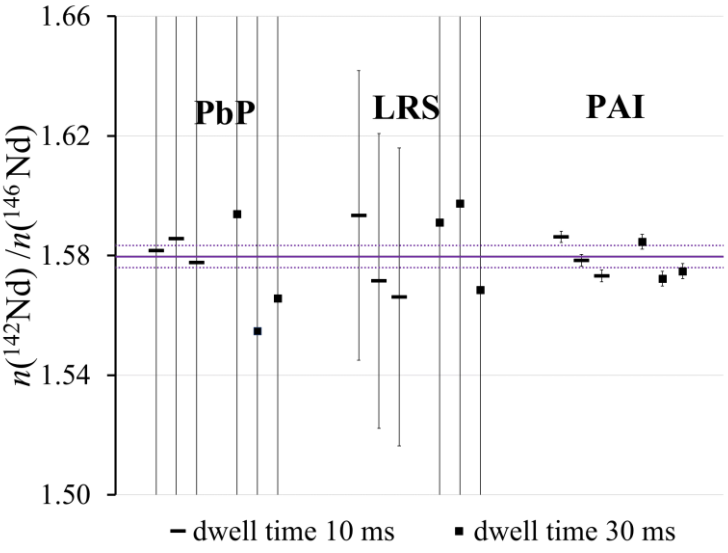


Figure 5.5 Precision of $n(^{142}Nd)/n(^{146}Nd)$ acquired using a mass window of 150 % and two different dwell times (10 & 30 ms) with HPIC-SF-ICP-MS and calculated using PbP, LRS and PAI

With a mass window of 50 %, to remove any contribution from the shoulders of the flat top spectral peak to the IR, and 10 ms dwell time, the effect of longer (total) acquisition times was investigated further by monitoring different numbers of nuclides. Two extreme cases were considered: the minimum number of nuclides (two) needed to obtain a ratio, and the maximum number of nuclides for a fission product element (seven in the case of Nd). The more nuclides

monitored per run, the larger the time lag between two consecutive data points, and hence, fewer data points are registered per chromatographic peak. This time lag between two consecutively measured data points explains why the precision on IRs calculated by using PbP and LRS is improved when fewer nuclides are monitored (example of $n(^{142}Nd)/n(^{146}Nd)$ in Figure 5.6). In the case of nuclear samples, however, the isotopic composition is unknown and monitoring all of the nuclides, of Nd for instance, is therefore required.

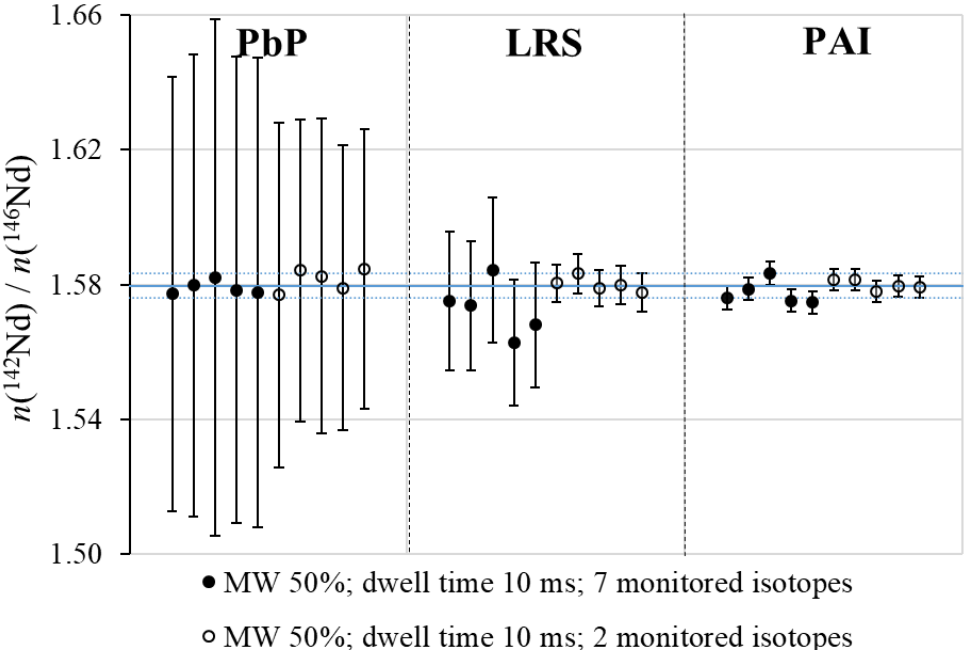


Figure 5.6 IR of $n(^{142}Nd)/n(^{146}Nd)$ acquired using a mass window of 50 % and two different numbers of nuclides monitored (2 & 7) with HPIC-SF-ICP-MS and calculated using PbP, LRS and PAI

The precision of IRs determined by using the three IRs calculation methods were investigated by measuring the Nd standard (JMC-311) 10 times on the same day, the results of which are presented in Table 5.7. The precisions of all the IRs calculated by using PAI were an order of magnitude better than when calculated by using PbP, and almost half of those when using the LRS method. That PbP results in a worse precision (for IRs from transient signals) compared to PAI and LRS is due to the sequential measurement of the different nuclides and has been reported elsewhere [5, 13-14]. In contrast, the poorest repeatability on the 10 Nd IRs was obtained with LRS and the best one with PAI, as is illustrated in Figure 5.7, which echoes the finding of Epov et al. [3] when only 50 % of the chromatographic peak is taken into account for IR calculation.

Moreover, the precision achieved with the three methods of calculation and four different mass windows have been compared with the theoretical precision (eq. 5.1), as shown in Figure 5.8 (also shown in Figure S5.3 in the appendix of this chapter). The precision obtained with PAI approached the theoretical precision the closest, independent of the mass window size. However, a mass window of 2 % is impractical because it results in only one sample per flat top peak, which prevents monitoring the mass calibration stability and leads to an underestimation of measurement precision as shown in Figure 5.8. A mass window of 25 % has

the advantage of 5 samples per peak that are located in the middle of the spectral flat top peak, as well as more data points being collected per chromatographic peak than is the case for mass windows of 50 or 150 % (see Figure S5.1 in the appendix of this chapter). Further investigation has shown that, with a mass window of 25 %, the linear regression of the K-bias versus the atomic masses of the monitored Nd nuclides passes through the point with coordinates (145.9131225 [9]; 1), which is not the case with mass windows of 50 & 150 %, as shown in Figure 5.9. Additionally, the sum of residuals on the linear regression of the K-bias versus the atomic masses of Nd nuclides was found to be smaller for a mass window of 25 % than for mass windows of 50 & 150 % (Figure 5.9). This illustrates that the data obtained fit the linear model for instrumental mass bias, and hence justifies the choice made. One last advantage of a mass window of 25 % is that the experimental precision approaches the theoretical precision the closest.

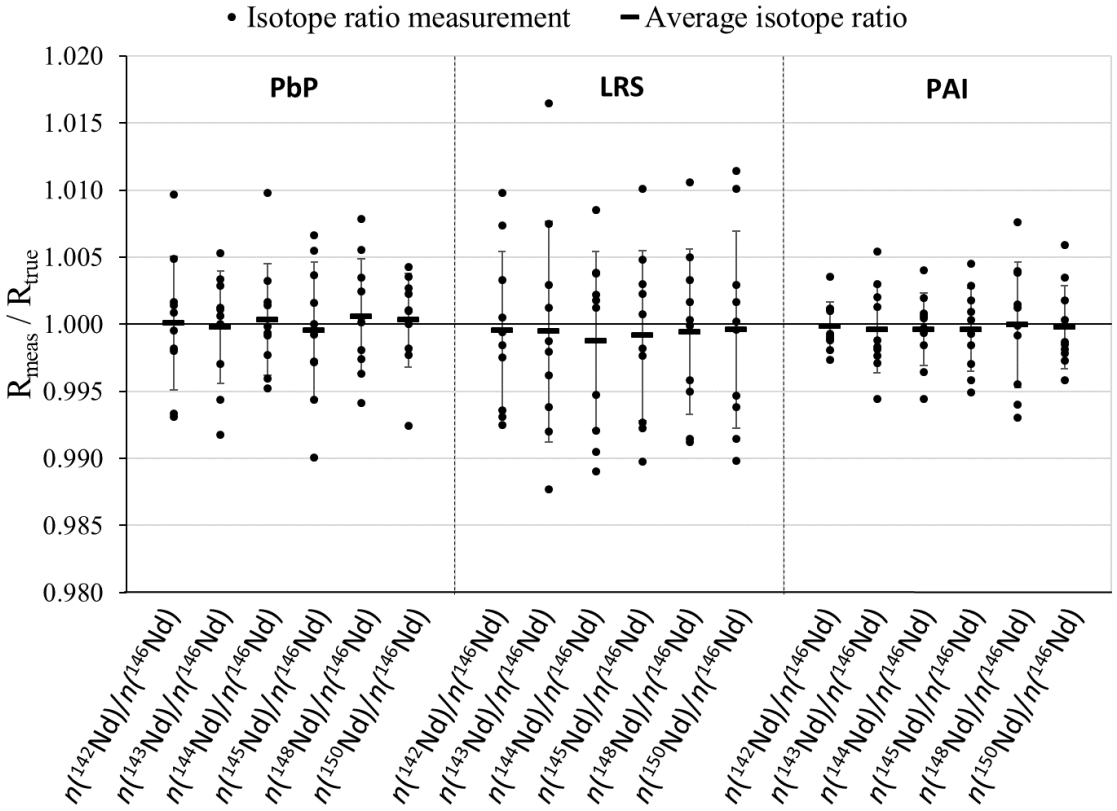


Figure 5.7 Repeatability on Nd IRs calculated using PbP, LRS and PAI and normalized to IUPAC values (the error bars represent ±1SD of the 10 calculated IRs)

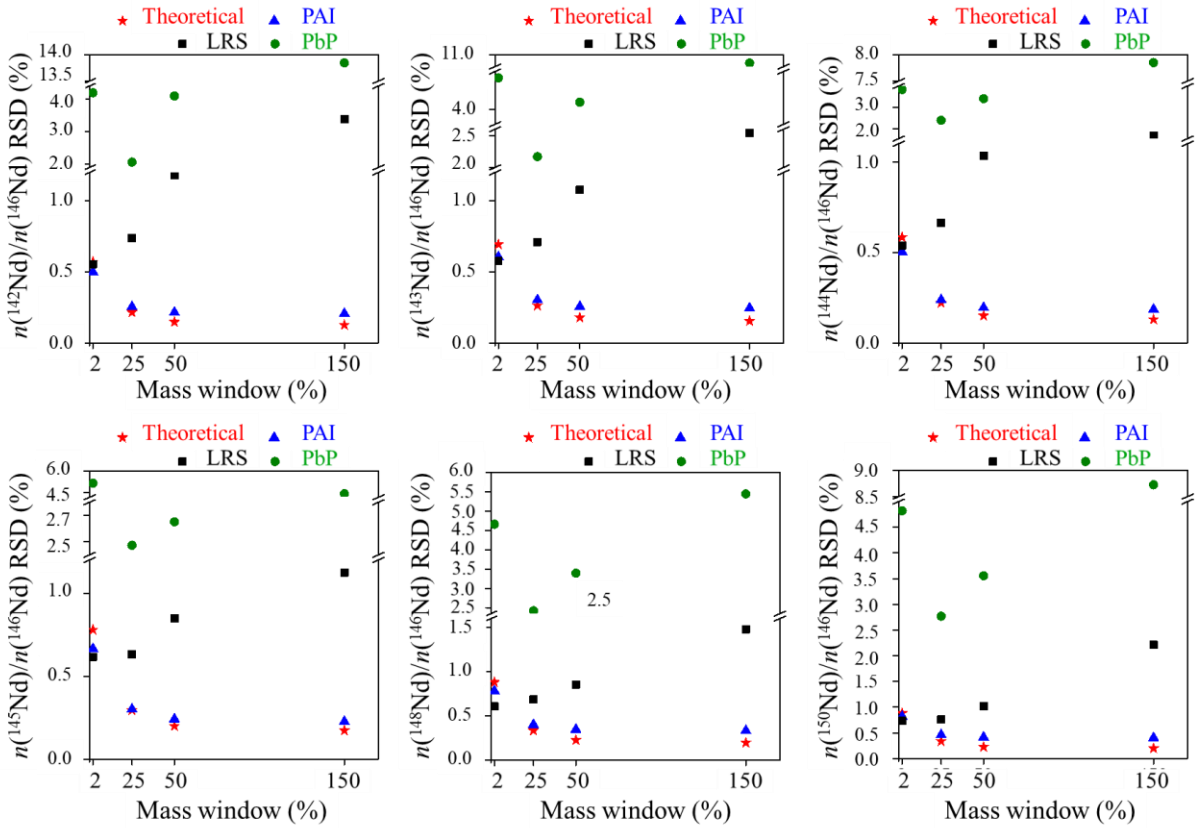


Figure 5.8 Theoretical and experimental precision of Nd IRs acquired using different mass windows (2, 25, 50 and 150 %) and calculated from transient signals as obtained using HPIC-SF-ICP-MS using PAI, PbP and LRS

Table 5.7 Precision on single IR measurement and repeatability of 10 Nd IR measurement results measured using HPIC-SF-ICP-MS and calculated using PbP, LRS and PAI

| IR | | $^{142}$Nd/ $^{146}$Nd | $^{143}$Nd/ $^{146}$Nd | $^{144}$Nd/ $^{146}$Nd | $^{145}$Nd/ $^{146}$Nd | $^{148}$Nd/ $^{146}$Nd | $^{150}$Nd/ $^{146}$Nd |
|---|---|---|---|---|---|---|---|
| Internal RSD range (%) | PbP | 2.1 – 2.6 | 1.9 – 3.1 | 2.0 – 2.5 | 2.1 – 2.8 | 2.3 – 2.8 | 2.3 – 3.3 |
| | LRS | 0.74 – 0.86 | 0.71 – 1.01 | 0.63 – 0.89 | 0.63 – 0.79 | 0.68 – 0.87 | 0.76 – 1.0 |
| | PAI | 0.25 – 0.26 | 0.30 – 0.31 | 0.24 | 0.30 – 0.31 | 0.40 – 0.41 | 0.46 – 0.47 |
| | theoretical | 0.22 | 0.26 | 0.22 | 0.30 | 0.33 | 0.33 |
| Repeatability RSD (%) | PbP | 0.50 | 0.42 | 0.42 | 0.51 | 0.43 | 0.35 |
| | LRS | 0.59 | 0.82 | 0.66 | 0.63 | 0.62 | 0.73 |
| | PAI | 0.18 | 0.33 | 0.27 | 0.31 | 0.47 | 0.31 |

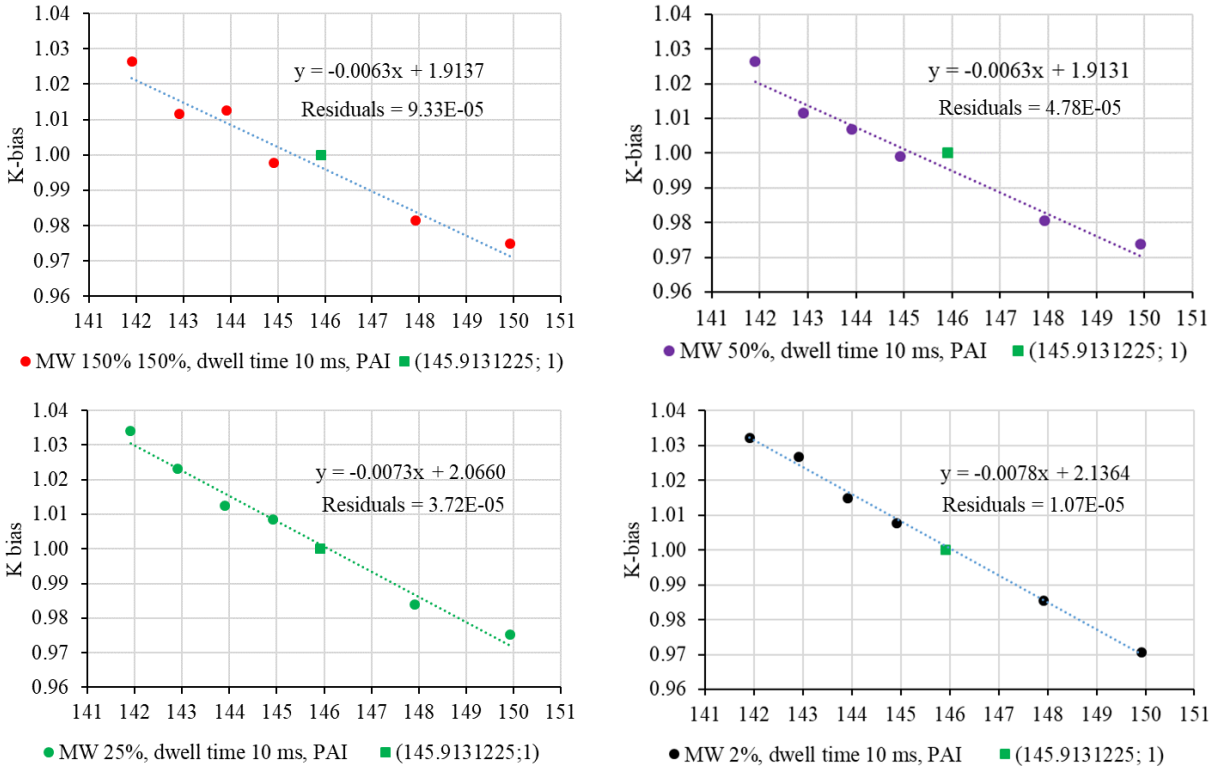


Figure 5.9 Mass bias correction factor (K-bias) over the monitored mass range for Nd IR determination using different mass windows (150, 50, 25 and 2 %)

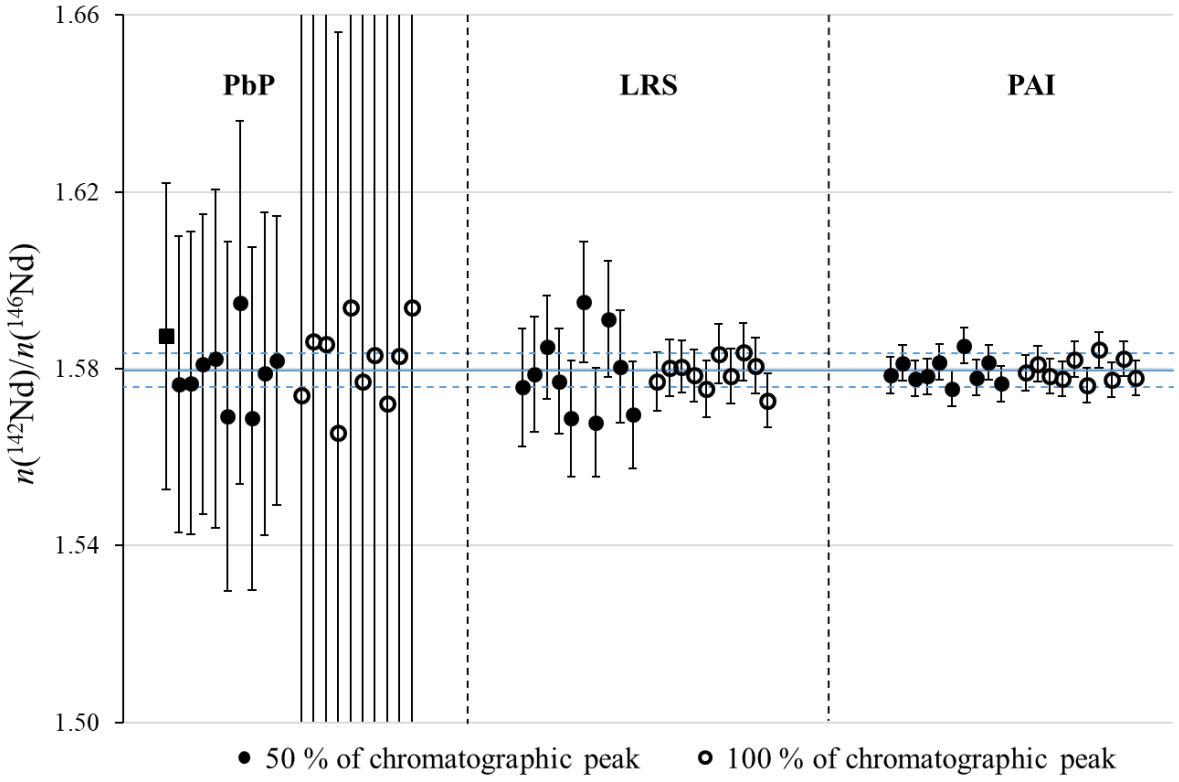


Figure 5.10 Effect of the chromatographic peak width percentage on the internal precision of $n(^{142}Nd)/n(^{146}Nd)$ IRs calculated using three different methods

Using a mass window of 25 %, the effect on the IR precision due to the portion of the chromatographic peak taken into account for IR calculation was investigated (Figure 5.10). It should be noted that by using 50 % of the chromatographic peak width around the peak apex for IR calculation, the chromatographic peak maximum was kept in the middle of the zone used for calculation. It can be seen from Figure 5.10 that the precision of IRs calculated by using PbP and 100 % of the chromatographic peak is more than double that of IRs determined using only the central 50 % of the chromatographic peak. This observation for the PbP method is due to the greater variation (standard deviation) in the IRs calculated along the chromatographic peak when the contribution of the peak shoulders, which have lower intensities and different IR values than the peak centre, is included in the average IR. Unlike the PbP method, the precision of IRs calculated by using the LRS method is improved by a factor of 2 when 100 % of the chromatographic peak is used instead of 50 % (Figure 5.10). This observation is in agreement with the literature stating the importance of starting and ending the IR calculation at the background of the chromatographic peak in LRS [3]. In contrast, no difference in the precision of IR calculated by using PAI was noted when 50 and 100 % portions of the chromatographic peak were used for calculation (Figure 5.10). This finding could be due to the significantly smaller area under the shoulders of the chromatographic peak compared to the centre (only 8 % difference between the areas integrated under 50 % and 100 % portions of the chromatographic peak).

Finally, the same Nd standard (10 $ng \cdot g^{-1}$ of Nd JMC-311) was measured on-line using HPIC-SF-ICP-MS and off-line using SF-ICP-MS on 5 days distributed over one month. The repeatabilities of the resulting IRs were compared. For both on-line and off-line measurements, the acquisition parameters consisted of a 10 ms dwell time and a 25 % mass window. Due to the dilution of the sample (and standard) in on-line HPIC-SF-ICP-MS measurements (injection loop and the admixing of the column effluent stream with the internal standard prior to introduction into the SF-ICP-MS nebulizer), the intensities at the apex of the chromatographic peaks of the Nd nuclides measured by on-line HPIC-SF-ICP-MS were lower than the intensities measured off-line using SF-ICP-MS without injecting the sample (or standard) onto the column. For example, the intensities at the apexes of the chromatographic peaks of $^{142}Nd$ and $^{150}Nd$ were respectively 16,524 and 3,773 counts when measured on-line using HPIC-SF-ICP-MS, whereas with continuous introduction of the Nd standard into the SF-ICP-MS unit offline, the intensities of $^{142}Nd$ and $^{150}Nd$ were 69,979 and 15,679 counts respectively. Table 5.8 indicates that the difference between the IRs measured on-line versus those measured off-line is not more than 0.15 %. Additionally, paired t-tests were performed using the data presented in Table 5.8. The calculated value of |t| was found to be 2.63 for the results of the on-line method compared to those of the off-line method, and 1.67 and 2.48 for the results of each method compared to the theoretical values, respectively. All the calculated |t| values were found to be less than the critical value ($t_5 = 3.36$) at P = 0.02. Therefore, the two methods, on-line HPIC-SF-ICP-MS and off-line SF-ICP-MS, do not differ significantly and their results are not different than the theoretical values at P = 0.02. Furthermore, no specific trend was found in relation to the standard deviations presented in Table 5.8. For example, in the case of the isotope ratios of $^{142,}$ $^{143,}$ $^{148}$ and $^{150}Nd$ relative to $^{146}Nd$, the standard deviation was lower with the on-line

measurements. However, in the case of the isotope ratios of $^{144 \text{ and } 145}$Nd relative to $^{146}$Nd, the opposite was observed – the standard deviation was higher with the on-line measurements.

Table 5.8 Comparison of Nd IRs in a 10 ng·g$^{-1}$ solution of Nd JMC-311 measured by online HPIC-SF-ICP-MS and by off-line SF-ICP-MS in 5 days

| IR | Theoretical value | On-line HPIC-SF-ICP-MS | | Off-line SF-ICP-MS | | Difference in ratio between on-line & off-line measurements |
|---|---|---|---|---|---|---|
| | IR* (U (k = 2)) | Average (1SD) | RSD (%) | Average (1SD) | RSD (%) | |
| $^{142}$Nd/$^{146}$Nd | 1.5797 (38) | 1.5801 (12) | 0.076 | 1.5784 (14) | 0.089 | 0.11 % |
| $^{143}$Nd/$^{146}$Nd | 0.7082 (20) | 0.7081 (12) | 0.17 | 0.7071 (17) | 0.24 | 0.14 % |
| $^{144}$Nd/$^{146}$Nd | 1.3845 (28) | 1.3849 (19) | 0.14 | 1.3837 (18) | 0.13 | 0.087 % |
| $^{145}$Nd/$^{146}$Nd | 0.4825 (11) | 0.4827 (13) | 0.27 | 0.4824 (10) | 0.21 | 0.062 % |
| $^{148}$Nd/$^{146}$Nd | 0.3349 (14) | 0.33476 (33) | 0.099 | 0.33491 (72) | 0.21 | 0.045 % |
| $^{150}$Nd/$^{146}$Nd | 0.3280 (17) | 0.32820 (30) | 0.091 | 0.32785 (38) | 0.12 | 0.11 % |

* Theoretical values of IRs were derived from IUPAC natural abundances [15].

The mass bias correction factors (K-bias) determined during the 5 days of on-line HPIC-SF-ICP-MS and off-line SF-ICP-MS measurements are shown in Figure 5.11. Figure 5.11 demonstrates that the K-bias decreases with increasing Nd nuclidic mass, relative to $^{146}$Nd. The linear correlation of the K-bias with the mass difference between the two nuclides in the IR of interest justifies the use of a single mass bias per atomic mass unit, ε (the one with the lowest uncertainty), to correct all IRs for mass bias (according to eq. 3.3). In such a way, expanded uncertainties on the IRs were lower than when individual ε values of the respective IRs were used. Additionally, it can be noted from Figure 5.12 that the K-bias values measured on-line are equal to those measured off-line when the error bars are taken into accounts. Figure 5.12 also shows that the mass bias correction factor determined from $n(^{145}\text{Nd})/n(^{146}\text{Nd})$ has the best repeatability (smallest SD, and hence the smallest RSD) amongst all the measured Nd IRs due to the smallest difference in nuclidic masses. Despite having the best repeatability, the K-bias determined for $n(^{145}\text{Nd})/n(^{146}\text{Nd})$ does not have the best internal precision, which was achieved with the K-bias determined for $n(^{142}\text{Nd})/n(^{146}\text{Nd})$, due to the higher abundance of $^{142}$Nd and hence the higher area under its chromatographic peak. Additionally, the larger difference in mass between $^{142}$Nd and $^{146}$Nd (4 atomic mass units) compared to $^{145}$Nd and $^{146}$Nd (1 atomic mass unit), results in a more expressed mass bias and a better determination of ε. Therefore, the ε determined using the latter K-bias was used to correct all the measured Nd IRs for mass bias. Additionally, the mass bias correction factors determined on-line and those determined off-line on the same day were found to be different by less than 1.1 %.

Overall, these results indicate that the best precision on an IR calculated from transient signals as obtained using HPIC-SF-ICP-MS is achieved when using a shorter dwell time (10 ms instead of 30 ms), a mass window of 25 % and by using the PAI method to calculate the IR (where only a 50 % portion of the chromatographic peak width around the peak apex is considered).

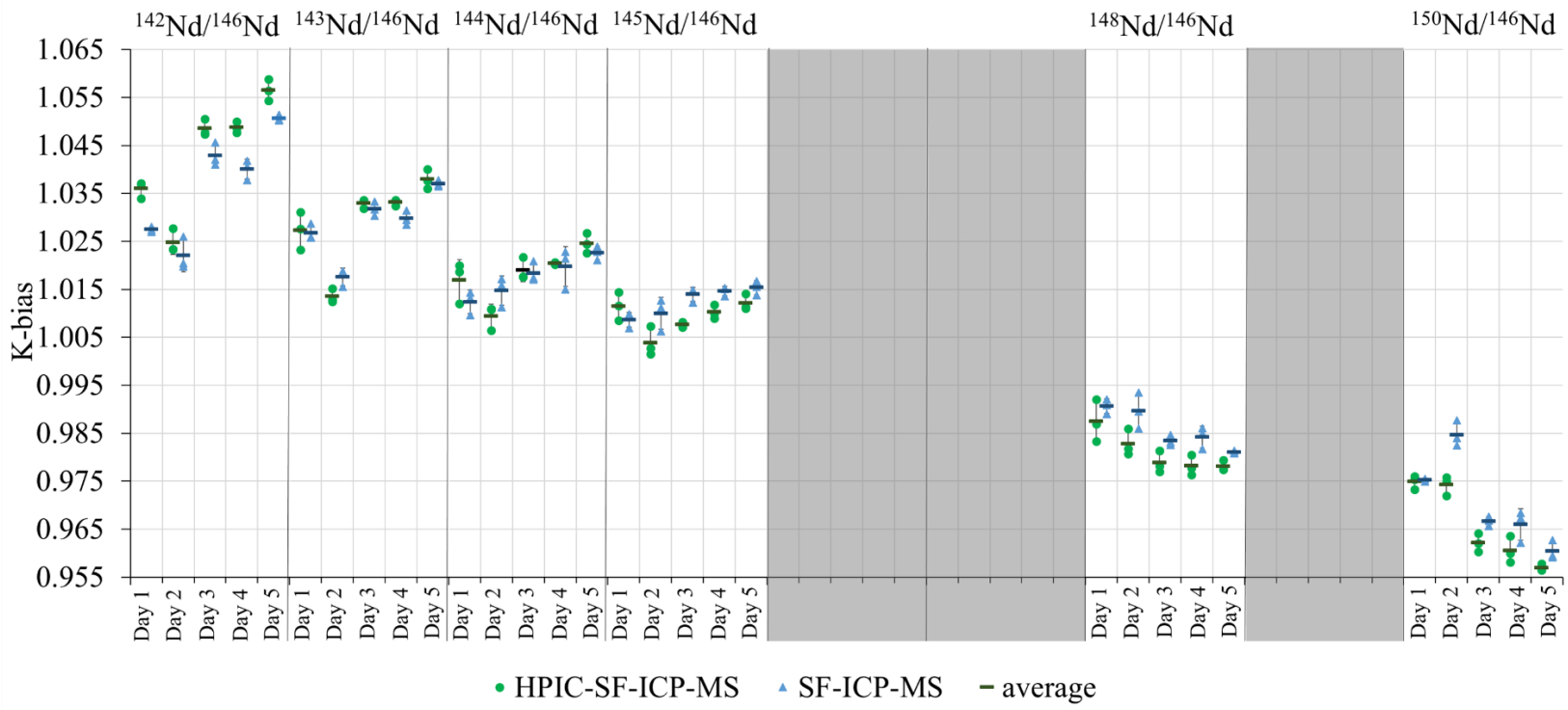


Figure 5.11 Instrumental mass bias correction factor determined using on-line HPIC-SF-ICP-MS and off-line SF-ICP-MS over 5 days

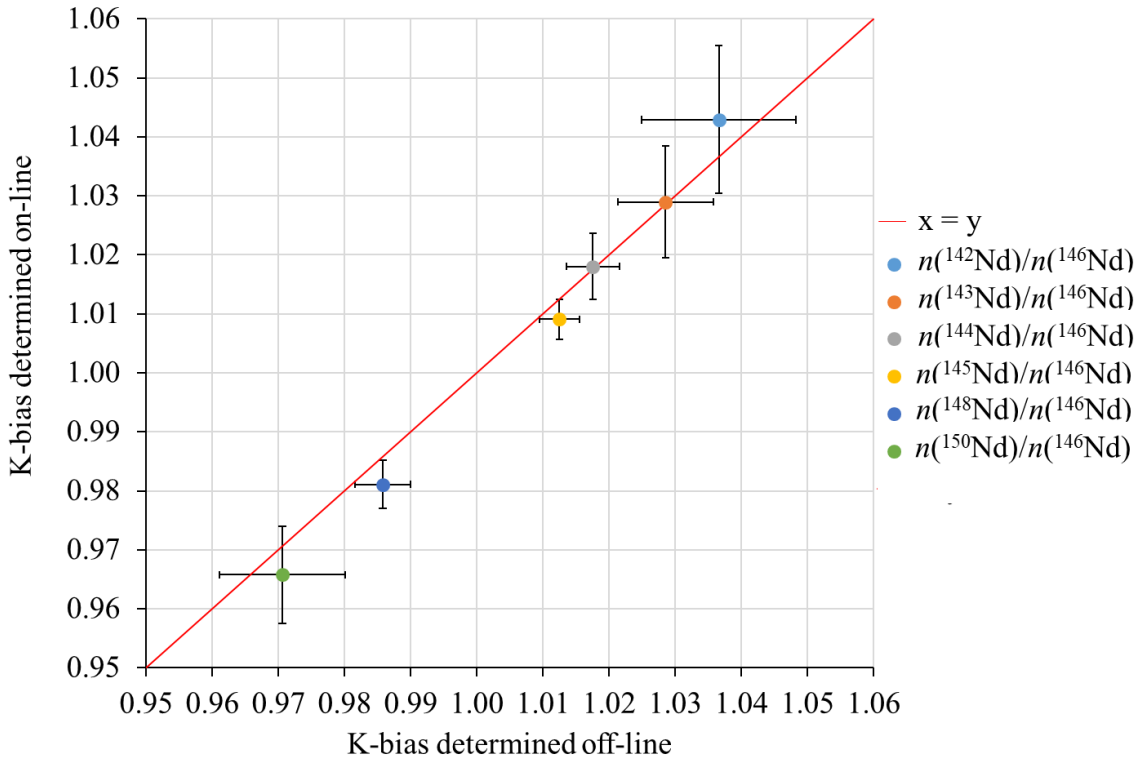


Figure 5.12 Average K-bias determined on-line using HPIC-SF-ICP-MS in 5 days versus average K-bias determined off-line using SF-ICP-MS in 5 days and their 1SD ranges

### 5.3.2 Isotope dilution

#### 5.3.2.1 UOx fuel

According to the literature, the best precision on an IR measurement is obtained with ratios close to unity [11, 16-17]. Existing knowledge of the isotopic composition of this sample and the spike was the basis for blend preparation. For determination of Pu and U via IDMS, the sample and the spike were mixed on a weight basis to obtain a blend containing equivalent amounts of the reference and the spiked isotope, as well as obtaining an IR close to unity in the blend. Satisfying these two conditions simultaneously in the case of Nd was not possible since almost 19% of the Nd in the sample is $^{146}$Nd, i.e. the enriched nuclide ($^{146}$Nd) of the spike. For Nd determination via IDMS, equivalent difference from the sample and spike isotopic compositions was achieved with an IR $n(^{148}\text{Nd})/n(^{146}\text{Nd})$ close to 0.1 in the blend. Based on Figure 5.13, the curve of the error multiplication factor $f(\text{R})$ versus the IR is relatively flat from 0.03 to 0.1, which means that between these two values, the magnification of the error associated with the IR in the blend is constant and thus the precision of the IDMS result is practically independent of the IR in the blend [16]. The error multiplication factor *f(R)* was calculated using eq. 5.4 [16] below, where $A^a$ and $A^b$ are the isotopic abundances of the lighter and heavier isotope, respectively. The isotopic abundances used to calculate *f(R)* were obtained from results of previous TIMS & alpha spectrometry analysis of the standard and samples from the same batch of UOx fuel.

$$f(R) = \frac{\left[\left(\frac{A^b}{A^a}\right)_{sample} - \left(\frac{A^b}{A^a}\right)_{spike}\right] R}{\left[R - \left(\frac{A^b}{A^a}\right)_{sample}\right]\left[\left(\frac{A^b}{A^a}\right)_{spike} - R\right]} \qquad \text{(eq. 5.4)}$$

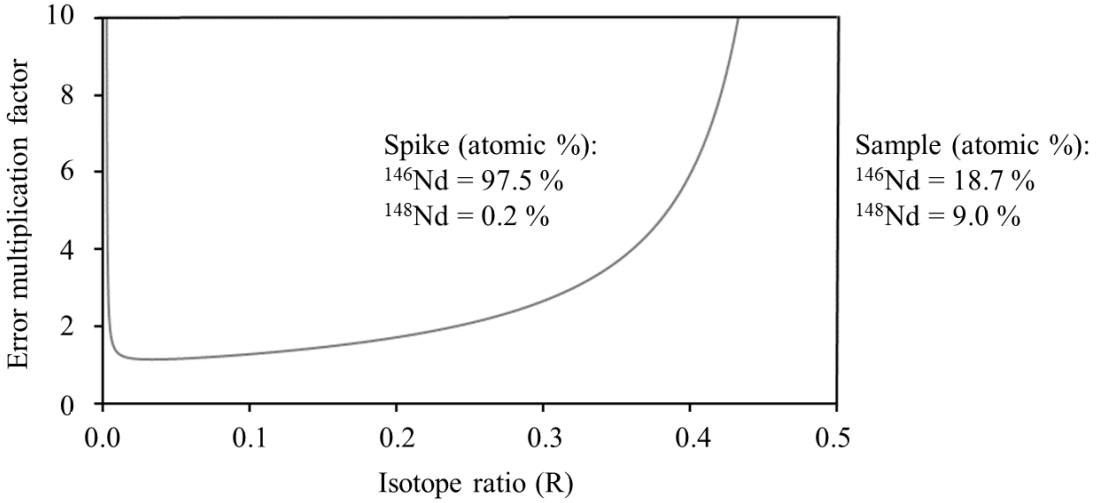


Figure 5.13 Error multiplication factor for IDMS determination of Nd as a function of $n(^{148}Nd)/n(^{146}Nd)$ (R) in the blend

Measurement of the isotopic composition of irradiated samples is essential because the composition will be different to that of the natural element composition (e.g. fission product Nd isotopic composition differs greatly – especially for $^{142}Nd$ – from that of natural Nd and is an integral part of the uncertainty budget). Since the samples analysed here by HPIC-ICP-MS had been measured previously by TIMS, information about the isotopic compositions of these specific samples was already available, which made it possible to calculate optimum spiking ratios and consider error magnification factors. Radiochemical laboratories, in the absence of specific information (e.g. irradiation history, theoretical estimates of burn-up credit etc.) about a nuclear sample, can rely to some extent upon their previous experience of analysing a range of nuclear fuels to estimate what the isotopic composition of an "unknown" fuel sample might be. The interested reader should also be aware that, for purposes of shipping nuclear fuel samples, there is already a requirement that the shipper provides certain information about the sample. Therefore, the radiochemical laboratory always has some information about the "unknown" sample. If, however, there were to be no information available about the isotopic composition of an "unknown" sample, it is precisely the speed of analysis achievable with the HPIC-ICP-MS methodology developed in this work that opens the possibility for a much quicker assessment of the isotopic composition of highly relevant elements (e.g. U, Pu, Nd) than possible with the established TIMS analyses (which rely on the longer conventional gravitational chromatographic separations).

During the isotope dilution analysis of UOx fuel using HPIC-SF-ICP-MS, Nd and Pu IRs were measured on-line, while the U peak was collected using fraction collection and the U IRs in the sample and the blend were measured later off-line by using SF-ICP-MS. This off-line collection results in a 174-fold dilution of the high U mass fraction prior to its introduction into the SF-ICP-MS, thereby avoiding the need to measure high intensity signals in analogue mode of the detector (which is not the conventional way of measuring IRs), or to introduce a more diluted

sample in to the HPIC for U determination only. The sample and the blend were measured three times using HPIC-SF-ICP-MS and the isotope dilution results were compared to those obtained using TIMS & alpha spectrometry for a sample of the same batch. The mass fractions of Nd, Pu and U in the UOx fuel when determined by using HPIC-SF-ICP-MS were found to be similar to those determined by TIMS & alpha spectrometry (Table 5.9), and, interestingly, the expanded uncertainties on the mass fractions determined for Nd and Pu by using transient signals were found to be better than or similar to those obtained by means of TIMS & alpha spectrometry. This demonstrates the good precision that can be obtained by using HPIC-SF-ICP-MS. Nevertheless, it should be noted that the expanded uncertainty (3.4 %), on the Nd elemental mass fraction obtained using isotope dilution TIMS & alpha-spectrometry for this sample, is an order of magnitude larger than the expanded uncertainties usually obtained using this method for other UOx SNF samples analysed at SCK CEN. The large expanded uncertainty reported for the off-line measurement of U could be associated with the collection of the uranium fraction and its 174-fold dilution prior to SF-ICP-MS analysis [18], thereby causing a significant decrease in the number of counts measured for the minor isotopes (e.g. ~ 18 counts for $^{234}$U compared to ~ 80,000 counts for $^{238}$U).

Overall, the repeatabilities (RSD) of the three mass fractions determined by using HPIC-SF-ICP-MS were found to be 0.14 and 0.18 %, for Nd and Pu, respectively, and 0.15 % for U when determined off-line subsequent to its isolation using HPIC-SF-ICP-MS.

Table 5.9 Mass fractions of Nd, Pu and U measured in UOx fuel in triplicate using HPIC-SF-ICP-MS and compared to a single measurement with TIMS & alpha spectrometry

| Element | HPIC-SF-ICP-MS mass fraction in fuel ($mg \cdot g^{-1}$) ± U (k = 2) | TIMS & alpha spectrometry mass fraction in fuel ($mg \cdot g^{-1}$) ± U (k = 2) | HPIC-SF-ICP-MS mass fraction/TIMS & alpha spectrometry mass fraction · 100 (%) ± U (k = 2) |
|---|---|---|---|
| Neodymium | 6.375 ± 0.039 | 6.47 ± 0.22 | 98.5± 3.4 |
| Plutonium | 8.380 ± 0.036 | 8.313 ± 0.021 | 100.81 ± 0.50 |
| Uranium | 762 ± 45 | 774.0 ± 2.0 | 98.5 ± 5.8 |

The amount fractions of Nd, Pu and U nuclides measured in the non-spiked sample using HPIC-SF-ICP-MS were found to be in agreement with those obtained by using TIMS & alpha spectrometry (Table 5.10). The amount fractions of Pu nuclides have been corrected for decay because the HPIC-SF-ICP-MS measurements were performed almost 5 months after the TIMS measurements. This correction was especially crucial for $^{241}$Pu, which decays to $^{241}$Am, with a short half-life (14.33 years) compared to the other Pu nuclides (see Table 1.2 in section 1.4.2). To account for the influence of the decay of Pu nuclides on the results obtained using HPIC-SF-ICP-MS, the TIMS date of analysis was considered the reference date (see Table 5.3). First, the mass bias corrected Pu IR ($R_{corr.i}$) from HPIC-SF-ICP-MS measurement of the SNF sample was corrected for the decay that took place using eq. 5.5, where $R_{decay\ corr.i}$ is the decay corrected and mass bias corrected IR of the corresponding Pu nuclide *i* relative to $^{239}$Pu, $\lambda_i$ is the decay correction factor per day calculated based on the half-life (in days) of the corresponding Pu nuclide *i* (eq. 5.6) and *t* is the time difference in days between the corresponding HPIC-SF-ICP-MS measurement date and the reference TIMS measurement date (see Table 5.3). The nuclide-

specific amount fraction percent ($Atom\ \%_{decay\ corr.,\ i}$) of nuclide *i* was then calculated according to eq. 5.7, where $\Sigma R_{decay\ corr.}$ is the sum of the decay corrected and mass bias corrected IRs.

$$R_{decay\ corr.,i} = R_{corr.,i} \cdot e^{-\lambda_i t} \quad \text{(eq. 5.5)}$$

$$\lambda_i = \frac{\ln(2)}{\tau_i} \quad \text{(eq. 5.6)}$$

$$Atom\ \%_{decay\ corr.,i} = \frac{R_{decay\ corr.,i}}{\Sigma R_{decay\ corr.}} \cdot 100 \quad \text{(eq. 5.7)}$$

The amount fraction of $^{142}$Nd determined in the sample had to be corrected for cross-contamination by $^{142}$Nd originating from the glass vial in which the sample stock solution was stored. Glass vials, similar to those in which the sample was stored, were filled with 2 % v/v $HNO_3$ and stored for 1 month. The average $^{142}$Nd concentration (0.062 ng·g$^{-1}$) in these solutions was then quantified (external calibration method) by ICP-MS (XSERIES 2, Thermo Fisher Scientific, Bremen, Germany), converted to an amount fraction and subtracted from the amount fraction of $^{142}$Nd originally determined in the sample.

Table 5.10 Nuclide-specific amount fractions of Nd, Pu and U measured in triplicate using HPIC-SF-ICP-MS and compared to a single measurement with TIMS & alpha spectrometry

| Nuclide | HPIC-SF-ICP-MS amount fraction (·100) ± U (k = 2) | TIMS & alpha spectrometry amount fraction (·100) ± U (k = 2) | HPIC-SF-ICP-MS/TIMS & alpha spectrometry · 100 ± U (k = 2) |
|---|---|---|---|
| $^{142}$Nd | 1.201± 0.011 | 1.096 ± 0.023 | 109.6 ± 2.5 |
| $^{143}$Nd | 12.046 ± 0.037 | 11.889 ± 0.022 | 101.32 ± 0.37 |
| $^{144}$Nd | 40.023 ± 0.066 | 40.065 ± 0.049 | 99.90 ± 0.20 |
| $^{145}$Nd | 14.802 ± 0.038 | 14.848 ± 0.017 | 99.69 ± 0.28 |
| $^{146}$Nd | 18.839 ± 0.024 | 18.740 ± 0.021 | 100.53 ± 0.17 |
| $^{148}$Nd | 8.781 ± 0.032 | 9.006 ± 0.086 | 97.5 ± 1.0 |
| $^{150}$Nd | 4.308 ± 0.023 | 4.355 ± 0.011 | 98.92 ± 0.58 |
| $^{238}$Pu | 3.825 ± 0.012* | 3.76 ± 0.22 | 101.8 ± 6.0 |
| $^{239}$Pu | 41.442 ± 0.038* | 41.38 ± 0.10 | 100.15 ± 0.26 |
| $^{240}$Pu | 31.369 ± 0.044* | 31.380 ± 0.084 | 99.97 ± 0.30 |
| $^{241}$Pu | 7.918 ± 0.025* | 7.945 ± 0.025 | 99.66 ± 0.44 |
| $^{242}$Pu | 15.443 ± 0.057* | 15.538 ± 0.051 | 99.39 ± 0.49 |
| $^{244}$Pu | 0.00263 ± 0.00023* | 0.0029 ± 0.0057 | 91.7 ± 182 |
| $^{233}$U | 0 | 0 | - |
| $^{234}$U | 0.0202 ± 0.0029 | 0.01924 ± 0.00068 | 105 ± 16 |
| $^{235}$U | 0.220 ± 0.013 | 0.21879 ± 0.00051 | 101.0 ± 6.0 |
| $^{236}$U | 0.665 ± 0.023 | 0.6615 ± 0.0025 | 100.5 ± 3.5 |
| $^{238}$U | 99.094 ± 0.031 | 99.1005 ± 0.0027 | 99.993 ± 0.031 |

* Corrected for decay with reference to the TIMS & alpha-spectrometry date of analysis (2019-10-08).

The expanded uncertainty on the amount fraction of each nuclide of Nd, Pu and U was determined according to the rules given in the Eurachem/CITAC guide CG 4 [6]. Contributors to the expanded uncertainty were identified (Figure 5.14), classified as type A (evaluated statistically) or type B errors (evaluated by other means, such as experience) [6, 19], evaluated and combined using the bottom up approach which is built into the GUM Workbench software. It was found that the mass bias correction (~ 1 % of the expanded uncertainty) and the raw measured IRs (~ 98 % of the expanded uncertainty) are the major contributors to the expanded uncertainty of the mass fraction determined by using isotope dilution HPIC-SF-ICP-MS (see Table T5.1 in the appendix of this chapter). This result is not surprising, as this is in agreement with what has been reported previously in the literature [16-17].

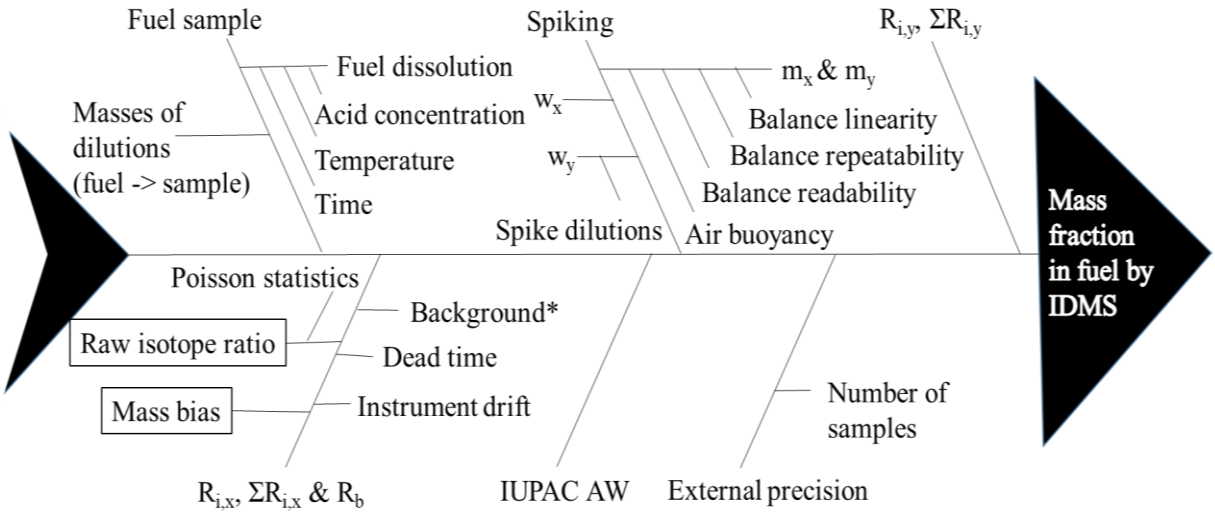


* Background refers to instrumental background as well as signal measured in the blank and has a major effect at mass fractions close to LOD

Figure 5.14 Fishbone diagram of uncertainty contributors to the mass fraction of an element determined using IDMS (major contributors have been outlined)

#### 5.3.2.2 Gd fuel

Compared to the UOx fuel, an additional spiking (with an isotopically enriched Gd material) was necessary to determine the mass fraction of Gd in the "Gd fuel" using IDMS. The amount of spike added was chosen such that the blend consisted of equal amounts of the sample and the spike, and resulted in an IR $^{157}Gd/^{156}Gd$ close to unity. IRs in the fractions of Pu, Nd and Gd eluting from the HPIC column were measured on-line using SF-ICP-MS and the collected U fraction was measured off-line using SF-ICP-MS, as was done for the UOx fuel. For the "Gd fuel", in contrast to the UOx fuel, three independent dilutions of the sample solution were prepared for IDMS. The results for the different elements are presented in Table 5.11. Good agreement was found between elemental mass fractions in the fuel determined by using HPIC-SF-ICP-MS and those determined by using TIMS & alpha spectrometry. Certain limitations were encountered when using HPIC-SF-ICP-MS for IDMS: the amount of Nd nuclides formed by fission depends on the irradiation conditions of the fuel, and therefore, at very low levels of fission, the amount of Nd nuclides present can be lower than the limit of detection. In addition, the quantification of $^{238}Pu$ was not possible due to its low mass fraction and the relatively high instrumental background (memory effects) at mass 238, compared to other monitored masses.

The nuclide amount fractions derived from the HPIC-SF-ICP-MS measurement of three samples were compared with those obtained by means of TIMS & alpha spectrometry analysis of the same SNF stock solution, as shown in Table 5.12. From the data in Table 5.12, it can be concluded that the nuclide amount fractions obtained by using HPIC-SF-ICP-MS were in agreement (maximum difference of ± 10 %) with those obtained by using TIMS & alpha spectrometry when different samples of the same batch are analysed.

Table 5.11 Mass fractions of Gd, Pu and U measured in "Gd fuel" in triplicate using HPIC-SF-ICP-MS and compared to a single measurement with TIMS & alpha spectrometry

| Element | HPIC-SF-ICP-MS mass fraction in fuel ($mg \cdot g^{-1}$) ± U (k = 2) (n=3) | TIMS & alpha spectrometry mass fraction in fuel ($mg \cdot g^{-1}$) ± U (k = 2) | HPIC-SF-ICP-MS mass fraction/TIMS & alpha spectrometry mass fraction · 100 ± U (k = 2) |
|---|---|---|---|
| Neodymium | - | 0.6291 ± 0.0096 | - |
| Gadolinium | 90.37 ± 0.28 | 90.36 ± 0.51 | 100.01 ± 0.64 |
| Plutonium | 5.443 ± 0.061 | 5.421 ± 0.010 | 100.40 ± 1.15 |
| Uranium | 816 ± 47 | 815.9 ± 2.2 | 100.1 ± 5.7 |

Table 5.12 Nuclide-specific amount fractions of Gd, Pu and U measured in three samples using HPIC-SF-ICP-MS and compared to a single measurement with TIMS & alpha spectrometry

| Nuclide | HPIC-SF-ICP-MS amount fraction (·100) ± U (k = 2) | TIMS & alpha spectrometry amount fraction (·100) ± U (k = 2) | HPIC-SF-ICP-MS / TIMS & alpha spectrometry 100 (%) ± U (k = 2) |
|---|---|---|---|
| $^{152}Gd$ | 0.157 ± 0.011 | 0.15537 ± 0.00086 | 100.8 ± 7.1 |
| $^{154}Gd$ | 2.059 ± 0.025 | 2.0489 ± 0.0069 | 100.4 ± 1.3 |
| $^{155}Gd$ | 1.974 ± 0.033 | 1.9663 ± 0.0058 | 100.4 ± 1.7 |
| $^{156}Gd$ | 33.098 ± 0.058 | 33.100 ± 0.051 | 99.99 ± 0.23 |
| $^{157}Gd$ | 0.492 ± 0.013 | 0.48342 ± 0.00036 | 101.8 ± 2.7 |
| $^{158}Gd$ | 40.327 ± 0.087 | 40.377 ± 0.021 | 99.88 ± 0.22 |
| $^{160}Gd$ | 21.897 ± 0.082 | 21.869 ± 0.049 | 100.13 ± 0.44 |
| $^{238}Pu$ | - | 0.1913 ± 0.0011 | - |
| $^{239}Pu$ | 85.05 ± 0.10* | 84.8615 ± 0.0099 | 100.23 ± 0.12 |
| $^{240}Pu$ | 11.413 ± 0.082* | 11.3900 ± 0.0059 | 100.20 ± 0.72 |
| $^{241}Pu$ | 3.032 ± 0.044* | 3.0994 ± 0.0034 | 97.8 ± 1.4 |
| $^{242}Pu$ | 0.500 ± 0.017* | 0.45818 ± 0.00079 | 109.1 ± 3.6 |
| $^{244}Pu$ | 0 | 0 | - |
| $^{233}U$ | 0 | 0 | - |
| $^{234}U$ | 0.0137 ± 0.0042 | 0.01350 ± 0.00012 | 102 ± 31 |
| $^{235}U$ | 1.74 ± 0.19 | 1.6165 ± 0.0025 | 108 ± 12 |
| $^{236}U$ | 0.112 ± 0.036 | 0.10235 ± 0.00015 | 109 ± 35 |
| $^{238}U$ | 98.14 ± 0.18 | 98.2676 ± 0.0026 | 99.87 ± 0.18 |

* Corrected for decay with reference to the TIMS & alpha-spectrometry date of analysis (2018-02-22).

## 5.4 Conclusions and outlook

The aim of this part of the project was to optimize the SF-ICP-MS data acquisition parameters and determine the best calculation method for obtaining precise IR measurements from transient signals, and to apply these to the accurate determination of Pu, U, Nd & Gd mass fractions in SNF by using isotope dilution HPIC-SF-ICP-MS. Using a mass window of 25 % and a dwell time of 10 ms with 20 samples per flat top peak gave the best performance. Although the three calculation methods (PbP, LRS and PAI) resulted in similar IR values from these transient signals, those calculated by PAI were found to have the best precision when only the central part (50 %) of the chromatographic peak was taken into consideration. Moreover, when using these acquisition parameters with isotope dilution HPIC-SF-ICP-MS, the nuclide-specific mass fractions of Pu, U, Nd & Gd obtained were in agreement with those obtained by using isotope dilution TIMS & alpha spectrometry for both types of SNF. Overall, isotope dilution HPIC-SF-ICP-MS resulted in accurate quantification of Pu, U, Nd and Gd mass fractions. For on-line measurement of Nd and Gd elemental mass fractions, the uncertainties were better than those obtained with TIMS & alpha spectrometry, in the case of Nd in UOx SNF and Gd in Gd SNF. Whereas in the case of on-line measurement of Pu elemental mass fraction, the uncertainties obtained were almost twice (in UOx SNF) and six times (in Gd SNF) worse than those obtained with TIMS & alpha spectrometry. For off-line measurement of a diluted U fraction, poorer measurement uncertainties were obtained than with TIMS. Isotope dilution HPIC-SF-ICP-MS has also proven to be a faster and safer method of analysis compared with gravitational chromatography followed by TIMS & alpha spectrometry, enabling the analysis of SNF samples in just two days and reducing the exposure of the operator to the radioactivity of the samples (automatic injection and online chromatography). However, the determination of nuclides present at low amounts in the samples was found to be limited by the LOD of the hyphenated method, the irradiation history of the fuel and the instrumental background.

In the case of the spent UOx and the “Gd fuel” measured, the optimized isotope dilution HPIC-SF-ICP-MS method provided a better precision than the TIMS and alpha spectrometry method for the quantification of Gd in “Gd fuel” and of Nd in UOx SNF with high levels of fission. However, isotope dilution HPIC-SF-ICP-MS cannot replace the ISO 17025 accredited TIMS and alpha spectrometry method for the precise and accurate determination of mass fractions of U, Pu and elements present in amounts close to the LOD. Nevertheless, HPIC-SF-ICP-MS is still a fast method to separate the elements of interest in a single injection and to determine their elemental mass fractions and nuclide-specific compositions in SNF samples based on external calibration and IR measurements respectively. This information can be invaluable in deciding the amounts of sample and spike (based on isotopic amount values from the certificate of the reference material) to be combined to produce the blend needed for subsequent IDMS analysis of SNF by the accurate ISO 17025 accredited TIMS and alpha spectrometry method.

Moreover, in the context of method optimization, the time needed to process the results obtained using HPIC-SF-ICP-MS has been significantly shortened. Details about the automation of data processing to obtain the mass fraction of the elements of interest in SNF will be presented in the following chapter.

## 5.5 References


[1] N. N. Wanna, A. Dobney, K. Van Hoecke, M. Vasile and F. Vanhaecke, "Quantification of uranium, plutonium, neodymium and gadolinium for the characterization of spent nuclear fuel using isotope dilution HPIC-SF-ICP-MS," *Talanta,* 2020.

[2] IAEA, "Characteristics and use of Urania-Gadolinia fuels," IAEA, Vienna, 1995.

[3] V. N. Epov, S. Berail, M. Jimenez-Moreno, V. Perrot, C. Pecheyran, D. Amouroux and O. F. Donard, "Approach to measure isotopic ratios in species using multicollector-ICPMS coupled with chromatography," *Analytical chemistry,* vol. 82, no. 13, pp. 5652-5662, 2010.

[4] E. M. Krupp and O. F. Donard, "Isotope ratios on transient signals with GC-MC-ICP-MS," *International Journal of Mass Spectrometry,* vol. 242, pp. 233 - 242, 2005.

[5] P. Rodriguez-Gonzalez, V. N. Epov, C. Pecheyran, D. Amouroux and O. F. Donard, "Species-specific stable isotope analysis by the hyphenation of chromatographic techniques with MC-ICPMS," *Mass Spectrom Rev,* vol. 31, no. 4, pp. 504-521.

[6] "Eurachem/CITAC Guide CG 4," 2012.

[7] E. Pagliano, Z. Mester and J. Meija, "Reduction of measurement uncertainty by experimental design in high-order (double, triple, and quadruple) isotope dilution mass spectrometry: application to GC-MS measurement of bromide," *Analytical and Biochemistry,* vol. 405, pp. 2879 - 2887, 2013.

[8] W. Kessel, "ISO/BIPM Guide: Uncertainty of measurement," in *DGQ-VDI/VDE meeting (1998),* Langen/Hessen, 1999.

[9] M. Wang, G. Audi, F. G. Kondev, W. J. Huang, S. Naimi and X. Xu, "The AME2016 atomic mass evaluation," *Chinese Physics C 41,* no. 030003, 2017.

[10] International Organization of Legal Metrology, "OIML R 111-1: 2004 (E)".

[11] P. Rodriguez-Gonzalez and J. Ignacio Garcia Alonso, "Mass Spectrometry: Isotope dilution mass spectrometry," in *Encyclopaedia of analytical science,* vol. 6, Elsevier, 2019.

[12] J. Szpunar and R. Lobinski, Hyphenated Techniques in Speciation Analysis, The Royal Society of Chemistry, 2003.

[13] J. Ignacio Garcia Alonso and P. Rodriguez-Gonzalez, Isotope Dilution Mass Spectrometry, The Royal Society of Chemistry, 2013.

[14] F. Gueguen, H. Isnard, A. Nonell, L. Vio, T. Vercouter and F. Chartier, "Neodymium isotope ratio measurements by LC-MC-ICP-MS for nuclear applications: investigation of isotopic fractionation and mass bias correction," *J Anal At Spectrom,* vol. 30, no. 2, p. 443–452, 2015.

[15] "The 2016 Atomic mass table," *Chinese physics C,* vol. 41, 2017.

[16] K. Heumann, “Determination of trace elements and elemental species using isotope dilution inductively coupled plasma mass spectrometry,” in *Isotopic analysis: fundamentals and applications using ICP-MS*, Wiley, 2012, pp. 189-233.

[17] M. Sargent, R. Harte and C. Harrington, “Guidelines for achieving high accuracy in isotope dilution mass spectrometry (IDMS),” Royal Society of Chemistry, 2002, pp. 1 - 34.

[18] V. C. Bradley, B. T. Manard, B. D. Roach, S. C. Metzger, K. T. Rogers, B. W. Ticknor, S. K. Wysor, J. D. Brockman and C. R. Hexel, “Rare earth element determination in uranium ore concentrates using online and offline chromatography couples to ICP-MS,” *Mineral*, vol. 10, no. 55, 2020.

[19] T. Meisel, “7 Quality control in isotope ratio applications,” in *Isotopic analysis: Fundamentals and applications using ICP-MS*, Wiley-VCH, 2012.

# Appendix chapter 5

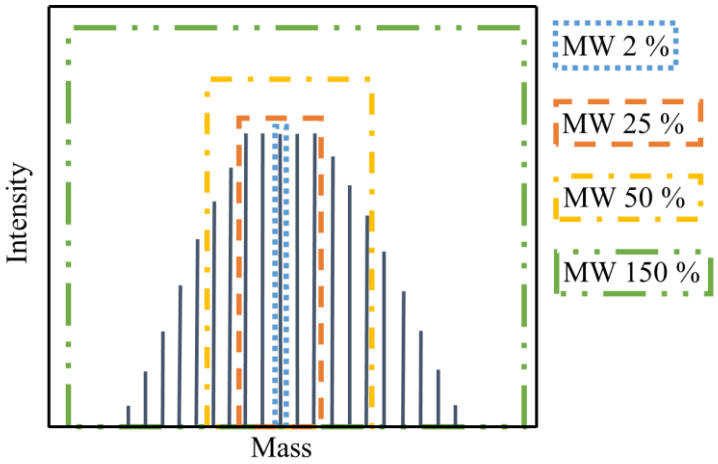


Figure S5.1 Schematic representation of the different mass windows (MW) used for the acquisition of a flat top peak consisting of 20 samples as obtained with SF-ICP-MS in low resolution mode

| | | |
|---|---|---|
| START | | |
| 1 | take up - Rinse 1 | 00/01 |
| 2 | Rinse 1 | 00/01 |
| 3 | take up - Blank 1 | 00/03 |
| 4 | Blank 1- Pu | 00/01 |
| 5 | Blank 1- U collection | 00/01 |
| 6 | Blank 1 - Lns 1 of 3 | 00/01 |
| 7 | Blank 1 - Nd | 00/01 |
| 8 | Blank 1 - Lns 2 of 3 | 00/01 |
| 9 | Blank 1- Gd | 00/01 |
| 10 | Blank 1 - Lns 3 of 3 | 00/01 |
| 11 | take up - Standard 1 | 00/05 |
| 12 | Standard 1 - Pu | 00/01 |
| 13 | Standard 1 - U collection | 00/01 |
| 14 | Standard 1 - Lns 1 of 3 | 00/01 |
| 15 | Standard 1 - Nd | 00/01 |
| 16 | Standard 1 - Lns 2 of 3 | 00/01 |
| 17 | Standard 1 - Gd | 00/01 |
| 18 | Standard 1 - Lns 3 of 3 | 00/01 |
| 19 | take up - IA | 01/01 |
| 20 | IA - Pu | 00/01 |
| 21 | IA - U collection | 00/01 |
| 22 | IA - Lns 1 of 3 | 00/01 |
| 23 | IA - Nd | 00/01 |
| 24 | IA - Lns 2 of 3 | 00/01 |
| 25 | IA - Gd | 00/01 |
| 26 | IA - Lns 3 of 3 | 00/01 |
| 27 | take up - ID | 01/02 |
| 28 | ID - Pu | 00/01 |
| 29 | ID - U collection | 00/01 |
| 30 | ID - Lns 1 of 3 | 00/01 |
| 31 | ID - Nd | 00/01 |
| 32 | ID - Lns 2 of 3 | 00/01 |
| 33 | ID - Gd | 00/01 |
| 34 | ID - Lns 3 of 3 | 00/01 |
| 35 | take up - Rinse 2 | 00/02 |
| 36 | Rinse 2 | 00/02 |
| 37 | take up - Blank 2 | 00/03 |
| 38 | Blank 2 - Pu | 00/01 |
| 39 | Blank 2 - U collection | 00/01 |
| 40 | Blank 2 - Lns 1 of 3 | 00/01 |
| 41 | Blank 2 - Nd | 00/01 |
| 42 | Blank 2 - Lns 2 of 3 | 00/01 |
| 43 | Blank 2- Gd | 00/01 |
| 44 | Blank 2 - Lns 3 of 3 | 00/01 |
| 45 | take up - Standard 2 | 00/05 |
| 46 | Standard 2 - Pu | 00/01 |
| 47 | Standard 2 - U collection | 00/01 |
| 48 | Standard 2 - Lns 1 of 3 | 00/01 |
| 49 | Standard 2 - Nd | 00/01 |
| 50 | Standard 2 - Lns 2 of 3 | 00/01 |
| 51 | Standard 2 - Gd | 00/01 |
| 52 | Standard 2 - Lns 3 of 3 | 00/01 |
| 53 | take up - Rinse 3 | 00/04 |
| 54 | Rinse 3 | 00/06 |
| STOP | | |

Figure S5.2 Screenshot of an isotope dilution sequence in the software of the "*Element 2"* used in this work for the analysis of a spent "Gd fuel"

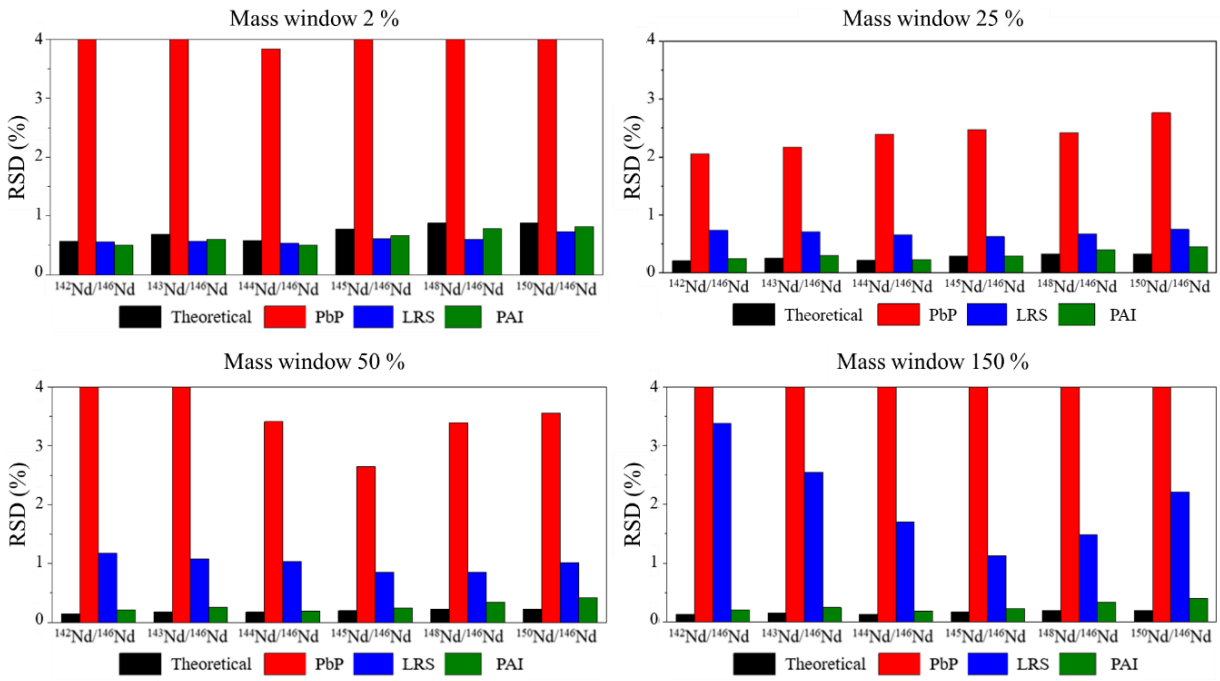


Figure S5.3 Comparison of the precision of different Nd IRs acquired using different mass windows (2, 25, 50 & 150 %) and calculated using different methods (PbP, LRS and PAI)

Table T5.1 Contributions of different parameters to the expanded uncertainty of the Nd mass fraction determined by IDMS

| Parameter | Type of uncertainty | Value | Standard uncertainty | Contribution to total uncertainty (%) |
|---|---|---|---|---|
| $M_{Nd\text{-}142}$ ($g \cdot mol^{-1}$) | Type B | 141.90772890 | 0.0000015 | < 0.1 |
| $M_{Nd\text{-}143}$ ($g \cdot mol^{-1}$) | Type B | 142.90981990 | 0.0000015 | < 0.1 |
| $M_{Nd\text{-}144}$ ($g \cdot mol^{-1}$) | Type B | 143.91009290 | 0.0000015 | < 0.1 |
| $M_{Nd\text{-}145}$ ($g \cdot mol^{-1}$) | Type B | 144.91257920 | 0.0000015 | < 0.1 |
| $M_{Nd\text{-}146}$ ($g \cdot mol^{-1}$) | Type B | 145.9131225 | 0.0000015 | < 0.1 |
| $M_{Nd\text{-}148}$ ($g \cdot mol^{-1}$) | Type B | 147.91689910 | 0.0000023 | < 0.1 |
| $M_{Nd\text{-}150}$ ($g \cdot mol^{-1}$) | Type B | 149.92090150 | 0.0000014 | < 0.1 |
| $m_{fuel}$ (g) | Type B | 6.10000 | 0.00061 | < 0.1 |
| $m_{V0}$ (g) | Type B | 517.8334 | 0.0517 | < 0.1 |
| $m_{V0\text{-}1}$ (g) | Type B | 0.9667 | 0.000097 | < 0.1 |
| $m_{V1}$ (g) | Type B | 11.2855 | 0.0011 | < 0.1 |
| $m_{V1\text{-}1}$ (g) | Type B | 0.874 | 0.000087 | < 0.1 |
| $m_{V2}$ (g) | Type B | 4.855 | 0.00049 | < 0.1 |
| $m_{v2\text{-}1}$ (g) | Type B | 0.52 | 0.000052 | < 0.1 |
| $m_{V3}$ (g) | Type B | 5.2238 | 0.00052 | < 0.1 |
| $m_{V3\text{-}1}$ (g) | Type B | 0.2561 | 0.000026 | < 0.1 |
| $m_{V4}$ (g) | Type B | 2.5831 | 0.00026 | < 0.1 |
| $m_x$ (g) | Type B | 0.52223 | 0.000052 | < 0.1 |
| $m_y$ (g) | Type B | 0.40178 | 0.000040 | < 0.1 |
| $w_y$ ($g \cdot g^{-1}$) | Type B | $10.0380 \cdot 10^{-9}$ | $0.0026 \cdot 10^{-9}$ | < 0.1 |
| $R_{142/146,\,y}$ | Type B | $4.4758 \cdot 10^{-3}$ | $0.0050 \cdot 10^{-3}$ | < 0.1 |
| $R_{143/146,\,y}$ | Type B | $3.0583 \cdot 10^{-3}$ | $0.0041 \cdot 10^{-3}$ | < 0.1 |
| $R_{144/146,\,y}$ | Type B | $7.915 \cdot 10^{-3}$ | $0.011 \cdot 10^{-3}$ | < 0.1 |
| $R_{145/146,\,y}$ | Type B | $6.5789 \cdot 10^{-3}$ | $0.0066 \cdot 10^{-3}$ | < 0.1 |
| $R_{148/146,\,y}$ | Type B | $2.3124 \cdot 10^{-3}$ | $0.0055 \cdot 10^{-3}$ | < 0.1 |
| $R_{150/146,\,y}$ | Type B | $1.0543 \cdot 10^{-3}$ | $0.0079 \cdot 10^{-3}$ | 0.2 |
| $R_{142/146,\,x}$ | Type A | 0.06298 | 0.00052 | < 0.1 |
| $R_{143/146,\,x}$ | Type A | 0.6096 | 0.0016 | 0.3 |
| $R_{144/146,\,x}$ | Type A | 2.0658 | 0.0041 | 2.1 |
| $R_{145/146,\,x}$ | Type A | 0.7745 | 0.0019 | 0.4 |
| $R_{148/146,\,x}$ | Type A | 0.4814 | 0.0014 | 40.5 |
| $R_{150/146,\,x}$ | Type A | 0.24149 | 0.00091 | < 0.1 |
| $R_{150/146,\,b}$ | Type A | 0.10906 | 0.00033 | 54.9 |
| ε | Type B | -0.01696 | 0.00057 | 0.9 |
| Nd mass fraction in fuel ($g \cdot g^{-1}$) | | $6.399 \cdot 10^{-3}$ | $0.035 \cdot 10^{-3}$ | |

# Chapter 6 – IDMS data analysis using R

This chapter provides an overview of the results obtained using the R code, which was developed to determine the mass fractions of uranium, plutonium, neodymium (Nd) and gadolinium (isotope dilution) and their corresponding nuclides from HPIC-SF-ICP-MS chromatograms. The R code was developed with the aim of saving time associated with data handling. The R code was written based on the Nd data that was obtained using HPIC-SF-ICP-MS and it is intended to be published in a separate manuscript.

## 6.1 Introduction

The analysis of data obtained from transient signals was found to be time-consuming and required handling data files with more than 700 data points for each Nd nuclide monitored (7 Nd nuclides were monitored in non-spiked samples and 2 Nd nuclides were monitored in spiked samples). Even though the processing of all data files belonging to one element required using the same equations and reference values, at least 3-4 working hours were required to calculate the mass fraction of one element using isotope dilution. This lengthy data handling process can be automated by using statistical computing languages to make it as simple and as quick as the click of a mouse button. A programming language allows humans to translate their thoughts into a set of instructions to be executed by computers. This set of instructions is commonly known as a code [1]. Various programming languages can be used for data analysis, such as Python [2], C++ [3] and R [4]. R is a free software for statistical computing and graphics and is named after the R language used in it [5]. R was originally written by Robert Gentleman and Ross Ihaka of the Statistics Department of the University of Auckland, and is currently maintained and updated by R core team members [5].While both Python and R are easier to learn than C++ for users without any programming background, Python is a general purpose language, whereas R was developed for statistics and consequently offers specific advantages, such as advanced data visualization features. Nevertheless, Python, C++ and R can be used together to combine their features to perform computationally-intensive tasks if needed. Based on its more dedicated nature, R was chosen for the statistical data handling required in the isotope dilution calculation based on transient HPIC-SF-ICP-MS signal data.

## 6.2 Methods

Using R, the chromatographic peaks were first plotted, after which the isotope ratios (IRs) could be derived. These ratios were then used in the isotope dilution calculation to determine the mass fraction of Nd, as well as its isotopic composition, in a UOx SNF sample.

### 6.2.1 Plotting the chromatographic peaks

To visualize the data, "*point geom*" was used in the "*ggplot*" function to create scatter plots of the time-resolved raw data for each Nd nuclide monitored. Horizontal "*facets"* were used to show all the nuclides on the same plot. A different colour was used in the point "*geom*" for each nuclide.

### 6.2.2 Calculating IRs

A Gaussian function was used to fit the chromatographic peaks of the Nd nuclides. Then, the area under the Gaussian curve was integrated and IRs were derived by dividing the peak area of a monitored nuclide by that of the reference nuclide ($^{146}$Nd) for the same element.

The raw IRs obtained using R were compared with those determined previously when using manual peak area integration (PAI) in Excel (discussed in section 5.2.3.3.iii of chapter 5).

### 6.2.3 Determination of isotopic composition and mass fraction of Nd using R

The raw IRs were then corrected for the bias caused by instrumental mass discrimination, by relying on an external correction method based on a standard-sample bracketing approach (see section 3.2.3 of chapter 3). The standard used for this mass bias correction was a Nd Johnson Matthey standard (JMC-311) with natural isotopic abundances. The mass bias corrected IRs were applied in the isotope dilution equation (see eq. 3.13 in section 3.2.6.3 of chapter 3) to calculate the mass fraction of Nd in the SNF sample and were also used to determine the isotopic composition of Nd in the SNF sample.

Uncertainty calculation has not yet been implemented in the code. Nevertheless, the results could be compared with those obtained previously by using Excel for the same SNF sample.

## 6.3 Results

### 6.3.1 Plotting the chromatographic peaks

Scatter plots obtained using R for the chromatographic peaks for the Nd nuclides monitored in the standard used are shown in Figure 6.1.

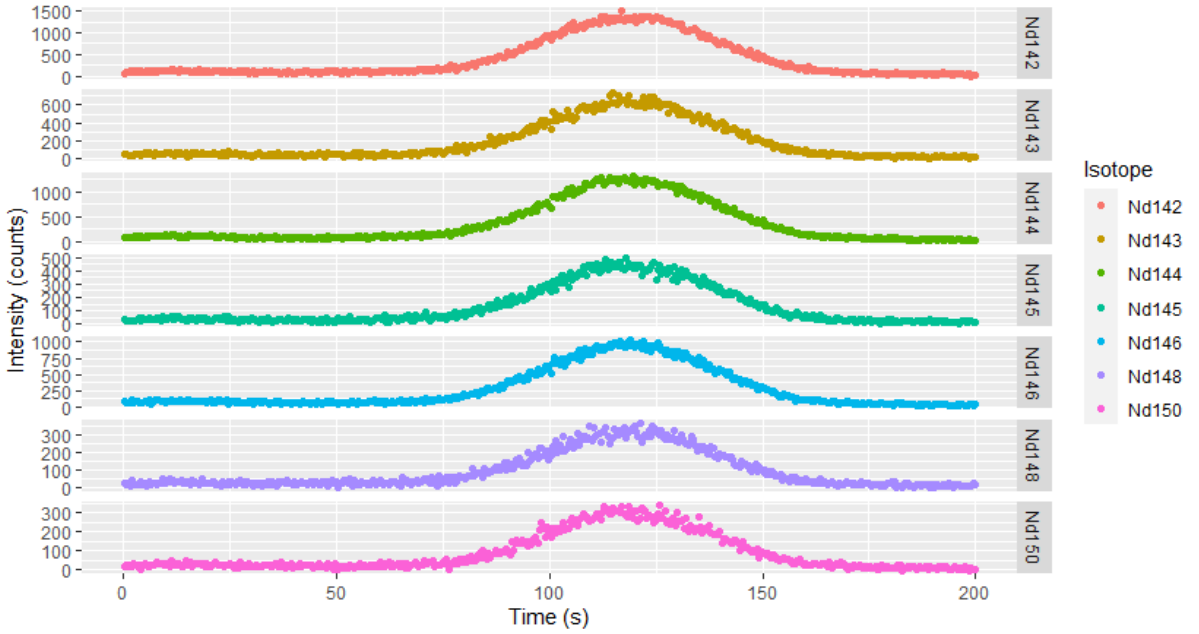


Figure 6.1 Scatter plots based on the raw data obtained for the Nd nuclides as obtained using HPIC-SF-ICP-MS

### 6.3.2 Calculating IRs

The Gaussian curves fitted through the chromatographic peak data of each Nd nuclide monitored in the standard used are illustrated in Figure 6.2. The chromatographic peak area was obtained by integrating the area between the Gaussian curve and the background of the curve throughout the total run time. The IRs obtained using PAI in R were found to be similar (within ± 2 %) to those obtained using PAI in Excel as shown in Table 6.1.

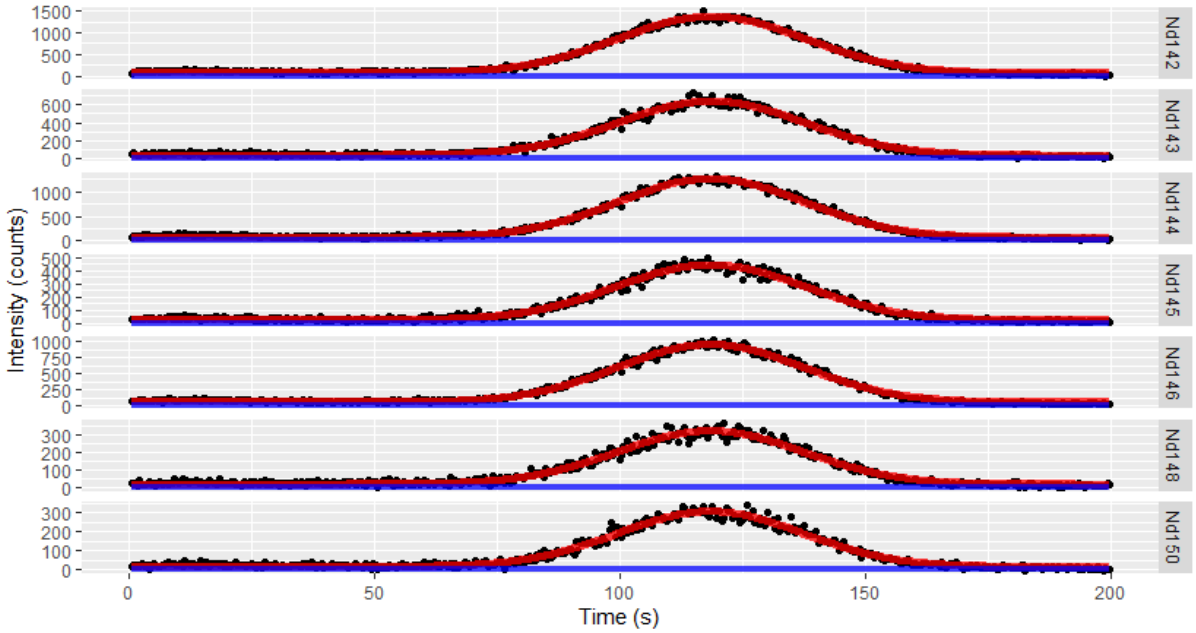


Figure 6.2 Gaussian fit (in red) and background (in blue) of the chromatographic peaks for the Nd nuclides monitored

Table 6.1 Comparison of raw neodymium IRs determined manually using PAI in Excel and using PAI in R for one injection of a Nd standard (JMC-311)

| IR | Determined using PAI in R | Determined using PAI in Excel | R/Excel · 100 (%) |
|---|---|---|---|
| $n(^{142}Nd)/n(^{146}Nd)$ | 1.5096 | 1.5218 | 99.20 |
| $n(^{143}Nd)/n(^{146}Nd)$ | 0.6891 | 0.6911 | 99.72 |
| $n(^{144}Nd)/n(^{146}Nd)$ | 1.3619 | 1.3654 | 99.74 |
| $n(^{145}Nd)/n(^{146}Nd)$ | 0.4674 | 0.4740 | 98.60 |
| $n(^{148}Nd)/n(^{146}Nd)$ | 0.3352 | 0.3364 | 99.65 |
| $n(^{150}Nd)/n(^{146}Nd)$ | 0.3366 | 0.3363 | 100.11 |

### 6.3.3 Determination of isotopic composition and mass fraction of Nd using R

In the UOx fuel sample, nuclide-specific amount fractions of Nd nuclides obtained by using R were in agreement (maximum 1.2 % difference) with those determined by using Excel, as shown in Table 6.2.

Table 6.2 Comparison of the nuclide-specific Nd amount fractions (·100) determined using R and manually using Excel in a UOx fuel sample

| | Determined using R | Determined using Excel | R/Excel · 100 (%) |
|---|---|---|---|
| $n(^{142}Nd)/n(Nd)$ | 1.820 | 1.842 | 98.81 |
| $n(^{143}Nd)/n(Nd)$ | 11.899 | 11.968 | 99.43 |
| $n(^{144}Nd)/n(Nd)$ | 39.875 | 39.903 | 99.93 |
| $n(^{145}Nd)/n(Nd)$ | 14.704 | 14.714 | 99.94 |
| $n(^{146}Nd)/n(Nd)$ | 18.761 | 18.682 | 100.4 |
| $n(^{148}Nd)/n(Nd)$ | 8.732 | 8.687 | 100.5 |
| $n(^{150}Nd)/n(Nd)$ | 4.209 | 4.205 | 100.1 |

* not corrected for cross-contamination with $^{142}Nd$ from the glass ampoule in which the stock solution of the sample was stored

Additionally, the Nd elemental mass fraction determined by isotope dilution using R was found to be 6.367 $mg \cdot g^{-1}$ in the UOx SNF sample, which is 99.50 % of the result calculated by using Excel for HPIC-SF-ICP-MS analysis and 98.40 % of that determined by using TIMS.

## 6.4 Conclusions and outlook

Data analysis and handling times were reduced significantly from a few hours to just a few minutes when using the R code to calculate the elemental mass fraction (isotope dilution) and the isotopic composition of Nd in SNF from HPIC-SF-ICP-MS data. Uncertainty calculation still needs to be implemented in the R code to provide a more complete basis upon which the performance of the R code can be compared with that of the manual approach. The R code will be extended to include the determination of plutonium, gadolinium and uranium mass fractions and nuclide-specific compositions in SNF based on on-line and off-line isotope dilution HPIC-SF-ICP-MS data. Ultimately, combining HPIC-SF-ICP-MS with rapid data analysis using R can be used for urgent SNF samples or exploratively before their analysis using isotope dilution TIMS and alpha spectrometry.

## 6.5 References

[1] T. Dalling, Programming for beginners, 2020.

[2] T. Drabas, Practical data analysis cookbook, Packt, 2016.

[3] Albatross, "A brief description," C++, [Online]. Available: https://www.cplusplus.com/info/description/. [Accessed 20 11 2020].

[4] R Core Team, R: A language and environment for statistical computing, Vienna: R Foundation for statistical computing, 2018.

[5] R foundation, "The R project for statistical computing," [Online]. Available: https://www.r-project.org/. [Accessed 20 11 2020].

# Chapter 7 – General conclusions and outlook

The aim of this work was to develop a method combining isotope dilution with HPIC-SF-ICP-MS to determine the elemental mass fractions and nuclide-specific compositions of uranium, plutonium, neodymium and gadolinium in SNF and to compare the performance of the novel method with an existing method based on isotope dilution TIMS after off-line column chromatography. The main achievements of this work and future perspectives are discussed in this chapter.

## 7.1 General conclusions

In **chapter 4**, the development and validation of an HPIC-based separation method were discussed. The elution program used to separate uranium, plutonium, neodymium and gadolinium from one another following a single sample injection onto a CS5A mixed-bed ion-exchange column in under 60 minutes was presented. The separation method was applied to a spent "Gd fuel" and a soil sample. To increase the signal intensities and verify the separation method, lanthanides were added to the spent "Gd fuel", and plutonium was added to the environmental soil sample (due to their respective low amounts in these samples). The separation resolution was independent of the type of matrix, whether SNF or soil matrix, which indicates that this separation method is applicable to widely differing sample matrices. HPIC-SF-ICP-MS can be used in conjunction with external calibration, to quantify plutonium, uranium, neodymium and gadolinium nuclides when present in spent "Gd fuel" and in environmental soil samples.

**Chapter 5** included the investigation of the effect of different data acquisition parameters and of different calculation methods on the uncertainties of isotope ratio (IR) data extracted from transient signals obtained using HPIC-SF-ICP-MS. Optimal data acquisition settings (mass window 25 %, 20 samples per peak, dwell time 10 ms) and the calculation method (peak area integration) providing the highest precision were identified and used to measure IRs in the context of nuclide-specific and elemental mass fractions determination using isotope dilution. The isotope dilution HPIC-SF-ICP-MS method developed was subsequently used for quantification of the mass fractions of plutonium, uranium, neodymium and gadolinium nuclides in two types of SNF samples (spent UOx and "Gd fuel"). Each sample type was measured in triplicate and the results obtained using isotope dilution HPIC-SF-ICP-MS were compared with those obtained by using isotope dilution TIMS and alpha spectrometry (an ISO 17025 accredited method). For the elemental mass fraction of neodymium in UOx SNF and that of gadolinium in the "Gd fuel", the corresponding expanded uncertainty (calculated using the bottom-up approach) obtained with isotope dilution HPIC-SF-ICP-MS was smaller than that obtained previously by using isotope dilution TIMS and alpha spectrometry (an ISO 17025 accredited method) for the same SNFs. However, for most of the nuclide-specific amount fractions determined based on IR measurements in UOx and "Gd fuel" samples, smaller

uncertainties were obtained using TIMS and alpha spectrometry than those obtained using HPIC-SF-ICP-MS. Therefore, it was concluded that the developed HPIC-SF-ICP-MS method can be used to rapidly determine the mass fractions of plutonium, uranium, neodymium and gadolinium in an unknown SNF, so that the optimum mixing ratio of spike and sample can be calculated prior to performing the lengthy isotope dilution TIMS and alpha spectrometry analyses.

## 7.2 Further investigations

### 7.2.1 Spent nuclear fuels

It would be interesting to evaluate the determination of the mass fractions of other nuclides than $^{148}$Nd which can be used as fission product monitors (such as $^{139}$La, $^{143+144}$Nd which includes $^{144}$Nd from the decay of $^{144}$Ce, $^{145+146}$Nd and $^{150}$Nd) using the nuclide-specific amount fractions measured in a SNF sample in combination with the elemental mass fraction determined using isotope dilution HPIC-SF-ICP-MS method developed in this work. When successful, such results could then be used to determine a burn-up value using each fission product monitor for quality assurance purposes (a common practice at SCK CEN).

### 7.2.2 Environmental samples

#### 7.2.2.1 Dealing with matrix composition of environmental samples

Investigating the application of this HPIC-SF-ICP-MS method to other types of environmental samples, such as urine, seawater and plant material, could be useful as the method developed shows a higher sample throughput (shorter measurement time per sample) than the currently used methods. For example, the HPIC-SF-ICP-MS developed in this work enables the chromatographic separation of uranium and the determination of its concentration in a soil sample in less than an hour, which offers a time saving compared to gravitational chromatography followed by alpha spectrometry, which for uranium, for example, takes three days due to its low activity levels in environmental samples. To investigate the applicability of HPIC-SF-ICP-MS to other types of environmental samples, the cation exchange capacity of the CS5A column (5 µeq) will have to be taken into account. Therefore, certified environmental standards can be used to determine the maximum amount of sample that can be injected onto the column in order not to exceed the column capacity. Knowing this would allow one to decide whether there is a need for (partial) removal of the sample matrix prior to sample loading or whether a simple dilute-and-shoot could be sufficient for environmental samples. Sample preparation methods to remove part of the sample matrix may include phosphate precipitation or sample digestion combined with evaporation of volatile matrix constituents.

Additionally, during a sample run, the third valve of the HPIC unit can be used to direct the column effluent to waste during the elution of matrix elements impurities (e.g. K, Ca, Na) to avoid contaminating the SF-ICP-MS with elements not meant to be measured. Also during column washing and conditioning prior to the next injection, the column effluent is directed to waste rather than to the ICP-MS introduction system.

#### 7.2.2.2 Improving the LOD for Pu in environmental samples

To measure plutonium nuclides at low concentrations in environmental samples (e.g. 10 fg of $^{238}$Pu per gram of soil), it would be interesting to investigate the use of a sample loop with a volume larger than 25 µL in conjunction with a concentrator column placed before the CS5A analytical column to increase the plutonium signal intensity, thereby facilitating its measurement along with uranium and some of the lanthanides. Commercially available cation concentrator columns such as MetPac CC-1 (Thermo Fisher Scientific) and Ionpac TMC-1 (Thermo Fisher Scientific) have capacities of 0.4 and 0.3 meq, respectively, and can be used in combination with CS5A columns. The use of such concentrator columns have been reported in the literature. For example, Perna et al.[1] published a study on the analysis of soil and sediment samples in which americium was concentrated on a TCC-II concentrator column connected to a CS5A column. The americium fraction eluting from the CS5A column was then collected and measured off-line by alpha spectrometry.

#### 7.2.2.3 Fast determination of U and lanthanide concentrations using external calibration or single standard addition

For samples not containing any plutonium, a method was developed to first elute the lanthanides from the CS5A column, followed by uranium. This was accomplished by using a gradient of 0.1-0.15 M oxalic acid at a pH of 4.5, followed by the isocratic elution using 0.1 M oxalic acid buffered to a pH of 0.6 with hydrochloric acid. This HPIC-SF-ICP-MS separation method could be tested on real environmental samples whereby external calibration or single standard addition to determine the elemental and nuclide-specific concentrations of uranium and the lanthanides in samples for which expanded uncertainties ≤10 % are fit-for-purpose. This could be applicable to monitor the concentrations of uranium, neodymium and gadolinium in underground or surface waters for example.

[1] L. Perna, J. Jernstrom, L. Aldave de las Heras, J. de Pablo and M. Betti, "Sample cleanup by on-line chromatography for the determination of Am in sediments and soils by alpha-spectrometry," Analytical Chemistry, vol. 75, pp. 2292-2298, 2003.

# Summary

Determining the nuclide-specific and elemental composition of spent nuclear fuel (SNF), which is fuel that has undergone irradiation in a nuclear reactor, is essential for criticality safety during nuclear waste management and for examining the performance of the fuel. Post-irradiation examination of SNF includes the determination of long-lived actinides, lanthanides (fission products) and neutron absorbers. Inductively coupled plasma-mass spectrometry (ICP-MS) is a sensitive analytical method that allows the measurement of stable and (sufficiently long-lived) radioactive nuclides (radionuclides). Isotope dilution mass spectrometry is an accurate and precise calibration method that can be used to determine nuclide-specific and elemental mass fractions of uranium (U), plutonium (Pu), neodymium (Nd) and gadolinium (Gd), based on isotope ratio (IR) measurements using ICP-MS or, alternatively, using thermal ionization mass spectrometry (TIMS) in combination with alpha spectrometry. Sector field (SF) ICP-MS is a single detector ICP-MS instrument well known for the flat top spectral peak shape at low mass resolution, which can be used to measure IRs sufficiently precisely. Coupling high-pressure ion chromatography (HPIC) on-line with ICP-MS (which is not possible with either TIMS or alpha spectrometry) offers a faster way to eliminate isobaric interferences compared with gravitational ion chromatography (which cannot be coupled on-line with ICP-MS), and reduces the analyst's exposure to radiation, as more diluted samples with lower activities suffice for the combination of HPIC (instrumentation can be placed inside a glovebox) and ICP-MS. The literature reports various kinds of ICP-MS instruments being coupled to HPIC for the characterization of SNF. However, the expanded uncertainty of isotope dilution when using HPIC-SF-ICP-MS to determine the mass fractions of U, Pu, Nd and Gd in SNF from the same sample injection has not been reported previously. Therefore, the aim of this work was to separate U, Pu, Nd and Gd and to determine their nuclide-specific composition (using IR measurements) and elemental mass fractions (using isotope dilution) in SNF by means of HPIC-SF-ICP-MS. To accomplish this, the work had four objectives: (1) to develop and validate a separation method for U, Pu and the lanthanides from one another upon a single sample injection using HPIC, (2) to optimize the SF-ICP-MS data acquisition parameters and to select the IR calculation method providing the most precise data, (3) to characterize different types of SNF using isotope dilution HPIC-SF-ICP-MS and (4) to evaluate the overall uncertainty budget of the elemental mass fractions determined using isotope dilution HPIC-SF-ICP-MS and compare it to that of an already implemented ISO 17025 accredited isotope dilution TIMS and alpha spectrometry method.

The first objective was tackled in different steps where, at each step, simulations with the Hydra/Medusa software package were performed to predict the speciation of U, Pu and the lanthanides in solution. The column used for the separation is a mixed-bed ion exchange IonPac CS5A (Dionex) column, preceded by an IonPac CG5A (Dionex) guard column. The separation method was developed using samples prepared by mixing mono-elemental standards, and was then validated by using a real SNF sample and an environmental soil standard (IAEA-375). Pu in the sample was oxidized to Pu(VI) with 40 nM $KMnO_4$ 12 hours prior to injection onto the column. In the final elution method, a gradient of 1 - 0.75 M nitric acid was used to elute Pu

and U as neutral plutonyl and uranyl nitrate complexes, respectively. The column was then washed with water before introducing a gradient of 0.1 – 0.15 M oxalic acid adjusted to a pH of 4.5 by using ammonium hydroxide to elute the lanthanides according to their decreasing ionic radius (from lanthanum to lutetium) as negatively charged oxalate complexes. This final elution method resulted in peak resolutions ranging from 1 to 1.7 for Pu, U and the lanthanides in a single run, in less than 60 minutes per sample. All analytes eluted as single peaks, thus enabling IR measurements. Limits of detection for $^{242}$Pu, $^{238}$U, $^{146}$Nd and $^{157}$Gd were found to be 0.015, 0.065, 0.055 and 0.050 $\mu g \cdot L^{-1}$, respectively. The separation method was found to be applicable to SNF and environmental soil matrices.

For the second objective, the SF-ICP-MS data acquisition parameters needed to be optimized to obtain precise IR measurements of Pu, Nd and Gd from transient signals. The eluting U peak was not suitable for on-line IR determination due to its excessive intensity. Therefore, the U eluting from the column was collected and measured later in a separate off-line SF-ICP-MS analysis using previously optimized data acquisition settings. The optimization of Pu, Nd and Gd IR measurements based on transient signals was accomplished by investigating different data acquisition parameters using repeated injections of the same Nd standard of natural isotopic composition. The effect of using four mass windows (2, 25, 50 and 150 %), two dwell times (10 and 30 ms) and two different numbers of nuclides monitored per run (2 and 7) was investigated. A mass window of 25 %, with 20 samples per flat top peak and a dwell time of 10 ms were found to give the best performance with transient signals in HPIC-SF-ICP-MS. Furthermore, the three most commonly used IR calculation methods (according to the literature), namely linear regression slope (LRS), point-by-point (PbP) and peak area integration (PAI), were compared for their accuracy and precision. Although the three calculation methods resulted in similar IR values, those calculated with PAI were found to have the best precision and repeatability when 50 % of the chromatographic peak width around the peak apex was integrated. This justifies the use of PAI, because the effects of sequential nuclide monitoring, causing peak skewness, is prevented in this calculation method. Moreover, the experimental precisions of Nd IRs obtained when using a mass window of 25 %, which acquires only the flat top region of the mass spectrometric peak, and calculated by using PAI were found to be the closest to the theoretical precision, derived from Poisson statistics. All of the IRs measured were corrected manually for mass discrimination using a linear model with the external standard measured in a sample-standard bracketing sequence. The raw IRs were first corrected automatically for detector dead time losses by the SF-ICP-MS software using an experimentally determined detector dead time value.

For the third objective, the optimization of on-line isotope dilution for the determination of Pu, Nd and Gd elemental mass fractions in two types of SNF had to be accomplished. The spikes and $KMnO_4$ were added to the samples at least 12 hours before the analysis, to ensure sufficient time for isotopic equilibration and to oxidise all Pu to Pu(VI). In the blend sample, the isotope amount ratios $n(^{148}\text{Nd})/n(^{146}\text{Nd})$, $n(^{242}\text{Pu})/n(^{239}\text{Pu})$, $n(^{233}\text{U})/n(^{238}\text{U})$ and $n(^{157}\text{Gd})/n(^{156}\text{Gd})$ were either close to unity or at the minimum of the error multiplication factor curve, for better precision. The elemental mass fractions of Nd, Pu and U were determined in triplicate in the UOx fuel by using isotope dilution HPIC-SF-ICP-MS and the results thus obtained were equal

to 98.5, 100.7 and 98.5 %, respectively, of those determined by means of the ISO 17025 accredited isotope dilution TIMS and alpha spectrometry method. In the "Gd fuel", the elemental mass fractions of Gd, Pu and U were determined in triplicate by using isotope dilution HPIC-SF-ICP-MS and the results thus obtained corresponded to 100.01, 100.11 and 100.1 %, respectively, of those determined by means of isotope dilution TIMS and alpha spectrometry. The determination of the Nd mass fraction in the "Gd fuel" was limited by both the LOD of the method and the low level of fission that had occurred in that particular fuel. The determination of $^{238}$Pu in the UOx fuel was limited by its low mass fraction in the sample and the higher instrumental background at $m/z$ = 238. For both types of fuel analysed, the nuclide amount fractions obtained by means of HPIC-SF-ICP-MS were in agreement (average difference of ± 2 % and maximum difference of 11 %) with those obtained by means of TIMS and alpha spectrometry. An R code was written for the rapid calculation of the Nd isotopic composition (using IR measurement) and its mass fraction (using isotope dilution) in SNF. The elemental mass fraction of Nd calculated using R was found to be 99.5 % of that calculated manually using Excel. The R code will be extended to include the elemental and nuclide-specific quantification of Pu, Gd and U based on on-line and off-line HPIC-SF-ICP-MS measurements, and to calculate the corresponding expanded uncertainties.

For the fourth objective, uncertainty budgets for the isotope dilution HPIC-SF-ICP-MS experiments were derived based on the bottom-up approach, following the Eurachem/CITAC guide CG4. The major contributors were found to be the mass bias correction (~ 1 %) and the raw IRs (~ 95 %) measured using HPIC-SF-ICP-MS. Uncertainty calculations were performed using GUM Workbench software. The expanded uncertainties associated with the elemental mass fractions of Nd in the UOx fuel and Gd in the "Gd fuel", obtained with on-line isotope dilution HPIC-SF-ICP-MS, were smaller than those obtained with isotope dilution TIMS and alpha spectrometry. However, this result was not the case for Pu elemental mass fractions, as their expanded uncertainties in both types of fuels were larger with isotope dilution HPIC-SF-ICP-MS than those obtained with isotope dilution TIMS and alpha spectrometry. Additionally, due to the ± 200-fold dilution of the U fraction collected prior to SF-ICP-MS analysis, large expanded uncertainties for the mass fractions of U in both types of fuel (almost 6 %) were obtained with off-line isotope dilution HPIC-SF-ICP-MS. For nuclide-specific amount fractions of Pu, U, Nd and Gd, determined based on IR measurements in non-spiked UOx and "Gd fuel" samples, smaller uncertainties were obtained using TIMS and alpha spectrometry than those obtained using HPIC-SF-ICP-MS except for most of the Pu nuclides and two Nd nuclides ($^{142}$Nd and $^{148}$Nd) in the UOx fuel sample.

Overall, isotope dilution HPIC-SF-ICP-MS was found to be a fast, safe, precise and accurate method to characterize SNF samples in three days: one day for the separation of U (to be collected off-line upon elution from the HPIC column), Pu, Nd and Gd and for the on-line measurement of Pu, Nd and Gd using HPIC-SF-ICP-MS, a second day for the off-line SF-ICP-MS measurement of the collected U and the data processing of U and one other element (Pu, Nd or Gd), and a third day to process the data of the remaining two elements. When the R code is finalized, it will be possible to reduce the data processing time of the four elements of interest

(U, Pu, Nd and Gd) to be done within less than one hour, which will permit to characterize SNF samples in less than two days.

# Samenvatting

Het bepalen van zowel de elementaire als de isotopische samenstelling van gebruikte kernbrandstof (SNF), dit is kernbrandstof die bestraald werd in een kernreactor, is essentieel voor de criticaliteit veiligheid bij het beheer van nucleair afval en het onderzoek naar de performantie van de kernbrandstof. Het onderzoek van SNF na de bestraling omvat het bepalen van langlevende actiniden, lanthaniden (fissieproducten) en neutronabsorbers. Inductief gekoppeld plasma-massaspectrometrie (ICP-MS) is een gevoelige analysemethode geschikt voor de bepaling van stabiele nucliden en voldoende langlevende radionucliden. Isotopendilutie massaspectrometrie is een accurate en precieze kalibratiemethode, gebaseerd op het berekenen van isotopenverhoudingen, die kan gebruikt worden bij de bepaling van nuclide-specifieke en elementaire massafracties van uranium (U), plutonium (Pu), neodymium (Nd) en gadolinium (Gd) met behulp van ICP-MS of thermische ionisatie massaspectrometrie (TIMS) (in combinatie met alfaspectrometrie). Een sector veld (SF) massaspectrometer is een ICP-MS toestel uitgerust met slechts één detector, maar genereert bij lage massaresolutie spectrale pieken met een vlakke top, die geschikt zijn voor het bepalen van isotopenverhoudingen met voldoende precisie. Het koppelen van hoge druk ionenchromatografie (HPIC) met ICP-MS (wat niet mogelijk is met TIMS, noch met alfaspectrometrie) biedt een snelle manier om isobare interferenties te elimineren en tegelijkertijd de blootstelling aan radioactieve straling te verminderen, in vergelijking met het afzonderlijk isoleren en analyseren van zuivere fracties m.b.v. respectievelijk kolomchromatografie (wat niet on-line kan gekoppeld worden met ICP-MS) en TIMS (met alfaspectrometrie). De lagere blootstelling is het gevolg van enerzijds de vermindering in staalvoorbereidingstijd en anderzijds de grotere verdunningsfactor van het SNF staal waarmee gewerkt wordt bij het laden van de HPIC kolom, die zich bovendien in een handschoenkast bevindt. In wetenschappelijke literatuur zijn diverse studies te vinden over de karakterisering van SNF m.b.v. HPIC gekoppeld aan diverse types ICP-MS toestellen. Echter, tot nu toe, rapporteert geen enkele studie geëxpandeerde meetonzekerheden op de massafracties van U, Pu, Nd en Gd in SNF bepaald d.m.v. isotopendilutie in combinatie met HPIC-SF-ICP-MS na een éénmalige staalinjectie. De overkoepelende doelstelling van dit werk was een methode ontwikkelen om U, Pu, Nd en Gd te isoleren uit SNF en te scheiden van elkaar om vervolgens hun isotopische samenstelling (m.b.v. isotopenverhoudingen)- en elementaire massafracties (m.b.v. isotopendilutie) te bepalen met HPIC-SF-ICP-MS. Deze doelstelling werd bereikt aan de hand van vier objectieven: (1) het ontwikkelen en valideren van een scheidingsmethode voor U, Pu en de lanthaniden vanuit een enkelvoudige staalinjectie in een HPIC-SF-ICP-MS opstelling; (2) het optimaliseren van de data-acquisitieparameters van het SF-ICP-MS toestel en het selecteren van de beste berekeningsmethode voor isotopenverhoudingen resulterend in de best haalbare precisie; (3) het karakteriseren van verschillende SNF stalen m.b.v. isotopendilutie HPIC-SF-ICP-MS; (4) het berekenen van de totale meetonzekerheid verkregen met de isotopendilutie HPIC-SF-ICP-MS methode en deze vergelijken met de meetonzekerheid verkregen met de ISO 17025 geaccrediteerde isotopendilutie TIMS (+ alfaspectrometrie) methode.

De eerste deeldoelstelling werd aangepakt in verschillende stadia, waarbij telkens Hydra/Medusa software werd gebruikt om de chemische speciatie van U, Pu en lanthaniden in oplossing te voorspellen. De kolommen die gebruikt werden voor de chemische scheidingen, Dionex Ionpac CS5A en CG5A, bevatten een gemengd bed ionenuitwisselingshars. De scheidingsmethode werd ontwikkeld door gebruik te maken van mono-element standaarden, die met elkaar gemengd werden tot multi-element standaarden met gepaste concentraties. Daarna werd de scheidingsmethode gevalideerd m.b.v. een echt SNF staal en een gecertificeerd bodemreferentiemateriaal (IAEA-375). Pu in het staal werd geoxideerd tot Pu(VI) door 40 nM $KMnO_4$ toe te voegen 12 h voorafgaand aan de injectie in het HPIC toestel. In de finale scheidingsmethode worden Pu en U geëlueerd als ongeladen plutonyl- en uranylnitraat complexen door gebruik van een gradiënt van 1 – 0.75 M $HNO_3$. Daarna werden de kolommen gewassen met water voorafgaand aan een gradiëntelutie van de lanthaniden in 0.10-0.15 M oxaalzuur dat vooraf door toevoeging van ammoniumhydroxide oplossing op een pH-waarde van 4.5 werd gebracht. Hierbij elueerden lanthaniden als negatief geladen oxalaatcomplexen, in volgorde van dalende ionenstraal, d.i. van lantaan naar lutetium. De finale scheidingsmethode leverde resoluties op tussen 1 en 1.7 voor de individuele pieken van lanthaniden en effectieve isolatie van Pu, U, Nd en Gd werd bereikt in minder dan 60 minuten per staalinjectie. Alle analietelementen elueerden als een enkelvoudige piek, geschikt voor het berekenen van isotopenverhoudingen. Detectielimieten voor enkele belangrijke nucliden waren 0.015, 0.065, 0.055, en 0.050 $\mu g \cdot L^{-1}$ voor respectievelijk $^{242}Pu$, $^{238}U$, $^{146}Nd$ en $^{157}Gd$. Bovendien bleek de scheidingsmethode geschikt voor zowel SNF als de bodemmatrix.

De tweede deeldoelstelling vereiste optimalisatie van de SF-ICP-MS data-acquisitieparameters met het oog op het bekomen van isotopenverhoudingen uit de transiënte signalen van Pu, Nd en Gd nucliden, met de best mogelijke precisie. De transiënte signalen van de uraniumnucliden waren niet geschikt voor het bepalen van isotopenverhoudingen wegens hun te hoge intensiteit door hun zeer hoge concentratie in SNF stalen. Daarom werd het kolomeffluent tijdens de elutie van U apart opgevangen en later off-line geïntroduceerd in het SF-ICP-MS toestel d.m.v. continue verstuiving, waarbij data-acquisitieparameters gebruikt werden die in een voorgaande studie optimaal bleken voor dit type monster. Voor optimalisatie van de bepaling van isotopenverhoudingen van Pu, Nd en Gd uit transiënte signalen werden herhaaldelijke injecties van dezelfde Nd standaardoplossing met natuurlijke isotopische samenstelling gebruikt. Het effect van verschillende data-acquisitieparameters, nl. van het *mass window* (2, 25, 50 en 150 %), de *dwell time* (10 en 30 ms) en aantal te monitoren isotopen (2 en 7), op de accuraatheid en precisie van isotopenverhoudingen werd onderzocht. Een *mass window* van 25 %, 20 punten per piek en een *dwell time* van 10 ms bleken de optimale instellingen voor het verkrijgen van isotopenverhoudingen uit de transiënte signalen. Bovendien werden drie methoden voor de berekening van isotopenverhoudingen uit transiënte signalen vergeleken inzake accuraatheid en precisie, nl. *linear regression slope* (LRS, richtingscoëfficiënt van de lineaire regressie), *point-by-point* (PbP, punt per punt) en *peak area integration* (PAI, integratie van piekoppervlak). Hoewel de drie berekeningswijzen resulteerden in gelijkaardige isotopenverhoudingen, werden de beste precisie (herhaalbaarheid) bekomen met de PAI methode, wanneer 50 % van de chromatografische piek werd geïntegreerd. Het is duidelijk dat in de PAI methode het negatieve effect van sequentiële meting van nucliden op de precisie

geëlimineerd wordt, in tegenstelling tot bij de PbP en LRS methoden. Bovendien sloten de experimentele precisies van de Nd isotopenverhoudingen verkregen bij een mass window van 25 %, waarbij enkel de vlakke top van de spectrale piek wordt gebruikt voor de berekeningen, en PAI als berekeningsmethode het beste aan bij de theoretische precisie bekomen op basis van de Poissonverdeling. Een correctie voor massadiscriminatie werd toegepast op alle bekomen isotopenverhoudingen, m.b.v. interne correctie via het lineaire model en externe correctie met een standaard gemeten in een "*sample-standard bracketing"* sequentie, waarbij afwisselend een staal en een standaard geïnjecteerd worden. Daarnaast werden alle intensiteiten vooraf automatisch gecorrigeerd voor de dode tijd van de detector.

In de derde deeldoelstelling werd de isotopendilutieprocedure geoptimaliseerd voor het *on-line* bepalen van de elementaire massafracties van Pu, Nd en Gd in twee types SNF. Spikes en $KMnO_4$ werden minstens 12 uur voorafgaand aan de analyse toegevoegd aan de monsters, zodat isotopisch evenwicht en oxidatie van Pu naar Pu(VI) kon bereikt worden. In het gemengde staal, alias de *blend*, werd de verhouding van het aantal nucliden van analiet- tot referentie-isotoop gekozen ofwel dichtbij een waarde van één, ofwel bij een waarde die aanleiding gaf tot een minimale foutenpropagatie, wat de precisie ten goede komt. Het betreft hier de volgende verhoudingen: $n(^{148}Nd)/n(^{146}Nd)$, $n(^{242}Pu)/n(^{239}Pu)$, $n(^{233}U)/n(^{238}U)$ en $n(^{157}Gd)/n(^{156}Gd)$. De elementaire massafracties van Nd, Pu en U in UOx kernbrandstof werden in drievoud bepaald d.m.v. isotopendilutie HPIC-SF-ICP-MS. Relatief ten opzichte van de resultaten bekomen met de ISO 17025 geaccrediteerde isotopendilutie TIMS en alfaspectrometrie methode bedroegen de elementaire massafracties respectievelijk 98.5, 100.7 en 98.5 %. In Gd-gedopeerde kernbrandstof werden elementaire massafracties van Gd, Pu en U, eveneens in drievoud bepaald, en werden gehaltes van respectievelijk 100.01, 100.11 en 100.1 % ten opzichte van de elementaire massafracties bekomen met TIMS en alfaspectrometrie gevonden. Bepaling van het Nd gehalte in de Gd-gedopeerde kernbrandstof werd bemoeilijkt door de detectielimiet van de methode en het lage aantal fissies dat had plaatsgevonden in deze kernbrandstof. De bepaling van $^{238}Pu$ in het UOx kernbrandstofstaal was niet mogelijk omwille van de lage concentratie in het staal en het verhoogde achtergrondsignaal op m/z = 238. Een goede overeenkomst tussen de met HPIC-SF-ICP-MS en TIMS + alfaspectrometrie bekomen nuclideconcentraties werd vastgesteld, met een gemiddeld verschil van ± 2 % en een maximaal verschil van 11 %. In het programma 'R' werd een programmeercode opgesteld voor de snelle berekening van de isotopische samenstelling (m.b.v. isotopenverhoudingen) en de massafractie (m.b.v. isotopendilutie) van Nd uit de chromatografische data gegenereerd door de HPIC-SF-ICP-MS opstelling. De automatisch berekende resultaten voor de elementaire massafractie m.b.v. de programmeercode in R stemden binnen ± 0.5 % overeen met de manueel berekende resultaten m.b.v. Microsoft Excel. De programmeercode in R zal nog uitgebreid worden, zodat ook nuclide-specifieke en elementconcentraties van Pu, U en Gd automatisch kunnen berekend worden, en er ook een meetonzekerheid gegenereerd wordt.

Om de totale meetonzekerheid op de resultaten verkregen via isotopendilutie HPIC-SF-ICP-MS te berekenen (de laatste deeldoelstelling van dit werk), werd een bottom-up benadering toegepast volgens de Eurachem/CITAC handleiding CG4. Hiervoor werd gebruik gemaakt van het GUM Workbench computerprogramma. De correctie voor massadiscriminatie (≈1 %) en de meting van de isotopenverhoudingen zelf (≈95 %) vormden de belangrijkste bijdragen tot de

totale meetonzekerheid. De geëxpandeerde onzekerheden op de elementaire massafracties van Nd in UOx kernbrandstof en van Gd in Gd-gedopeerde kernbrandstof waren kleiner wanneer ze bepaald werden met de nieuwe on-line isotopendilutie HPIC-SF-ICP-MS methode dan met de gevestigde TIMS methode. Het omgekeerde werd echter vastgesteld voor Pu. Tot slot,voor U werden hoge geëxpandeerde onzekerheden (bijna 6 %) op de massafracties bekomen m.b.v. de off-line isotopendilutie HPIC-SF-ICP-MS methode, als gevolg van de bijna 200-voudige verdunning van de U fractie. Met TIMS en alfaspectrometrie kunnen eveneens kleinere onzekerheden op de nuclide-specifieke concentraties, door het bepalen van isotopenverhoudingen in ongespiked SNF staal, verkregen worden dan met de HPIC-SF-ICP-MS. Een uitzondering hierop werd vastgesteld voor de meeste Pu nucliden en twee Nd nucliden ($^{142}$Nd en $^{148}$Nd) in het UOx kernbranstofstaal.

Over het algemeen kan gesteld worden dat de isotopendilutie HPIC-SF-ICP-MS methode een snelle, veilige, precieze en accurate methode is om SNF monsters te karakteriseren in slechts drie dagen tijd: één dag voor de isolatie van U, dat afzonderlijk wordt opgevangen, Pu, Nd en Gd en de on-line bepaling van Pu, Nd en Gd, een tweede dag voor de off-line meting en de berekening van de resultaten voor U en voor één ander element (Pu, Nd of Gd), en een derde dag voor het berekenen van de resultaten voor de tweeresterende elementen en rapportering. Eens de programmeercode in R uitgebreid is en ook de andere elementen omvat, kan de berekening van de resultaten voor alle elementen uitgevoerd worden in minder dan één uur, waardoor de totale analysetijd beperkt wordt tot slechts twee dagen.

# List of publications

**Journal publications**

1. N.N. Wanna, K. Van Hoecke, A. Dobney, M. Vasile and F. Vanhaecke, Quantification of uranium, plutonium, neodymium and gadolinium for the characterization of spent nuclear fuel using isotope dilution HPIC-SF-ICP-MS, Talanta, 221 (2021), doi: 10.1016/j.talanta.2020.121592.

2. N.N. Wanna, A. Dobney, K. Van Hoecke, M. Vasile, T. Cardinaels and F. Vanhaecke, Determination of the lanthanides, uranium and plutonium by means of on-line high-pressure ion chromatography coupled with sector field inductively coupled plasma-mass spectrometry to characterize nuclear samples, Journal of Chromatography A, 1617 (2020), doi: 10.1016/j.chroma.2019.460839.

**Oral presentations at international conferences, workshops and events**

1. *Developing a safe, fast and accurate isotope dilution method to characterize spent nuclear fuel using HPIC-SF-ICP-MS*, 14th ENEN PhD Event: European nuclear education network, via web-conferencing, 16 November 2020.

2. *Developing a safe, fast and accurate isotope dilution method to characterize spent nuclear fuel using HPIC-SF-ICP-MS*, UK NMSUG meeting 2020: Nuclear Mass Spectrometry User Group, via web-conferencing, 15 October 2020.

3. *IDMS for the characterization of spent nuclear fuel*, CEA sub-group GT2 "Mass spectrometry and isotope dilution" meeting 2020, via web-conferencing, 23 June 2020.

4. *Optimization of isotope ratio measurement for lanthanides, uranium and plutonium using HPIC-SF-ICP-MS*, 2020 Winter Conference on Plasma Spectrochemistry, Tucson, USA, 13-18 January 2020.

5. *Developing and validating a HPIC-SF-ICP-MS method for separating and measuring isotope ratios of Pu, U and lanthanides to characterize spent nuclear fuel*, RANC 2019: 2nd International conference on Radioanalytical and Nuclear Chemistry, Budapest, Hungary, 5-10 May 2019.

6. *Ion chromatography and mass spectrometry: a match made in a glovebox*, Working group on Atomic Spectrometry meeting 2018, Utrecht, Netherlands, 18 December 2018.
   ➔ **Invited speaker**

**Poster presentations**

1. *Quantification of U, Pu, Nd & Gd for the characterization of spent nuclear fuel using isotope dilution HPIC-SF-ICP-MS*, BNS PhD Contest 2020: Belgian Nuclear Society, via web-conferencing, 26 November 2020.

2. *Separation and isotope ratio measurements of lanthanides and uranium, using HPIC-SF-ICP-MS, for characterization of spent nuclear fuel*, RadChem 2018: 18th Radiochemical conference, Mariánské Lázně, Czech Republic, 13-18 May 2018.
   ➔ **Prize in student poster competition**

3. *Development and validation of HPLC-SF-ICP-MS methodologies for characterization of spent nuclear fuel*, ENYGF 2017: European Nuclear Young Generation Forum, Manchester, UK, 11-16 June 2017.